4th MERIS data reprocessing
Evolutions and Validation report

Ref.: MER4RP Validation Report

Version: 1.0

Date: 01/04/2019

4th MERIS data reprocessing
Evolutions and Validation report

Ref.: MER4RP Validation Report
Version: 1.0
Date: 01/04/2019
Page: ii

Signatures

	Name	Company / Institute	Signature
Book captain	Véronique Bruniquel	ACRI-ST	
with the contributions from the MERIS QWG members (by alphabetic order of company/institute)	Ludovic Bourg Nicolas Lamquin Christophe Lerebourg Richard Santer	ACRI-ST	
	Bahjat Alhammoud	ARGANS	
	Gerald Moore	Bio-Optika	
	Carsten Brockmann Roland Doerffer Ana Ruescas	Brockmann Consult	
	Marc Bouvet	ESA	
	Jürgen Fischer	FUB	
	Didier Ramon	Hygeos	
	Nadine Gobron	JRC	
	Vincenzo Vellucci David Antoine	LOV	
	Francis Zagolski	PARBLEU	
	Constant Mazeran	SOLVO	
	Jadu Dash Luke Brown	University of Southampton	
Validated by	Philippe Goryl	ESA	

Distribution list

Public distribution

Changes Log

Version	Date	Changes
1.0	01/04/2019	Initial version

4th MERIS data reprocessing
Evolutions and Validation report

Ref.: MER4RP Validation Report
Version: 1.0
Date: 01/04/2019
Page: iii

Table Of Content

4th MERIS data reprocessing

Evolutions and Validation report

Ref.:   MER4RP Validation Report

Version: 1.0

Date: 01/04/2019

Page: iv

4th MERIS data reprocessing

Evolutions and Validation report

Ref.: MER4RP Validation Report

Version: 1.0

Date: 01/04/2019

Page: v

List Of Figures

4th MERIS data reprocessing
Evolutions and Validation report

Ref.: MER4RP Validation Report
Version: 1.0
Date: 01/04/2019
Page: vi

4th MERIS data reprocessing

Evolutions and Validation report

Ref.: MER4RP Validation Report

Version: 1.0

Date: 01/04/2019

Page: vii

4th MERIS data reprocessing
Evolutions and Validation report

Ref.: MER4RP Validation Report
Version: 1.0
Date: 01/04/2019
Page: viii

4th MERIS data reprocessing

Evolutions and Validation report

Ref.:   MER4RP Validation Report

Version: 1.0

Date: 01/04/2019

Page: ix

4th MERIS data reprocessing
Evolutions and Validation report

Ref.: MER4RP Validation Report
Version: 1.0
Date: 01/04/2019
Page: x

4th MERIS data reprocessing
Evolutions and Validation report

Ref.: MER4RP Validation Report
Version: 1.0
Date: 01/04/2019
Page: xi

4th MERIS data reprocessing

Evolutions and Validation report

Ref.: MER4RP Validation Report

Version: 1.0

Date: 01/04/2019

Page: xii

4th MERIS data reprocessing

Evolutions and Validation report

Ref.: MER4RP Validation Report

Version: 1.0

Date: 01/04/2019

Page: xiii

List Of Tables

1 Introduction

1.1 Scope of the document

This document corresponds to the "4th MERIS data reprocessing evolutions and validation report" prepared by the MERIS Quality Working Group (QWG) in the frame of the MERIS 4th Level-1 (L1) and Level-2 (L2) products reprocessing (MER4RP). It presents the evolutions implemented for the 4th data reprocessing and aims at qualifying and quantifying the accuracy of the products generated.

1.2 Structure of the document

This document is split into several chapters:

- This chapter introduces the document;

- Chapter 2 presents all the Level 1 and Level 2 evolutions implemented in the 4th MERIS data processors whether it be in terms of algorithm evolutions, Auxiliary Data File (ADF) changes or output products format. The Look-Up Tables (LUTs) evolutions are also presented;

- Chapter 3 corresponds to the validation report. It provides an assessment of the performance of the MER4RP products;

- Chapter 4 acknowledges the in situ data providers;

- Chapter 5 lists the scientific publications cited in this document.

1.3 Reference documents

1.3.1 ATBD documentation

This table below lists the MERIS ATBD documentation.

ID	MERIS ATBD title
ATBD-2.1 & 2.2	Cloud Albedo and Cloud Optical Thickness - V3.1 – 22/08/2011
ATBD-2.3	Cloud Top Pressure - V4.2 – 30/06/2011
ATBD-2.4	MERIS L2 Algorithm for Total Column Water Vapour
ATBD-2.6	Case-2 (Sediment) Bright Pixel Atmospheric Correction - V5.3 – 31/03/2017
ATBD-2.7	Atmospheric Correction over the Ocean (Case 1 Waters)
ATBD-2.9	Pigment Index Retrieval in Case-1 Waters
ATBD-2.10	MERIS & OLCI Uncertainties Assessment for FAPAR and Rectified Channels
ATBD-2.12	Pigment Index, Sediment and Gelbstoff Retrieval from directional Water-leaving Reflectances using Inverse Modeling Technique dated on 19/03/2015

	Ref.:	MER4RP Validation Report
4th MERIS data reprocessing	Version:	1.0
Evolutions and Validation report	Date:	01/04/2019
	Page:	2

ATBD-2.13	Sunglint flag algorithm - V4.3 – 18/07/2011
ATBD-2.15	Land Aerosol retrieval algorithm update for the MERIS 4th reprocessing - V1.0 – 21/11/2016
ATBD-2.17	Pixel Identification
ATBD-2.18	Photosynthetically Available Radiation (PAR)
ATBD-2.22	MERIS Terrestrial Chlorophyll Index
ATBD-2.23	Surface Pressure
ATBD-2.24	Vicarious calibration - V2.0 – 28/07/2017
ATBD-2.25	Alternative Atmospheric Correction Procedure for Case 2 Water Remote Sensing using MERIS
ATBD-2.26	Variation of the barometric pressure with altitude (P-z) - V1.4 – 30/09/2018
ATBD-2.27	The MERIS O_2 Apparent Pressures over Land (P_1) and Water (P_{scat}) Surfaces - V2.2 – 13/09/2018
ATBD-2.28	Pressure Adjustment over Water in the MERIS Ground-Segment Processor (MEGS-9) - V2.1 – 15/12/2018

1.3.2   Reference documents

The table below lists the other reference documents.

ID	Title	
RD-1	https://earth.esa.int/web/guest/software-tools/content/-/article/amorgos-40p1-4410#_101_INSTANCE_2B0w_matmp	
RD-2	Sentinel-3 OLCI Gaseous Correction ATBD, ref. S3-L2-SD-03-C03- FUB-ATBD_GaseousCorrection	V2.0 – 04/08/2010
RD-3	MERIS Sentinel-3 like L1 and L2 Product Format Specification	V1.0 – 26/09/2017
RD-4	The new modelling of the Rayleigh optical thickness (ROT) used in the MERIS 4th reprocessing	V1.0 – 30/09/2018
RD-5	Generation of MERIS O_2 look-up tables with the apparent pressure over land (P_1) and water (P_{scat}) surfaces for MEGS-9	V1.2 – 15/12/2018
RD-6	Specification of the scientific contents of the MERIS level-1b & 2 auxiliary data products", ref. PO-RS-PAR-GS-0002 (ProdSpec)	V3-D – 31/03/2018
RD-7	Reference Model Document for the Ocean Branch	V6.1 – 31/10/2017
RD-8	Generation of the MERIS Ocean-Aerosol LUTs with the NASA/GSFC climatology	V1.2 – 30/06/2017
RD-9	MERISAT porting in linux – MERISAT detail design of optimization & complementary recipes for LUTs generation	V1.B – 30/06/2011

1.4 Acronyms

The definition of the acronyms used in this document is provided hereafter:

AAOT   Aqua Alta Oceanographic Tower

4th MERIS data reprocessing

Evolutions and Validation report

Ref.:   MER4RP Validation Report

Version: 1.0

Date: 01/04/2019

Page: 3

AD	Applicable Document
ADF	Auxiliary Data File
AERONET	AErosol RObotic NETwork
AOP	Apparent Optical Property
AOT	Aerosol Optical Thickness
ARVI	Atmospherically Resistant Vegetation Index
ATBD	Algorithm Theoretical Basis Document
ATSR	Along-Track Scanning Radiometer
BOA	Bottom Of the Atmosphere
BOUSSOLE	BOUée pour l'acquiSition d'une Série Optique à Long termE
BPAC	Bright Pixel Atmospheric Correction
BRDF	Bidirectional Reflectance Distribution Function
BRR	Bottom Rayleigh Reflectance
C2RCC	Case-2 Regional CoastColour
CCC	Canopy Chlorophyll Content
CCD	Charge-Coupled Device
CCI	Climate Change Initiative
CDOM	Coloured Dissolved Organic Matter
CEFAS	Centre for Environment, Fisheries and Aquaculture Science
CMG	Climate Modeling Grid
DDV	Dense Dark Vegetation
DEM	Digital Elevation Model
DIMITRI	Database of Imaging Multispectral Instrument and Tool for Radiometric Intercomparison
ECMWF	European Centre for Medium-Range Weather Forecasts
ENVISAT	ENVIronment SATellite (ESA platform)
EO	Earth Observation
ESA	European Space Agency
ESFT	Exponential Sum Fitting Technique
ESU	Elementary Sampling Unit
FMF	Fine-Mode Fraction
FOV	Field Of View
FR	Full Resolution
GSFC	Goddard Space Flight Center
IOP	Inherent Optical Properties
IS / ISME	In-Situ / In-Situ MERIS
L0, L1, L2, L3	Level-0, Level-1, Level-2, Level-3
LAI	Leaf Area Index
LARS	Land-Aerosol Remote-Sensing
LCC	Land Cover Classification
LUT	Look-Up Table
MER2RP	2nd MERIS data Reprocessing
M3RP/MER3RP	3rd MERIS data Reprocessing
M4RP/MER4RP	4th MERIS data Reprocessing

4th MERIS data reprocessing

Evolutions and Validation report

Ref.: MER4RP Validation Report

Version: 1.0

Date: 01/04/2019

Page: 4

MERIS	Medium Resolution Imaging Spectrometer
MERMAID	MEris MAtchup In-situ Database
MGVI	MERIS Global Vegetation Index
MOBY	Marine Optical BuoY
MODIS	Moderate-Resolution Imaging Spectroradiometer
MOMO	Matrix Operator MOdel (RTC)
MTCI	MERIS Terrestrial Chlorophyll Index
NASA/GSFC	National Aeronautics and Space Administration/Goddard Space Flight Center
NetCDF	Network Common Data Form
NIR	Near-InfraRed
NN	Neural Network
NOMAD	NASA bio-Optical Marine Algorithm Data set
OC	Ocean Colour
OC4ME	MERIS chlorophyll algorithm
OLCI	Ocean and Land Colour Instrument
OZA	Observation Zenithal Angle
PAR	Photosynthetically Active Radiation
PCD	Product Confidence Data
PFS	Product Format Specification
PROSPECT	Model of leaf optical properties spectra
QWG	Quality Working Group
RC	Radiometric Calibration
RD	Reference Document
RGB	Red/Green/Blue
RH	Relative Humidity
RMSE	Rool Mean Square Error
ROT	Rayleigh Optical Thickness
RP	Re-Processing
RPD	Relative Percentage Difference
RR	Reduced Resolution
RSH	Rayleigh Scale Height
RTC / RTM	Radiative Transfer Code / Radiative Transfer Model
S3	Sentinel-3 (ESA satellite)
SAA	Sun Azimutal Angle
SAIL	Canopy bidirectional reflectance model
SAM	Standard Aerosol Model
SDI	Soil Discrimination Index
SeaWiFS	Sea-viewing Wide Field-of-view Sensor
SIO	South Indian Ocean
SO	Successive Orders of the scattering code (RTC)
SPG	South Pacific Gyre
SSA	Single Scattering Albedo
SZA	Solar Zenithal Angle

4th MERIS data reprocessing

Evolutions and Validation report

Ref.: MER4RP Validation Report

Version: 1.0

Date: 01/04/2019

Page: 5

TOA	Top Of the Atmosphere
TOSA	Top Of the Standard Atmosphere
TSM	Total Suspended Matter
US62	US62 standard atmospheric model (or profile)
VIS	VISible
XML	eXtensible Markup Language

1.5 Definitions

Statistical estimators used in this document are descrived below (x_i stands for the reference in-situ measurement, y^i stands for the MERIS measurement):

$$RPD = \frac{1}{N} \sum_{i=1}^{N} \frac{y_i - x_i}{x_i}$$

$$|RPD| = \frac{1}{N} \sum_{i=1}^{N} \frac{|y_i - x_i|}{x_i}$$

$$MAD = \frac{1}{N} \sum_{i=1}^{N} y_i - x_i$$

$$RMSE = \sqrt{\frac{1}{N} \sum_{i=1}^{N} (y_i - x_i)^2}$$

4th MERIS data reprocessing

Evolutions and Validation report

Ref.: MER4RP Validation Report

Version: 1.0

Date: 01/04/2019

Page: 6

2 4th MERIS data reprocessing evolutions

This chapter presents the evolutions of the 4th MERIS data reprocessing, also called MER4RP in this document. For more details, please refer to the corresponding ATBDs or technical documentation such as the Product Format Specification (PFS).

2.1 Product format change

The format of MERIS L1 and L2 products generated in the frame of the MER4RP is aligned with the Sentinel-3 format (S3-like format)

Nature of the change: *Product format*

A major evolution of the MER4RP is related to the data formatting: the ENVISAT data format (.N1) is given up in favour to the Sentinel-3 like format ([RD-3]) based on a folder of netCDF files including a xml manifest file.

The S3-like format includes multi-file products packages with xml Manifest (descriptive header) and NetCDF data files.

2.2 Change of the auxiliary data

2.2.1 Meteo data

The source of the meteo data is now ECMWF Era-Interim

(http://www.ecmwf.int/en/research/climate-reanalysis/era-interim)

Nature of the change: *Dynamic Auxiliary Data Files (ADF)*

The MER4RP now requires the use of atmospheric profiles of relative humidity and temperature. They are extracted from the European Centre for Medium range Weather Forecast (ECMWF) Era-Interim files and included in the L1 and L2 products.

2.2.2 Improved a priori masks

The a priori surface classification masks (land/sea, tidal areas and in-land-waters) are significantly upgraded and are in line with those used by the OLCI data processing.

Nature of the change: *ADF values / Algorithm*

4th MERIS data reprocessing

Evolutions and Validation report

Ref.:   MER4RP Validation Report

Version: 1.0

Date: 01/04/2019

Page: 7

A new MERIS/ATSR land/water, inland water, coastline and intertidal mask at 300 m resolution in S3 format has been generated combining different state-of-the-art input data sets. The same auxiliary dataset is also used in the Sentinel-3 ground segment.

The base product for all new masks is the water body mask at 300 m spatial resolution, produced within the ESA Land Cover CCI project. This base product was refined in areas where it has shown some weaknesses, to produce the best possible land/water mask. This optimized mask then served as a baseline for derivation of all other products, i.e. the coastline, the tidal and the inland water masks, to ensure consistency between the products.

For more details, see Technical Note "Sentinel-3 – Land-Water Mask".

2.3   Level 1 evolutions

2.3.1   Geolocation

The geolocation is improved: parallax and orographic corrected latitude, longitude and altitude are given per pixel.

Nature of the change*: Algorithm*

The MER4RP includes the Amorgos-like ortho-geolocation scheme ([RD-1]).

The algorithm provides 3D georeferencing (lon, lat, alt) at each pixel. Those values are computed at *instrument* pixels, according to most accurate platform navigation and attitude (depending on available input files) as the first intersection of the pixel (CCD element) line-of-sight with the Earth surface modelled by a Digital Elevation Model (DEM; GETASSE v3 - http://earth.esa.int/services/amorgos/download/getasse/) on top of the ellipsoid surface. They are then affected to a given product pixel in the same regridding process as the radiometry. In other word, the acquisition geometry and radiometry are self-consistent. The geocoordinates obtained above are referred to as ortho-geolocation as they are fully corrected for the satellite to ground parallax. The principle of the retrieval is sketched on Figure 2-1.

Product pixels outside the actual instrument swath are geolocated by interpolation between the surrounding tie-points; the latter are defined equaly spaced along the theoretical swath (intersection of the ellipsoid and the vertical plane joining the platform at a given time and perpendicular to the satellite ground track), their altitude is as such set to 0 as lying on the ellipsoid by definition.

4th MERIS data reprocessing
Evolutions and Validation report

Ref.: MER4RP Validation Report
Version: 1.0
Date: 01/04/2019
Page: 8
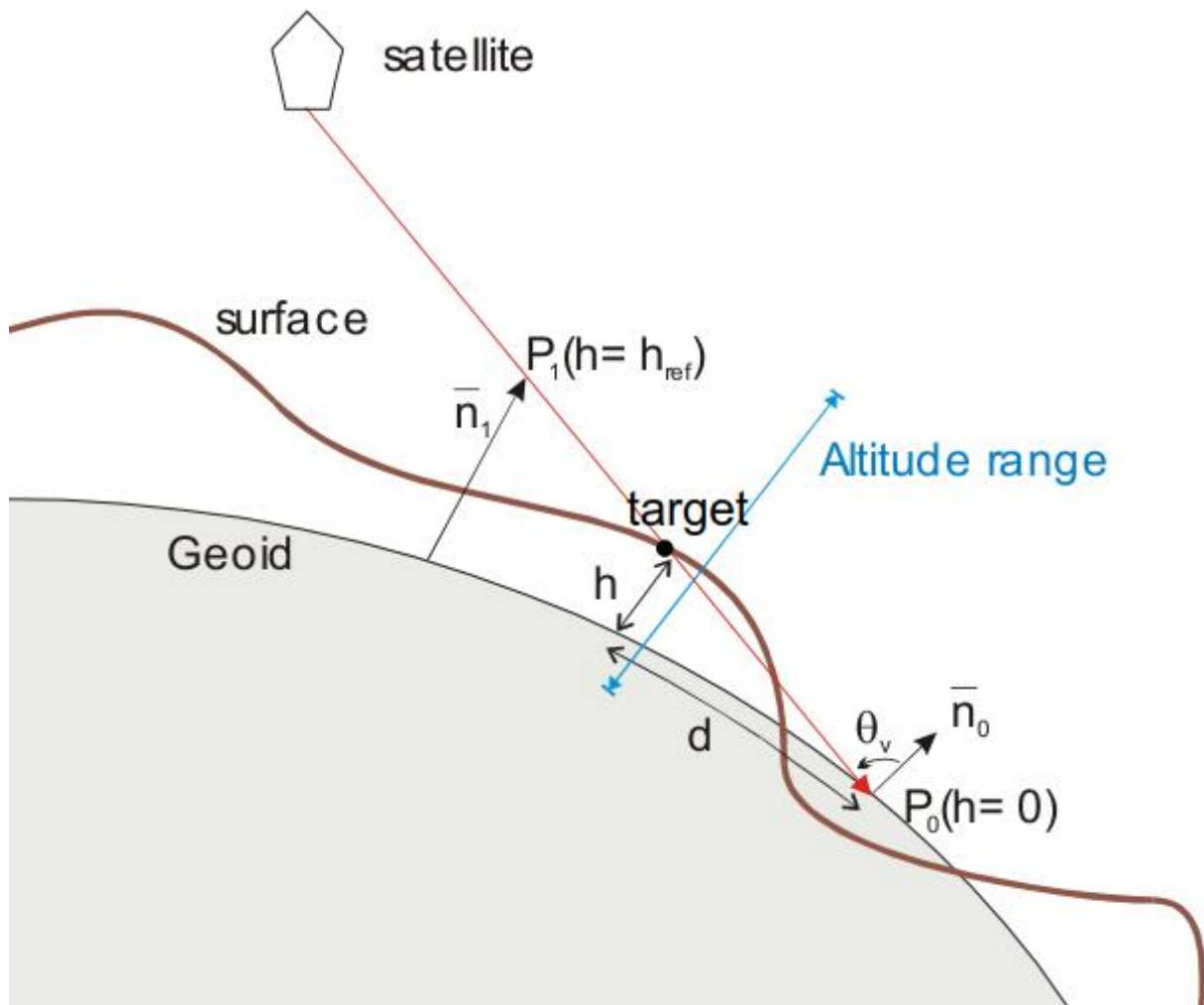
Figure 2-1: Principle of the ortho-geolocation: the coordinates retrieved for a pixel are now those of the target (black circle) instead of the first intersection with the ellipsoid (P₀)

2.3.2 Level 1 calibration

The L1 calibration is updated based on a reanalysis of the complete mission in-flight calibration dataset. It includes in particular a revised diffuser ageing methodology accounting also for the ageing of the reference diffuser.

Nature of the change: ADF values

The MER4RP, taking place after the end of the mission, is the opportunity to revise the radiometric Gain Model. Obviously, the instrument degradation shall be refillted to the whole mission Radiometric Calibration (RC) dataset, and the diffuser ageing reassessed from the same dataset.

4th MERIS data reprocessing
Evolutions and Validation report

Ref.:   MER4RP Validation Report
Version: 1.0
Date: 01/04/2019
Page: 9

2.3.2.1 How does a refreshed ageing model behave with degradation?

Current methodology for the determination of ageing gives slightly different ageing estimates according to the duration of the data set included in the analysis. Figure 2-2 shows the ageing rates versus wavelength as derived from the first 3 years of mission (used for the 2nd MERIS data reprocessing, also called MER2RP) and from the whole mission. The difference can reach about 15% of the ageing rate in the blue.
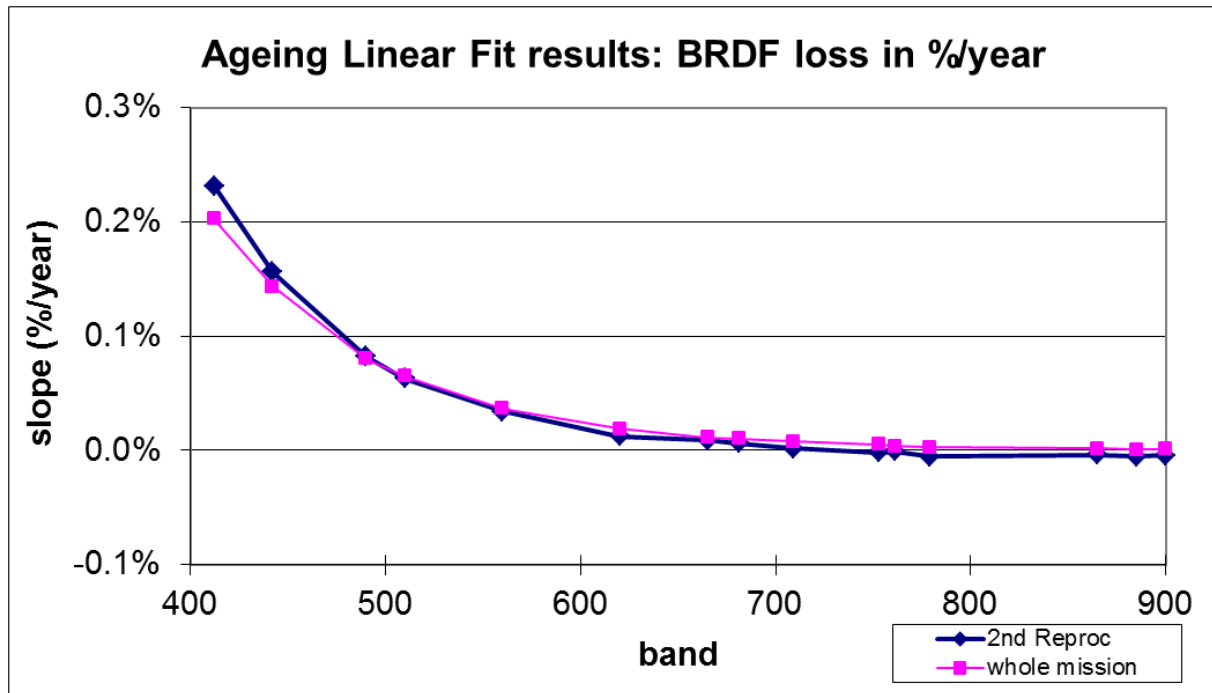
Figure 2-2: Ageing rate versus wavelength from restricted data range (blue line, MER2RP values based on 2.8 years of data with 10 ageing sequences) and whole mission (10 years, 39 ageing sequences).

Figure 2-3 generalises this comparison over time all along the mission: ageing is determined as soon as 2 ageing sequences are available and then re-evaluated each time a new sequence is available. Ageing rates are then plotted against the duration since launch ("year of available data") for each channel. One can see that large oscillations occur during the first two years, likely to be linked with the bidirectional reflectance distribution function (BRDF) discrepancies between the two diffusers, and seriously questioning the relevance of an ageing estimation, at least for operational use, before a minimum of two yearly cycles correctly sampled are gathered. The second point highlighted by the figure is the slower and more regular trend that can be seen from about year 3 toward the end of the mission: this is interpreted as the impact of diffuser 2 ageing on the results, as the latter is not accounted for in the ageing computation.

4th MERIS data reprocessing

Evolutions and Validation report

Ref.:   MER4RP Validation Report

Version: 1.0

Date: 01/04/2019

Page: 10
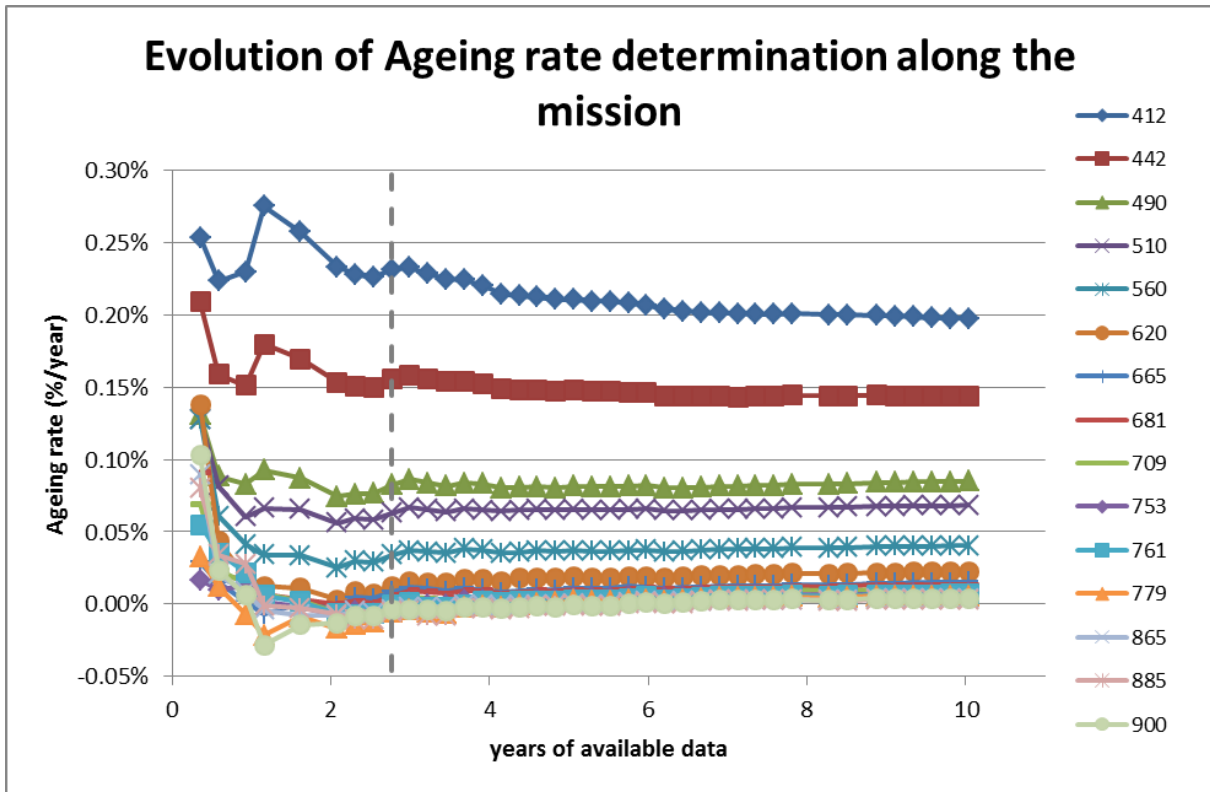
Figure 2-3: Evolution of the determination of the ageing rate versus mission duration. 1st operational value has been derived from 2.8 years of data (dashed vertical line).

Ageing estimation and modelling are embedded into the gain analysis that provides the Instrument Degradation Model. As a consequence, refreshing the degradation model using whole mission data implies refreshing the ageing model on the same data set unless specific precautions are taken. On the basis of this known limitation, the MER2RP ageing model was used for the degradation model derived for the MER3RP.

On the contrary, recent attempts to refresh the degradation model using the whole mission data set have shown that a blindly refreshed ageing model introduces discrepancies in the way instrument degradation is seen from each diffuser data. Just to make things clear: if ageing is accurately corrected for both diffusers, the relative evolution of gains with time should behave the same with diffuser 1 or diffuser 2 data, since every other acquisition condition is identical.

The impact of neglecting diffuser 2 ageing is pointed at by the analysis of the performances of a refreshed set of ageing and degradation models using the MER3RP methodology but the whole mission data set. Results are summarized below: Figure 2-4 and Figure 2-5 clearly show that the models refreshment significantly improves the stability over time. Figure 2-6 confirms that refreshed models have much better performances but it also shows that neglecting ageing of diffuser 2, if self-compensated for diffuser 1 through the degradation model, limits the overall performance for diffuser 2 data.

4th MERIS data reprocessing

Evolutions and Validation report

Ref.:   MER4RP Validation Report

Version: 1.0

Date: 01/04/2019

Page: 11
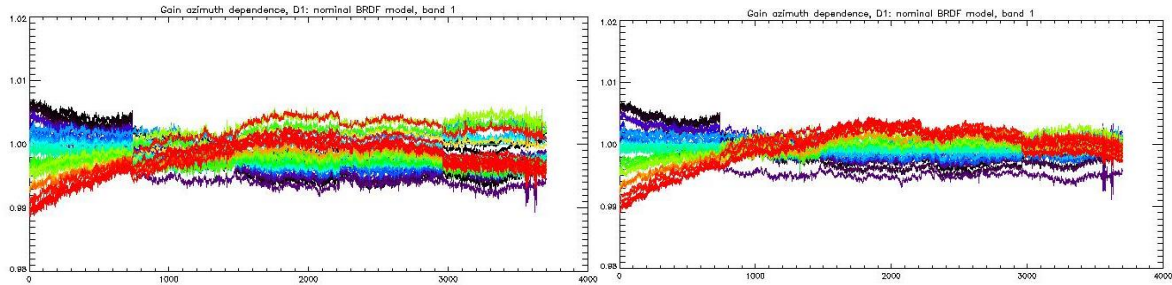
Figure 2-4: Relative gain comparison over the mission for band 1 (gain normalisation reference is an average over the set or orbits within 27.5±0.25 degrees), and using the MER3RP models (left) and refreshed whole-mission ones (right).The x axis is pixel index, and the colour represents time (from oldest in blue to most recent in red).
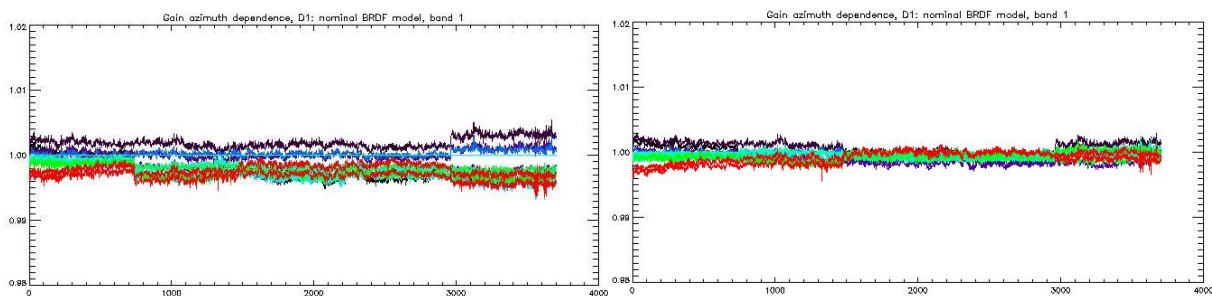
Figure 2-5: same as Figure 2-4 but for Sun azimuth angles limited to 27.5±2 degrees
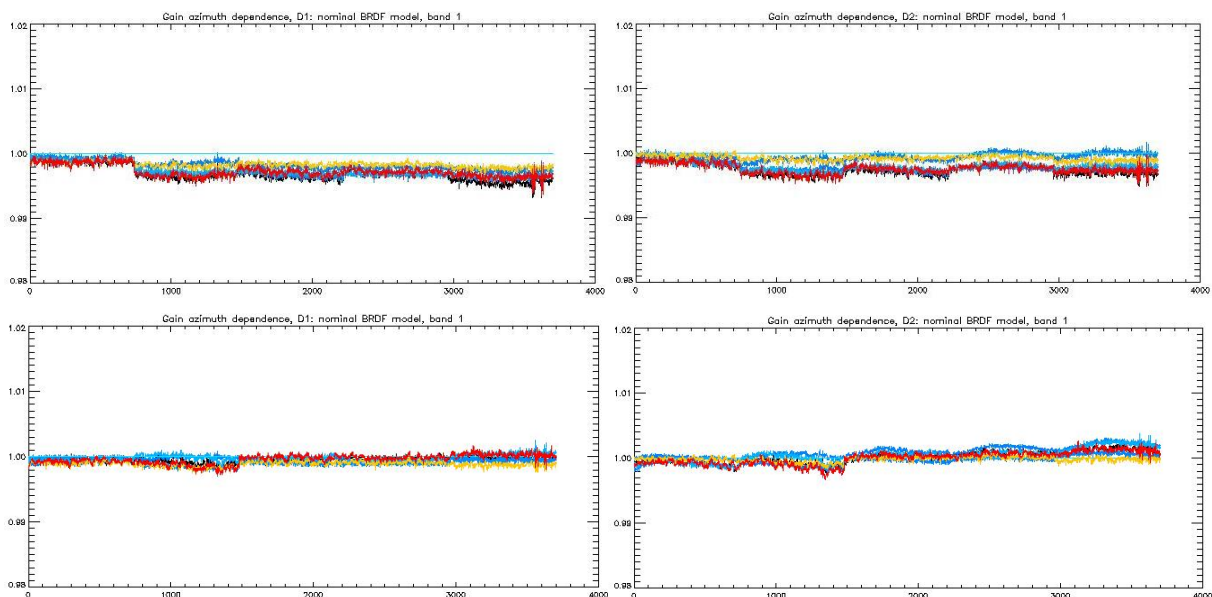
Figure 2-6: Comparison of gain modelling performance (in terms of stability over time) when applied to diffuser 1 (left) and diffuser 2 (right) data, and for the MER3RP model (top) and the refreshed model (bottom); all data restricted to SZA in 27.5±0.5 degrees. The x axis is pixel index, and the colour represents time (from oldest in blue to most recent in red).

Figure 2-7 shows the overall consistency of diffuser one and diffuser 2 data as potential source for the degradation modelling when corrected using the refreshed ageing model: slight discrepancies remain between the two evolution curves (averaged over each camera FOV) starting with camera 2 and increasing toward camera 5.

4th MERIS data reprocessing

Evolutions and Validation report

Ref.: MER4RP Validation Report

Version: 1.0

Date: 01/04/2019

Page: 12

All these results justified the need for revisiting the way ageing is modelled and applied to gains before the degradation modelling.
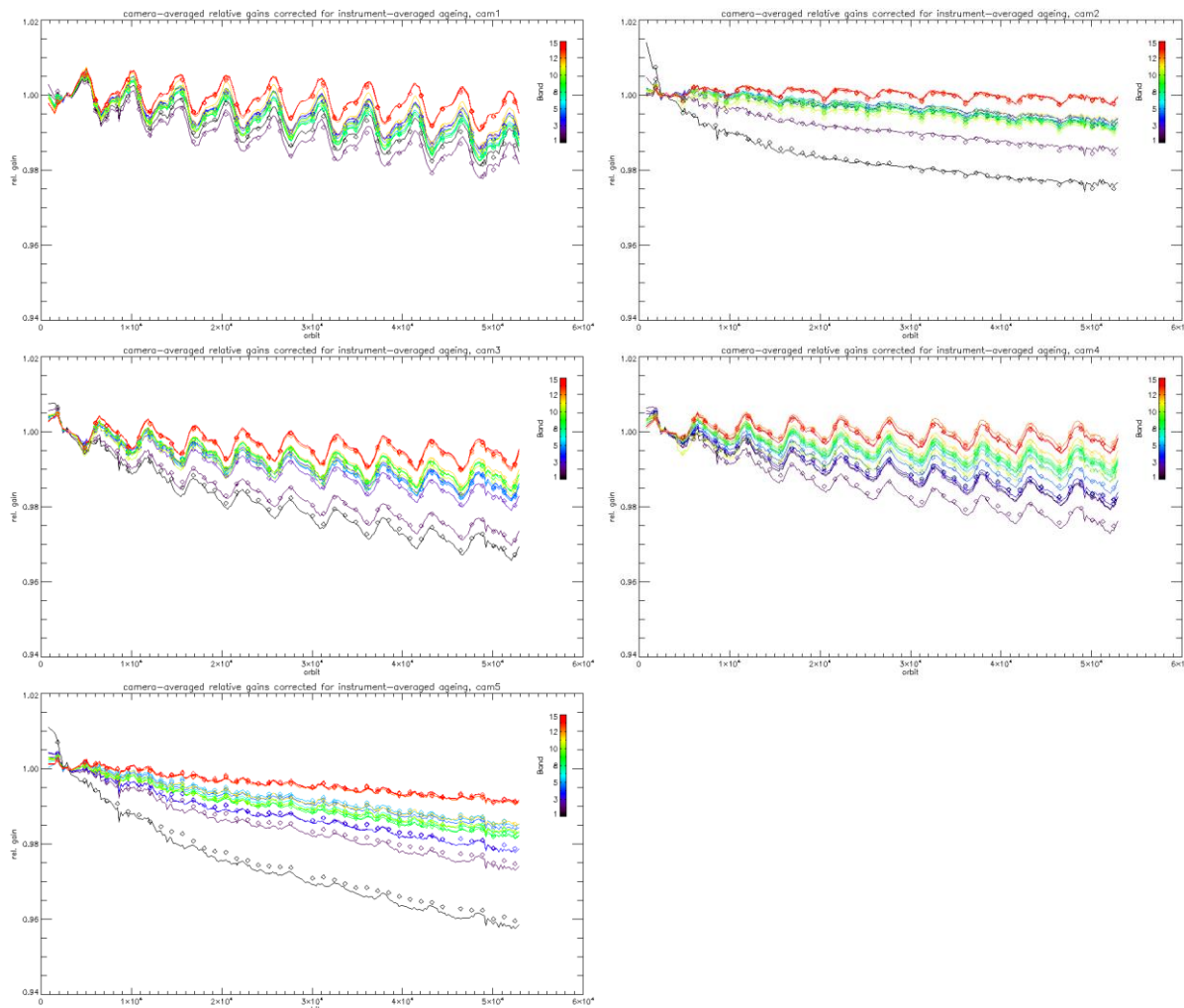
Figure 2-7: Camera-averaged instrument degradation as derived using an ageing model determined following current methodology from the whole mission dataset. Solid lines are diffuser-1 ageing corrected gains, symbol are diffuser-2 gains (not corrected for ageing, consistently with ageing modelling methodology).

2.3.2.2   Introducing ageing of diffuser 2

As ageing can reach 2% in the blue and considering the exposure ratio between diffuser 2 and diffuser 1 (about 0.1), one can see that ageing of diffuser 2 is no longer negligible at the end of the mission. Indeed, ignoring it gives slightly different ageing estimates according to the duration of the data set included in the analysis.

Strictly speaking, ageing A(t) can be defined such that:

$$BRDF(d,t,\lambda) = (1-A(t-t_{ref})) \cdot BRDF(d,t_{ref},\lambda) \qquad (1)$$

4th MERIS data reprocessing
Evolutions and Validation report

Ref.:   MER4RP Validation Report
Version: 1.0
Date: 01/04/2019
Page: 13

where d is a given diffuser, t_{ref} is a reference time representative of the characterisation data; A(t) expresses the relative loss of reflectance between times t and t_{ref}. The acquisition geometry is not introduced in the equation as ageing is assumed isotropic.

On the assumption that diffuser ageing is only related to its exposure to UV radiation, t_{ref} can be set to launch or – pragmatically – to the date of the first in-flight ageing calibration sequence.

The in-flight data acquired to monitor diffuser ageing is a set of 2 radiometric calibrations occurring on 2 successive orbits using diffuser 1 on orbit N and diffuser 2 on orbit N+1. It is known since BRDF characterisation that some differences are to be expected (see Figure 2-3), and hence to be discarded from ageing determination, as being of the same order of magnitude that the ageing (of the order of the percent).

What we measure in-flight is:

$$X = G(t).L \text{ with } L = BRDF(t) * E0 * \cos(SZA) \quad (2)$$

where G is the instrument gain and X the calibration counts (corrected for dark and smear). The ratio of two gains acquired with the 2 diffusers at quasi –identical geometry is thus proportional to the ratio of the two BRDF at the same instant.

It is known from ground characterisation that the diffusers BRDF relative difference has a small sensitivity to geometry hence the ratio of (corrected) counts, or of gains between the 2 diffusers can be considered as the ratio of the respective ageing factors time the ratio of the BRDFs at a reference time (e.g. beginning of mission).

The exposure rate of the two diffusers has been rather regular throughout the mission and can in first approximation be considered constant, from one year after launch on (Figure 2-8).
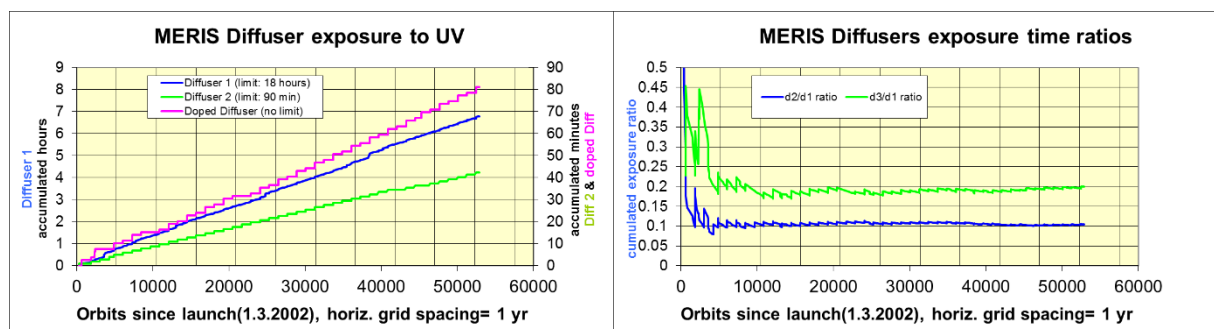
Figure 2-8: Cumulated exposure of the 3 MERIS diffusers (left) and corresponding exposure ratios (right).

Up to the MER3RP, the assumption was that diffuser 2 ageing was negligible. Thus the time series of ageing measurement could be rewritten:

$X(d1,t)/X(d2,t) = BRDF(d1,tref)/BRDF(d2,tref).(1-A(t-t_{ref}))$
where $A(t-t_{ref})$ is the relative loss of reflectance of diffuser 1 due to ageing between t_{ref} and t.

4th MERIS data reprocessing

Evolutions and Validation report

Ref.: MER4RP Validation Report

Version: 1.0

Date: 01/04/2019

Page: 14

As BRDF($d1,t_{ref}$)/BRDF($d2,t_{ref}$) can be replaced by X($d1,t_{ref}$)/X($d2,t_{ref}$), one gets:

X($d1,t$)/X($d2,t$) – X($d1,t_{ref}$)/X($d2,t_{ref}$) = A($t-t_{ref}$) BRDF($d1,t_{ref}$)/BRDF($d2,t_{ref}$)
and on the (verified) assumption that the BRDF ratio between the 2 diffusers is very close to 1 this further simplifies to:

$$\boxed{\text{X}(d1,t)/\text{X}(d2,t) - \text{X}(d1,t_{ref})/\text{X}(d2,t_{ref}) \approx \text{A}(t-t_{ref})}\ (3)$$

This is the formula that has been used so far to derive the operational version of the ageing correction, and A(t) proved to be fairly linear with time, with residual oscillation likely due to small discrepancies in the bi-directionality of the two diffusers, as shown on Figure 2-9.
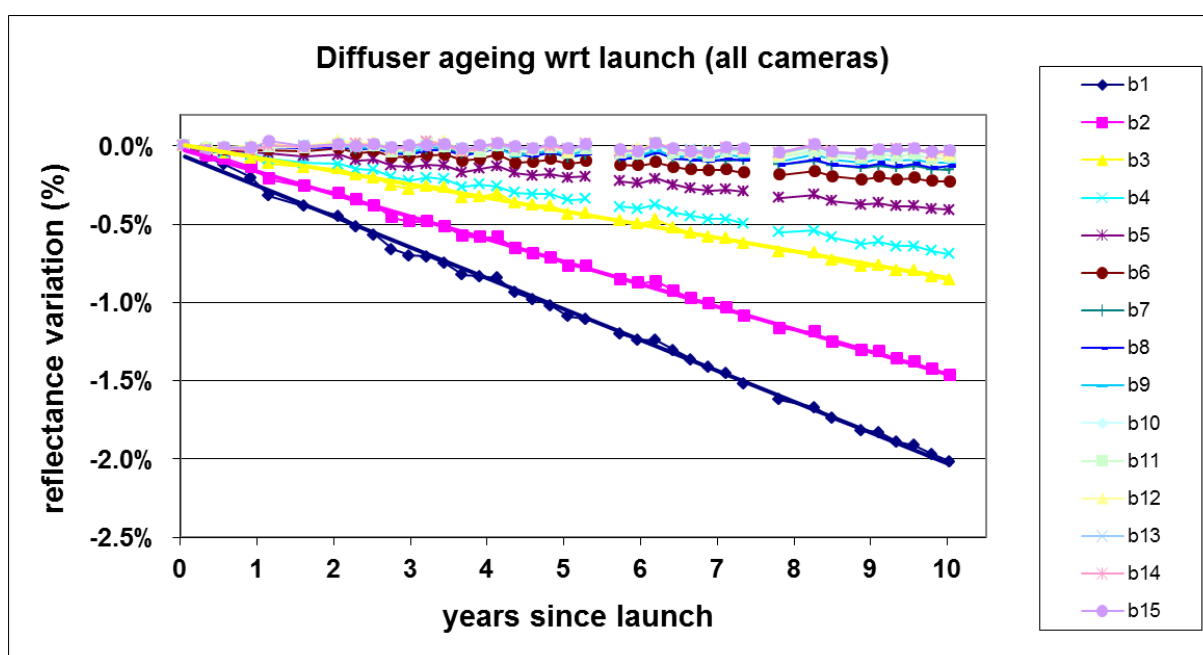
Figure 2-9: Ageing data and fit as derived using the MER3RP methodology over the whole mission.

Introducing ageing of diffuser 2 allows expressing the counts ratio as:

X($d1,t$)/X($d2,t$) = BRDF($d1,tref$)/BRDF($d2,tref$).(1-A($t-t_{ref}$))/(1-A($\alpha.(t-t_{ref})$))
where α is the cumulated exposure ratio.

Let's use Δt as ($t-t_{ref}$) in the following and we get:

(1-A(Δt))/(1-A($\alpha.\Delta t$)) = X($d1,t$)/X($d2,t$) / (X($d1,t_{ref}$)/X($d2,t_{ref}$)).

As A(Δt) is small and close to linear, A($\alpha\Delta t$) is very small and can be considered an epsilon, so that equation above rewrites:

(1-A(Δt))*(1+A($\alpha.\Delta t$)) = X($d1,t$)/X($d2,t$) / (X($d1,tref$)/X($d2,tref$)) or

(1-A(Δt)+A($\alpha.\Delta t$)-A(Δt)A($\alpha.\Delta t$)) = X($d1,t$)/X($d2,t$) / (X($d1,tref$)/X($d2,tref$))

4th MERIS data reprocessing

Evolutions and Validation report

Ref.: MER4RP Validation Report

Version: 1.0

Date: 01/04/2019

Page: 15

And on the assumption that $A(\Delta t)$ can be accurately approximated by a proportional term $(b. \Delta t)$, we get

$$1 - b.(1-\alpha).\Delta t - \alpha.(b.\Delta t)^2 = X(d1,t)/X(d2,t) \,/\, (X(d1,tref)/X(d2,tref)) \quad (4)$$

Once the quadratic fit is done, b can be easily determined. It is also very likely that the quadratic term can be neglected and a linear fit replacing the time abscissa by a contracted one would give the same results:

$$1 - b.(1-\alpha).\Delta t \approx X(d1,t)/X(d2,t) \,/\, (X(d1,tref)/X(d2,tref))$$

$$b.(1-\alpha).\Delta t \approx 1 - X(d1,t)/X(d2,t) \,/\, (X(d1,tref)/X(d2,tref)) \quad (5)$$

Equation 5 has been tested on the available data and compared to previous results, those used for the MER2RP and MER3RP, derived from the first 2.8 years of data, and the same methodology using the whole mission. New results are very similar to early results in the blue while the old method using the full data set better match new results in the red-NIR (Figure 2-10).
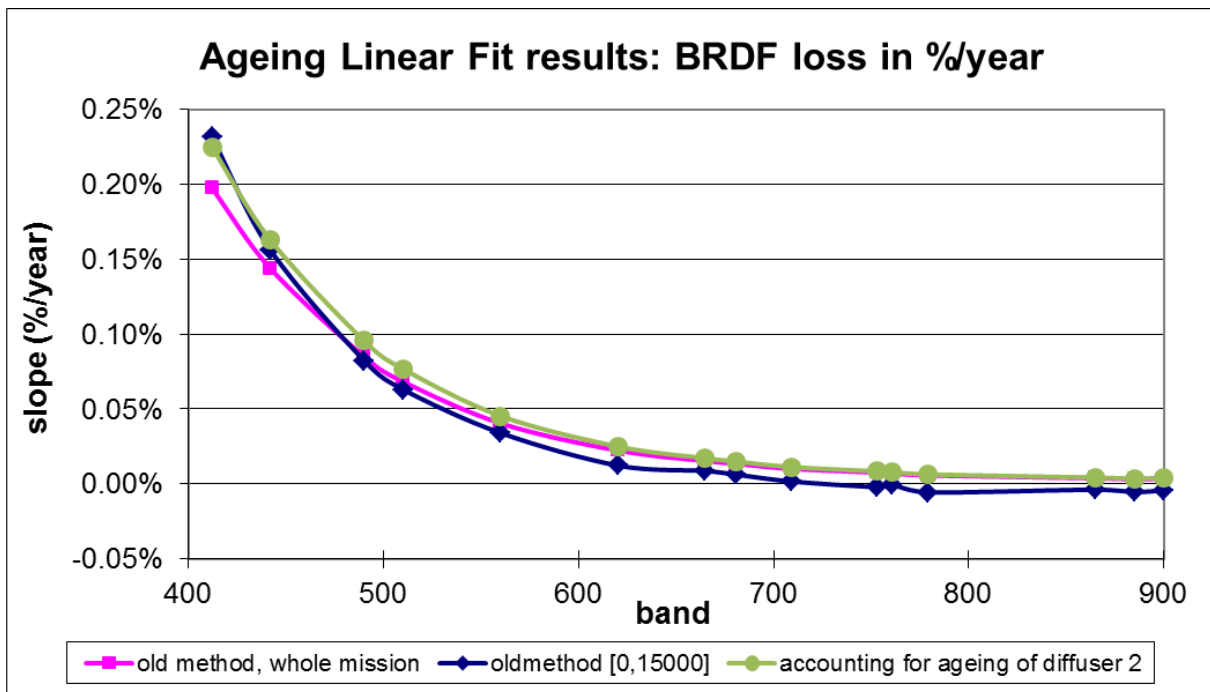
Figure 2-10: Same as Figure 2-2, with results of new method (from whole data set) on top.

As expected, the normalisation used in the new methodology (ratio to reference instead of subtraction) does not change significantly the evolution data set, thus justifying a posteriori the simplified approach used so far. The main change is brought by the use of the contracted time scale, and fairly equivalent results are obtained from the data set normalised by subtraction, as shown on Figure 2-11. The new formulation, however, needs fewer approximations and allows a more straightforward approach to account for diffuser 2 ageing.

4th MERIS data reprocessing
Evolutions and Validation report

Ref.: MER4RP Validation Report
Version: 1.0
Date: 01/04/2019
Page: 16
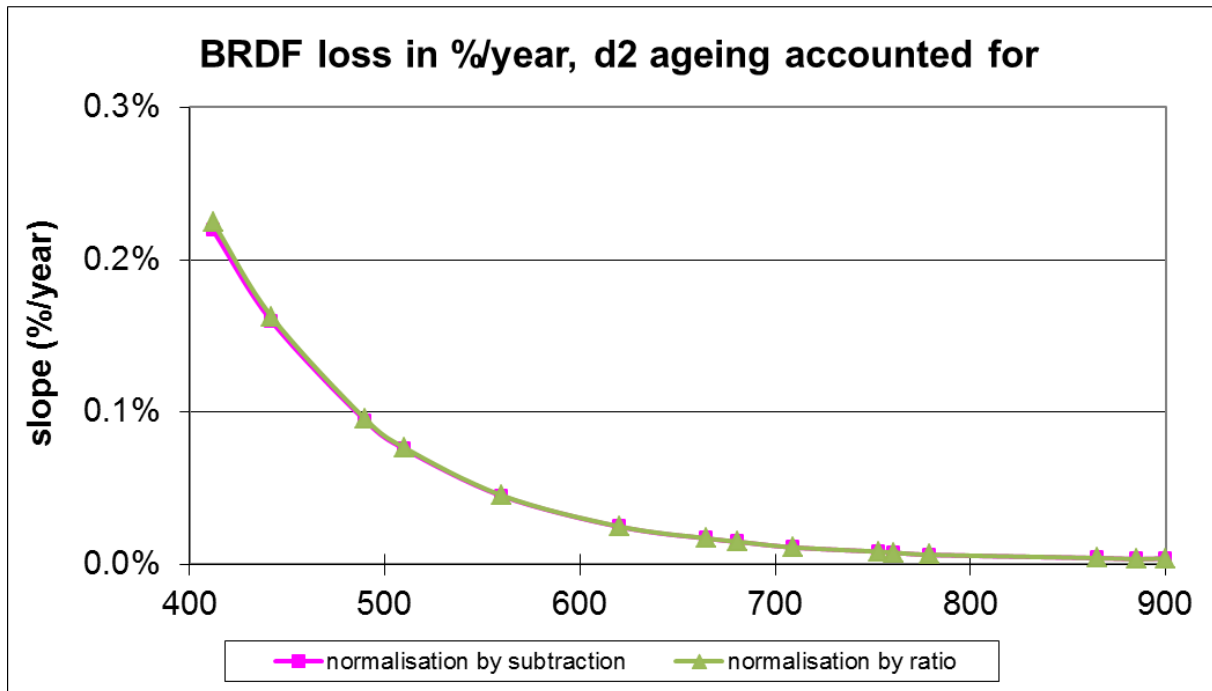
Figure 2-11: Comparison of results obtained for linear fits of diffusers ratios normalised by subtraction (pink line, eq. 3) or by ratio (green line, eq. 5). Note that in both cases, diffuser 2 ageing is accounted for through contraction of the time scale.

The ageing model derived as described above allows various options: with and without introducing a second-degree term (i.e. linear or quadratic fits); with and without considering ageing of diffuser 2; and finally considering global averages or per-camera ones.

All options have been applied to D1 gains (using normal time scale) and to D2 gains (using time scale contracted by the exposure ratio) in order to assess the agreement between the instrument degradation ("true" gain variation with time) as seen with the two diffusers.

The results of the various fits are presented on Figure 2-12 and do not show large differences. However, one can see a slight underestimation in the blue when D2 ageing is ignored, and for per camera results, a systematic increase of the dispersion with from camera 1 to camera 5.

4th MERIS data reprocessing
Evolutions and Validation report

Ref.:   MER4RP Validation Report
Version: 1.0
Date: 01/04/2019
Page: 17
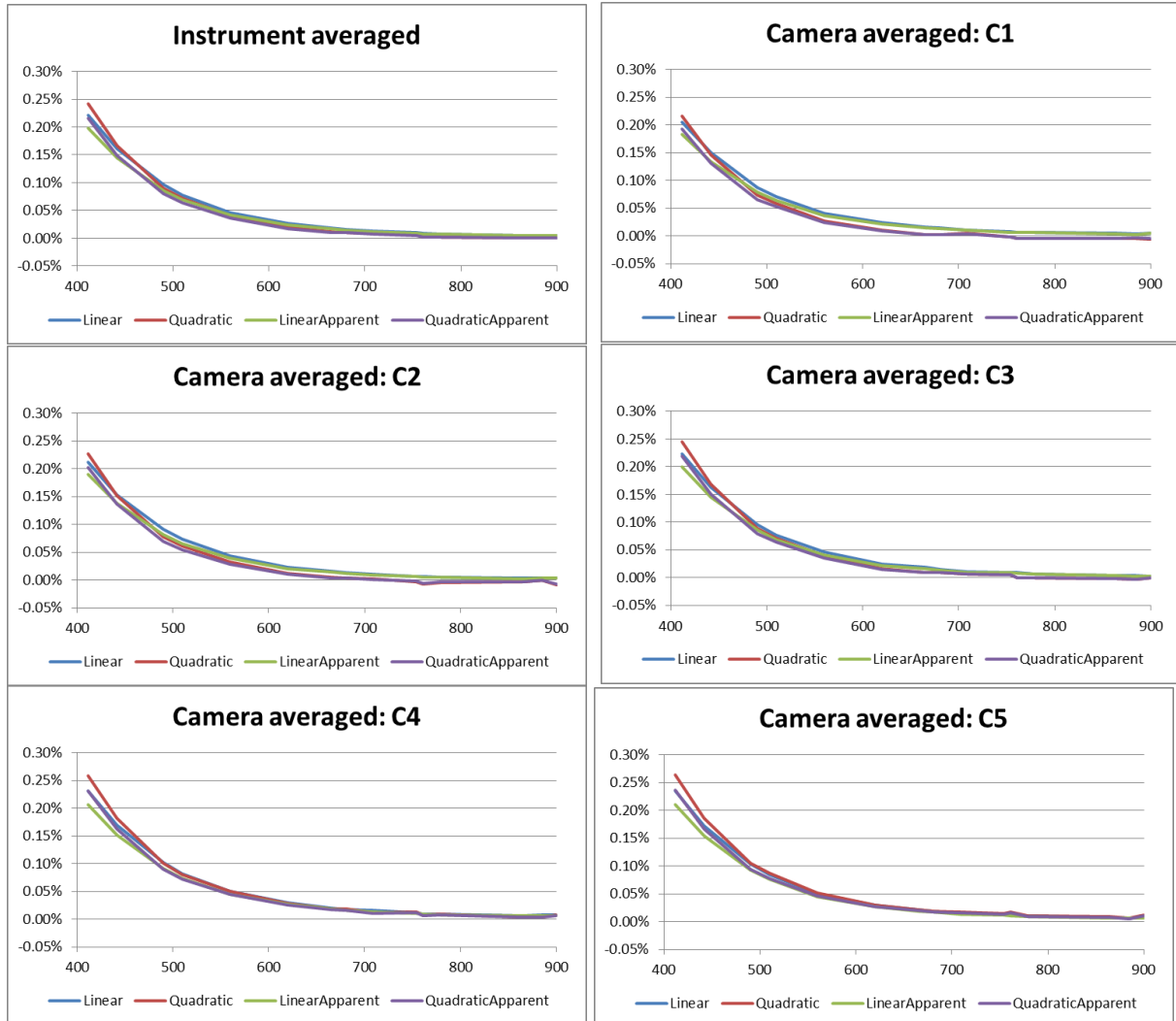
Figure 2-12: Ageing yearly slopes for all methods (curve colours) and for the global fit (top left) and per-camera ones (from top right to bottom right for cameras 1 to 5).

A performance metrics has been defined to allow selecting the method providing the best consistency between the two diffusers in terms of instrument degradation.

The metrics is defined as follows:

- instrument degradation is defined as relative ageing corrected gain evolution: independent of diffuser, D1 & D2 data shall be consistent

- within Ageing evaluation process, gains can be corrected for ageing and match estimated at ageing orbits:

- P(b,m) = $\sqrt{\frac{1}{N}\sum_{ageings}\left(\frac{\overline{G_m^{d1}}(t)}{G_m^{d1}(t_0)} - \frac{\overline{G_m^{d2}}(t)}{G_m^{d2}(t_0)}\right)^2}$

- where $\overline{G_m^{di}}(t)$ is the camera-averaged gain at orbit t for diffuser #i hence $\frac{\overline{G_m^{d2}}(t)}{G_m^{d2}(t_0)}$ is a camera-average estimate of degradation at t wrt t_0

4th MERIS data reprocessing
Evolutions and Validation report

Ref.: MER4RP Validation Report
Version: 1.0
Date: 01/04/2019
Page: 18

It cannot be considered as a quantitative absolute performance estimator but should be enough for comparisons between methods. Its meaning is the RMS distance between the camera-averaged instrument degradation as derived from D1 or D2 at ageing orbits, or between symbols and solid lines in Figure 2-13 below.
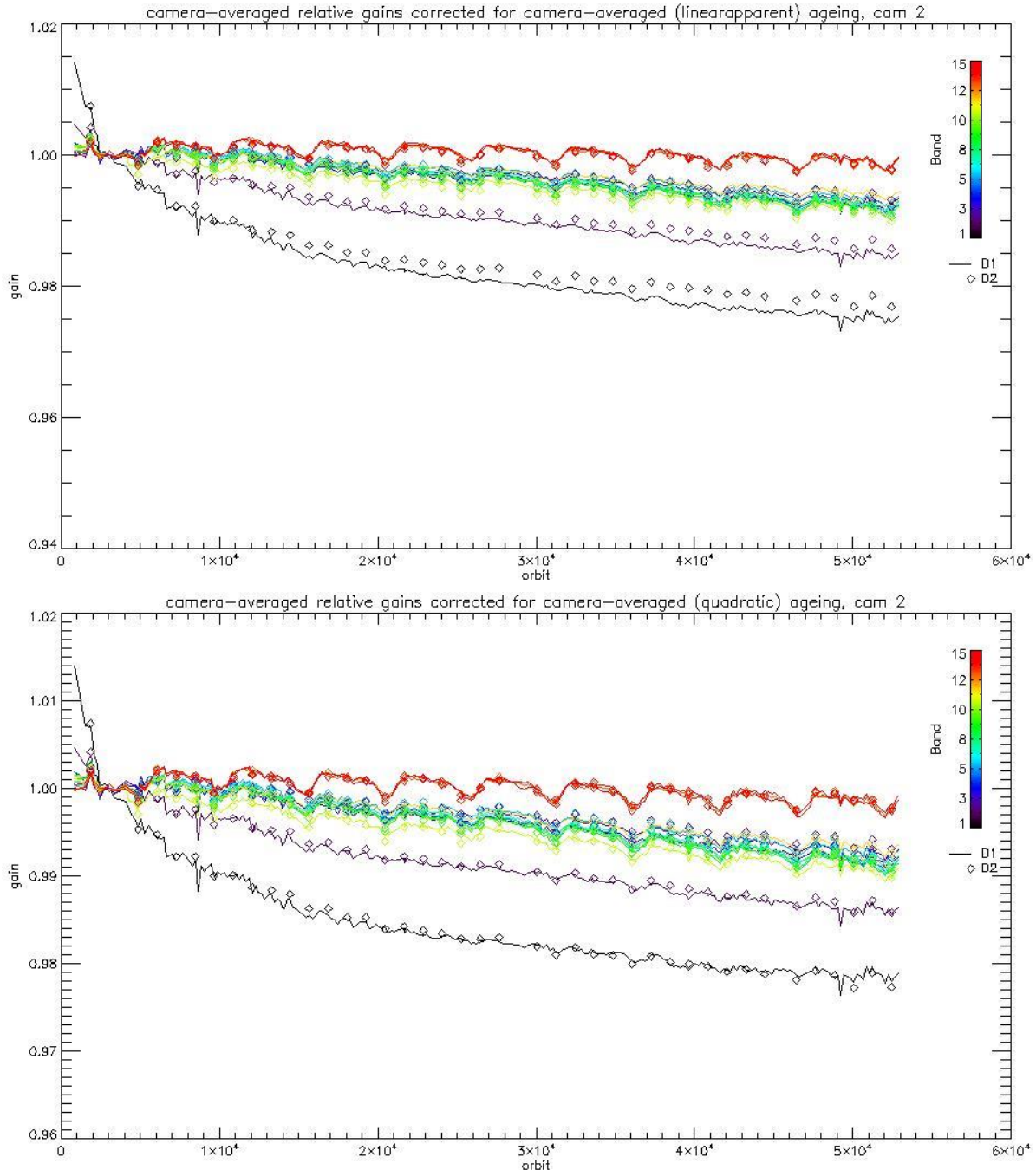
Figure 2-13: Camera averaged degradation for both diffusers (D1: solid, D2: symbols) for Camera 2, ignoring D2 ageing (top, RP3 method) and accounting for D2 ageing (bottom, revised methodology).

The performance estimates for six of the 8 options are shown below: global fit or per camera one, then RP3 method (no D2 ageing, linear fit) and two RP4 options: D2 ageing considered, linear or quadratic fit. The improvement brought by (a) considering D2 ageing, (b) using a

4th MERIS data reprocessing
Evolutions and Validation report

Ref.:   MER4RP Validation Report
Version: 1.0
Date: 01/04/2019
Page: 19

quadratic fit and (c) using per-camera fits is obvious despite the simple expression of the performance estimator. **This is thus the method that has been selected for the MER4RP**.
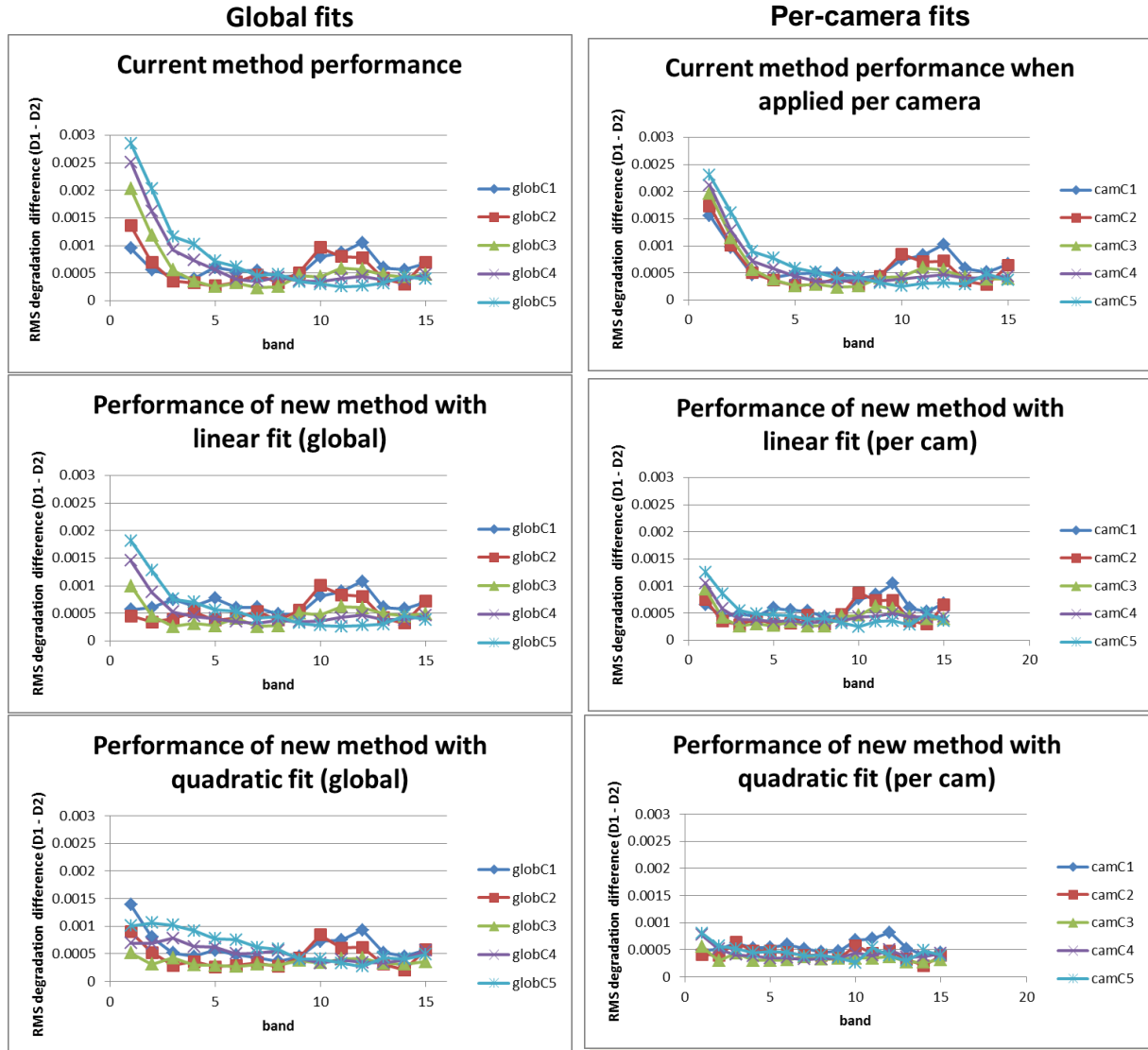
Figure 2-14: Performance estimates for the six methods: global (left) end per-camera (right) fits, D3 aging ignored (top), D2 ageing considered and linear fit (centre), D2 ageing considered and quadratic fit (bottom).

2.3.2.3   Instrument degradation modelling and reference gains

The lessons learnt from the MER2RP and MER3RP are the following:

1.   MERIS gains show dependency to Sun Azimuth Angles (SAA). Taking a reference SAA as the one where BRDF model fits best to characterisation data (27.5), one can show that gains at given SAAs normalised to that reference do show a deviation that increases with the ΔSAA, as a more or less white curved across-track trend (Figure 2-15)

4th MERIS data reprocessing
Evolutions and Validation report

Ref.:   MER4RP Validation Report
Version: 1.0
Date: 01/04/2019
Page: 20
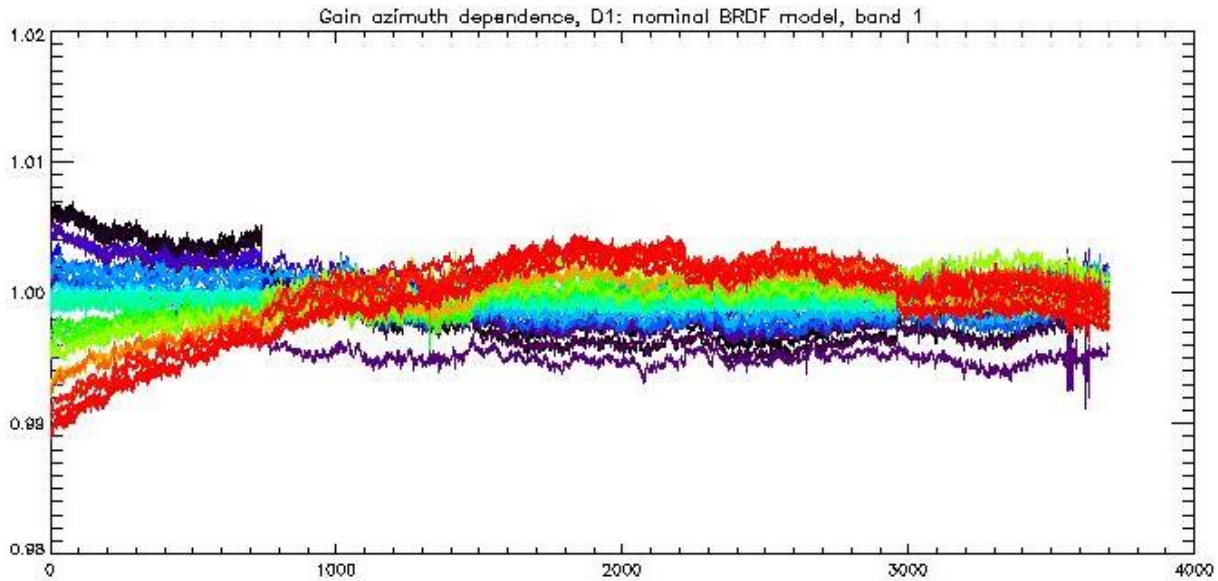
Figure 2-15: normalized gains for band 1 across the mission (colour code represents ⊿SAA)

2. 2nd RP gains were shown to have significant pixel-to-pixel variability, introducing visually identifiable striping. They were based on diffuser 2, from selected SAAs within 27.5 ± 0.2 degrees.

3. 3rd RP gains had very low pixel-to-pixel variability, but significantly higher steps at camera interfaces than 2nd RP ones. They were based on diffuser 1, with selected SAAs also within 27.5 ± 0.2.

Reasons for the last two points lie in the selected diffuser: D1 has much more acquisitions and allows better reducing the diffuser speckle by averaging, while showing larger discontinuities at camera interfaces, linked to larger reflectance variability across its surface (known from characterisation).

These lessons taken into account, a method was defined to benefit from both diffusers in a single gain model. Diffuser 1 was used to derive the degradation model and the reference gains, as for 2nd RP, but reference gain cross-track shape has been corrected using diffuser 2 data to restore smother camera transitions.

The degradation model has been trained on diffuser 1 data, after aging correction according to the selected fits as described in previous section. The fit methodology is the same as for previous assessments (RP2 and RP3) but trained on the whole mission dataset.

The reference gain (absolute gain at start of mission, further affected by the Degradation model before use to process a given L0) has been derived in two steps:

1. A first version has been derived from diffuser 1 fully corrected gains, similarly to RP2, but with a refined data selection, now based on paired symmetric delta-SAA with respect to the reference one instead of taking all gains within a small SAA range: the SAA have been sorted and the median selected as the reference (27.35 instead of the

4th MERIS data reprocessing

Evolutions and Validation report

Ref.: MER4RP Validation Report

Version: 1.0

Date: 01/04/2019

Page: 21

theoretical "best" value of 27.5, Figure 2-16); then a sorted distribution of the SAA difference with respect to that reference has been built (Figure 2-17), and best match pairs defined (Figure 2-18). The relevance of the method has been verified by comparing each pair average with a reference orbit (one with its SAA as close as possible to the reference value): and example is shown on Figure 2-19 for band 2 with a very small residual (despite one outlier).
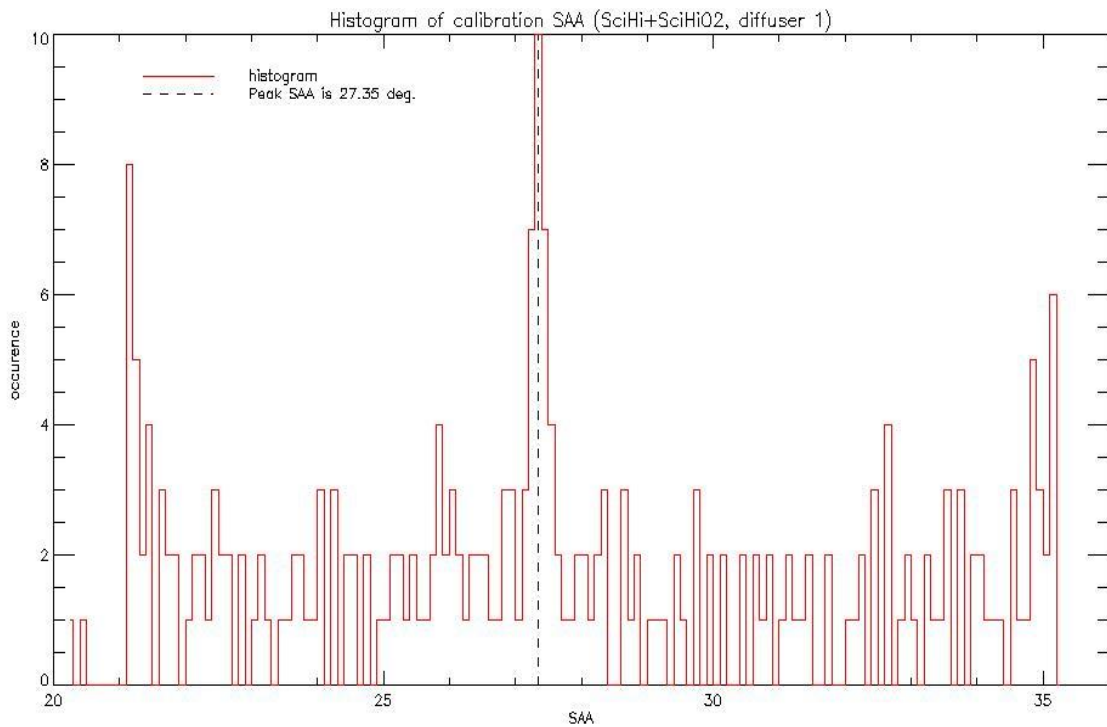
Figure 2-16: RC's SAA histogram
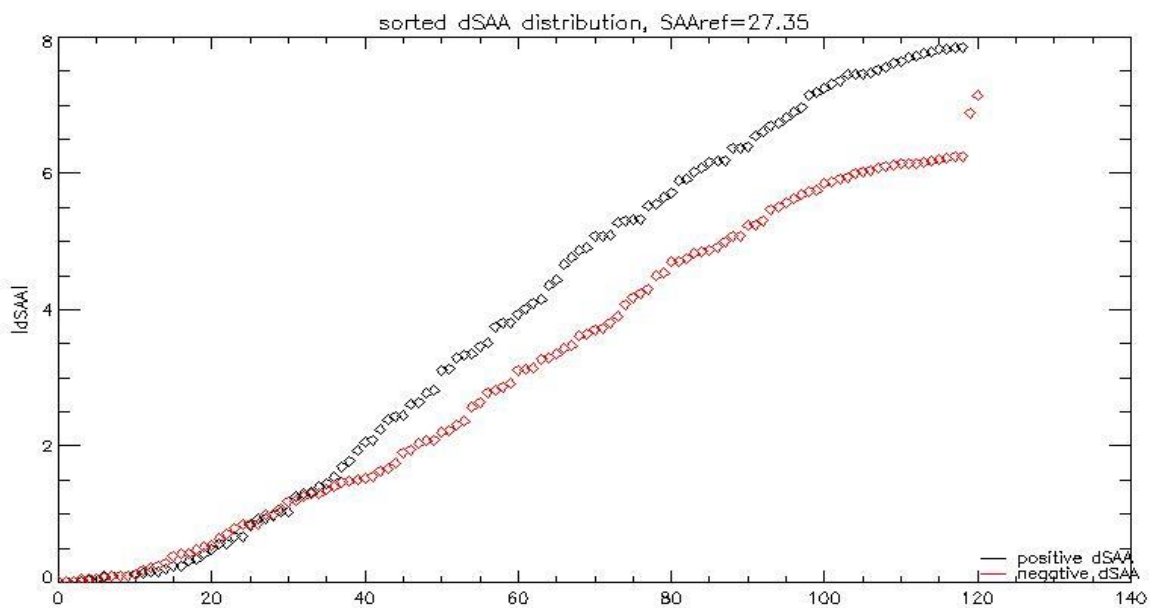
Figure 2-17: RC's SAA sorted distribution for negative ΔSAA (red) and positive ones (black)

4th MERIS data reprocessing

Evolutions and Validation report

Ref.:   MER4RP Validation Report

Version: 1.0

Date: 01/04/2019

Page: 22
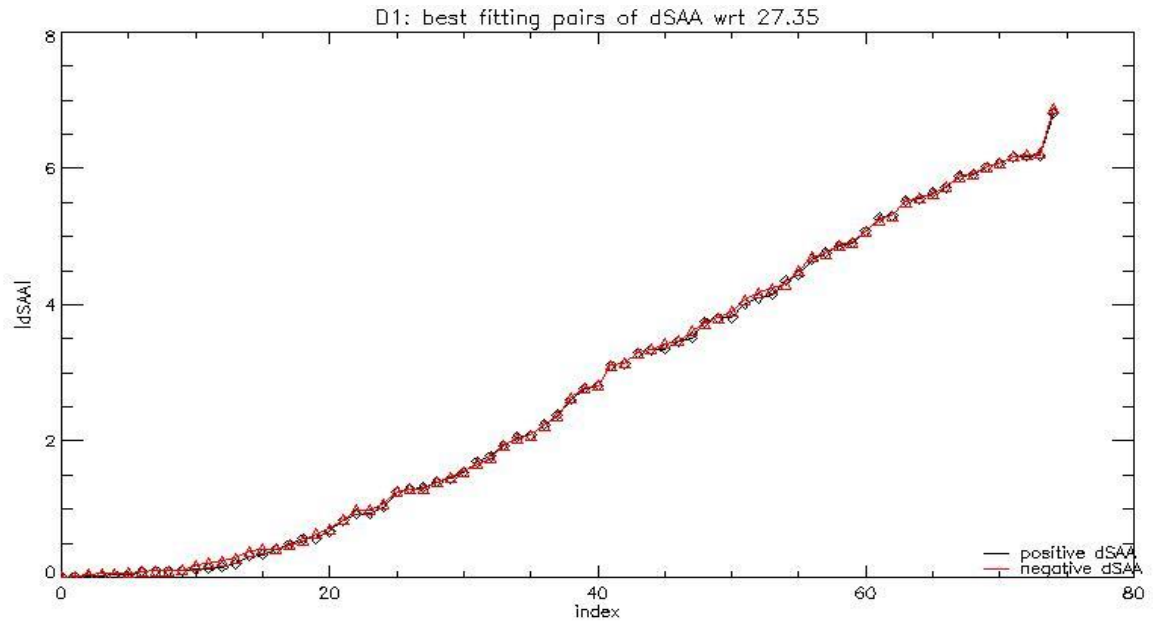
Figure 2-18: Best match pairs of RC ΔSAAs
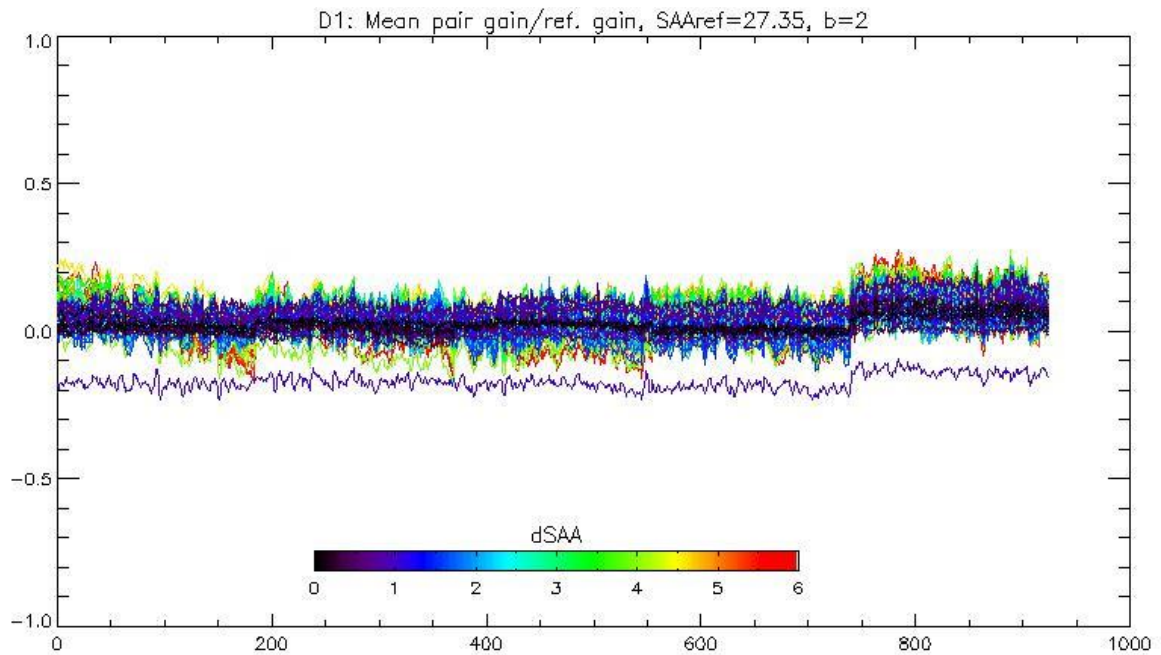
Figure 2-19: Residual for b2: pair average over reference orbit

2. As the same methodology is not applicable to diffuser 2 (it ends up with only 5 pairs, not enough for noise reduction), the overall spatial behavior of the diffuser 1 over diffuser 2 gain ratios have been modelled (Figure 2-20) and used to correct diffuser 1 reference gain, thus reducing discontinuities at camera interfaces.

4th MERIS data reprocessing

Evolutions and Validation report

Ref.:   MER4RP Validation Report

Version: 1.0

Date: 01/04/2019

Page: 23
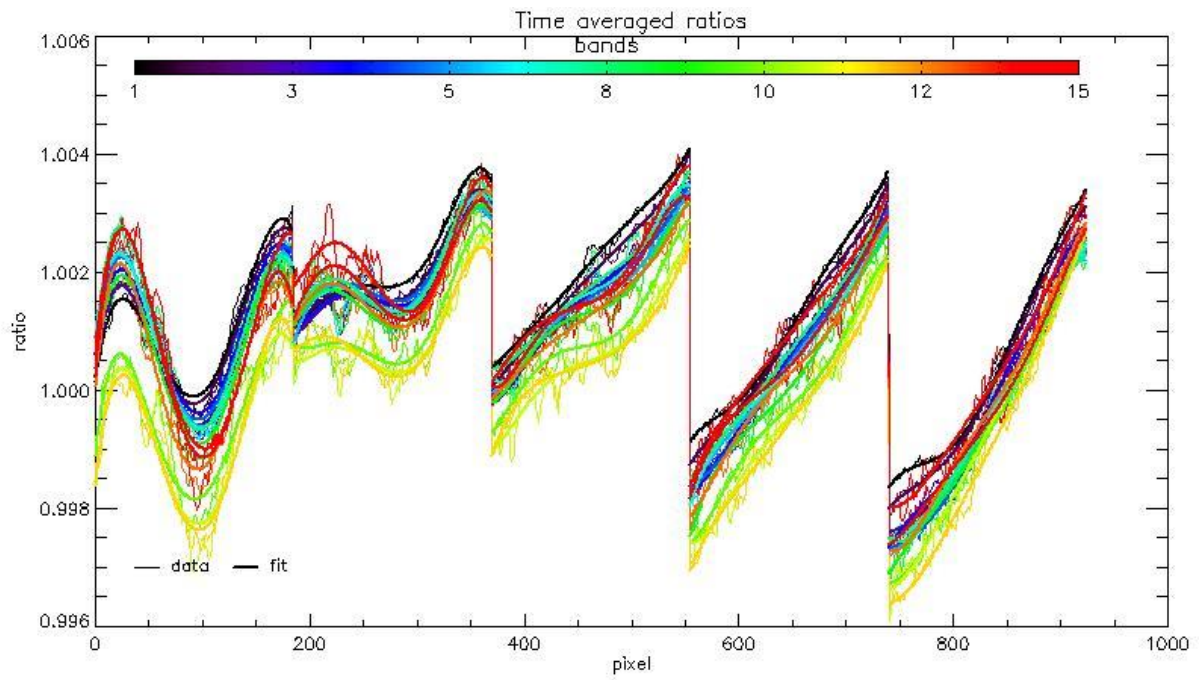
Figure 2-20: Time average (thin) and model (thick) D1/D2 ratio for each band

4th MERIS data reprocessing
Evolutions and Validation report

Ref.: MER4RP Validation Report
Version: 1.0
Date: 01/04/2019
Page: 24

2.4 Level 2 evolutions

2.4.1 Pre-processing

2.4.1.1 New modelling of Rayleigh Optical Thickness

The model of Bodhaine et al. (1999) is selected for the computation of the Rayleigh Optical Thickness in the MERIS spectral bands.

Nature of the change: ADF values

A new modelling of the Rayleigh optical thickness (ROT) is adopted for the MER4RP. The latter, described by Bodhaine et al. (1999), relies on the first principles of the *Rayleigh* scattering theory to better account for the spectral dependence of the molecular scattering cross-section. It includes the variability of refractive index and mean molecular weight of air, due to the presence of the carbon dioxide (CO_2) in the atmosphere, and presents a latitude-dependence through an accurate determination of the acceleration of gravity at anywhere on the Earth's surface.

A global average abundance of 390 ppm in CO_2 could be chosen as representative value for the whole period of the MERIS mission (2002−2012). Indeed, as illustrated in Table 2-1, an increasing of 20 ppm in the CO_2 concentration, does not impact the ROT. For the MER4RP, the ROT is then computed with this nominal value of CO_2 abundance and for a set of latitudes varying from 0 to 90° by step of 1°. All these details are given in [RD-4]. A comparison with the approximation of Hansen and Travis (1974) that was employed for the MER3RP is reported in Table 2-1.

Table 2-1: ROT computed at the 15 MERIS wavelength for a standard barometric pressure (1013.25 hPa) with (a) the approximation Hansen & Travis (H&T) that was used in the MER3RP, and (b) the new modelling of Bodhaine et al. (Bod) for a latitude (lat) of 45° and three values of the CO_2 abundance.

λ (nm)	ROT (H&T)	ROT (Bod): lat.=45° and 3 amounts in CO2		
		380 ppm	390 ppm	400 ppm
412.500	0.3152799628	0.3169589110	0.3169609852	0.3169630593
442.500	0.2359103470	0.2369950740	0.2369966265	0.2369981790
490.000	0.1551552838	0.1557451794	0.1557462009	0.1557472225
510.000	0.1317138017	0.1321818222	0.1321826896	0.1321835569
560.000	0.0899122270	0.0901888423	0.0901894345	0.0901900268
620.000	0.0594333719	0.0595929177	0.0595933093	0.0595937009
665.000	0.0447297235	0.0448402753	0.0448405701	0.0448408649
681.250	0.0405621315	0.0406597603	0.0406600276	0.0406602949
708.750	0.0345582111	0.0346380162	0.0346382439	0.0346384717

4th MERIS data reprocessing
Evolutions and Validation report

Ref.: MER4RP Validation Report
Version: 1.0
Date: 01/04/2019
Page: 25

λ (nm)	ROT	ROT (Bod): lat.=45° and 3 amounts in CO_2		
	(H&T)	380 ppm	390 ppm	400 ppm
753.750	0.0269437926	0.0270024160	0.0270025936	0.0270027712
761.875	0.0258015792	0.0258571700	0.0258573400	0.0258575101
778.750	0.0236167217	0.0236666217	0.0236667774	0.0236669330
865.000	0.0154592423	0.0154892560	0.0154893579	0.0154894598
885.000	0.0140987984	0.0141257208	0.0141258137	0.0141259067
900.000	0.0131757415	0.0132006062	0.0132006930	0.0132007799

2.4.1.2   Variation of the barometric pressure with the altitude P(z)

The computation of the surface pressure over land and inland waters is improved considering the per-pixel altitude and an improved relationship of barometric pressure with the altitude.

Nature of the change: Algorithm

The objective is a more sophisticated surface pressure determination over land and inland waters, considering the local variation of the barometric pressure with the altitude. In this new approach, the surface pressure at a given altitude 'alt', p(z=alt), is evaluated from the pressure at mean sea level, p(z=0), and the atmospheric profile in temperature (T) and relative humidity (RH) provided by meteo ancillary files. This new methodology, so-called the 'P-z' algorithm, is fully described in ATBD-2.26. The altitude is derived from a digital elevation model (DEM). Meteorological data are given at tie-points resolution then interpolated at pixel resolution, one tie-point corresponding to 16x16 pixels in the reduced resolution (RR) mode or 64 x 64 in the full resolution (FR) mode.

For the MER4RP, temperature (T) and relative humidity (RH) profiles from ECMWF are added to the meteorological annotations of the L1 products used as input to the L2 processing. These atmospheric profiles are available at tie-points and discretized over Np pressure levels from a pressure at 1000 hPa down to 300 hPa, which is enough to cover all the possible range of altitudes. The profiles are interpolated at pixel resolution so that p(z) is computed for each pixel.

Compared with MER3RP, this new surface pressure determination is now also performed on water pixels allowing continuity in the barometric pressure between land and water pixels. Indeed, the altitude from the DEM (over land but also over water) departs from the geoid altitude used in the ECMWF gridding so that the mean sea level has to be adjusted to the actual sea level (*i.e.* z and not 0). This is also the case for the pressure. Examples of the new product and difference with the previous determination from the MER3RP are displayed on Figure 2-21.

4th MERIS data reprocessing
Evolutions and Validation report

Ref.: MER4RP Validation Report
Version: 1.0
Date: 01/04/2019
Page: 26
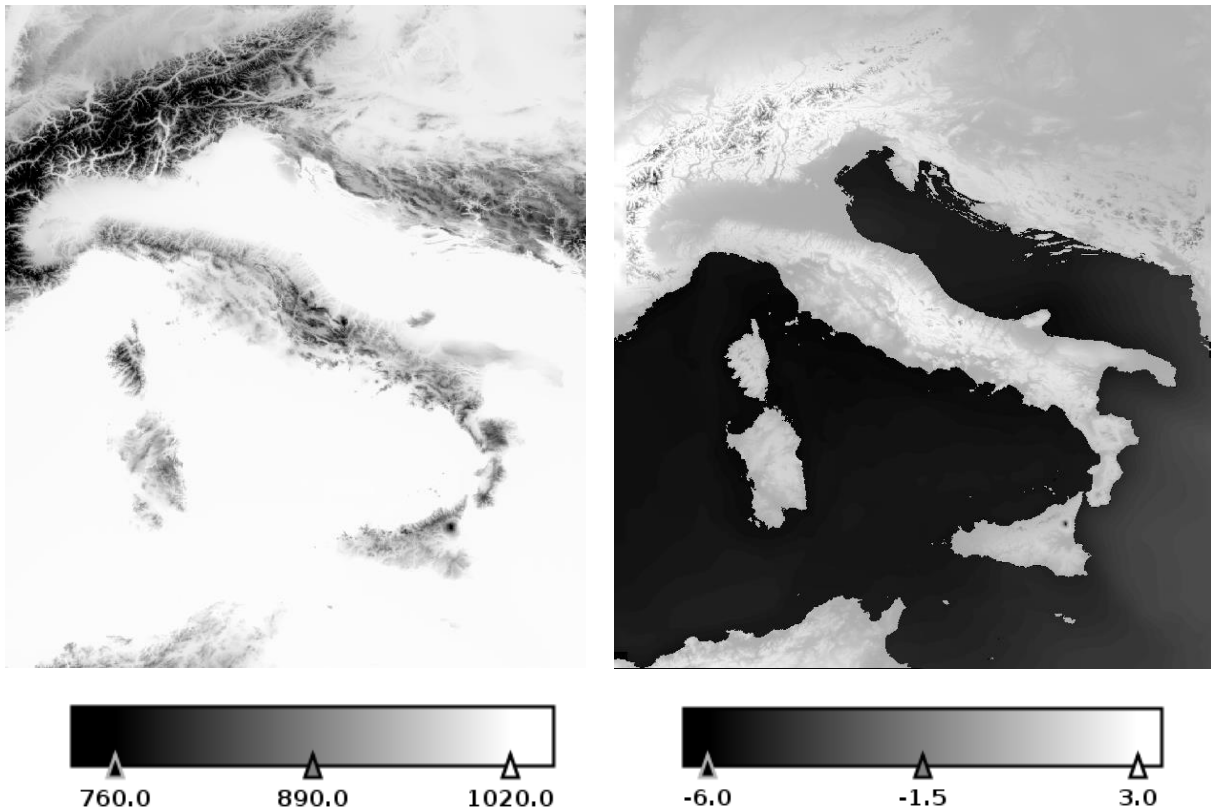
Figure 2-21: New estimate of the surface pressure P(z) (left, and difference (δP) with the previous determination employed in the MER3RP (right). Both the two pressure scales are expressed in hPa..

2.4.1.3 Gaseous correction

The computations of H_2O, O_2 and O_3 transmissions have been revised and the NO_2 absorption has been added in the total gaseous atmospheric transmittance.

Nature of the change: ADF values / Algorithm

The gaseous corrections have been refreshed according to the OLCI ATBD ([RD-2]) as follows:

1. Introduction of the nitrogen dioxide (NO_2) transmission, estimated with a climatological value of the NO_2 concentration (u_{NO_2}) and an absorption cross-sections extracted from the spectroscopic database of Bogumil et al. (2003);

2. Revision of the ozone (O_3) absorption cross-section derived from the spectroscopic database of Chehade et al. (2013). This optical parameter presents a better temperature-dependence; see Bouvet (2017) for more details;

3. Improved H_2O transmission computations using multiple cross-sections and total column water vapour amount from meteo forecast (applicable to all channels but 709 and 900 nm);

4. Contrary to the OLCI ATBD available at that time, H2O correction at 709 nm has been kept unchanged with respect to MERIS 3rd RP algorithm: the amount of absorber is

4th MERIS data reprocessing
Evolutions and Validation report

Ref.:   MER4RP Validation Report
Version: 1.0
Date: 01/04/2019
Page: 27

derived from the apparent absorption at 900 nm and transferred to the 709 nm channel using predefined laws (polynomials) accounting for the actual central wavelength of the 709 nm channel.

2.4.1.4   Smile correction moved to processing branches

The smile correction is performed through the pressure (or Rayleigh) adjustment by using an equivalent Rayleigh optical thickness. It is separately achieved for the water and the land branch.

Nature of the change: ADF values / Algorithm

Removing the smile effect in the MERIS acquisitions consists in the correction of the reflectance at top of the atmosphere (TOA) from the pixel (detector) wavelength to the nominal one (centre waveband). This correction is applied in a first step as a correction of the Rayleigh scattering after the gaseous correction in the 'land' and the 'water' branch. The small spectral shift, resulting from the difference between nominal and actual (pixel) wavelengths, corresponds to the introduction of an equivalent Rayleigh optical thickness (ROT) for each pixel. This Rayleigh adjustment is fully detailed in ATBD-2.28 and is applied separately for the water and the land branches, according to their specific algorithm to estimate the Rayleigh scattering. In a second step, Rayleigh corrected reflectance is further corrected in each branch for the residual spectral variation by a first order Taylor approximation (this second step has not evolved in the MER4RP processing).

2.4.2   Pixel identification

2.4.2.1   Radiometric land/water reclassification

The radiometric land/water reclassification has been revised following upgrades of the a-priori masks: (1) Reclassified pixels outside the tidal areas remain in their original branch; (2) The Flood and Dry Fallen masks have been added.

Nature of the change: ADF values / Algorithm

The radiometric land/water reclassification relies on the same tests as the one defined in the MER3RP. The latter exploit the basic differences in the spectral signatures of ground targets: while the reflectance decreases from the red to the near-infrared (NIR) region over water, it increases over land vegetation or remains more or less constant over bare soils. More, knowing that the water body strongly absorbs in the NIR domain, its reflectance is lower than that of most land surfaces. Thus, the radiometric land/water reclassification relies in testing the 'red-NIR' spectral slope and the absolute threshold on the NIR reflectance.

Pixels which are classified a-priori as 'land', and radiometrically reclassified as 'water', will trigger the «ES_FLOODED_RADIOMETRIC» flag. For the pixels classified a-priori as 'water'

4th MERIS data reprocessing
Evolutions and Validation report

Ref.: MER4RP Validation Report
Version: 1.0
Date: 01/04/2019
Page: 28

and radiometrically reclassified as 'land', the « DRYFALLEN_RADIOMETRIC » flag will be raised.

2.4.2.2   Cloud screening and snow/ice masking

Cloud screening is improved thanks to the use of Neural Network derived from the ESA Climate Change Initiative (CCI) programme.

Nature of the change: ADF values / Algorithm

The cloud screening has been significantly revised from the MER3RP to the MER4RP. The traditional tests based on whiteness and brightness, as well as on height of the scattering surface, have been simplified. More, a neural network (NN) well trained on manually classified pixels has been added. The latter developed in the frame of the ESA CCI programme. The NN provides classes of thick clouds, semi-transparent clouds, and cloud-free pixel classes. A snow/ice class is also computed. These classes are combined with some of the MER3RP tests based on brightness and whiteness features, as well as with a test on normalised snow index.

The main contributor to the final cloud screening is the neural net. The combination of these tests results in the cloud flags « CC_CLOUD » and « CC_CLOUD_AMBIGUOUS », which are mutually exclusive. An example is given in Figure 2-22.
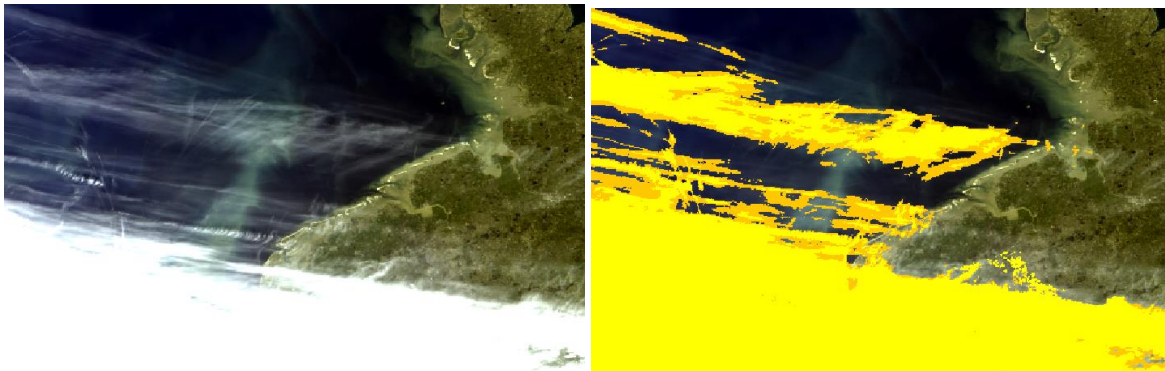
Figure 2-22: Example of cloud (yellow) and CC_CLOUD_AMBIGUOUS flags for MERIS 20.04.2005 over the North Sea and the area of northern Netherland and northern Germany. Note that the bright stripe off the Dutch coast is in the water and not cloud.

2.4.2.3   Cirrus mask

Cloud screening is enriched with semi-transparent cirrus clouds detection using the O₂ absorption.

Nature of the change: ADF values / Algorithm

4th MERIS data reprocessing

Evolutions and Validation report

Ref.: MER4RP Validation Report

Version: 1.0

Date: 01/04/2019

Page: 29

Except over bright cloud pixels, the MERIS O_2 transmittance is defined as the ratio in TOA reflectance between the absorbing band B_{11} (760.625 or 761.875 nm) and a pseudo-band 11 (free of O_2 gaseous absorption) as an interpolated value between the bands B_{10} (753.75 nm) and B_{12} (778.75 nm).

A Rayleigh correction is applied for a standard barometric pressure of 1013.25 hPa. The latter is now done with a dedicated O_2-Rayleigh transmittance look-up table (LUT) (see Section 2.5 and [RD-5] for more details). Over bright land pixels, it will inform mainly on the pressure at the surface level with a minor contribution of aerosols. Over dark water pixels under clear sky, it will give some indications about the vertical distribution of aerosols after a correction for the coupling term between the atmospheric scattering and the Fresnel reflection at bottom of the atmosphere (BOA).

The O2 transmittance is converted into an apparent pressure (i.e. P_{scat} over water and P_1 over land), using the US62 standard atmospheric model (ATBD-2.27). The determination of P_{scat} has been improved firstly, with an applicable domain based on a better formalism through the Rayleigh correction and a simplified 'aerosol-Fresnel' coupling term, and secondly, with the introduction of the Sun glint correction. In presence of cirrus, P_{scat} substantially decreases and is used for flagging pixels contaminated by thin clouds. Over land, the surface being quite bright in the O_2 absorption band (*i.e.* it is the opposite situation to the water case), P_1 can be also used for the cirrus cloud detection.

2.4.2.4 Multi-branch processing

Similarly to the OLCI processing, MER4RP processing is now controlled according to the observed surface type, namely Marine, Land and Cloud.

Nature of the change*: Algorithm*

Similarly to the OLCI processing, the MER4RP processing is now controlled according to the observed surface type, namely Marine, Land and Cloud. Each branch provides its own products, independently of the others, and can be activated or disabled separately. As they all share the same pre-processing steps, all branches are implemented in the same processor and can be acticated at the same time.

2.4.3 Water Vapour processing

The Water Vapour retrieval has been upgraded using the 1D-var algorithm.

Nature of the change*: ADF values / Algorithm*

4th MERIS data reprocessing
Evolutions and Validation report

Ref.: MER4RP Validation Report
Version: 1.0
Date: 01/04/2019
Page: 30

2.4.4 Water processing

2.4.4.1 Pressure adjustment and smile correction

Handling of the molecular scattering is improved using a new modelling of the ROT, an accurate pixel elevation, a new surface pressure determination, and a new pressure adjustment.

Nature of the change*: ADF values / Algorithm*

The model of Bodhaine et al. (1999) is selected for computing the ROT at the standard barometric pressure (1013.25 hPa). Moreover, the Rayleigh scattering contribution to the TOA signal is also improved thanks to the better accuracy on the pixel geolocation and altitude introduced in Section 2.3.1 and the new surface pressure determination described in Section 2.4.1.2.

New Pressure adjustment

One major evolution for the MER4RP is the new pressure adjustment scheme implemented in the '*water*' branch. This adjustment results from the difference between the standard barometric pressure (1013.25 hPa) and the estimated surface pressure derived from ECMWF measurements.

Different pressure adjustments have been done based firstly, on a decomposition of the TOA signal compatible with the formalism used for the atmospheric correction, and secondly, on the approximations of atmospheric scattering functions. The conceptual approach of the modelling is to produce a TOA reflectance after the removal of the gaseous absorption which corresponds to the 'Atmosphere-Ocean' system observed by MERIS but for a reference pressure. These pressure adjustments, designed to account for realistic variations of the pressure at sea level, correctly fulfilled this objective but revealed some limitations when considering inland waters at significant elevations.

The 5S decomposition of the TOA signal is employed in the MER4RP to perform the pressure adjustment. It provides this corrected TOA reflectance with an adapted formalism (forward or backward) depending on the sign of the correction in ROT ($d\tau_R$) associated with an elementary molecular layer removed (positive $d\tau_R$ value) or added (negative $d\tau_R$ value) at TOA (ATBD-2.28). It was not the case in the MER3RP in which all the adjustments were algebraic and therefore symmetrical in $d\tau_R$. In this new pressure (or Rayleigh) adjustment, the coupling between the Rayleigh scattering in the elementary molecular layer and the 'atmosphere-ocean' system below this one is accounted for. Another difference with the MER3RP is the use of LUTs with the Rayleigh scattering functions computed with the successive orders of the scattering code (RTC/SO) for this elementary molecular layer.

With the new *Rayleigh* LUTs, the pressure adjustment can be shared between the different algorithms, *i.e.* the Bright Pixel Atmospheric Correction (BPAC; ATBD-2.6), the Neural Network (NN) atmospheric correction (see ATBD-2.25), and the standard atmospheric

4th MERIS data reprocessing

Evolutions and Validation report

Ref.:   MER4RP Validation Report

Version: 1.0

Date: 01/04/2019

Page: 31

correction over Case-1 waters (ATBD-2.27). It applies at the beginning of the '*water*' branch for the two atmospheric correction procedures and replaces the former adjustments. Indeed, the three pressure (or Rayleigh) adjustments induced by the change in the ROT modelling (*i.e.* the model of Bodhaine et al.), the impact of the smile effect (*i.e.* the wavelength-shift correction), and the pressure adjustment (*i.e.* the variation of the barometric pressure) can be achieved in a same time insofar as they are all performed with an equivalent ROT shift.

The 6S formalism suggests accounting for the coupling between the *Lambertian* reflection at BOA and the atmospheric scattering. This term is implemented in the new pressure adjustment but it could be also included in the *Rayleigh* correction for the BPAC (even if it remains small in the NIR region) to derive the water reflectance. Indeed, this coupling can be significant in the blue domain.

This new pressure adjustment has been evaluated on the marine reflectance (ρ_w) at Aqua Alta Oceanographic Tower (AAOT). Results stressed the existence of a bias around 10% of ρ_w. This bias being symmetrical with respect to the reference pressure, a final interpolation scheme on ρ_w derived from adjustments at the two bracketing reference pressures is then suggested to finally reduce it by a factor of 10 (see ATBD-2.28 for more details).

2.4.4.2   Bright Pixel Atmospheric Correction

The atmospheric correction over coastal waters is better handled thanks to the improvement of the BPAC. The numerical inversion has been totally revised, now based on a spectral matching algorithm (χ2 minimisation) on five NIR bands, considering input uncertainty at each channel.

Nature of the change: *Algorithm (revision of the inversion method) and ADF values (only Case2_S threshold)*

MER3RP known issue: Previous implementation of BPAC (ATBD 2.6, issue 5.3) has shown to fail over coastal waters when combined with NIR vicarious calibration (ATBD 2.24, issue 1.0), due to too strong sensitivity of the inversion to the radiometry. Furthermore, previous inversion was limited to moderately turbid waters (less than about 50 g/m^3) first, because of erroneous H2O transmittance in B$_{09}$ (708.75nm) and B$_{14}$ (885 nm) with growing turbidity, and second, due to the multiple-minima issue when using only three bands.

MER4RP evolution: Importantly, the BPAC model is strictly identical to previous version, for both the atmospheric part (aerosol signal) and marine part (particulate IOPs and AOPs). The same also applies for the three unknowns of the inversion: BPAC keeps retrieving aerosol reflectance (amplitude and shape) and particulate backscattering in the NIR region. Only the numerical inversion has been totally revised, now based on a spectral matching algorithm (χ^2 minimisation) on five NIR bands, considering the input uncertainty at each channel. This evolution also concerns the first guess estimate, no more based on a 3-band iterative scheme, but on the admissible range of particulate backscattering given the actual

4th MERIS data reprocessing
Evolutions and Validation report

Ref.: MER4RP Validation Report
Version: 1.0
Date: 01/04/2019
Page: 32

radiometry in the NIR region and realistic range of aerosol content encountered in nature. Last, because this algorithm generally retrieves higher backscattering than the previous version (due to residual glint, thin clouds, etc.), the threshold on TSM used to raise Case2_S flag (sediment-dominated Case2 waters) has been changed from 0.75 to 1.5 g/m^3.

In term of impact, the spectral matching algorithm on five bands makes BPAC more robust to radiometric noise, calibration and modelling error in the NIR region. At high turbidity, input uncertainties in the χ^2 play an important role in lowering importance of bands B_{09} and B_{14}. The use of five bands cancels the multiple-minima issue (i.e. when particulate is interpreted as aerosol over very turbid waters). The new BPAC tends to harmonise performance of the downstream clear water atmospheric correction among various water types (from clear to moderately turbid) and extend MERIS data over extremely turbid waters (TSM > 100 g/m^3).

2.4.4.3 Clear water atmospheric correction

A new set of aerosol models, based on a Ahmad et al. (2010), has been included in the Atmospheric Correction LUTs which have been extended to several reference pressure levels for allowing the application of the atmospheric correction algorithm to the in-land waters at significant elevations.

Nature of the change: ADF values / Algorithm

New set of aerosol models

For the MER3RP, a set of 16 standard aerosol models (SAMs) was employed to process the atmospheric correction over ocean: *i.e.* 12 models from Shettle and Fenn (1979) including maritime, coastal and rural aerosols with four values of relative humidity (RH = 50, 70, 90 and 99 %), 3 'blue-aerosol' models corresponding to the small particles (Santer and Zagolski, 2010), and a particular model 'whiter than white' (*i.e.* an assemblage composed of a maritime model with a RH of 99% in the boundary layer, and 'free-aerosol' in the troposphere and stratosphere). These 16 SAMs were completed with 18 DUST models from Moulin et al. (2001) for describing absorbing smokes or Saharan/Asian dusts.

Because these SAMs present a spectral discontinuity in their inherent optical properties (IOPs), the MERIS QWG took the decision to replace them for the MER4RP by a more recent set of models proposed in Ahmad et al. (2010), also known as the NASA/GSFC Models.

This new set of models is based on a micro-physical description of the aerosols through the retrieval of standard vertical size distributions of particles associated with their refractive indices from ground-based radiometric measurements provided by the Aerosol Robotic Network (AERONET) database. These models were developed on the assumption that the aerosols in coastal and open ocean conditions could be represented by a binormal size distributions, one being continental (water soluble + dust-like + soot-like) and defined by the fine mode and the other naturally oceanic (sea salt) and characterized by the coarse mode. The seasonal variation of RH on the growth of fine and coarse mode aerosols is accounted

4th MERIS data reprocessing
Evolutions and Validation report

Ref.: MER4RP Validation Report
Version: 1.0
Date: 01/04/2019
Page: 33

for. Thus, the NASA/GSFC set of models is built with 8 values of RH (RH={30%, 50%, 70%, 75%, 80%, 85%, 90%, 95%}) and 10 fine-mode fractions per RH, varying from 0 to 1 (*i.e.* FMF={0%, 1%, 2%, 5%, 10%, 20%, 30%, 50%, 80%, 95%}) to reconstruct the particle size distributions. This yields to 80 models to which is added the original set of 18 DUST models to complete the new aerosol database used as input to atmospheric correction over water (see RD-6 and RD-7 for more details).

New set of reference pressure levels

For MER3RP, all the LUTs with atmospheric scattering functions (*i.e.* reflectance and transmittance) were generated over three wind-roughened black sea surfaces for a standard barometric pressure of 1013.25 hPa and a ROT derived from the formulation of Hansen and Travis.

To perform the new pressure adjustment scheme implemented in the 4th MERIS data processor (see § 2.4.4.1), the atmospheric and Rayleigh LUTs need to be extended to several reference pressure levels. A set of six reference pressures (P_{ref}) is selected for allowing the application of this pressure (or Rayleigh) adjustment to the TOA reflectance over inland and open waters: P_{ref} = {1040, 1013.25, 970, 900, 800, 700} hPa.

Thus, for the MER4RP, the Rayleigh LUTs (reflectance and transmittance) have been recomputed for the same set of wind-roughened black sea surfaces and the same regular Sun/view geometry as for the MER3RP, but for each of six values of P_{ref}. For the 'Ocean-Aerosol' LUTs, the atmospheric scattering functions have been regenerated for each value of P_{ref} and the NASA/GSFC models only. In other words, the atmospheric LUTs associated with the 18 DUST models remain unchanged (*i.e.* they were calculated at a standard pressure of 1013.25 hPa) and have been introduced in the new 'Ocean-Aerosol' ADF produced per value of P_{ref} (see § 2.5 for more details).
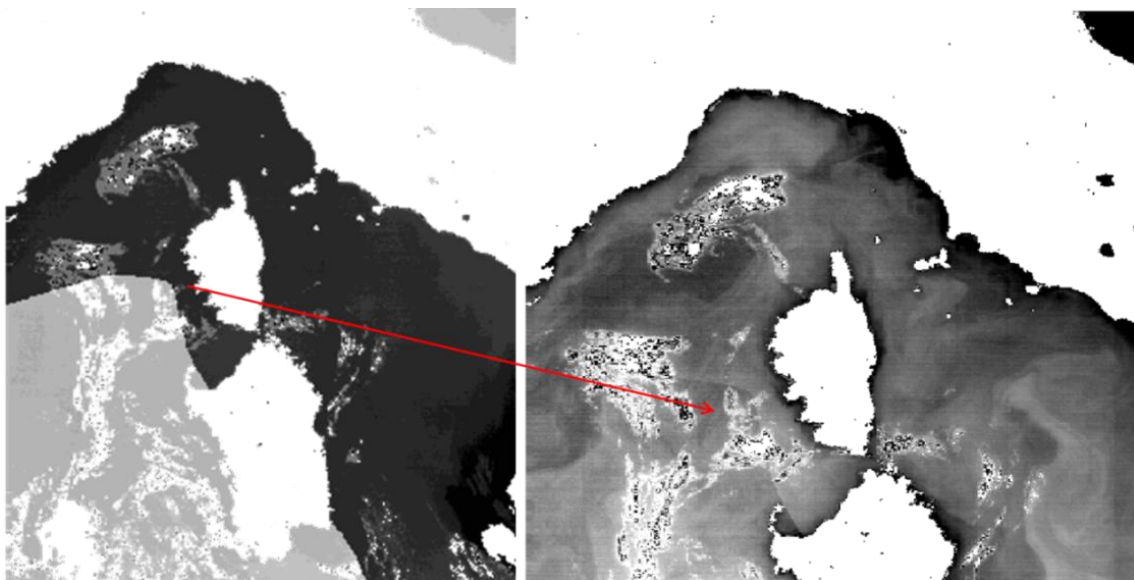
Figure 2-23: Illustration of the impact due to a lack of interpolation in the RH levels through the selection of 2 bracketing aerosol models that belong to two different classes of RH. Left: index of selected model (the closest to the actual value of RH). Right: retrieved marine reflectance.

4th MERIS data reprocessing

Evolutions and Validation report

Ref.: MER4RP Validation Report

Version: 1.0

Date: 01/04/2019

Page: 34

In the aerosol remote-sensing algorithm, the selection of the two bracketing NASA/GSFC models requires the consideration of the two reference pressure levels bracketing the target pressure, but also the two bracketing RH levels. In fact, in the case where the two selected models present two distinct values of RH, a discontinuity clearly appear in the retrieval of the marine reflectance, as illustrated inFigure 2-23.

Therefore, dealing with both the RH dependence in the NASA/GSFC models and the new pressure adjustment scheme, two main changes have been brought in the standard atmospheric correction algorithm over Case-1 waters:

- Adaptation to the new pressure adjustment scheme: As fully described in ATBD-28, by means of the new pressure adjustment the TOA reflectance corrected for the gaseous absorption in the NIR region is adjusted at two reference pressure levels, P_{ref1} and P_{ref2}, bracketing the actual target pressure (P_{pix}). P_{ref1} is assumed to be the closest pressure to P_{pix}. The TOA reflectance adjusted at P_{ref1} is used as input to the standard atmospheric correction for retrieving the aerosol model, the mixing ratio, and the first value of the marine reflectance, $\rho_{w,1}$. The last quantity should not depend on the pixel pressure. However, it is not actually the case due to lack of precision in the modelled pressure which may be farther from the target pressure (see RD-8 for more details). Therefore, in order to reduce the potential bias in the marine reflectance, the best choice consists in the extraction of the aerosol parameters at P_{ref1} and their propagation to P_{ref2} through an interpolation in the atmospheric scattering LUTs. The latter allow the retrieval of the second value of the marine reflectance, $\rho_{w,2}$. A final interpolation in ROT is then applied one these two extractions ($\rho_{w,1}$ and $\rho_{w,2}$) to get the final value of the marine reflectance, ρ_w with an acceptable bias.

- Adaptation to the RH dependence in the NASA/GSFC models: In the aerosol remote-sensing algorithm, a preselection of model candidates to the atmospheric correction is performed to get the two values of RH among the 8 classes of RH, bracketing the ECMWF value of RH over the target. When selecting only the models from the class for which the RH dependence is the closest to the target one, the retrieved marine reflectance exhibits some artefacts in the RH discretization of this class (Figure 2-24). The best way to reduce them consists in the use of two classes of RH for which their values bracket the target one. Interpolations are then performed on the intermediate results derived from the two bracketing RHs, so that the two values of the marine reflectance ($\rho_{w,1}$ and $\rho_{w,2}$) at P_{ref1} and P_{ref2} are still extracted and interpolated with the approach described above. An illustration of this improvement is displayed in Figure 2-25.

4th MERIS data reprocessing

Evolutions and Validation report

Ref.:   MER4RP Validation Report

Version: 1.0

Date: 01/04/2019

Page: 35
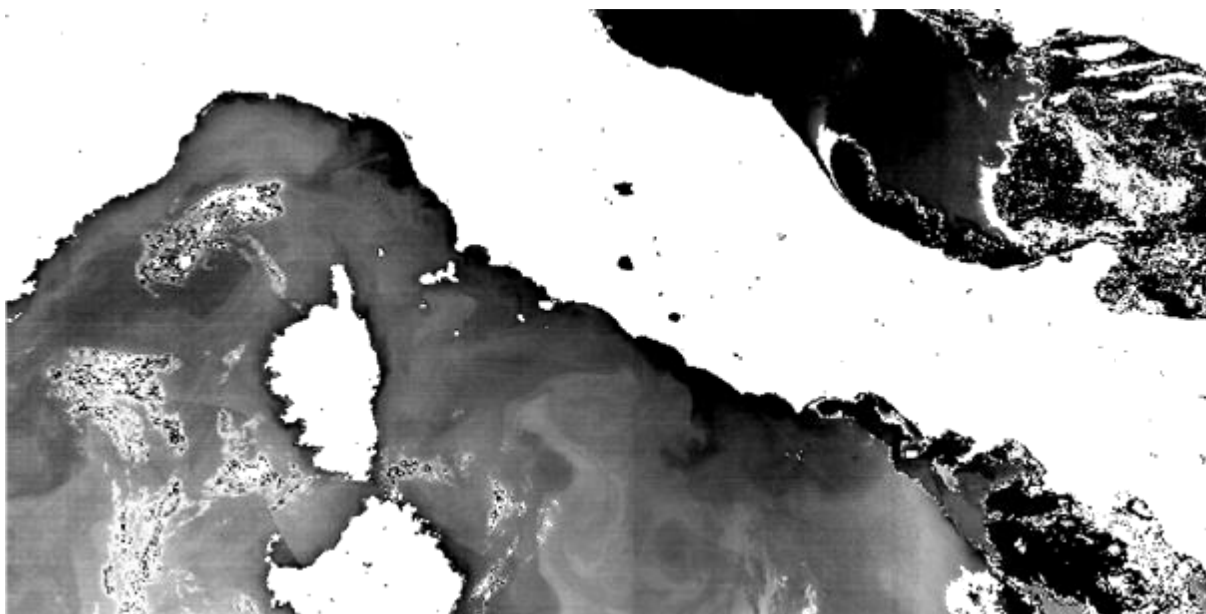
Figure 2-24: Marine reflectance retrieved over the North-Eastern Mediterranean Sea and the South-Western Adriatic Sea, using the RH dependence within the selected class of aerosols and without interpolation on the bracketing RH levels. Some artefacts are clearly visible over open waters located west of Corsica.
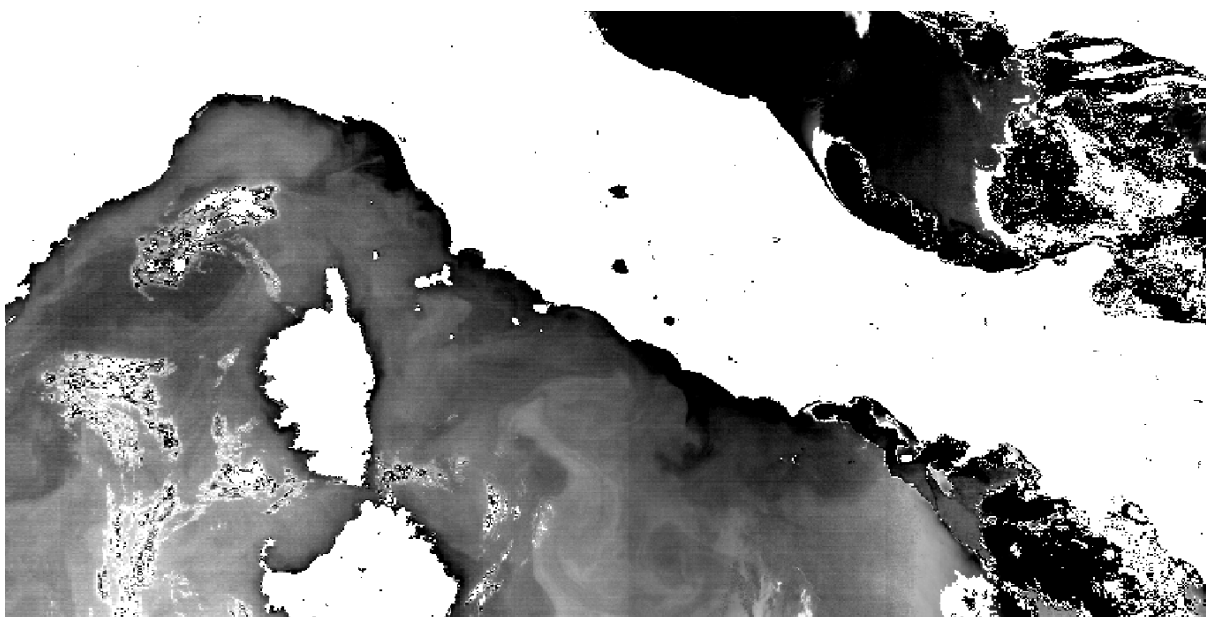
Figure 2-25: Same legend as for Figure 2-24 but with interpolation on the bracketing RH levels. Some improvements appear over open waters located west of Corsica.

2.4.4.4   *Propagation of radiometric uncertainty*

The propagation of TOA radiometric uncertainty through the L2 water processing chain down to BOA has been implemented to provide water-leaving reflectance uncertainties

Nature of the change: *ADF values / Algorithm*

4th MERIS data reprocessing
Evolutions and Validation report

Ref.: MER4RP Validation Report
Version: 1.0
Date: 01/04/2019
Page: 36

The uncertainty propagation scheme of OLCI (ATBD S3-L2-SD-01-C01-ACR-TN, 2013) has been implemented. This scheme considers the propagation of TOA radiometric uncertainty through the L2 processing chain down to BOA where it finally provides water-leaving reflectance uncertainties. Currently, this scheme is specifically limited to the clear water atmospheric correction where atmospheric path reflectance uncertainties in the NIR bands are propagated to the VIS bands and contribute to the total uncertainty budget. Uncertainties due to the model are not accounting for.

An example is shown below over the Southern Indian Ocean (SIO) at 412.5 nm. Water-leaving reflectance is scaled between 0.04 and 0.06, the associated uncertainty between 2 10^{-4} and 10^{-3} corresponds to about 1%.

M01_rho_w [-]

0.04	0.05	0.06

M01_rho_w_err [-]

2.0E-4	6.0E-4	0.001
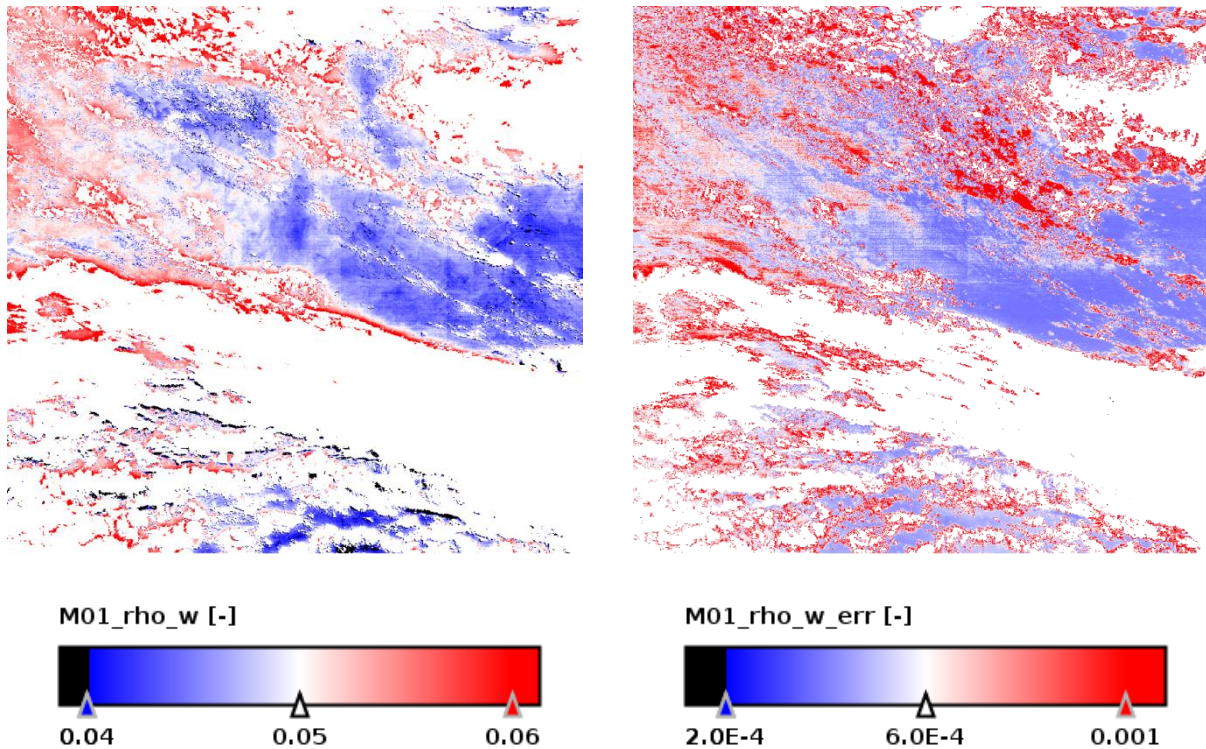
Figure 2-26: Water-leaving reflectance at 412 nm over SIO (left) and its uncertainty (right). Rhow scale: 0.04 - 0.06; uncertainty scale: 2 10^{-4} - 10^{-3}.

2.4.4.5 Vicarious adjustment

Vicarious gains in the VIS region have been recomputed to account for modified L1 calibration, atmospheric correction upgrades and updated in-situ measurement datasets.

Vicarious adjustment in the NIR region (relative to one band) is discarded because the new BPAC is more robust to errors in the NIR domain and spectrally aligns the path reflectance for each pixel.

Nature of the change*: Algorithm (gains computation and application) and ADF values (gains values)*

4th MERIS data reprocessing

Evolutions and Validation report

Ref.: MER4RP Validation Report

Version: 1.0

Date: 01/04/2019

Page: 37

By definition of system vicarious calibration, vicarious gains must be computed each time there is a change in the Level-1 and Level-2 processing chain, hence the initial need to recompute values for MER4RP; the in situ data at BOUSSOLE and MOBY have also evolved. Moreover, the NIR vicarious gains computed over oligotrophic gyres in the MER3RP were doubtful: assumption of perfect calibration of B_{09} (708.75 nm) and B_{12} (778.75 nm) is not demonstrated and the uncertainty on the modelled marine signal at 709 nm has large impact on gains in B_{13} (865 nm) and B_{14} (885 nm).

MER4RP evolution: VIS vicarious gains have been recomputed to account for modified L1 calibration, atmospheric correction upgrades and updated in-situ measurement datasets. An algorithmic evolution is required following the new pressure adjustment over water, which now defines water-leaving reflectance at two bracketing reference pressures (noted P_{ref1} and P_{ref2} below) and linearly interpolates them to produce the final Level-2 reflectance:

$$\rho_w^{P_{ref1}}(\lambda) = \frac{\rho_{gc}^{P_{ref1}}(\lambda) - \rho_{path}^{P_{ref1}}(\lambda)}{t_d^{P_{ref1}}(\lambda)} \text{ and } \rho_w^{P_{ref2}}(\lambda) = \frac{\rho_{gc}^{P_{ref2}}(\lambda) - \rho_{path}^{P_{ref2}}(\lambda)}{t_d^{P_{ref2}}(\lambda)}$$

$$\rho_w(\lambda) = (1 - \varepsilon)\, \rho_w^{P_{ref1}}(\lambda) + \varepsilon\, \rho_w^{P_{ref2}}(\lambda) \text{ with } \varepsilon = \frac{\tau_1 - \tau}{\tau_1 - \tau_2}$$

On a pixel-per-pixel basis, and for a given wavelength, the vicarious gain that forces the atmospheric correction to exactly retrieve the in situ marine reflectance ρ_w^{IS} is now given by:

$$g(\lambda) = \frac{\rho_w^{IS}(\lambda) + (1 - \varepsilon)\, \rho_{path}^{P_{ref1}}(\lambda) / t_d^{P_{ref1}}(\lambda) + \varepsilon\, \rho_{path}^{P_{ref2}}(\lambda) / t_d^{P_{ref2}}(\lambda)}{(1 - \varepsilon)\, \rho_{gc}^{P_{ref1}}(\lambda) / t_d^{P_{ref1}}(\lambda) + \varepsilon\, \rho_{gc}^{P_{ref2}}(\lambda) / t_d^{P_{ref2}}(\lambda)}$$

Regarding the NIR region, the new BPAC (MERIS ATBD 2.6) dynamically aligns the radiometry. It justifies to not use anymore the MER3RP adjustment (i.e. gains are set to unity in the NIR bands). The implementation ensures that the spectral alignment is performed whether the BPAC has converged or not (same alignment on all pixels).

The computation of the mission average vicarious gains in the VIS domain uses the methodology of the MER3RP, i.e. the computation of median gains per macropixels and the weighted-mean of these median gains. The macropixels have been selected to avoid contamination by clouds and Sun, as well as to be the most homogeneous.

The weighting of the individual macropixel median gains is done by using the associated uncertainties (radiometric uncertainty and standard deviation as well as in situ uncertainty).

Final gains are computed per site (here, BOUSSOLE and MOBY separately), and a weighted interpolation is performed between the two. At 620 nm (B_{06}), BOUSSOLE is missing, to provide continuity weighted average of the neighbouring gains at 560 (B_{05}) and 665 nm (B_{07}) is performed so as to provide a value for BOUSSOLE which is then used to average with MOBY. Final gains are displayed in Figure 2-27.

4th MERIS data reprocessing

Evolutions and Validation report

Ref.: MER4RP Validation Report

Version: 1.0

Date: 01/04/2019

Page: 38
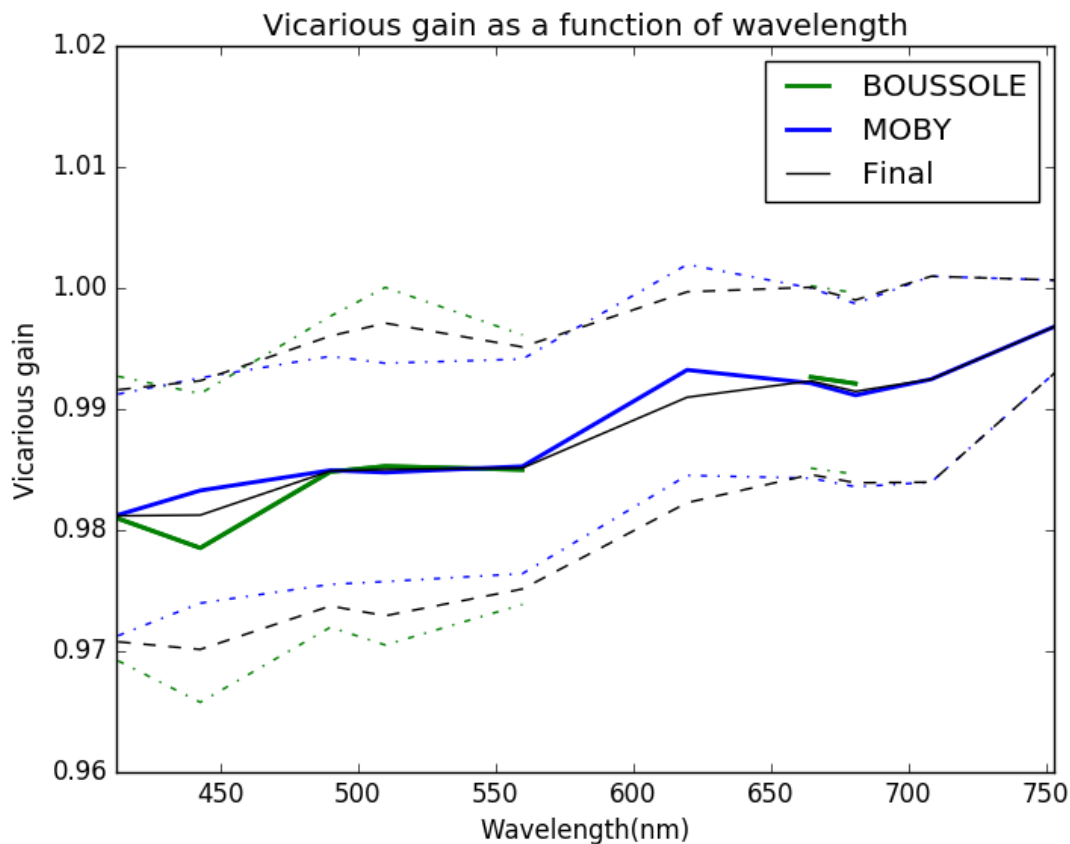
Figure 2-27: Final vicarious gains (green: BOUSSOLE, blue: MOBY, black: final).

2.4.4.6   Case-1 Ocean Colour processing

The Case-1 Ocean Colour algorithm has been upgraded in two main aspects:

- Introduction of the computation of the diffuse attenuation coefficient at 490 nm K_d(490), according to (Morel et al, 2007)

- Computation of Ocean Colour products uncertainties by propagation of the radiometric uncertainty through the OC algorithms

Nature of the change: *Algorithm / ADF values*

The Case-1 Ocean Colour processing has evolved with:

- ADF update: the f/Q and Gothic R LUTs have been updated from delivery of new LUTs by LOV: hyperspectral LUTs of f & Q that have been converted to f & Q at MERIS channels, updated Gothic R table with finer Sun zenith and wind speed sampling.

- Addition of KD_490 (Morel 2007; S3-L2-SD-03-C10-LOV-ATBD_OC_Products, 05/10/2012)

- Propagation of radiometric uncertainty through OC4Me_CHL and KD_490M07 (ATBD S3-L2-SD-01-C01-ACR-TN, 2013)

4th MERIS data reprocessing
Evolutions and Validation report

Ref.: MER4RP Validation Report
Version: 1.0
Date: 01/04/2019
Page: 39

2.4.4.7 Case 2 Ocean Colour processing

The Case-2 Ocean Colour algorithm has been upgraded considering:

- a new bio-optical model derived from NOMAD data set and extended for Case-2 water with 5 components;

- an atmospheric correction based on the GEN_TOA Coastcolour atmosphere model, which includes a variable ground pressure;

- the uncertainties calculation.

Nature of the change*: Algorithm / ADF values*

For retrieving Case-2 water optical variables (IOPs) and concentrations of chlorophyll and total suspended matter (TSM) the bio-optical model and the alternative atmospheric correction procedure have been changed. Furthermore, a procedure was added to compute the uncertainties of the retrieved IOPs and concentrations.

Details can be found in the Case-2 water ATBD 2.25.

Bio-optical model

The bio-optical model is based on the NOMAD data set, which has been extended to higher concentrations to cover Case-2 water conditions.

The analysis of the NOMAD data base has shown that at least five optical components are necessary to describe the variability of the water leaving radiance spectra of Case-1 and Case-2 waters; these are listed as:

- spectral absorption coefficient of phytoplankton pigments, *ap*

- spectral absorption coefficient of detritus, *ad*

- spectral absorption coefficient of CDOM, *ag*

- spectral scattering coefficient of small particles, *bp*

- spectral scattering coefficient of large (white) particles, *bw*

All spectral coefficients are normalized to unity at 442.5 nm (MERIS B_{02}).

The absorption spectra of detritus, *ad,* and gelbstoff, *ag,* are parametrized by

$ad(\lambda) = ad\_443 * exp(-ex\_ad*(\lambda-443))$

$ag(\lambda) = ag\_443 * exp(-ex\_ag*(\lambda-443))$

The exponents *ex_ad* and *ex_ag* have been determined from the NOMAD data set. Since both have a large overlap the upper value (95% percentile) of *ex_ag* and the lower end (5% percentile) of *ex_ad* were used to bracket most of the absorption spectra of *ad* and *ag*.

4th MERIS data reprocessing
Evolutions and Validation report

Ref.: MER4RP Validation Report
Version: 1.0
Date: 01/04/2019
Page: 40

Ex_ag =0.025

ex_ad =0.0074

The spectral scattering coefficients of particles are defined as:

bp(λ) =((443.0/λ)**ex_bp) * conc_bpart

bw(λ) =((443.0/λ)**ex_bw) * conc_bwit

with

> *ex_bp =1.87 // with Bb = 0.018 from the Petzold phase function*
>
> *ex_bw =0.0 // with Bb = 0.008*
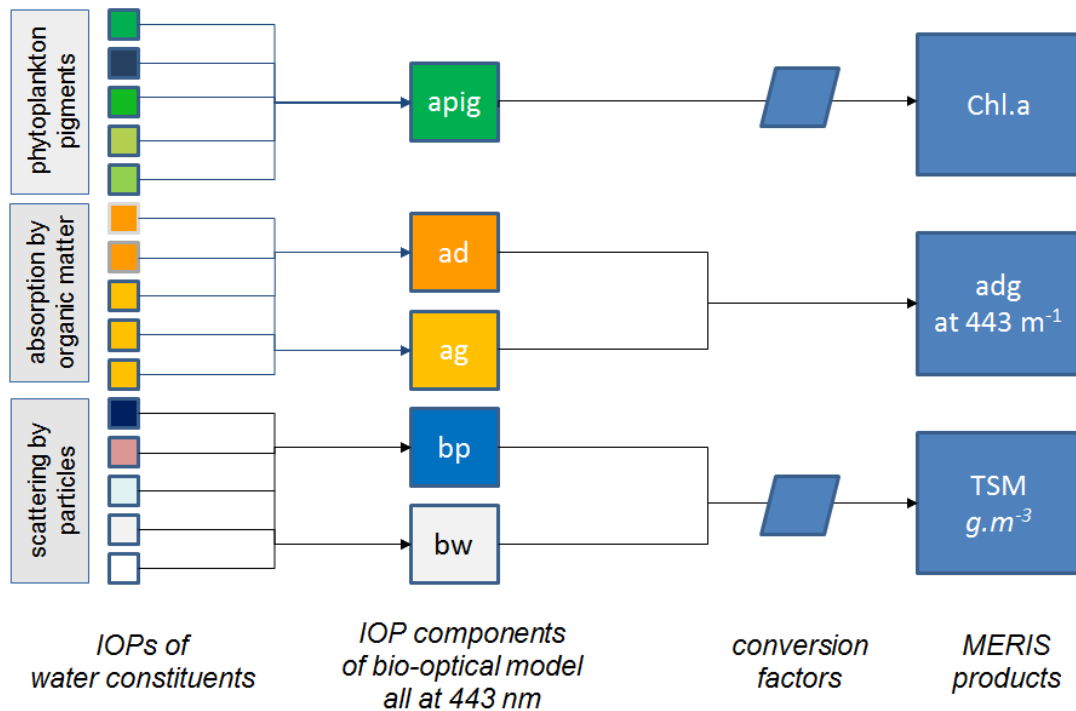
Figure 2-28: Scheme of the bio-optical model

The phytoplankton pigment absorption spectrum is derived from the mean NOMAD absorption spectrum (Table 2-2).

Table 2-2: Relative absorption of phytoplankton pigments

Band / λ	1/412	2/443	3/489	4/510	5/560	6/620	7/665	8/681	9/708
rel. a	0.95	1.0	0.64	0.42	0.15	0.124	0.242	0.247	0.098

The mass concentrations of chlorophyll (chl) and total suspended matter (TSM) are computed from the corresponding IOPs (*ap, bp and bw*) by using the following conversion coefficients:

4th MERIS data reprocessing
Evolutions and Validation report

Ref.: MER4RP Validation Report
Version: 1.0
Date: 01/04/2019
Page: 41

chl = 21.0*(ap)^(1.04)

tsm = (bp+bw)*1.73

The absorption (*resp.* scattering) spectra of *ad* and *ag* (*resp. bp* and *bw*) are regarded as the lower and upper end of the natural range of only one component so that finally only three components are provided as products to the user: *ap, adg, btsm*.

One has to be aware of the fact that the natural variability of all these components is high. Also the conversion of *ap* into *chl* has an uncertainty of about a factor of 2, as the NOMAD data show.

Atmospheric correction

The atmospheric correction is based on the Coast-Colour Atmospheric model (the 'GEN_TOA' developed by Zagolski and Santer). For each simulation run (case) a random value of the following parameters is selected from a uniform distribution:

- Sun zenith angle: 0 -75 deg

- View zenith angles: 0 – 60 deg

- View azimuth angle: 0 -180 deg

- Aerosol optical thickness (AOT at 550 nm): 0 – 0.8

- Angstrom exponent: 0 – 2.5

- Wind speed: 0 – 10 m s-1

- Water temperature: 0 – 36 deg C

- Salinity: 0 – 43 ‰

- Sea-level surface pressure 800 – 1040 hPa (8 steps)

Using the 'GEN_TOA' tool the path radiance reflectances and the up/down transmittances are computed and combined with the HYDROLIGHT simulations of water-leaving radiance reflectances.

From the HYDROLIGHT simulations a forward NN is trained, which has the IOPs, angles, wind speed, temperature and salinity as input, and determines the water leaving radiance reflectances as output. For each case of the atmosphere, 9 randomly selected cases of IOPs are used to compute the water reflectances. The water reflectances are transported to TOA using the up and downward transmittances. Finally, a randomly selected uncertainty of 1% is added to the TOA reflectances.

From this data set the following neural networks are trained:

- Auto-associative NN for determining out of scope cases: aaNN

- Bi-directional water leaving-radiance reflectances, rtosa_rw_NN

4th MERIS data reprocessing
Evolutions and Validation report

Ref.:   MER4RP Validation Report
Version: 1.0
Date: 01/04/2019
Page: 42

- Bi-directional path radiance reflectances: rtosa_rpath_NN

- Downward and upward transmittances: rtosa_td_NN, rtosa_du_NN

No correction for atmospheric gas absorption is included in this procedure. This will be applied in another section of the MERIS ground processor before.

Uncertainties

Uncertainties of the five IOPs are computed from the deviations between the IOPs, which have been used to simulate the water reflectance, and the corresponding IOPs from the rw_iop_NN. From these case-by-case deviations the uncertainty NN is trained with the five IOPs as input and the 5 uncertainties as output. These numbers include uncertainties, which are mainly induced by the following factors:

- Ambiguities, when IOPs are derived from reflectances

- Saturation effects, which occur at high concentrations

- Masking effects, when one IOP dominates the water reflectance spectrum

- Imperfect NN

This determination of uncertainties requires that the measured spectrum has to be tested if it is in scope of the data cube used to simulate the water reflectances, which, however, is part of the Case-2 water processor (see ATBD 2.25).

The uncertainties are provided in absolute units (a or b expressed in m^{-1}).
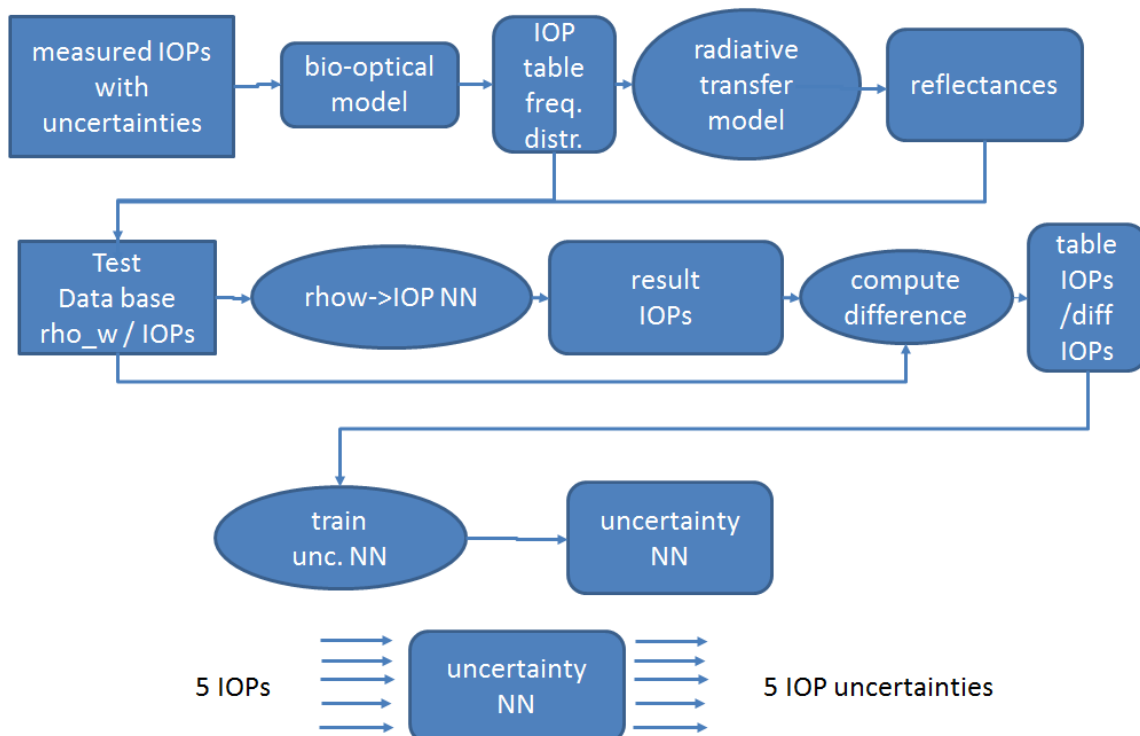
Figure 2-29: Scheme of the computation of uncertainties

4th MERIS data reprocessing

Evolutions and Validation report

Ref.: MER4RP Validation Report

Version: 1.0

Date: 01/04/2019

Page: 43
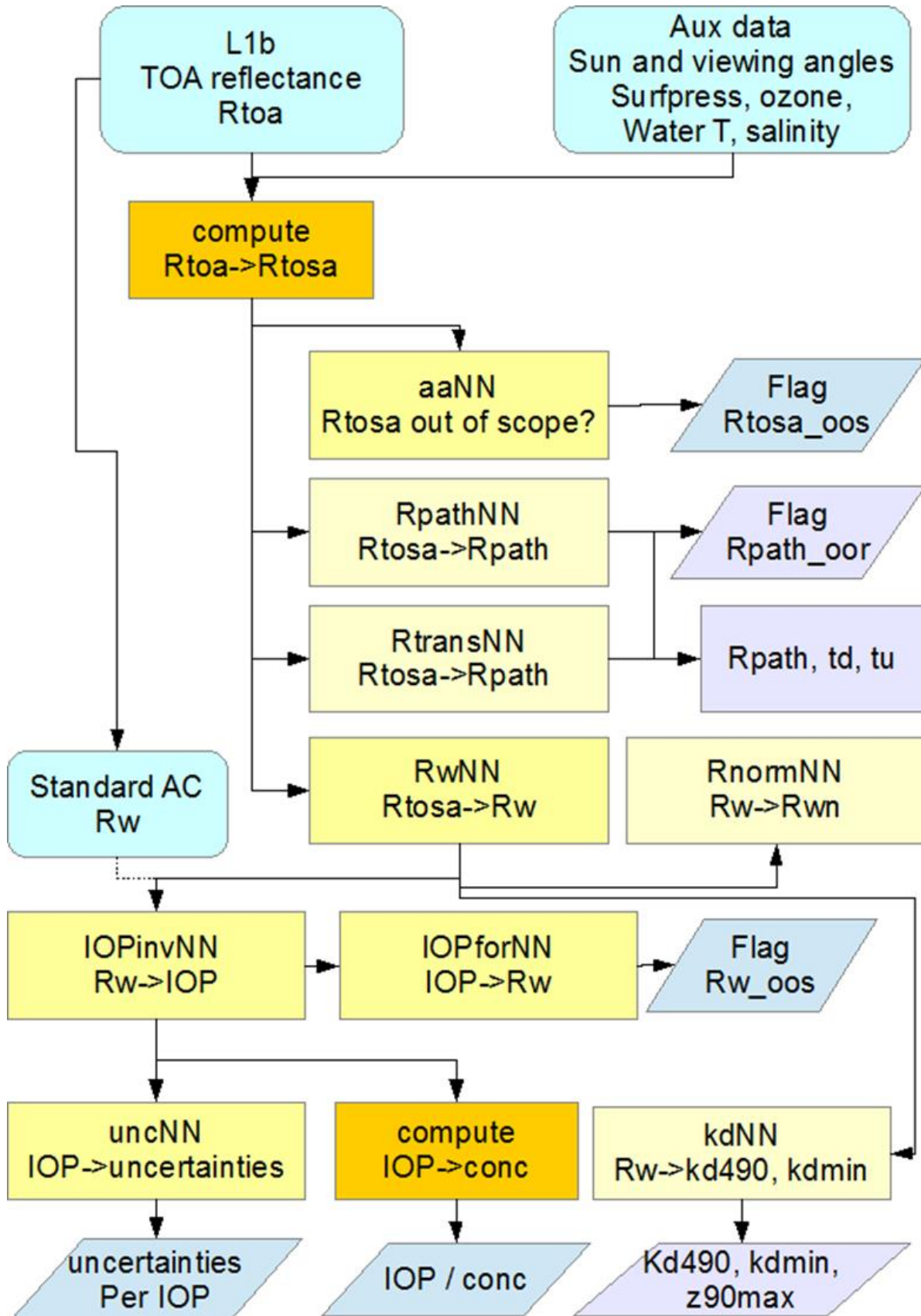
Figure 2-30: The system of neural networks for Case-2 water

4th MERIS data reprocessing
Evolutions and Validation report

Ref.: MER4RP Validation Report
Version: 1.0
Date: 01/04/2019
Page: 44

2.4.5 Land Processing

2.4.5.1 Atmospheric corrections over land

Pressure adjustment and smile correction: Handling of molecular scattering is improved using accurate pixel elevation, better modelling of the relationship between pressure and elevation, better modelling of the Rayleigh optical thickness (*Bodhaine et al., 1999*) and improved correction of meteorological variation of atmospheric pressure.

Nature of the change: *Algorithm / ADF values*

The smile correction, the pressure adjustment, and the latitude-dependence of the ROT (Bodhaine et al., 1999) are fully accounted for through a correction performed with an equivalent ROT shift as done over water targets. The ROT employed in this adjustment corresponds to the actual (or observed) value of ROT over the target, *i.e.* the theoretical ROT adjusted to the pixel wavelength, the local pressure computed with the new surface pressure determination (*i.e.* the 'P-z' algorithm), and the new modelling of ROT. After the removal of atmospheric effects, the smile correction is finally performed on the Bottom of Rayleigh Reflectance (BRR).

2.4.5.2 Land aerosols remote sensing (AOT at 442 nm (T442) and Angström exponent (A442))

All evolutions and their validation are described in [ATBD-2.15].

The BRDF model of the Land Aerosol Remote Sensing (LARS) targets has been revised.

Nature of the change: *ADF values and Algorithm*

There is no more reference to the Dense Dark Vegetation (DDV) concept and related LUT's. Now, $\widetilde{\rho_{LARS}}$, the LARS directional reflectance normalized to a reference direction ($\widetilde{\theta_s} = 45°, \widetilde{\theta_v} = 0°, \widetilde{\phi} = 0°$) is linearly related to the observed ARVI (It was the LARS albedo related to the ARVI in MER3RP).

$$\widetilde{\rho_{LARS}} = \alpha_{\widetilde{\rho}}(lat, lon, month, \lambda) \cdot ARVI_{LARS}^{TOA} + \beta_{\widetilde{\rho}}(lat, lon, month, \lambda)$$

The regression coefficients $\alpha_{\widetilde{\rho}}$ and $\beta_{\widetilde{\rho}}$ are stored in LUT's for a spatial grid of 0.5° and a monthly basis.

Following *Vermote et al., 2009*, the LARS BRDF is modeled as:

$$\rho_{LARS}(\theta_s, \theta_v, \phi) = \widetilde{\rho_{LARS}} \frac{1 + VF_1(\theta_s, \theta_v, \phi) + RF_2(\theta_s, \theta_v, \phi)}{1 + VF_1(45,0,0) + RF_2(45,0,0)}$$

4th MERIS data reprocessing
Evolutions and Validation report

Ref.: MER4RP Validation Report
Version: 1.0
Date: 01/04/2019
Page: 45

where the F1 kernel is the Ross-Thick kernel corrected for the hot spot feature and the F2 kernel is the Li Sparse Reciprocal one. The model free parameters V (Volume scattering term within the canopy) and R (Surface scattering term related to surface roughness) are derived from Surface Reflectance time series. They are also linearly correlated with the observed ARVI. A set of regression coeffcients $(\alpha_R, \beta_R, \alpha_V, \beta_V)$ are computed on a monthly basis for a spatial grid of 0.5° and stored in LUT.

The input data source to the calculation of these new LUTs is the MODIS surface reflectance product, namely 'MOD09CMG collection 5' for the period from 2003 to 2007.

In the MER3RP, the LARS BRDF was considered equal to the DDV BRDF (20 models).

It is complemented by other LUT corresponding to the coupling term between the land surface and the atmosphere. They are built from the angle integration of BRDF kernels, F_1 and F_2. The only difference between the MER3RP and the MER4RP is the replacement of the dimension corresponding to 20 DDV models by two different kernels (F_1 and F_2).

The aerosol Angstroem exponent climatology has been updated.

Nature of the change: ADF values

This ADF is used to choose the aerosol model for deriving the main AOT product at 442.5 nm (**T_442**). In the MER3RP, the aerosol model was fixed to a refractive index of 1.44 and an Angstroem exponent of 1.

The procedure to build the new ADF is defined by the following steps:

- Used the data source namely 'MODIS Aqua Land Aerosol Monthly Level-3 (L3) product on the CMG grid (1°x1°), MYD08_M3 collection 6' and select the dataset is 'Deep_Blue_Angstrom_Exponent_Land_Mean_Mean';

- Compute the monthly means for the period from 2003 to 2012;

- Calculate the yearly means for backup in case of lacking monthly means;

- Fill remaining gaps of the backup with an average value of 1.5;

- Rely the Angstroem exponent with the model from MODIS to a model number. There are 78 models with Angstroem exponent varying from 0 to 2.5 by step of 0.1, for three refractive indices (1.33, 1.44, 1.55). Only the value of 1.44 is kept.

A new product is introduced T442_ALPHA and a quality index Q.

Nature of the change: Algorithm

The AOT at 442 nm using the Angstroem exponent retrieved from the image (averaged in 8RR x 8RR pixels boxes), **T442_ALPHA**, is also calculated.

4th MERIS data reprocessing

Evolutions and Validation report

Ref.:   MER4RP Validation Report

Version: 1.0

Date: 01/04/2019

Page: 46

A quality index **Q**, related to the surface darkness through the ARVI (Q=0 meaning a low ARVI or bright target, and Q>8 corresponds toDDV) is also added to the L2 product.

2.4.5.3   Land products

2.4.5.3.1 MGVI

Uncertainty estimates are now provided for the MGVI

2.4.5.3.1.1   MGVI uncertainty estimates

Nature of the change: *Algorithm (MGVI uncertainty estimates)*

MER3RP known issue: The MGVI is subject to uncertainty due to errors in the input top-of-aerosol reflectance values, however a quantitative estimate of this uncertainty was not previously provided.

MER4RP evolution: Uncertainty estimates are now provided for the MGVI, based on uncertainty propagation calculations and estimated model errors.

2.4.5.3.2 MTCI

The MTCI range limit has been extended; the associated flags have been revised and the uncertainty is now esimtated.

2.4.5.3.2.1   MTCI range limit

Nature of the change: *ADF values (MTCI range limits)*

MER3RP: The range of MTCI values was previously restricted to the range from 0 to 5.5. However, some investigations suggested that this range could be extended without increasing the probability of incorportating saturated pixels.

MER4RP evolution: The range limits of possible values of MTCI have been updated so that they MTCI values between 0 and 6.5 are now considered valid.

2.4.5.3.2.2   MTCI uncertainty estimates

Nature of the change: *Algorithm (MTCI uncertainty estimates)*

MER3RP known issue: The MTCI is subject to uncertainty due to errors in the input top-of-aerosol reflectance values, however a quantitative estimate of this uncertainty was not previously provided.

4th MERIS data reprocessing

Evolutions and Validation report

Ref.: MER4RP Validation Report

Version: 1.0

Date: 01/04/2019

Page: 47

MER4RP evolution: Uncertainty estimates are now provided for the MTCI, based on uncertainty propagation calculations. The standard uncertainty associated with the MTCI is determined using that associated with the top-of-aerosol reflectance values in each band. It is calculated as

$$\mu(MTCI) = \sqrt{\begin{aligned} &\left(\frac{1}{\rho_{708.75} - \rho_{681.25}}\right)^2 \cdot \mu(\rho_{753.75})^2 \\ &+ \left(\frac{\rho_{681.25} - \rho_{753.75}}{(\rho_{708.75} - \rho_{681.25})^2}\right)^2 \cdot \mu(\rho_{708.75})^2 \\ &+ \left(\frac{\rho_{753.75} - \rho_{708.75}}{(\rho_{708.75} - \rho_{681.25})^2}\right)^2 \cdot \mu(\rho_{681.25})^2 \end{aligned}}$$

where $\mu(MTCI)$ is the standard uncertainty associated with the MTCI, whereas $\mu(\rho_{753.75})$, $\mu(\rho_{708.75})$ and $\mu(\rho_{681.25})$ are the standard uncertainties associated with the top-of-aerosol reflectance values in MERIS B_{10} (753.75 nm), B_{09} (708.75 nm) and B_{08} (681.25 nm).

2.4.5.3.3 MTCI quality flags

Nature of the change: *Algorithm (MTCI quality flags)*

MER3RP known issue: The quality of the MTCI may be influenced by several non-canopy factors, however quality flags to identify pixels that could be affected by these factors were not previously provided.

MER4RP evolution: A number of new quality flags are now provided for soil, viewing and illumination geometry, range and radiometry, enabling the best quality pixels to be selected by the user.

The poor soil flag is based on the soil discrimination index (SDI), and is used to identify pixels corresponding to bare soil or very sparse vegetation that may provide less reliable MTCI values when compared to those acquired over denser vegetation (Table 1). The SDI takes the form

$$SDI = \frac{\rho_{NIR}/\rho_{red}}{\rho_{red}/\rho_{green}} = \frac{\rho_{753.75}/\rho_{681.25}}{\rho_{681.25}/\rho_{560}}$$

where $\rho_{753.75}$, $\rho_{681.25}$, and ρ_{560} are top-of-aerosol reflectance values in MERIS B_{10} (753.75 nm), B_{08} (681.25 nm) and B_{05} (560 nm).

The viewing and illumination geometry flag makes useful the observer zenith angle (OZA) and the solar zenith angle (SZA) to determine whether the angular characteristics associated with each pixel are best, good, fair or poor with respect to the calculation of the MTCI and the potential bidirectional reflectance distribution function (BRDF) effects (Table 1).

The good 'range' flag means that the calculated MTCI values are well included within the range limits (0 to 6.5). The 'bad radiometry' flag identifies pixels for which the MTCI values are not provided. This could be due to the fact that they are outside the range limits (0 to

4th MERIS data reprocessing
Evolutions and Validation report

Ref.: MER4RP Validation Report
Version: 1.0
Date: 01/04/2019
Page: 48

6.5), or were calculated from bad top-of-aerosol reflectance values, which are identified using a series of spectral tests (Table 1).

Table 1: Summary of MTCI quality flags and the conditions under which they are raised.

Flag	Condition
LP_QS_MTCI_POOR_SOIL	SDI ≤ 0.9
LP_QS_MTCI_BEST_GEOMETRY	Default
LP_QS_MTCI_GOOD_GEOMETRY	OZA > 30° AND OZA ≤ 40° SZA > 40°
LP_QS_MTCI_FAIR_GEOMETRY	OZA ≤ 40° SZA ≤ 40°
LP_QS_MTCI_POOR_GEOMETRY	OZA > 40°
LP_QS_MTCI_GOOD_RANGE	MTCI > 0 AND MTCI ≤ 6.5
LP_QS_MTCI_BAD_RADIOMETRY	MTCI ≤ 0 OR MTCI > 6.5 OR $\rho_{681.25} \leq 0$ OR $\rho_{681.25} \geq 0.2$ OR $\rho_{708.75} \leq 0$ OR $\rho_{753.75} \leq 0.1$ OR $\rho_{753.75} - \rho_{681.25} < 1\ 10^{-6}$ OR $\rho_{865} - \rho_{681.25} < 0.05$

2.4.6   Flags

The flags are split into categories and/or branch product; PCDs become Product Confidence "PC" associated to the product.

Nature of the change: *ADF values / Algorithm*

The new product format allows to store more flags in the product.

A new naming convention has been introduced to split the flags into categories and/or branch product:

- "ES" earth surface flags (e.g. ES_LAND_MAP, ES_COASTLINE, ES_TIDAL_MAP…). These flags characterise the surface of a pixel regardless of the current observation condition. I.e. a pixel called "ES_LAND_MAP" or "ES_LAND_RADIOMETRIC" is above land, and not ocean, regardless of the cloud conditions. The flags which have "_MAP" in their names are taken from a static auxiliary dataset, while flags having "_RADIOMETRIC" in their names are derived from test using the MERIS measurement. This allows to react on changing conditions but is only possible where the surface is seen, i.e. no clouds.

- "CC" cloud classification flags (e.g. CC_CLOUD, CC_CLOUD_SURE, CC_CIRRUS…)

- "CO" common flags (e.g. CO_INVALID, CO_COSMETIC, CO_DUPLICATED…). These flags are mainly copied from the Level 1b product

- The following flags are specific for the 3 processing branches, i.e. land, water and cloud processing. The flag names have 3 parts XX_YY_ZZZZZ. XX identifies the processing

4th MERIS data reprocessing

Evolutions and Validation report

Ref.:   MER4RP Validation Report

Version: 1.0

Date: 01/04/2019

Page: 49

branch, i.e. WP (water product), LP (land product), CP (cloud product). YY marke the type of the flag and ZZZZ is the individual flag.

- "WP" water product

    - "WP_QS" quality and science flags (e.g. WP_QS_WHITE_CAPS, WP_QS_BPAC_ON…)

    - "WP_PC" product confidence flags (e.g. WP_PC_CHL_OC4ME_FAIL, WP_PC_T865_FAIL…)

- "CP" cloud product

    - "CP_QS" quality and science flags (e.g. CP_QS_OUT_OF_RANGE_COT…)

    - "CP_PC" product confidence flags (e.g. CP_PC_COT_FAIL…)

- "LP" land product

    - "LP_QS" quality and science flags (e.g. LP_QS_OUT_OF_RANGE_MTCI…)

    - "LP_PC" product confidence flags (e.g. LP_PC_MTCI_FAIL…)

Until MER3RP, the quality indicator where assigned to measurement data set and named "Product Confidence Flag" (PCD), e.g. PCD_15. The value PCD == TRUE indicated poor quality. This was confusing for unexperienced users.

In the new system, there is for each variable (e.g. OC4ME) one product confidence flag (e.g. 'LP_PC_OC4ME_FAIL'). The name of the flag is now consistent with the TRUE/FALSE state.

4th MERIS data reprocessing
Evolutions and Validation report

Ref.: MER4RP Validation Report
Version: 1.0
Date: 01/04/2019
Page: 50

2.5 LUTs evolution

This section described the evolution of LUTs used as inputs to the standard atmospheric correction algorithms over land and water, following the changes and improvements brought in the L2 algorithms implemented in the MER4RP. We restrict here to a brief description of LUTs generated by Parbleu for the MER4RP. For more details about the computations of LUTs and the formatting of ADFs, the reader must refer to RD-6.

The LUTs that either evoluted or created for the MER4RP are listed hereafter:

▪ ROT_bod[λ, lat]

  ◆ This new LUT contains the values of ROT computed at the 15 MERIS wavelengths (λ) with the model of Bodhaine et al. (1999), for a standard barometric pressure of 1013.25 hPa and a set of 91 latitudes (lat) varying from 0 to 90º with a step of 1º. These calculations have been conducted for a CO_2 abundance of 390 ppm that is a global average value for the whole period of the MERIS mission (value reached in 2007).

  ◆ Rather to regenerate all the MERIS LUTs dependent on ROT for the MER4RP that represents a heavy task, the QWG decided to apply the new pressure (or Rayleigh) adjustment scheme with an equivalent ROT shift to account for this change in the modelling.

  ◆ This 'ROT_bod' LUT is used as input to the new pressure (or Rayleigh) adjustement scheme introduced in the MER4RP.

  ◆ <u>LUT dimensions</u>: 15 λ x 91 lat

▪ RSH[lat]

  ◆ This new LUT includes the values of the Rayleigh scale height (RSH; H_R) at sea level (z=0), computed with the standard US62 model for a set of 91 latitudes (lat) varying from 0 to 90º with a step of 1º. This LUT describes the variation of the acceleration gravity (g) with the latitude (lat).

  ◆ This 'RSH' LUT is used as input to the new surface pressure determination (so-called the 'P-z' algorithm) implemented in the MER4RP.

  ◆ <u>LUT dimension</u>: 91 lat

▪ dRho_Ray[sza, vza, raa, rot]

  ◆ This new LUT comprises the values of the Rayleigh reflectance calculated for the elementary molecular layer used in the new pressure (or Rayleigh) adjustment scheme. They have been generated with an in-house tool developed by ParBleu. The latter provides as output the Rayleigh reflectance of an elementary layer characterized by 21 values of ROT (rot is ranged from 0 to 0.1 by a step of 0.005)

4th MERIS data reprocessing
Evolutions and Validation report

Ref.: MER4RP Validation Report
Version: 1.0
Date: 01/04/2019
Page: 51

for the MERIS Sun/view geometries defined by 23 solar zenith angles (*sza* includes the zenith direction plus the first 22 *Gaussian* angles from the quadrature defined for 24 discrete directions in zenith), 13 view zenith angles (*vza* includes the nadir direction plus the first 12 *Gaussian* angles from the same quadrature as for *sza*), and 25 relative azimuth angles (*raa* is regularly spaced from 0 to 180° by a step of 7.5°).

◆ This 'dRho_Ray' LUT is used as input to the new pressure (or Rayleigh) adjustement scheme implemented in the MER4RP.

◆ <u>LUT dimensions</u>: 23 *sza* x 13 *vza* x 25 *raa* x 21 *rot*

▪ dTrs_Ray[*sza*, *rot*]

◆ This new LUT contains the values of the Rayleigh transmittance (diffuse + direct) for the downward atmospheric path of the elementary molecular layer. They are generated with the same tool as for the Rayleigh reflectance LUT (dRho_Ray), using as inputs the same sets of ROT (21 *rot*) and solar zenith angle (23 *sza*).

◆ By using the principle of reciprocity, the *Rayleigh* transmittance (diffuse + direct) for the upward atmospheric path could be directly extracted from dTrs_Ray[*sza*, *rot*] for the first 13 values of *sza* (given in an increasing order).

◆ This 'dTrs_Ray' LUT is used as input to the new pressure (or Rayleigh) adjustement scheme implemented in the MER4RP.

◆ <u>LUT dimensions</u>: 23 *sza* x 21 *rot*

▪ Faer[iaer, λ, aot550]

◆ This LUT describes the spectral dependence factor of the aerosol optical thickness (AOT) in the atmospheric column, for each of aerosol assemblages over ocean (*iaer*), each of the 15 MERIS wavelengths (λ), and each of the six (non-null) pre-selected values of total AOT at 550 nm (AOT550). The spectral dependence factor (f_{aer}) is normalized to the reference wavelength at 865 nm.

◆ A set of 80 assemblages are built with the NASA/GSFC aerosol models (8 RHs x 10 FMFs) using the same model in each of three major aerosol layers (*i.e.* the boundary or 'mixing' layer, the troposphere and the stratosphere). For each class of RH, a particular assemblage, namely the 'whiter than white', has been defined with the model corresponding to a FMF of 95% in the boundary layer and 'free-aerosol' in the upper atmosphere.

◆ IOPs of the aerosols (*i.e.* the scattering phase matrix, the extinction and scattering coefficients, and the single scattering albedo) have been recomputed with the *Mie*'s theory for each of 80 NASA/GSFC models. The extinction coefficients have been recombined with the values of AOT550 in the three major layers to provide the f_{aer}-factor for each of 88 assemblages (*iaer*). While the upper atmosphere is

4th MERIS data reprocessing

Evolutions and Validation report

Ref.: MER4RP Validation Report

Version: 1.0

Date: 01/04/2019

Page: 52

optically frozen with an AOT550 fixed to 0 for each of 8 particular assemblages and, 0.025 in the troposphere and 0.005 in the stratosphere for each of 80 other assemblages, the mixing layer is optically variable with an $aot550$ in {0.01, 0.03, 0.1, 0.3, 0.5, 0.8}.

- The values of f_{aer}-factor for the 18 DUST assemblages from the previous generation (MER3RP) have been kept being stored at the end of this new 'Faer' LUT.

- This 'Faer' LUT is used as input to the aerosol remote-sensing algorithm over water implemented in the MER4RP. However, it should be noted that the f_{aer} values are obsolete for the 88 assemblages but useful for the DUSTs to estimate the atmospheric transmittance with the approximation of Gordon and Wang (1994).

- <u>LUT dimensions</u>: 106 $iaer$ x 15 λ x 6 $aot550$

- AOT865[$iaer$, $aot550$]

  - This LUT provides the AOT at 865 nm (AOT865) in the atmospheric column, for each of the 106 aerosol assemblages (including the DUSTs) over ocean and each of 6 values of AOT550 in the mixing layer. The values of AOT865 have been refreshed only for the 88 assemblages (including the particular ones).

  - The values of AOT865 for the 18 DUST assemblages from the previous generation (MER3RP) have been kept to be stored at the end of this new 'AOT865' LUT.

  - This 'AOT865' LUT is used as input to the aerosol remote-sensing algorithm over water implemented in the MER4RP.

  - <u>LUT dimensions</u>: 106 $iaer$ x 6 $aot550$

- SSA[$iaer$, λ]

  - This LUT describes the single scattering albedo (SSA) of aerosols in the atmospheric column, for each of the 106 aerosol assemblages (including the DUSTs) over ocean and each of the 15 MERIS wavelengths (λ). The values of SSA have been refreshed only for the 88 assemblages (including the particular ones).

  - The values of SAA for the 18 DUST assemblages from the previous generation (MER3RP) have been kept to be stored at the end of this new 'SSA' LUT.

  - This 'SSA' LUT is used as input to the aerosol remote-sensing algorithm over water implemented in the MER4RP. As for the 'Faer' LUT, only the SSA values associated with the DUST assemblages are really employed for estimating the atmospheric transmittances with the approximation of Gordon and Wang (1994).

  - <u>LUT dimensions</u>: 106 $iaer$ x 15 λ

4th MERIS data reprocessing
Evolutions and Validation report

Ref.:   MER4RP Validation Report
Version: 1.0
Date: 01/04/2019
Page: 53

- Rho_Ray[λ, w_s, sza, vza, raa]

  - This LUTs provides the Rayleigh reflectances simulated at each of the 15 MERIS wavelengths (λ) over 3 wind-roughened black sea surfaces (w_s =1.5, 5, 10 m.s^{-1}), for all the Sun/view geometries described by 23 solar zenith angles (sza), 13 view zenith angles (vza) and 25 relative azimuthal angles (raa), and a given reference pressure (P_{ref}). The angular geometry is the same as that for the 'dRho-Ray' LUT. For these computations, the Rayleigh scattering is modelled with an anisotropic molecular phase function using a depolarization factor of 0.0279, with a ROT derived from the formulation of Hansen and Travis (1974) and a vertical distribution of the molecules according to an exponential decrease weighted by a RSH of 8 km. Moreover, the Sun glint contribution is not accounted for.

  - This 'Rho_Ray' LUT has been generated with the MERIS auxiliary data tool (MERISAT; RD-9) for each P_{ref} selected in {1040, 1013.25, 970, 900, 800, 700} hPa, that yields to a production of 6 'Rho_Ray' LUTs.

  - These 'Rho_Ray' LUTs are used as input to the standard atmospheric correction algorithm implemented in the MER4RP.

  - <u>Number of LUTs:</u>   6 'Rho_Ray' LUTs associated with 6 values of P_{ref}.

  - <u>LUT dimensions:</u>   15 λ x 3 w_s x 23 sza x 13 vza x 25 raa

- XC[$iaer$, λ, w_s, sza, vza, raa, k]

  - This LUT gives the coefficients of a second order polynomial, expressing the ratio in TOA reflectance between a realistic scattering atmosphere (aerosols + molecules) and a pure molecular scattering atmosphere, Rho_Path/Rho_Ray, as function of AOT in the atmospheric column. These polynomial coefficients (k=[0;2]) depend on the aerosol assemblage ($iaer$), the MERIS wavelength (λ), the wind-speed above sea level (w_s), and the Sun/view geometries (sza, vza, raa) as described above for the 'Rho_Ray' LUT.

  - An intermediate TOA reflectance LUT, Rho_Path[λ, w_s, sza, vza, raa, $aot550$, $iaer$], has been recomputed at eéeach of the 15 MERIS wavelengths (λ) over 3 wind-roughened black sea surfaces (w_s =1.5, 5, 10 m.s^{-1}), for all the Sun/view geometries (23 sza, 13 vza, 25 raa) as described for the 'dRho-Ray' LUT, for each of the 11 assemblages composed with the 10 models from a given class of RH plus one particular assemblage (FMF=95%), for each of the 7 pre-selected values of total AOT550 including the pure Rayleigh case ($aot550$ in {0, 0.01, 0.03, 0.1, 0.3, 0.5, 0.8}), and for a given reference pressure (P_{ref}). For these computations, the Rayleigh scattering is modelled as for the 'Rho_Ray' LUT and the aerosol scattering with the assemblages as described above (see 'Faer' LUT). Moreover, the Sun glint contribution is not included in these TOA simulations.

  - Both the radiative transfer computations and the application of the polynomial fit on Rho_Path/Rho_Ray to extract the sets of coefficients (k) have been achieved with MERISAT. This 'XC' LUT has been provided for each class of RH chosen in {30%,

4th MERIS data reprocessing
Evolutions and Validation report

Ref.:   MER4RP Validation Report
Version: 1.0
Date: 01/04/2019
Page: 54

50%, 70%, 75%, 80%, 85%, 90%, 95%} and each P_{ref} selected in {1040, 1013.25, 970, 900, 800, 700} hPa, that yields to a production of 48 'XC' LUTs.

- Moreover, the sets of polynomial coefficients provided at a standard barometric pressure (1013.25 hPa) for the 18 DUST assemblages in the previous generation (MER3RP) have been stored in each of the 48 'XC' LUTs. To maintain the same dimension in '*iaer*' (a total of 34 assemblages was used for the MER3RP), we duplicated five times the results obtained for the particular assemblage.

- These 'XC' LUTs are used as input to the standard atmospheric correction algorithm over water implemented in MER4RP.

- <u>Number of LUTs:</u>   48 'XC' LUTs associated with the 6 values of P_{ref} and 8 values of RH.

- <u>LUT dimensions:</u>   34 *iaer* x 15 λ x 3 w_s x 23 *sza* x 13 *vza* x 25 *raa* x 3 k

- Tdown[*iaer, w_s, λ, sza, aot550*]

   - This LUT provides the total (direct + diffuse) downward atmospheric transmittance computed at each of the 15 MERIS wavelengths (λ) over 3 wind-roughened black sea surfaces (w_s =1.5, 5, 10 m.s⁻¹), for illumination conditions as described for the 'dRho-Ray' LUT (23 *sza*), for each of the 11 assemblages composed with the 10 models from a given class of RH plus 1 particular assemblage (FMF=95%), for each of the 7 pre-selected values of total AOT550 including the pure Rayleigh case (*aot550* in {0, 0.01, 0.03, 0.1, 0.3, 0.5, 0.8}), and for a given reference pressure (P_{ref}). Both the Rayleigh and the aerosol scattering are modelled as for the 'XC' LUT. This 'Tdown' LUT includes the coupling term between the atmospheric scattering and the Fresnel reflection at BOA.

   - The radiative transfer computations have been completed with MERISAT, and a 'Tdown' LUT has been provided for each class of RH chosen in {30%, 50%, 70%, 75%, 80%, 85%, 90%, 95%} and each P_{ref} selected in {1040, 1013.25, 970, 900, 800, 700} hPa. This yielded to a production of 48 'Tdown' LUTs.

   - These 'Tdown' LUTs are employed as input to the standard atmospheric correction algorithm over water implemented in MER4RP.

   - <u>Number of LUTs:</u>   48 'Tdown' LUTs associated with the 6 values of P_{ref} and 8 value of RH.

   - <u>LUT dimensions:</u>   16 *iaer* x 3 w_s x 15 λ x 23 *sza* x 7 *aot550*

- Tup[*iaer, λ, vza, aot550*]

   - This LUT provides the total (direct + diffuse) upward atmospheric transmittance computed at each of the 15 MERIS wavelengths (λ) over a black surface, for viewing conditions (13 *vza*) as described for the 'dRho-Ray' LUT, for each of the 11 assemblages composed with the 10 models from a given class of RH plus 1

4th MERIS data reprocessing
Evolutions and Validation report

Ref.:   MER4RP Validation Report
Version: 1.0
Date: 01/04/2019
Page: 55

particular assemblage (FMF=95%), for each of the 7 pre-selected values of total AOT550 including the pure Rayleigh case (*aot550* in {0, 0.01, 0.03, 0.1, 0.3, 0.5, 0.8}), and for a given reference pressure (P_{ref}). Both the Rayleigh and the aerosol scattering are modelled as for the 'XC' LUT.

- The radiative transfer calculations have been achieved with MERISAT, and the 'Tup' LUT has been provided for each class of RH chosen in {30%, 50%, 70%, 75%, 80%, 85%, 90%, 95%} and each P_{ref} selected in {1040, 1013.25, 970, 900, 800, 700} hPa. This yielded to a production of 48 'Tup' LUTs.

- These 'Tup' LUTs are employed as input to the standard atmospheric correction algorithm over water implemented in the MER4RP.

- <u>Number of LUTs:</u>   48 'Tup' LUTs associated with the 6 values of P_{ref} and 8 values of RH.

- <u>LUT dimensions:</u>   16 *iaer* x 15 λ x 13 *vza* x 7 *aot550*

- MERIS-O2_Filters [*ifilt*]

   - This LUT describes the smile of the O_2 band for each period of the MERIS mission. It is defined by two sets of 21 shifted O_2 filters of 0.1 nm around two nominal wavebands at 760.25 nm (1st period; before December 24th, 2002) and 761.75 nm (2nd period; after December 24th, 2002). The spectral overlapping between these two smiles yields to a set of 33 O_2 filters (*ifilt*), the centre wavelengths are stored in this LUT. They are ranged from 759.5 to 762.7 nm.

   - These O_2 filters have been used by FUB to produce the set of *k*-binning coefficients in each atmospheric layer of the US62 standard profile (20 layers). The latter are employed for estimating the O_2 transmission function in each atmospheric layer with the help of an exponential sum fitting technique (ESFT).

   - <u>LUT dimension:</u>   33 *ifilt*

- TO2-Ray_Ocean[*ifilt*, *sza*, *vza*, *raa*]

   - This LUT describes the O_2–Rayleigh transmittance over ocean in the 33 shifted O_2 filters (*ifilt*), and for all the Sun/view geometries (23 *sza*, 13 *vza*, 25 *raa*) as described for the 'dRho-Ray' LUT. Compared with the previous LUT used in the MER3RP (it was based on the primary scattering approximation), this LUT presents now an azimuth-dependence. It has been computed with the RTC/MOMO over a wind-roughened black sea surface (w_s = 5 m.s^{-1}) at a standard barometric pressure (1013.25 hPa) under two molecular atmospheres, *i.e.* for an absorbing and a non-absorbing O_2 atmosphere. The Rayleigh scattering is modelled in the same manner as in the 'Rho_Ray' LUT. Because the TOA signal output by the MOMO includes the Sun glint contribution, a specific scheme has been proposed by ParBleu for removing it from the TOA signal (see RD-5 for more details).

4th MERIS data reprocessing
Evolutions and Validation report

Ref.: MER4RP Validation Report
Version: 1.0
Date: 01/04/2019
Page: 56

- This 'TO2-Ray_Ocean' LUT is used as input to the 'Pscat' algorithm implemented in the MER4RP, for the Rayleigh correction of the O_2 atmospheric transmittance over water.

- LUT dimensions: 33 *ifilt* x 23 *sza* x 13 *vza* x 25 *raa*

- TO2-Ray_Land[*ifilt*, *sza*, *vza*, *raa*]

  - This LUT describes the O_2−Rayleigh transmittance over land in the 33 shifted O_2 filters (*ifilt*), and for all the Sun/view geometries (23 *sza*, 13 *vza*, 25 *raa*) as described for the 'dRho-Ray' LUT. As for the 'TO2-Ray_Ocean' LUT, it has been generated with the RTC/MOMO over a black land surface at a standard barometric pressure (1013.25 hPa) under two molecular atmospheres, *i.e.* for an absorbing and a non-absorbing O_2 atmosphere.

  - This new 'TO2-Ray_Land' LUT replaces the previous one with the correction factor of the surface pressure retrieval (C[*iaer*, *M*, ρ]) used in the MER3RP.

  - This 'TO2-Ray_Land' LUT is employed as input to the 'P1' algorithm implemented in MER4RP, for the Rayleigh correction of the O_2 atmospheric transmittance over land.

  - LUT dimensions: 33 *ifilt* x 23 *sza* x 13 *vza* x 25 *raa*

- TO2-aer_fact[*ifilt*, *sza*, *vza*, *raa*]

  - This LUT comprises the corrective factor for the O_2−aerosol transmittance over ocean, in the 33 shifted O_2 filters (*ifilt*), and for all the Sun/view geometries (23 *sza*, 13 *vza*, 25 *raa*) as described for the 'dRho_Ray' LUT. This factor is computed as the ratio of the O_2−aerosol transmittance over a black surface (*i.e.* calculated with the ESFT coefficients) and the O_2−aerosol transmittance accounting for the coupling between the aerosol scattering and the Fresnel reflection at BOA. This LUT has been generated with an in-house tool developed by ParBleu, in which a Junge's power law defined by a refractive index of 1.44 and an Angstroem exponent of -0.4 has been selected as default model.

  - This LUT replaces the 3 previous LUTs with the Fresnel reflection coefficient, the ratio in aerosol phase function between the forward and backward scattering directions, and the O_2 transmittance for the 'aerosol-Fresnel' coupling term, used in the MER3RP.

  - This 'TO2-aer_fact' is used as input to the 'Pscat' algorithm implemented in the MER4RP, for correcting the Rayleigh-corrected O_2 transmittance over water for the 'aerosol-Fresnel' coupling term.

  - LUT dimensions: 33 *ifilt* x 23 *sza* x 13 *vza* x 25 *raa*

4th MERIS data reprocessing

Evolutions and Validation report

Ref.: MER4RP Validation Report

Version: 1.0

Date: 01/04/2019

Page: 57

- TO2_atm[*ifilt, ipress, sza, vza*]

    - This LUT includes the O_2 atmospheric transmittance in the 33 shifted O_2 filters (*ifilt*), at the 20 pressure levels (*ipress*) varying from TOA to sea surface, and for all the Sun/view zenith angles (23 *sza*, 13 *vza*) as described for the 'dRho_Ray' LUT. It has been generated with an in-house tool developed by ParBleu, which recomputes the O_2 transmittances in the 20 atmospheric layers of a given profile (*here*, the US62 standard model) with the ESFT coefficients in the 33 shifted O_2 filters.

    - This 'TO2_atm' is used as input to the 'Pscat' algorithm implemented in the MER4RP.

    - <u>LUT dimensions</u>:   33 *ifilt* x 20 *ipress* x 23 *sza* x 13 *vza*

4th MERIS data reprocessing
Evolutions and Validation report

Ref.: MER4RP Validation Report
Version: 1.0
Date: 01/04/2019
Page: 58

3 Verification/Validation results

3.1 L1

3.1.1 Radiometry validation

The assessment of the L1 radiometry validation will be performed using DIMITRI after the availability of the MER4RP archive.

3.1.2 Geometric validation

The Amorgos geolocation accuracy has been validated in a specific project GlobCover making extensive use of MERIS FRS data geolocated by the Amorgos post-processing software. The results are described in a dedicated peer reviewed publication:

Bicheron, Patrice; Amberg, Virginie; **Bourg, Ludovic**; Petit, David; Huc, Mireille; Miras, Bastien; Brockmann, Carsten; Hagolle, Olivier; Delwart, Steve; Ranera, Franck; Leroy, Marc; Arino, Olivier. Geo-location assessment of MERIS Globcover ortho-rectified products. IEEE Transactions on Geoscience and Remote Sensing, 49(8):2972 – 2982, (2011). DOI: 10.1109/TGRS.2011.2122337. (On-line here).

The paper abstract summarises the geolocation performance as follows: "*Final results are very satisfactory with an absolute geolocation error of 77 meters rms and a relative geolocation error of 51 meters rms.*"

The results obtained with the Amorgos algorithm embedded in the MERIS Level 1 processor have been succesfully validated against the Amorgos results, quoting the validation report (PO-RP-ACR-GS-0014, Issue 1r0, 15/07/2011): "*mean altitude difference is virtually null with an extreme of 1 m, i.e. 1 coding step, mean ground distance is about 6 cm with a maximum of less 30 cm*".

3.2 Surface classification

Validation method
Validation using PixBox database
L2 and L3 visual inspection

Accuracy goal	MER3RP estimated quality	MER4RP estimated quality
95%	73.5% – 99.5%	96.5%

4th MERIS data reprocessing
Evolutions and Validation report

Ref.: MER4RP Validation Report

Version: 1.0

Date: 01/04/2019

Page: 59

3.2.1 New static land-water mask

Validation of the land/water mask was carried out using 25815 randomly distributed sample points from the PixBox data set.

The "PixBox" database software was developed by M. Zühlke of Brockmann Consult GmbH on the basis of BEAM-VISAT specifically for the purpose of pixel collection. It allows to assign, show and store one or more characteristics for any of pixel on satellite image. Possible attributes are shown in the figure below.
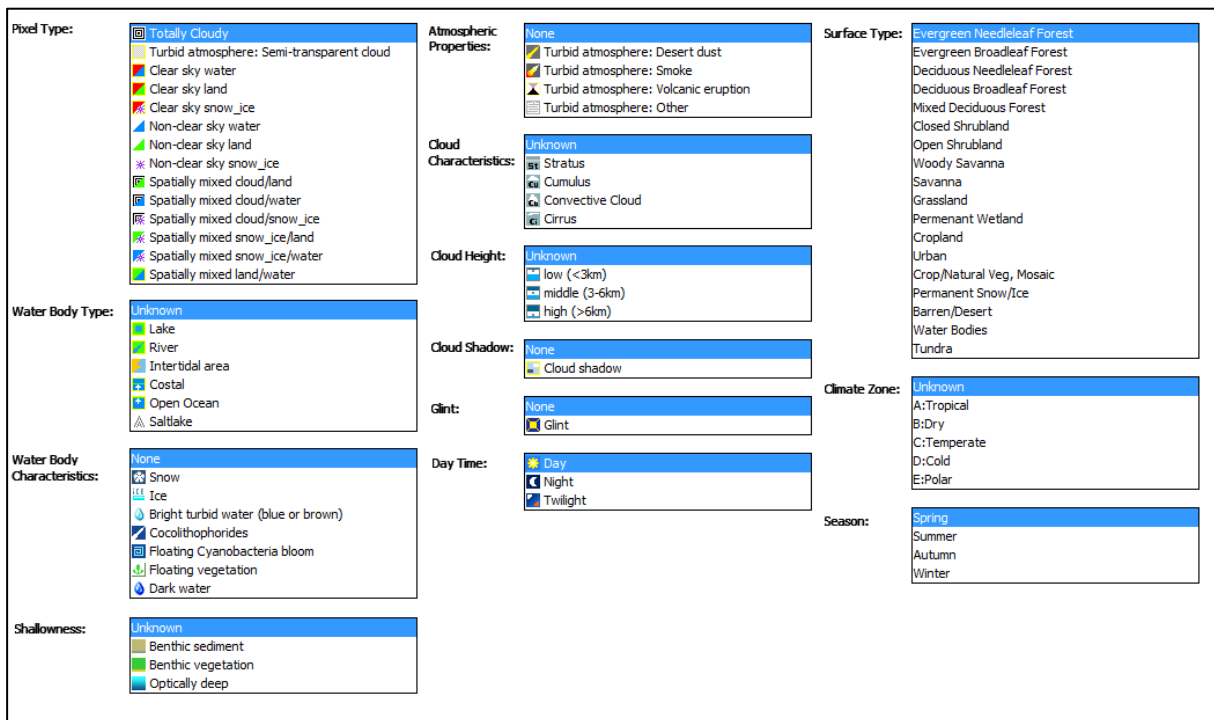
Pixbox's objective is the accumulation of information from satellite images collected solely on the basis of expert opinion. The satellite data may be represented as black-white and RGB images on the computer screen using the linear combination of the available channels. The expert decides which of the pixels to be considered, and then, based solely on his own experience, he assigns some properties (e.g., " cloudless case", "semi-transparent clouds", "coastline", "seaweed", "sun glint", "sand storm", etc.) for each selected pixel to attribute it. The pixel will be ignored, if the expert has a doubt in the determination of its properties.

The information is collected in the form of the "original geo referenced satellite (L1b) data" + "assigned expert attributes" for each selected pixel and is stored as a database. It can be used, for example, for the validation of various automatic techniques.

The "PixBox" database comprises 110,000 samples as shown in the image below.

4th MERIS data reprocessing

Evolutions and Validation report

Ref.: MER4RP Validation Report

Version: 1.0

Date: 01/04/2019

Page: 60

The validation points are shown in Figure 3-1. The dataset is a subset of the complete PixBox database and comprises 16484 land and 9331 water pixels. The classification of these sample points is based on Envisat MERIS RR data. Each sample point was classified by visual interpretation. Thus 100% accuracy is given for these validation points.
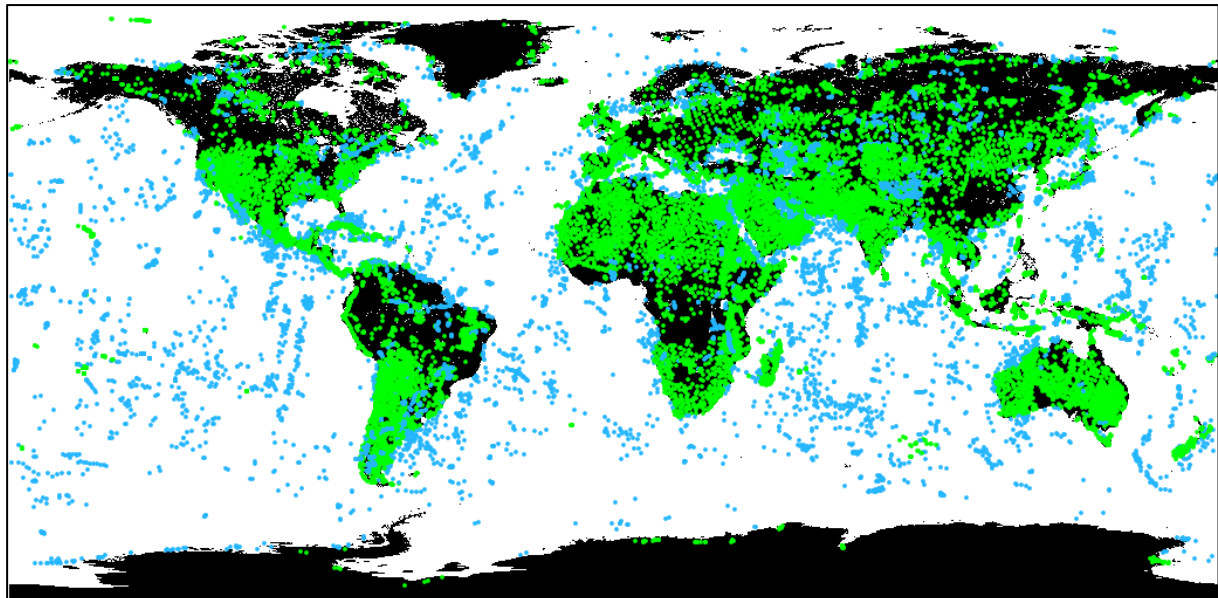
Figure 3-1: 250 randomly distributed sample points.

At these validation points the classification value of the land/water mask was extracted and validated against the sample point classification.

4th MERIS data reprocessing
Evolutions and Validation report

Ref.: MER4RP Validation Report
Version: 1.0
Date: 01/04/2019
Page: 61

The accuracy assessment was conducted using a confusion matrix and calculating producer's, user's and overall accuracy. The results are shown in Table 3-1.

Table 3-1: Confusion matrix showing producer's, user's and overall accuracy.

		Validation Data		
		Land	Water	Row Total
Classification Data	Land	15874	293	16167
	Water	610	9038	9648
	Column Total	16484	9331	25815

Producer's Accuracy	
Water	96.30%
Land	96.86%

User's Accuracy	
Water	98.19%
Land	93.68%

Overall Accuracy	96.50%

The overall accuracy for the land/water mask is 96.5%

3.2.2 Earth Surface flags

The surface classification flags are prefixed by "ES_" which stands for "Earth Surface". They are flags indicating if the pixel is over land or ocean. In the Level 2 product there are two land/ocean flags: one couple which originate from static background maps and which can be identified by the postfix "_MAP", and a second couple which are the result of the radiometric reclassification. The latter can be identified by the postfix "_RADIOMETRIC". Further there are the ES_COASTLINE, ES_TIDAL, and ES_INLAND_WATER flags which all originate from static maps. The ES_FLOODED_RADIOMETRIC and ES_DRY_FALLEN_RADIOMETRIC flags result from reclassification using the actual measurement, as described in chapter 2.4.2.1. An overview of the flags is provided in Figure 3-2.

	Ref.:	MER4RP Validation Report
4th MERIS data reprocessing	Version:	1.0
Evolutions and Validation report	Date:	01/04/2019
	Page:	62

ES_LAND_MAP	Maths		0.5	ES.LAND_MAP
ES_LAND_RADIOMETRIC	Maths		0.5	ES.LAND_RADIOMETRIC
ES_OCEAN_MAP	Maths		0.5	ES.OCEAN_MAP
ES_OCEAN_RADIOMETRIC	Maths		0.5	ES.OCEAN_RADIOMETRIC
ES_COASTLINE	Maths		0.5	ES.COASTLINE
ES_TIDAL_MAP	Maths		0.5	ES.TIDAL_MAP
ES_INLAND_WATER_MAP	Maths		0.5	ES.INLAND_WATER_MAP
ES_FLOODED_RADIOMETRIC	Maths		0.5	ES.FLOODED_RADIOMETRIC
ES_DRY_FALLEN_RADIOMETRIC	Maths		0.5	ES.DRY_FALLEN_RADIOMETRIC

Figure 3-2: Overview of the Earth Surface flags

All Earth Surface flags have been examined by visual inspection of 10 individual images, both in RR and FR resolutions. The following series of images shows the resulting classification at the example of the MERIS scene over central Europe of 23.12.2008.

Figure 3-3 shows the RGB of the scene, with no flags overlaid. The contrast is stretched to better visualise the land and water surface, and to distinguish clouds and thin clouds. Figure 3-4 shows the same RGB but with the ES_LAND_MAP flag overlaid in green. The flag has a transparency of 50% so that different shared of green allow to see the underlying radiometry. All land contours are correctly located. One can see that the land area is also indicated below clouds. This is a new feature which was not available in previous (re)-processings.

The ES_LAND_RADIOMETRIC would look identical at this scale of reduction and is thus not shown. The ES_OCEAN_MAP has been proven to be the complement to the land flag.

4th MERIS data reprocessing

Evolutions and Validation report

Ref.: MER4RP Validation Report
Version: 1.0
Date: 01/04/2019
Page: 63
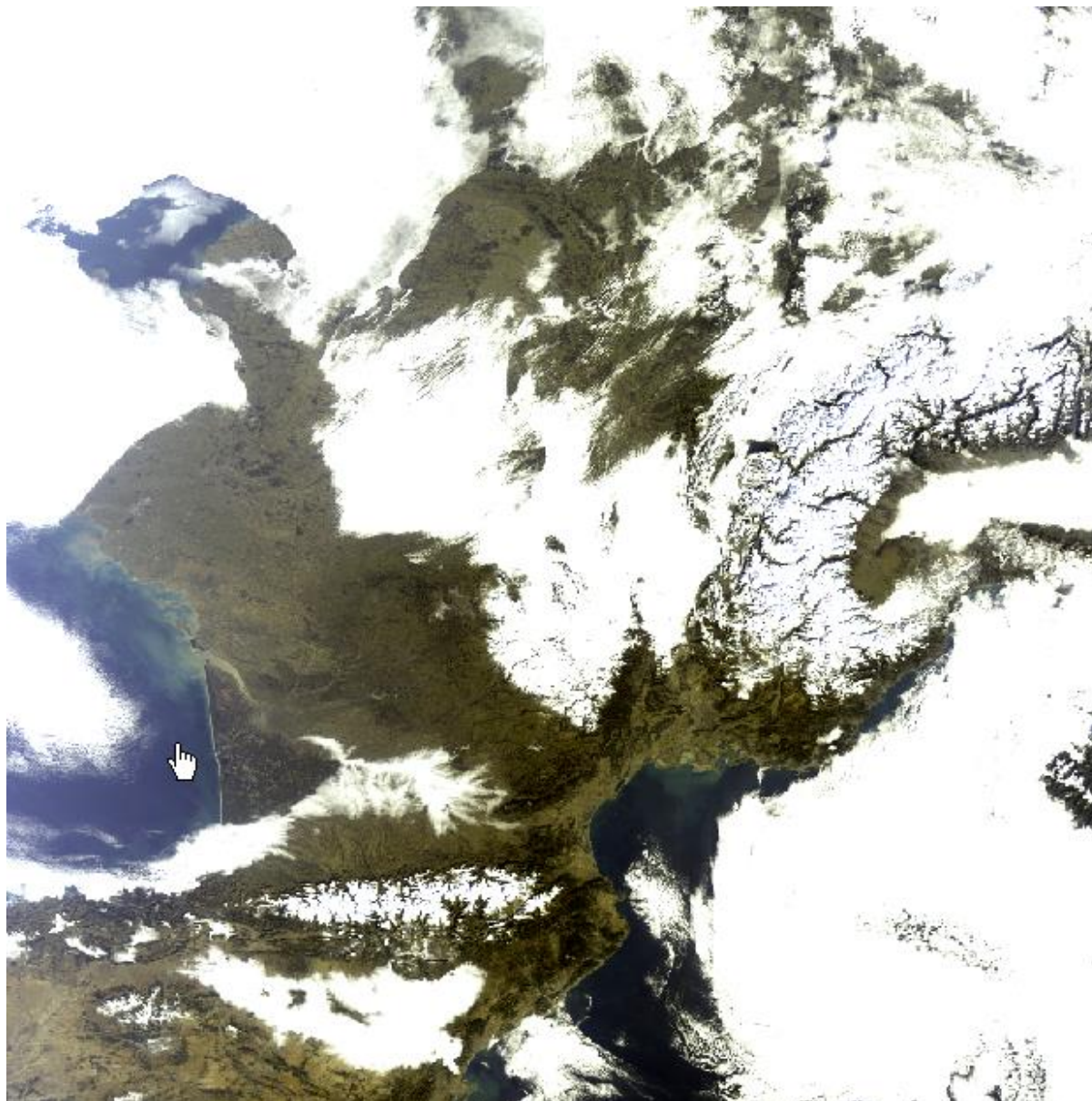
Figure 3-3: Top-of-atmosphere radiances, RGB. MERIS scene of 23.12.2008 over central Europe.

4th MERIS data reprocessing
Evolutions and Validation report

Ref.: MER4RP Validation Report
Version: 1.0
Date: 01/04/2019
Page: 64
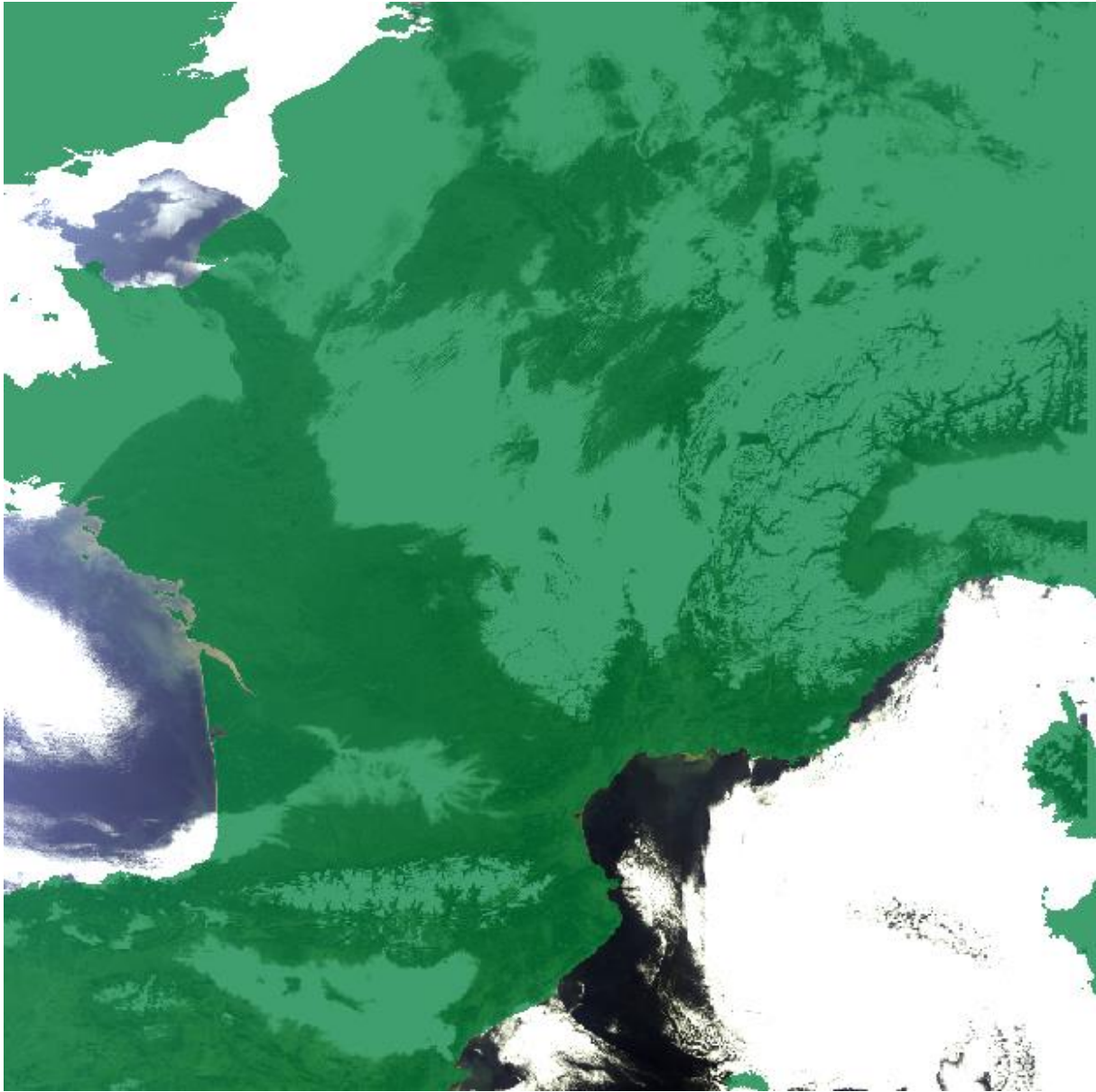
Figure 3-4: Same as above but with the "ES_LAND_MAP" overlaid.

4th MERIS data reprocessing
Evolutions and Validation report

Ref.: MER4RP Validation Report
Version: 1.0
Date: 01/04/2019
Page: 65
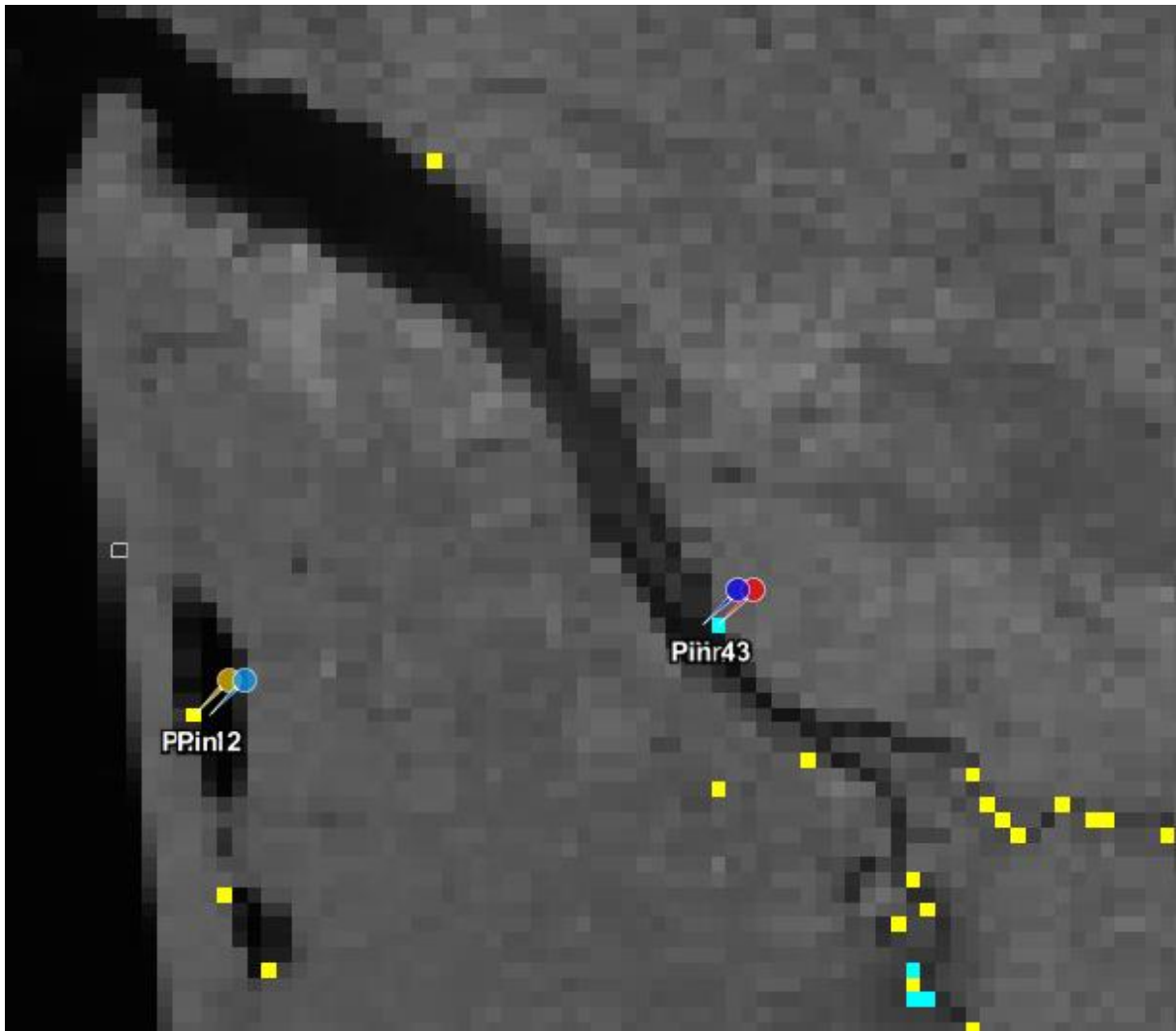
Figure 3-5: Enlargement of the area of the Gironde estuary, showing pixels which are marked as "ES_DRY_FALLEN" (yellow) and "ES_FLOODED_RADIOMETRICALLY" (blue). 4 pixels are marked.

A validation of the correct processing of the radiometric reclassification is shown in Figure 3-5 and Figure 3-6. Figure 3-5 shows a magnification of the estuary of the Gironde. Yellow marked pixels are those which are water in the static map and reclassified as land, while bue ones are land in the static map and reclassified as water. The first are flagged as "ES_DRYFALLEN" while the second ones are flagged "ES_FLOODED_RADIOMETRICALLY".

Two of those pixels are investigated to verify the correctness of the flag. Pin1 is the dry falls pixel, and Pin2 is a direct neighbour of that pixel, which was water in the static map and which was not reclassified. Pin3 is a "ES_FLOODED_RADIOMETRIC" pixel, and Pin4 a neighbour which is not reclassified. The 4 spectra of these pixels are shown in Figure 3-6. Pin1 has an almost identical shape and magnitude as Pin2 in the VIS, up to 675nm. However, it then expresses a clear red-edge signal which identifies it as vegetation. The neighbour pixel 2 remains decreasing as expected for water. The reclassification of pixel 1, and not-reclassification of pixel 2 is correct.

4th MERIS data reprocessing
Evolutions and Validation report

Ref.: MER4RP Validation Report
Version: 1.0
Date: 01/04/2019
Page: 66
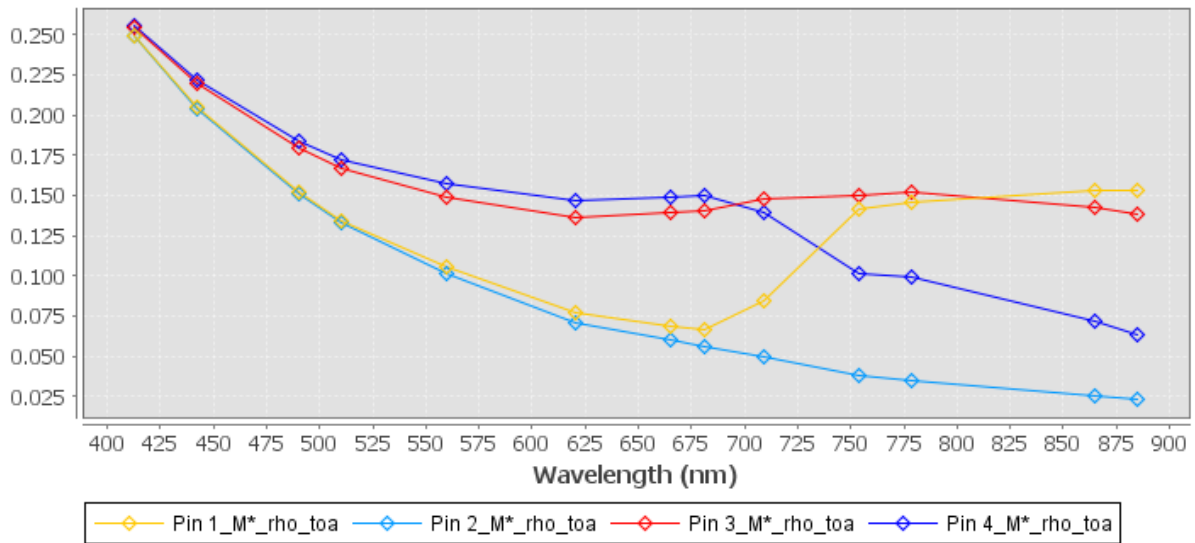
Figure 3-6: Spectra (top-of-atmosphere) of the 4 pixels indicated in the figure above.

The example of pixels 3 and 4 is more difficult. Both pixels are comparably bright in blue, but still possible as turbid water. The gentle increase of the spectrum from 620 nm to 675 nm is difficult to explain. The strong decrease of pixel 4 towards the NIR identifies it as water, while the additional increase of pixel 3, and finally the large difference in absolute reflectance between pixels 3 and 4 identifies pixel 3 as land. The reclassification of pixel 4 as water is probably correct.

3.2.3   Cloud Classification flags

CC_CLOUD	Maths		0.5	CC.CLOUD
CC_CLOUD_AMBIGUOUS	Maths		0.5	CC.CLOUD_AMBIGUOUS
CC_CIRRUS	Maths		0.5	CC.CIRRUS

Figure 3-7: Overview of the Cloud Classification flags

3.2.3.1   Level 2 visual inspection

A total number of 12 products have been processed for visual inspection, in both RR and FR resolution. These products include scenes selected specifically for an assessment of the clouds screening (comprising different cloud and snow situations) and scenes which were selected for validation of ocean and land products, but which also include cloud and serve thus as random samples. Overall, the cloud screening is working satisfactory. The RR and FR products are consistent.

As an example, the scene of 20.04.2005 over Europe is shown in Figure 3-8 - Figure 3-10.

4th MERIS data reprocessing

Evolutions and Validation report

Ref.: MER4RP Validation Report

Version: 1.0

Date: 01/04/2019

Page: 67
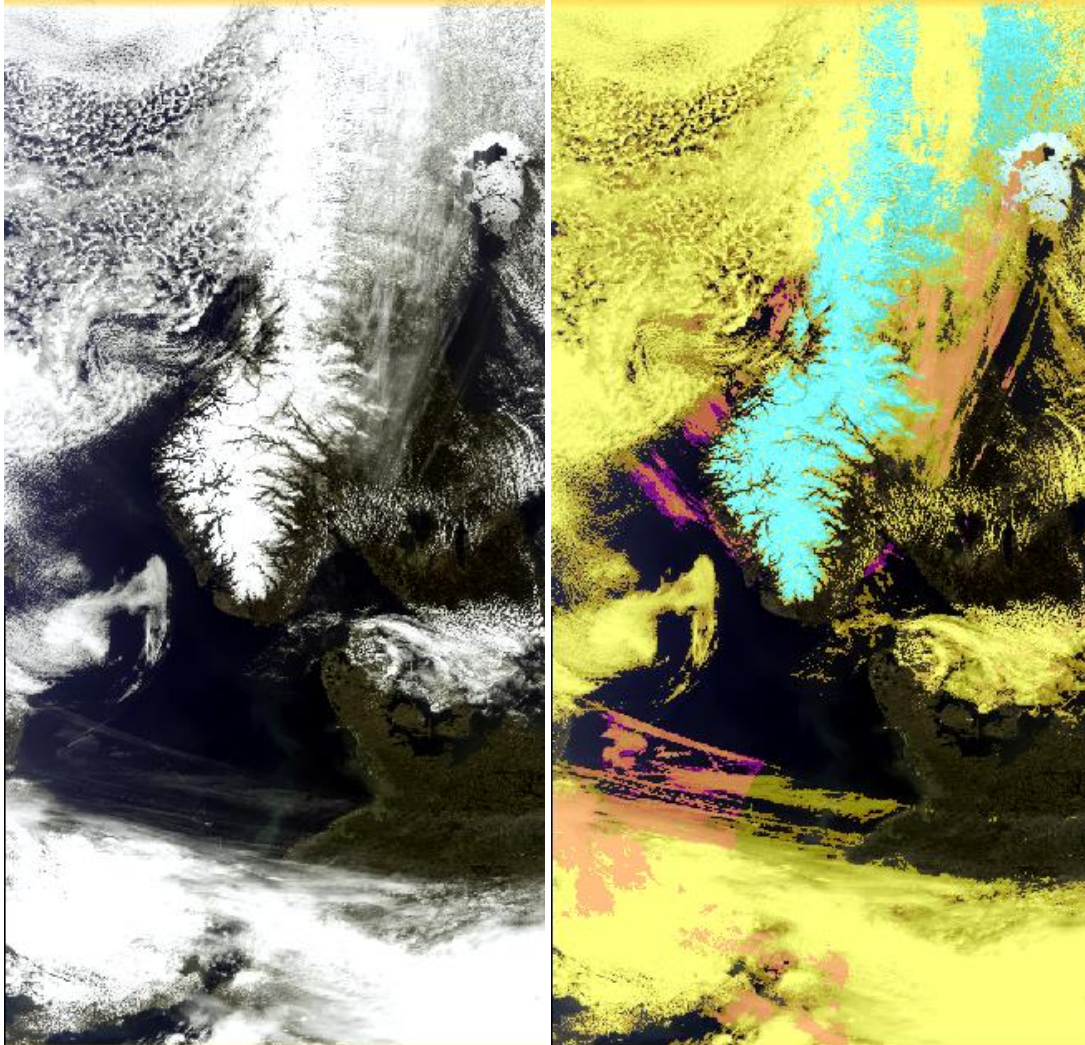
Figure 3-8: MERIS scene of 20.04.2005 over Europe. Left: RGB, Right: RGB with flags overlay: CC_CLOUD (yellow), CC_CLOUD_AMBIGUOUS (orange), CC_CIRRUS (purple), WPQS_SeaIce (light blue1), LP_QS_SNOW_ON_LAND (light_blue2)

4th MERIS data reprocessing
Evolutions and Validation report

Ref.: MER4RP Validation Report
Version: 1.0
Date: 01/04/2019
Page: 68
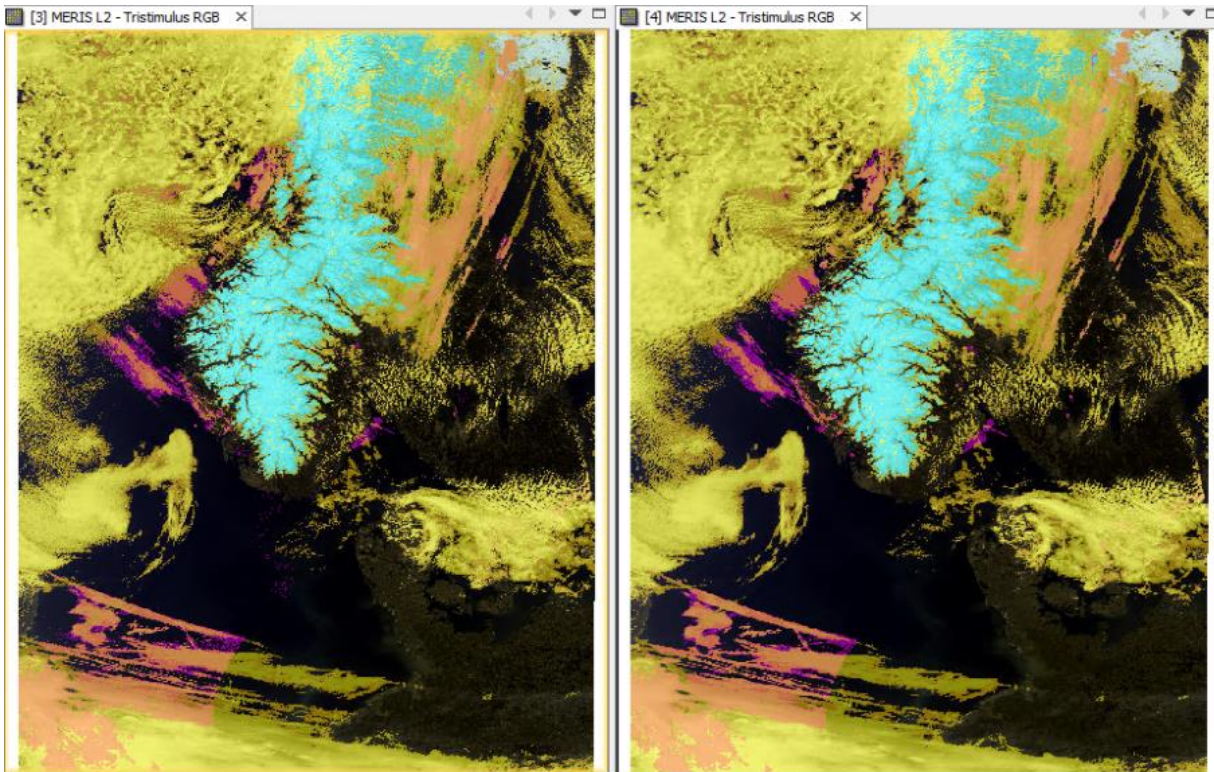
Figure 3-9: Comparison of RR (left) and FR products (right) with cloud and snow/ice flags overlaid.
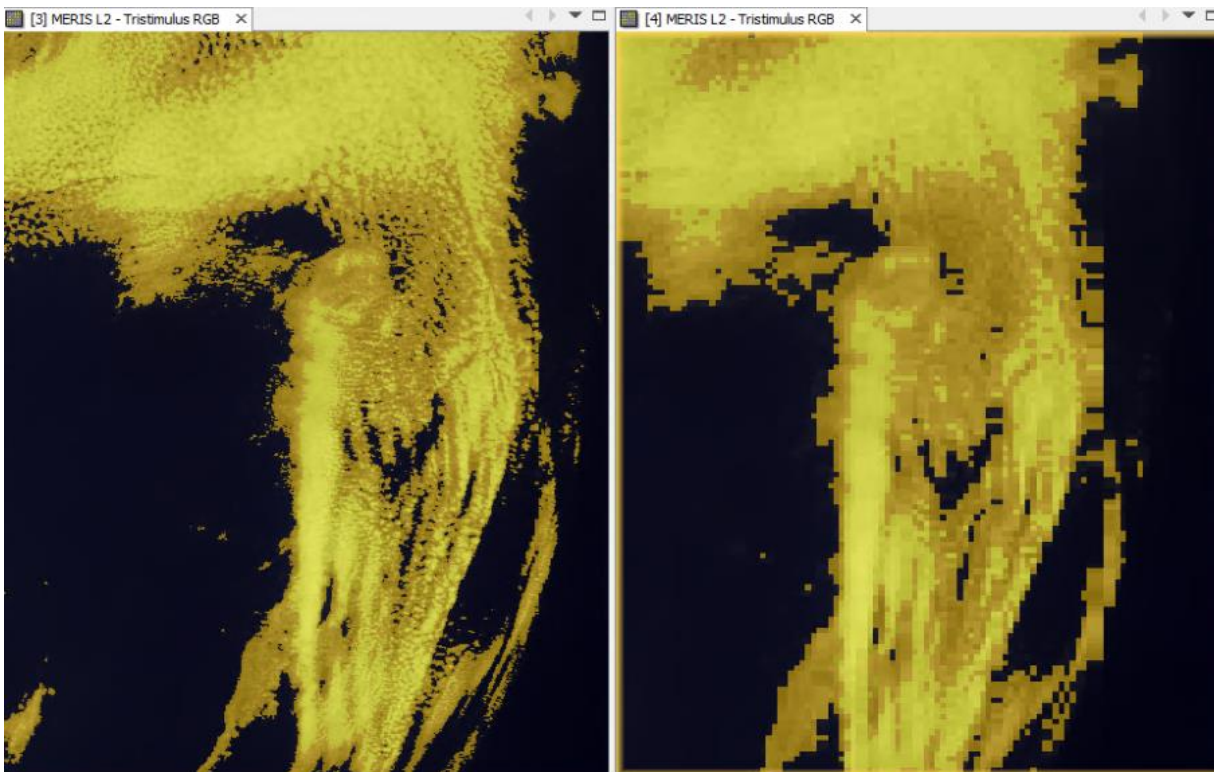
Figure 3-10: Enlargement of the cloud structure in the central western part of the above image, showing full size of the FR image. RR: right, FR: left.

4th MERIS data reprocessing

Evolutions and Validation report

Ref.: MER4RP Validation Report

Version: 1.0

Date: 01/04/2019

Page: 69

3.2.3.2 Level 3 inspection

Monthly composites of various products and flags contained in the Level 2 products were generated. Mean values were calculated for the products, e.g. OC4ME, and occurence of flags was calculated for the flags (e.g. 60% CC_CLOUD indicates that 60% of the pixels falling into a binning cell had CC_CCLOUD=TRUE). Systematic errors, such as no clouds in the western parts of a swath, would become visible in these composites.

The conclusions from this inspection are:

- No systematic error could be established.

- The occurrence of the 'DO_CLOUD' flag (Figure 3-11), as well as the cloud fraction (Figure 3-12), agree with the expected cloud patterns.

- The cloud classification along the Antarctic coast requires further attention as not all clouds may be detected under low sun conditions. This is not visible in all parameters but, for example, the 'CASE-S' flag (Figure 3-13).

- The distribution and absolute value of the HAZE_OVER_WATER flag suggests that these pixels are likely to include also omission errors of the cloud flagging (Figure 3-14).

Some examples are presented below.
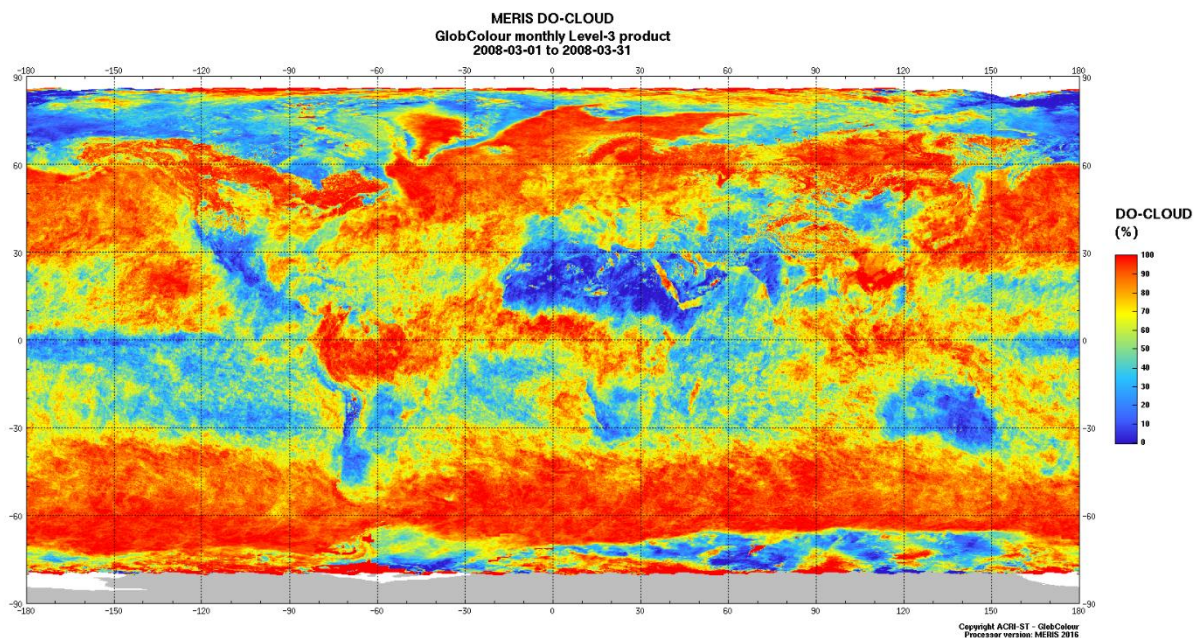
Figure 3-11: DO_CLOUD monthly occurrence, March 2008

4th MERIS data reprocessing

Evolutions and Validation report

Ref.: MER4RP Validation Report

Version: 1.0

Date: 01/04/2019

Page: 70
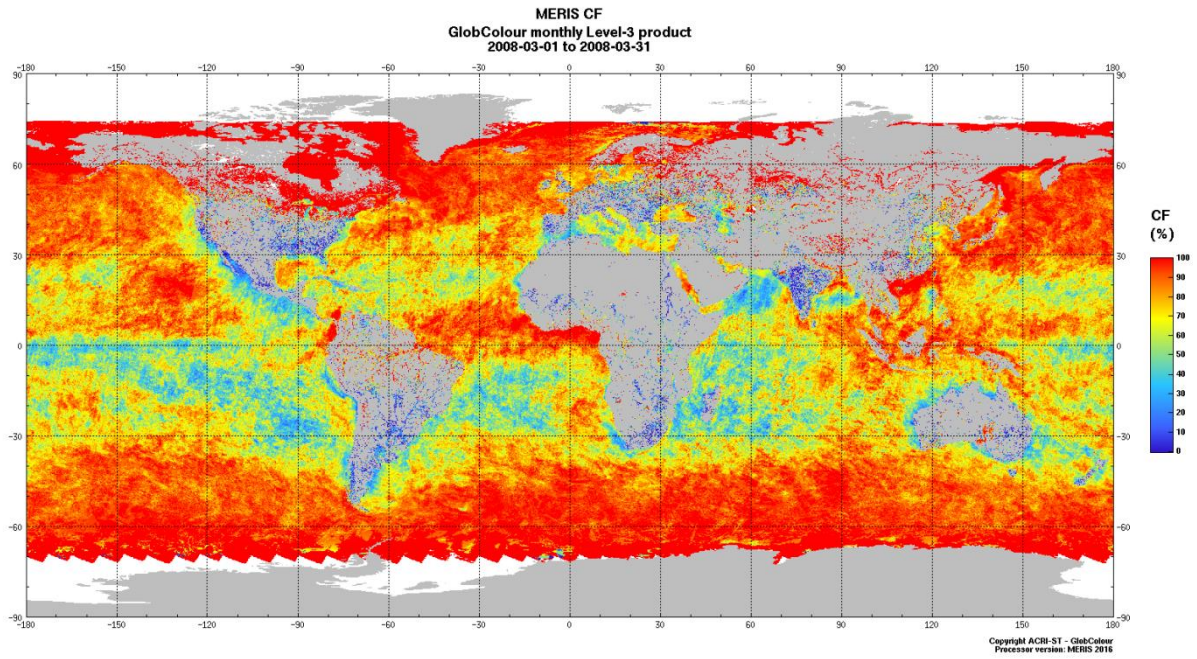
Figure 3-12: Cloud Fraction, March 2008
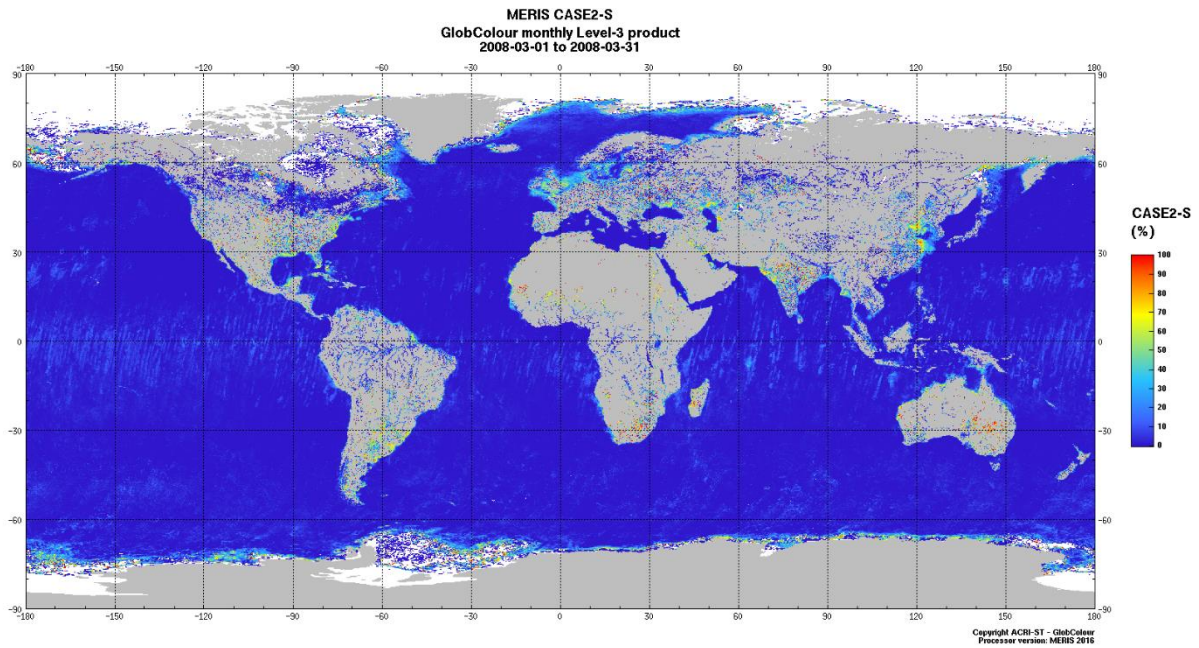
Figure 3-13: Case2-S flag occurrence, March 2008

4th MERIS data reprocessing

Evolutions and Validation report

Ref.: MER4RP Validation Report

Version: 1.0

Date: 01/04/2019

Page: 71
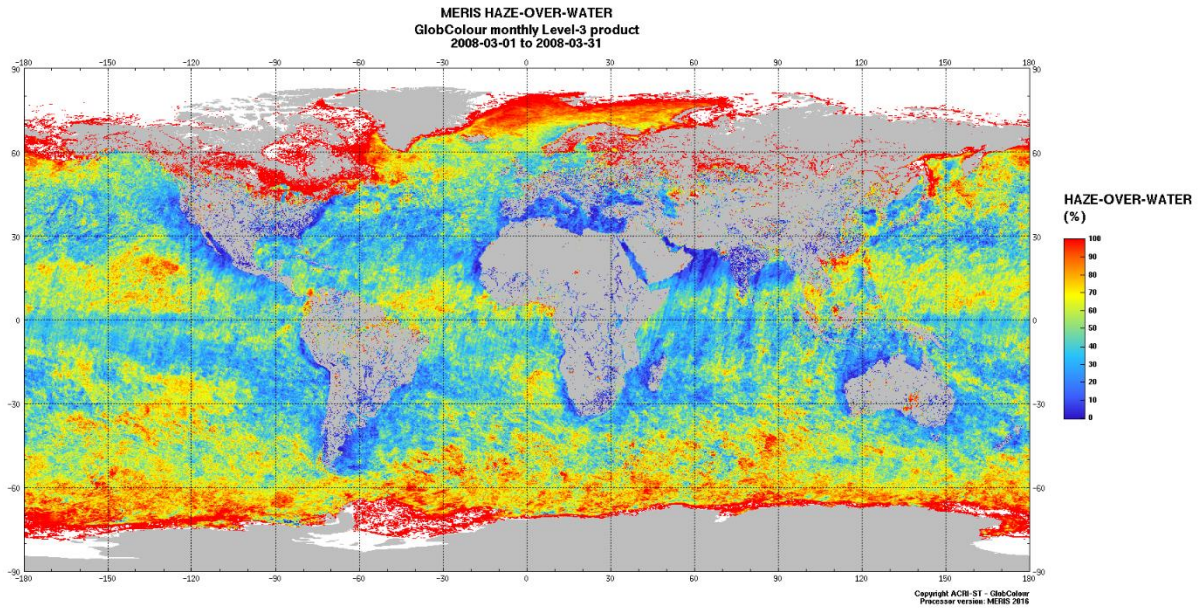
Figure 3-14: HAZE_OVER_WATER monthly occurrence, March 2008.
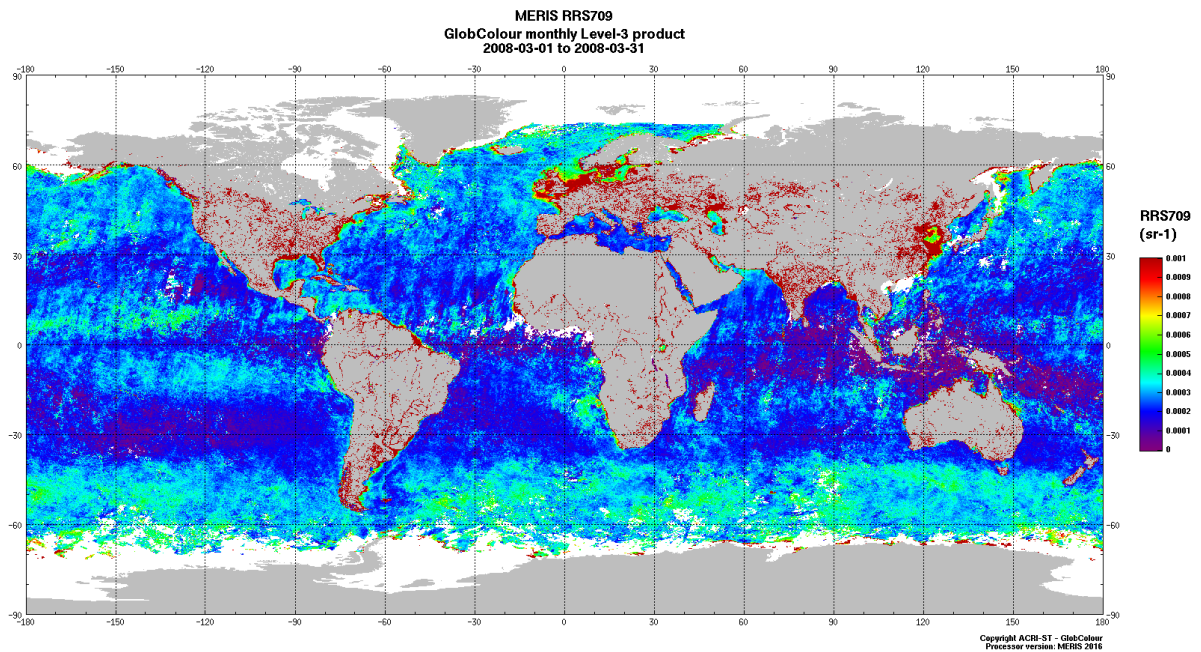
Figure 3-15: RRS709 monthly mean for the period March 2008. No errors due to systematic issues with the cloud screening are visible.

4th MERIS data reprocessing

Evolutions and Validation report

Ref.: MER4RP Validation Report

Version: 1.0

Date: 01/04/2019

Page: 72
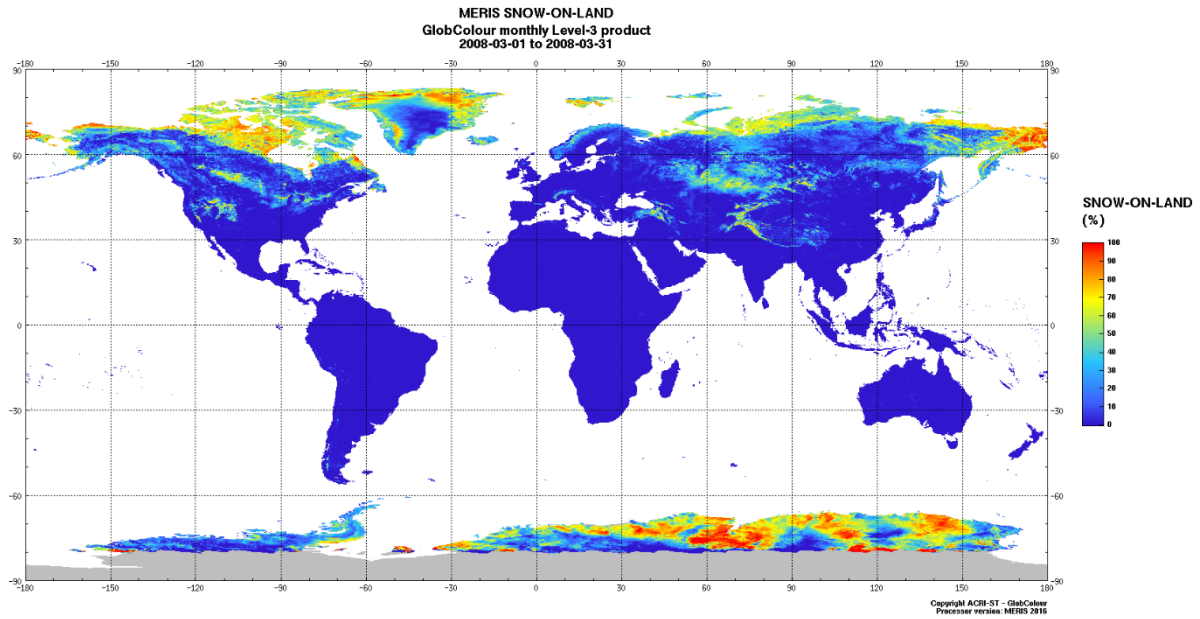
Figure 3-16: Snow on land, monthly occurrence, for the period March 2008

3.2.3.3 Known Issues

- The cloud flagging may flag bright beaches as clouds. This results in a scattered flagging of the coastline as clouds. An example is shown in Figure 3-17.

- The CC_CIRRUS flag is accidently interrupted. An example is shown in Figure 3-18

4th MERIS data reprocessing

Evolutions and Validation report

Ref.: MER4RP Validation Report

Version: 1.0

Date: 01/04/2019

Page: 73
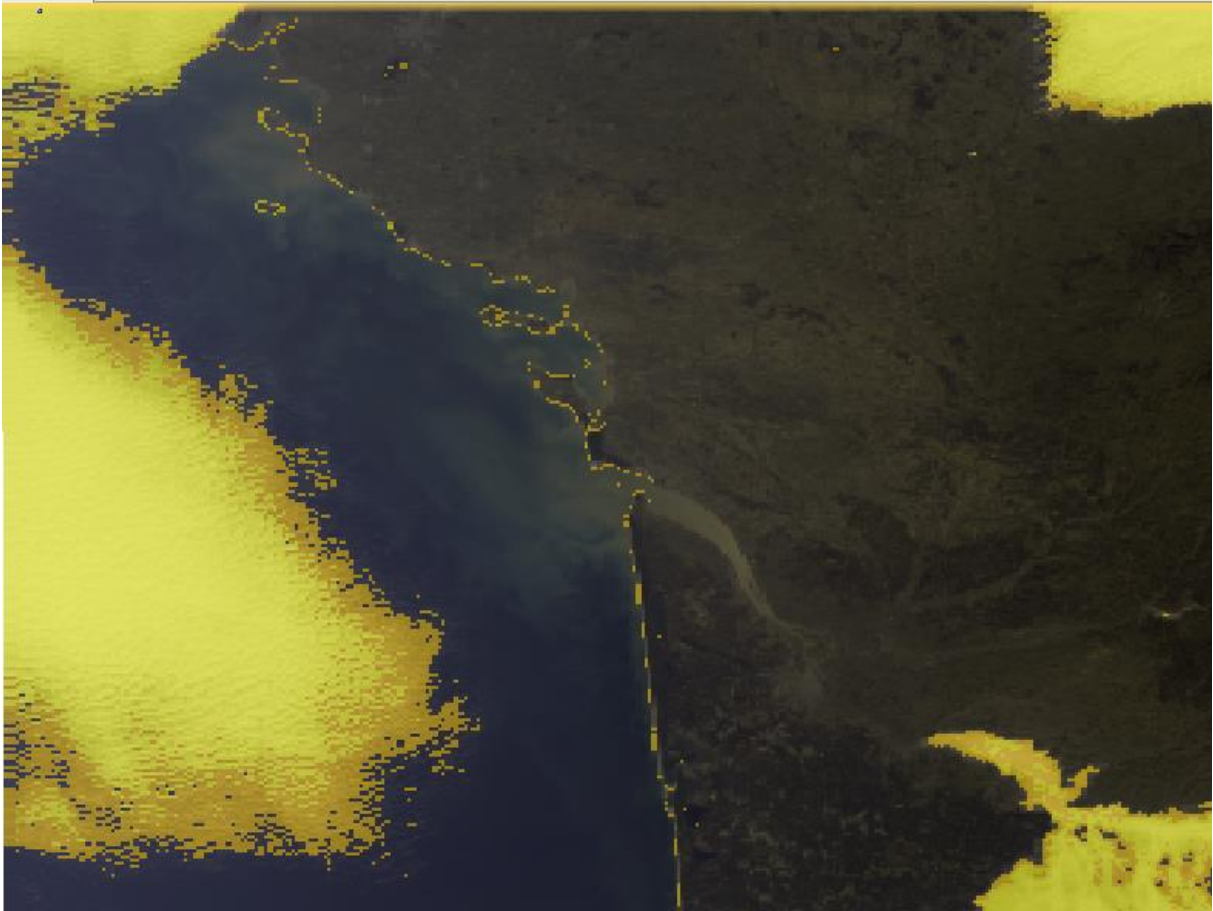
Figure 3-17: Coastline flagged as cloud.

	Ref.: MER4RP Validation Report
4th MERIS data reprocessing	Version: 1.0
Evolutions and Validation report	Date: 01/04/2019
	Page: 74
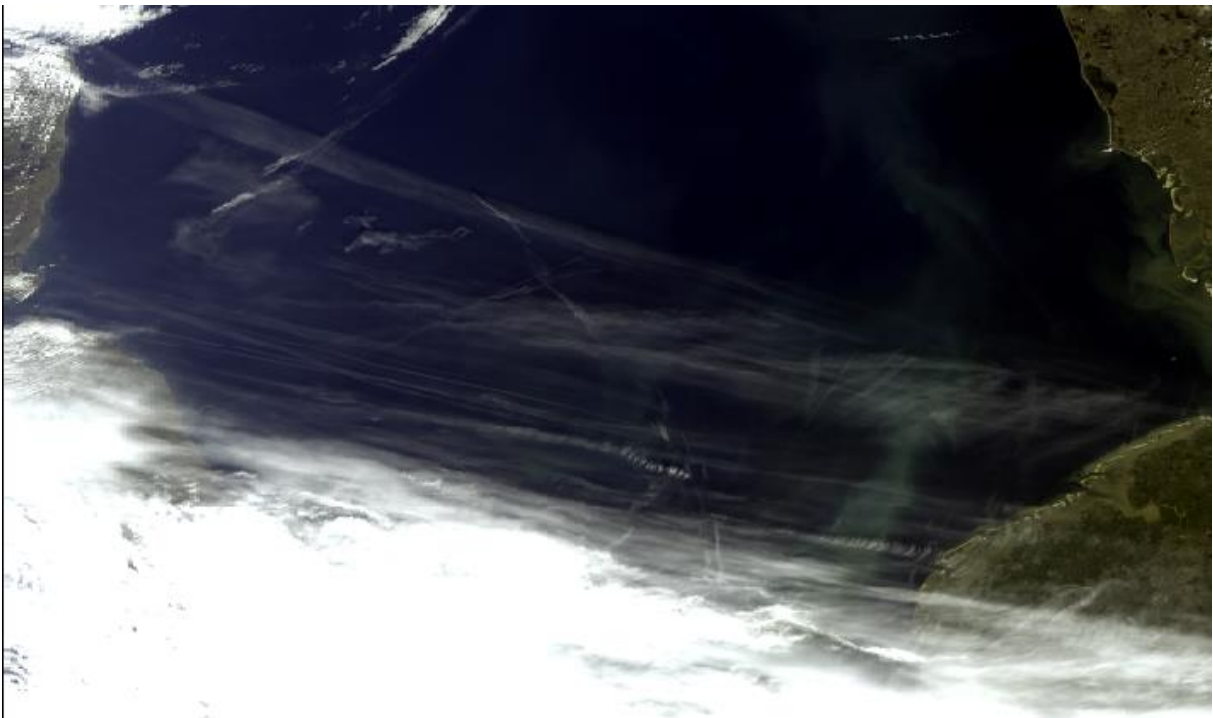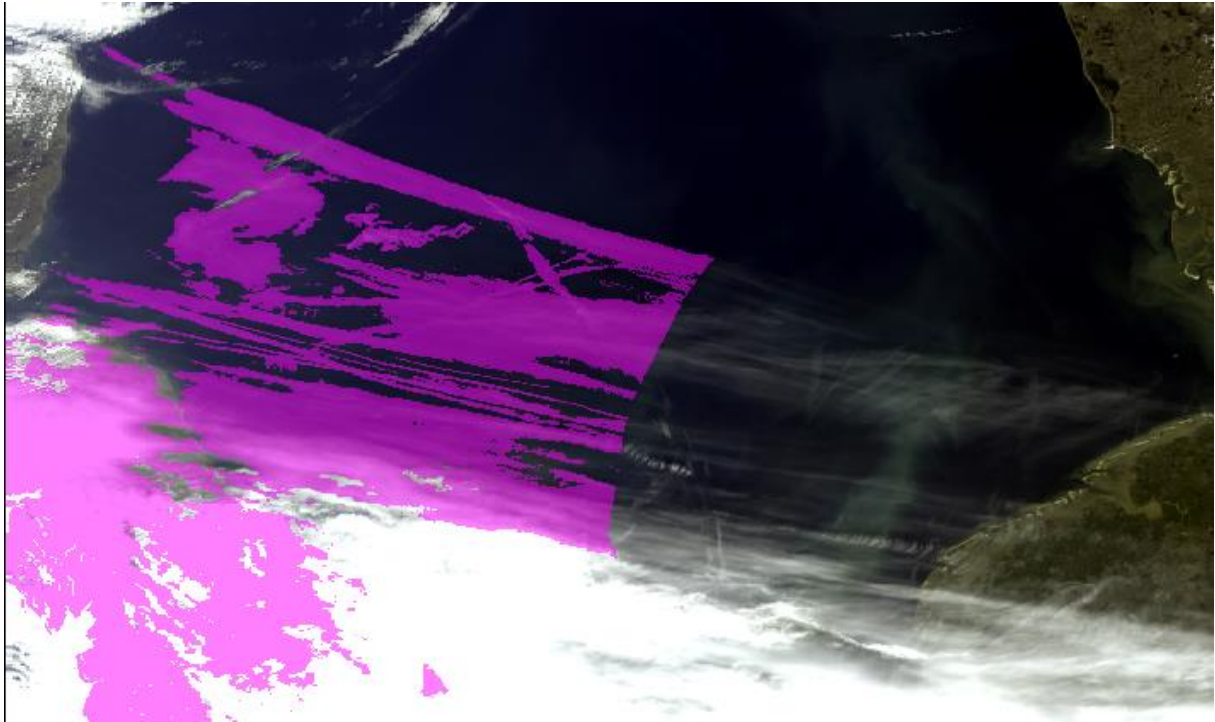
Figure 3-18: Cirrus flag interrupted. MERIS scene 20.04.2005, North Sea. Top: RGB, strongly contrast stretched. Bottom: Same but with CC_CIRRUS flag overlaid.

4th MERIS data reprocessing
Evolutions and Validation report

Ref.: MER4RP Validation Report
Version: 1.0
Date: 01/04/2019
Page: 75

3.3   Ocean products

3.3.1   Water-Leaving Reflectance (Mxx_rho_w)

Validation method
Validation using the MERMAID database
Comparisons between MER3RP and MER4RP matchups and L3 monthly products
Comparisons with MODIS and SeaWIFS L3 monthly products and time series

Accuracy goal	MER3RP estimated quality	MER4RP estimated quality
	(*) Case-1 waters, for wavelengths up to 560 nm: ▪ RPD < 5.0% ▪ RMSE < 4.15×10^{-3} Case-2 waters: ▪ RPD < 12.7% ▪ RMSE < 6.2×10^{-3}	

Case-1:
0.002 RMSE in the blue (ATBD2.7, v5.1, July 2011) or 5% RPD in blue band (Gordon, 1997)
	(**) For wavelengths up to 560 nm:
	
	▪ RPD better than
	   - 5.1% (Case-1 Ref)
	   - 24.6% (Case-1)
	   - 41.4% (Case-1/2 Ref)
	   - 117.6% (Case-1/2)
	   - 76% (Case-2)
	
	▪ RMSE better than
	   - 2.53×10^{-3} (Case-1 Ref)
	   - 2.77×10^{-3} (Case-1)
	   - 5.83×10^{-3} (Case-1/2 Ref)
	   - 3.51×10^{-3} (Case-1/2)
	   - 5.65×10^{-3} (Case-2)
		MER4RP results are better than those of MER3RP
		Accuracy goal is almost achieved
		
		For wavelengths up to 560 nm:
		
		▪ RPD better than
		   - 4.4% (Case-1 Ref)
		   - **5.7% (Case-1)**
		   - 12.2% (Case-1/2 Ref)
		   - 34.9% (Case-1/2)
		   - 19.1% (Case-2)
		
		▪ RMSE better than
		   - 2.52×10^{-3} (Case-1 Ref)
		   - **1.96×10^{-3} (Case-1)**
		   - 3.08×10^{-3} (Case-1/2 Ref)
		   - 2.59×10^{-3} (Case-1/2)
		   - 6.52×10^{-3} (Case-2)
		
		Detailed results in Table 3-3 to Table 3-7.

(*) Results as reported in the MER3RP validation report, ref. A879-NT-017-ACR_v1.0 dated on 09/10/2012, based on data includes both calibration (MOBY and BOUSSOLE) and validation data.

(**) Results obtained with the same methodology and datasets as MER4RP.

3.3.1.1   Validation on MERMAID matchups

Comparisons can be made between validations of the MER3RP and the MER4RP based on the MERMAID database (see acknowledgments of in situ data providers on top of this

4th MERIS data reprocessing

Evolutions and Validation report

Ref.: MER4RP Validation Report

Version: 1.0

Date: 01/04/2019

Page: 76

document). Such database provides match-ups between in situ measurements and satellite water-leaving reflectances. In this chapter we compare validation statistics obtained from both reprocessings. Note that between the MER3RP and the MER4RP in situ data may also have been reprocessed. However, both resulting matchup database span the same time period. In-situ water-leaving reflectances can be provided either as "IS" or "ISME", the latter being corrected from the solar irradiance by using the theoretical irradiance provided by the MERIS processing.

We draw attention on the necessary careful selection of the match-ups according to the Level 2 processing flags. As in MER3RP, cloudy and glinted pixels are removed as well as pixels where atmospheric correction has failed. For MER3RP, it traduces by removing all pixels with raised LAND, CLOUD, ICE_HAZE, HIGH_GLINT, MEDIUM_GLINT, PCD_19 or PCD_1_13 flags. For MER4RP, it traduces by removing all pixels with raised CLOUD, HAZE_OVER_WATER, WHITE_SCATT, HIGHGLINT, MEGLINT, RHO_W_FAIL, AC_FAIL.

Results are first shown by means of histograms relating the satellite fully-normalized water-leaving reflectance to the corresponding in situ reflectances after filtering from cloudy and glint conditions. Each figure shows the result for MER3RP on the left and MER4RP on the right. The MER4RP validation shows less bias than the MER3RP validation, the standard deviation being quite similar.

Figure 3-19: Differences between in situ and satellite fully-normalized water-leaving reflectances at 412 nm. MER3RP (left) and MER4RP (right).

4th MERIS data reprocessing
Evolutions and Validation report

Ref.: MER4RP Validation Report
Version: 1.0
Date: 01/04/2019
Page: 77

Figure 3-20: Differences between in situ and satellite fully-normalized water-leaving reflectances at 443 nm. MER3RP (left) and MER4RP (right).
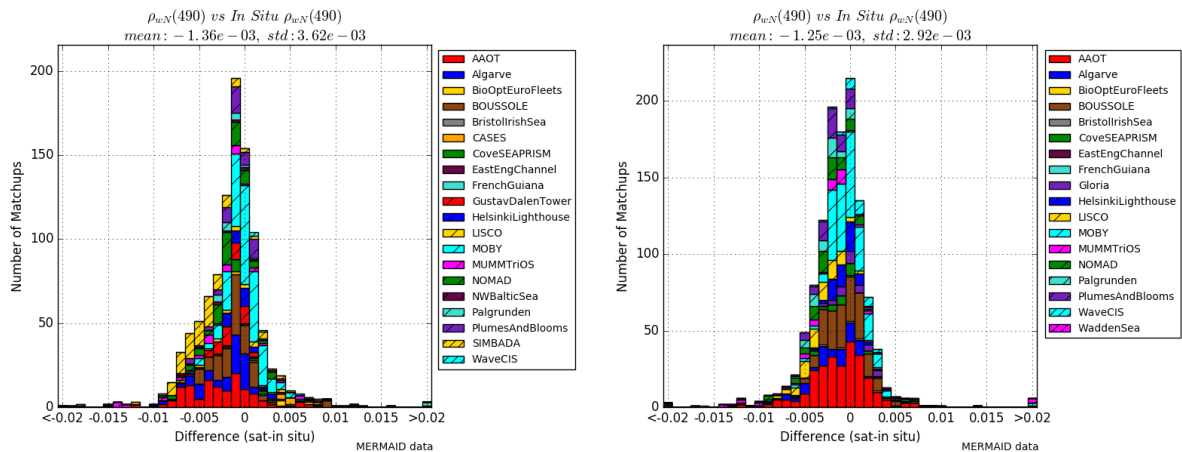
Figure 3-21: Differences between in situ and satellite fully-normalized water-leaving reflectances at 490 nm. MER3RP (left) and MER4RP (right).
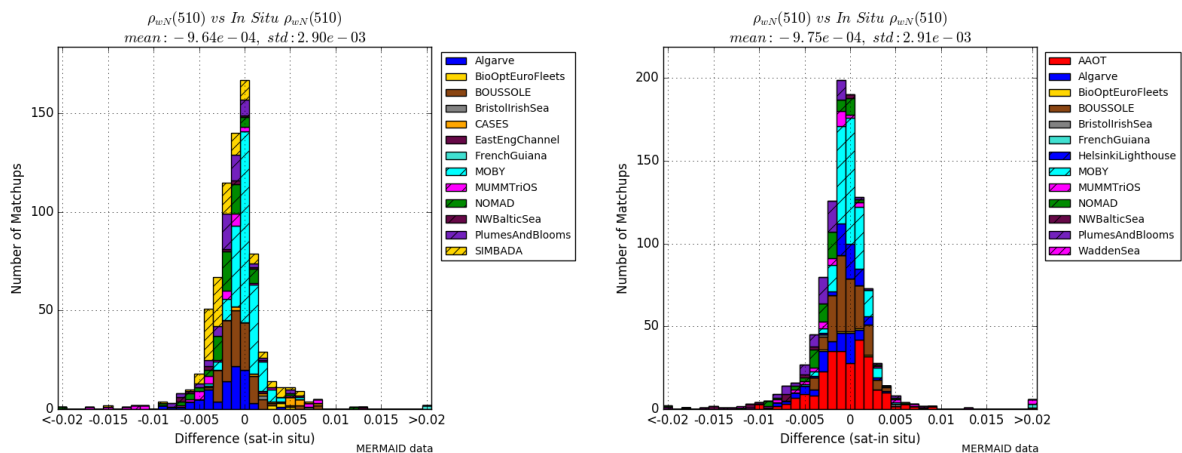
Figure 3-22: Differences between in situ and satellite fully-normalized water-leaving reflectances at 510 nm. MER3RP (left) and MER4RP (right).

4th MERIS data reprocessing
Evolutions and Validation report

Ref.: MER4RP Validation Report
Version: 1.0
Date: 01/04/2019
Page: 78
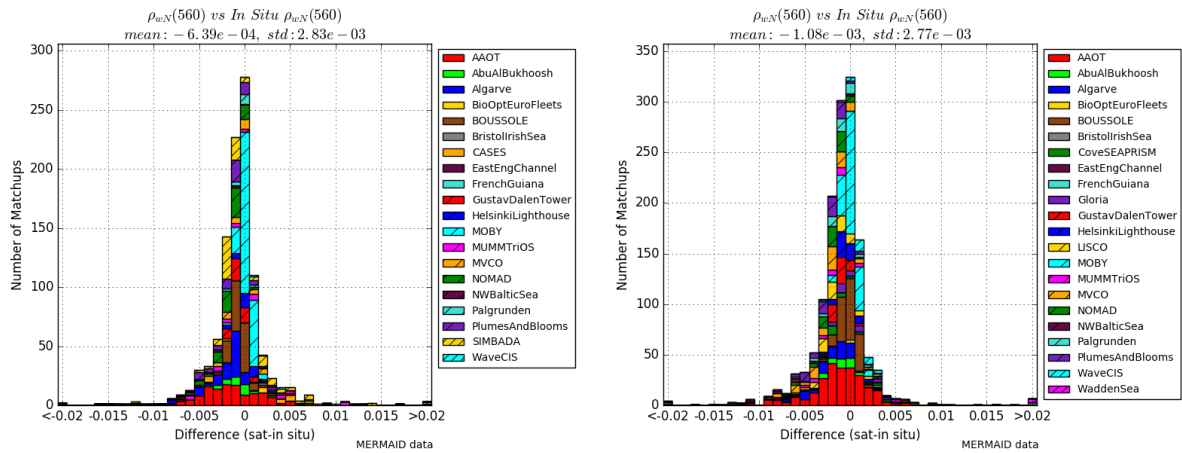
Figure 3-23: Differences between in situ and satellite fully-normalized water-leaving reflectances at 560 nm. MER3RP (left) and MER4RP (right).
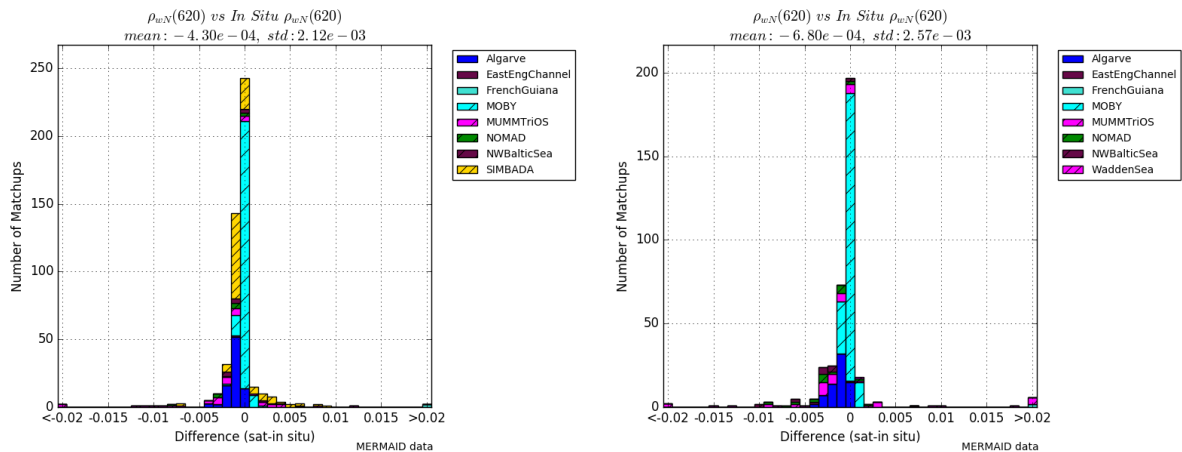
Figure 3-24: Differences between in situ and satellite fully-normalized water-leaving reflectances at 620 nm. MER3RP (left) and MER4RP (right).
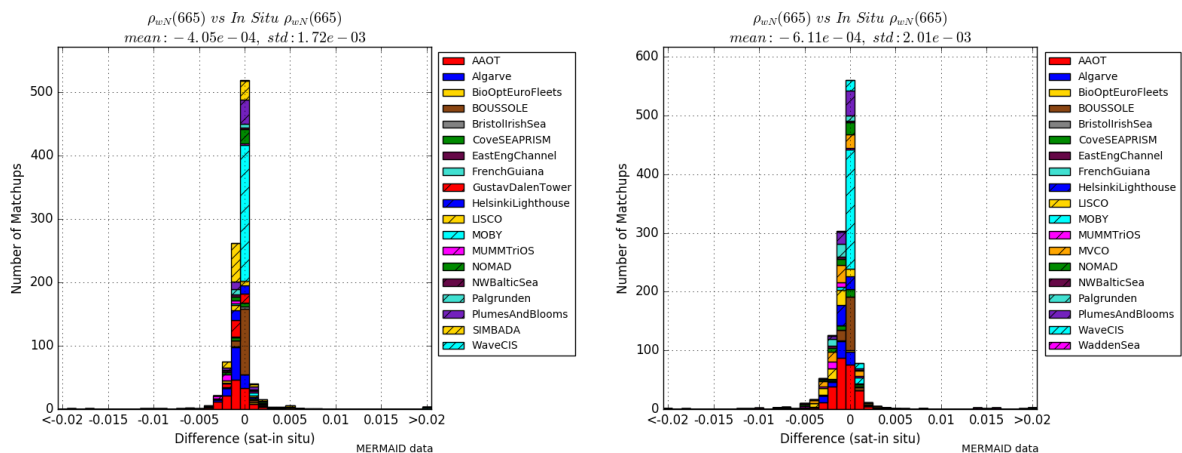
Figure 3-25: Differences between in situ and satellite fully-normalized water-leaving reflectances at 665 nm. MER3RP (left) and MER4RP (right).

4th MERIS data reprocessing

Evolutions and Validation report

Ref.: MER4RP Validation Report

Version: 1.0

Date: 01/04/2019

Page: 79
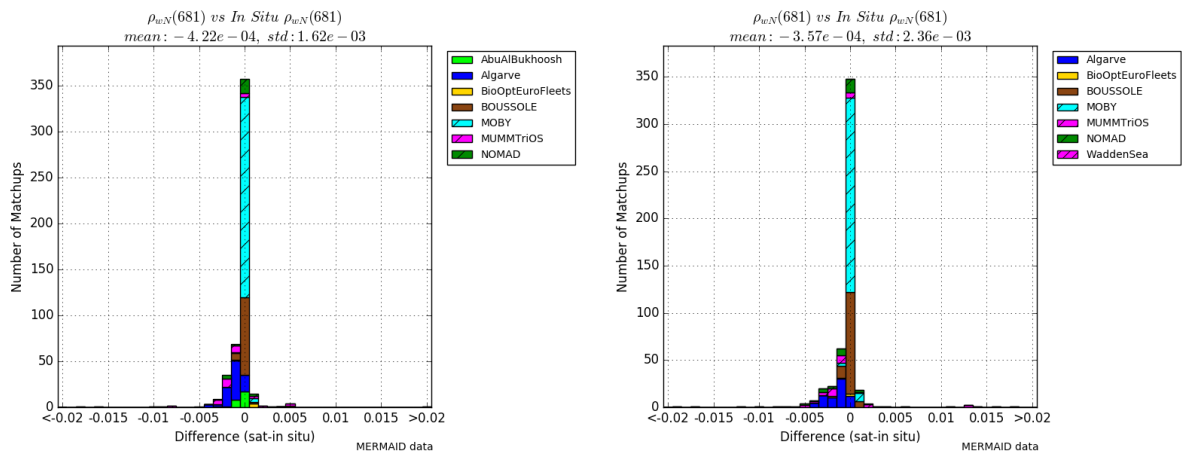
Figure 3-26: Differences between in situ and satellite fully-normalized water-leaving reflectances at 681 nm. MER3RP (left) and MER4RP (right).
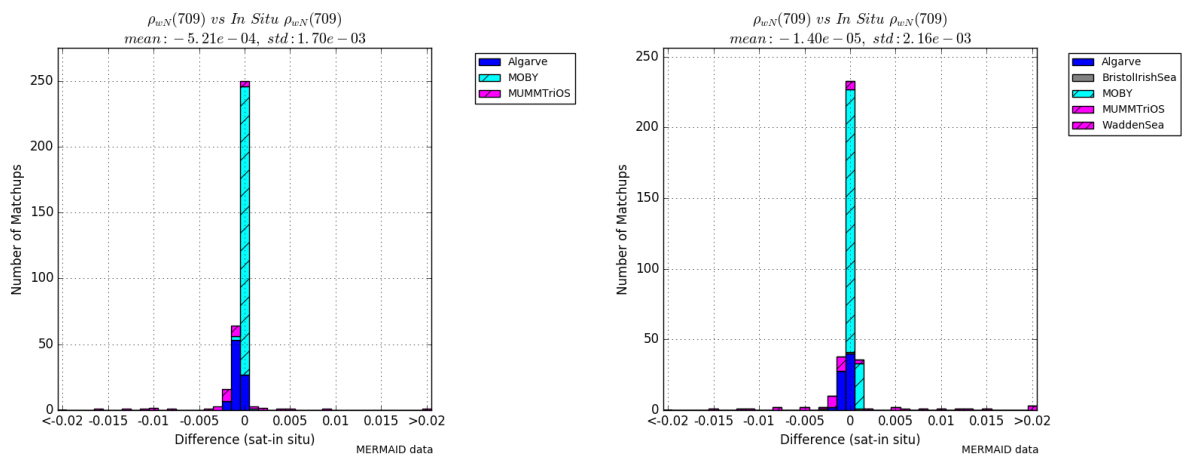
Figure 3-27: Differences between in situ and satellite fully-normalized water-leaving reflectances at 709 nm. MER3RP (left) and MER4RP (right).
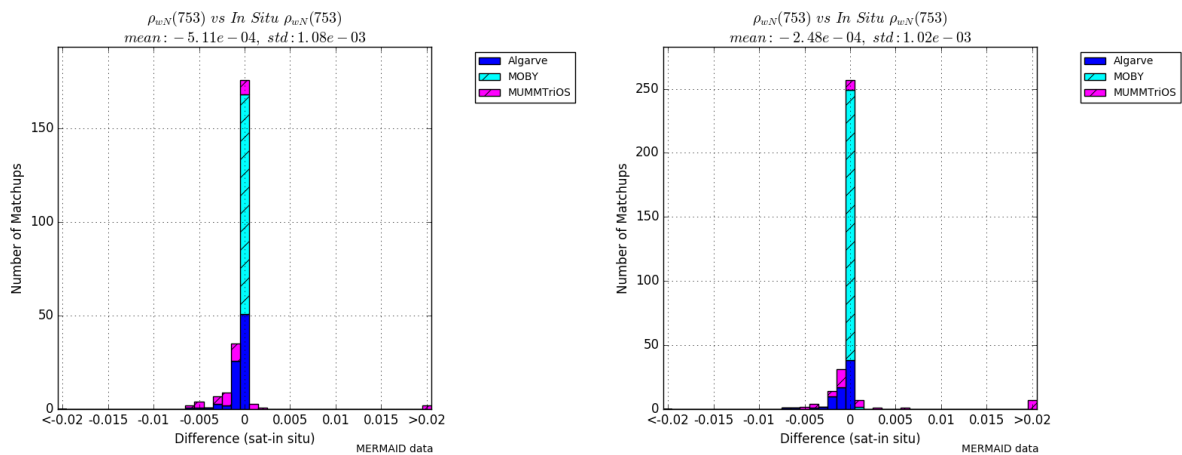
Figure 3-28: Differences between in situ and satellite fully-normalized water-leaving reflectances at 753 nm. MER3RP (left) and MER4RP (right).

4th MERIS data reprocessing

Evolutions and Validation report

Ref.: MER4RP Validation Report

Version: 1.0
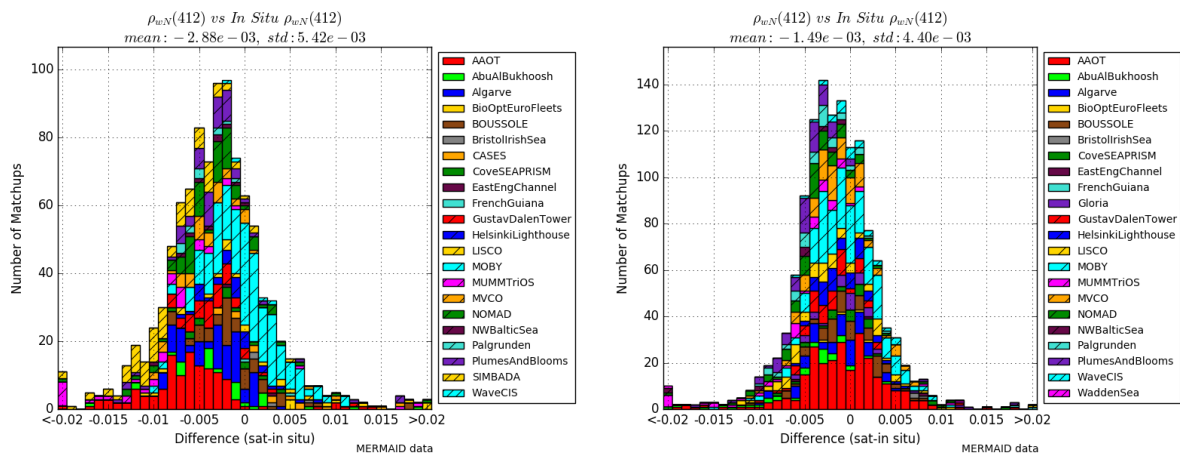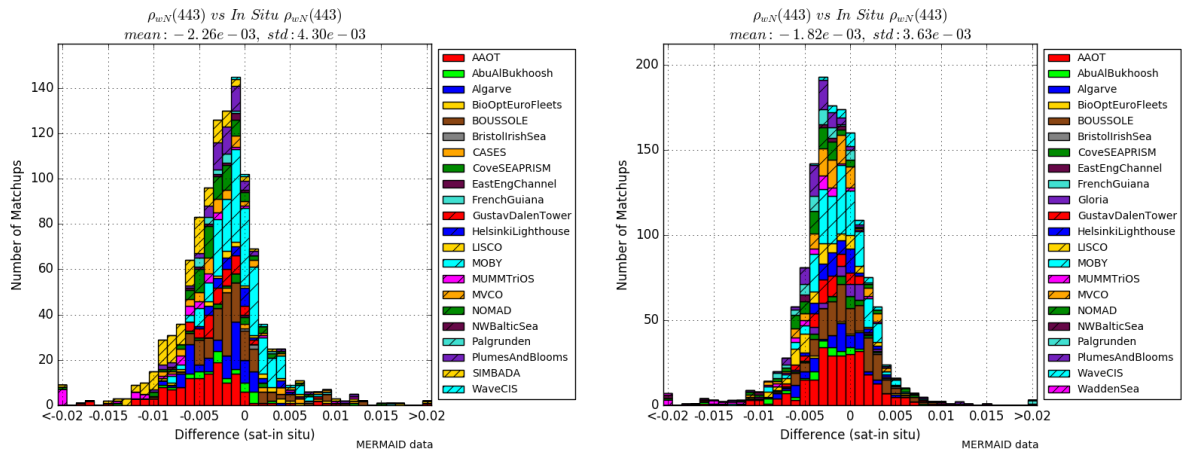
Date: 01/04/2019

Page: 80
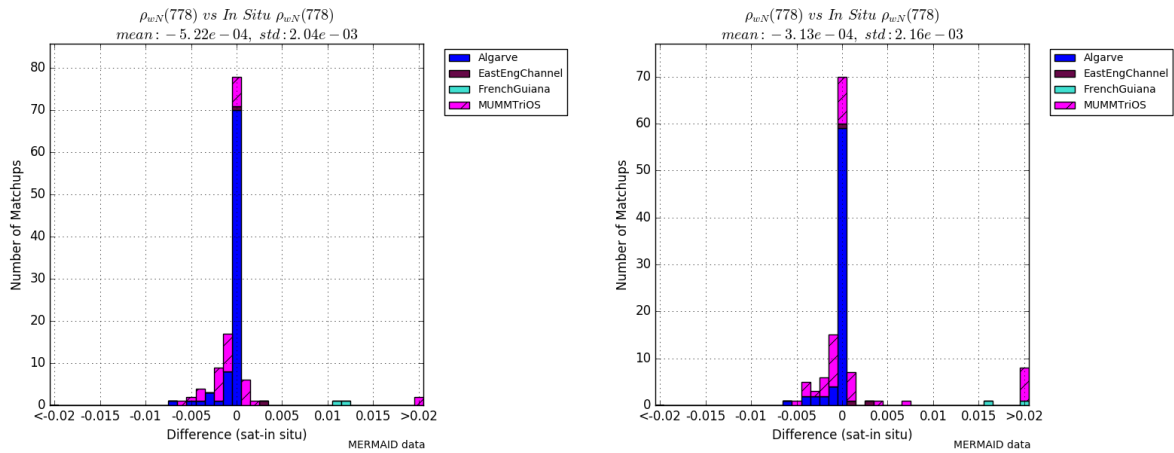
Figure 3-29: Differences between in situ and satellite fully-normalized water-leaving reflectances at 778 nm. MER3RP (left) and MER4RP (right).
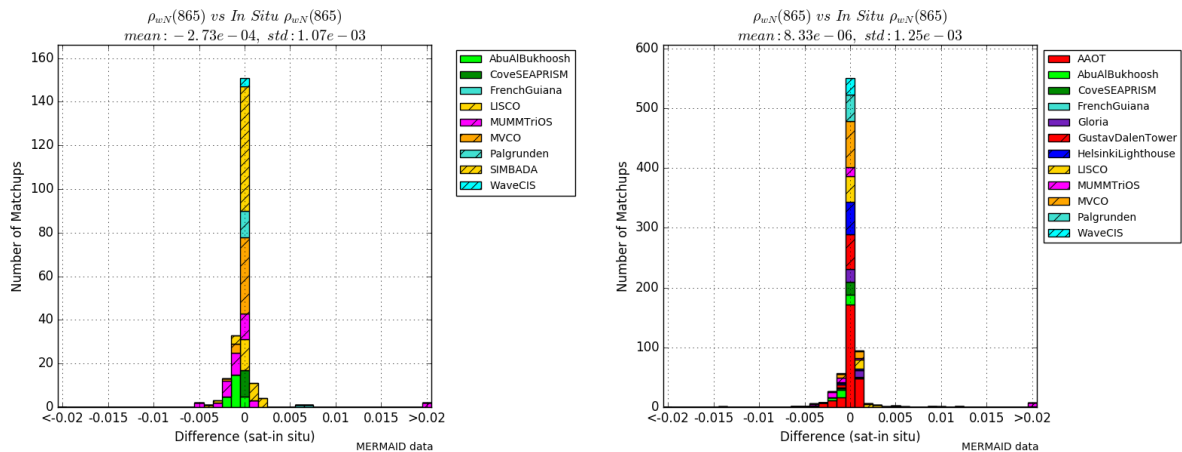
Figure 3-30: Differences between in situ and satellite fully-normalized water-leaving reflectances at 865 nm. MER3RP (left) and MER4RP (right).

These comparisons can further be subdivided per validation site, separating Case-1, Case-2, and mixed waters (Case-1/2) as well as reference sites (Ref). Data from reference sites are assumed to be of better quality. To do so the categorization presented in Table 3-2 is used:

Table 3-2: List of the MERMAID sites used in this comparison, categorization into Case-1, Case-2, or mixed waters (1/2) as well as reference sites (Ref).

Site name	Category	Site name	Category
BOUSSOLE	Case-1 (Ref)	AbuAlBukhoosh	Case-2
MOBY	Case-1 (Ref)	BristolIrishSea	Case-2
Algarve	Case-1	CoveSEAPRISM	Case-2
BSHSummerSurvey	Case-1	EastEngChannel	Case-2
Gloria	Case-1	FrenchGuiana	Case-2
PortCoast	Case-1	LISCO	Case-2

4th MERIS data reprocessing

Evolutions and Validation report

Ref.: MER4RP Validation Report

Version: 1.0

Date: 01/04/2019

Page: 81

WaveCIS	Case-1	MUMMTriOS	Case-2
AAOT	Case-1/2 (Ref)	MVCO	Case-2
NOMAD	Case-1/2 (Ref)	Palgrunden	Case-2
BioOptEuroFleets	Case-1/2	PlumesAndBlooms	Case-2
GustavDalenTower	Case-1/2		
HelsinkiLighthouse	Case-1/2		
NWBalticSea	Case-1/2		

Results are presented following this order (Case-1 first, reference site first, alphabetical order into subdivisions).

Figure 3-31 to Figure 3-43 then present the means and standard deviations of the differences associated to each site for M3RP (red or pink) and M4RP (blue or cyan) using "IS" or "ISME" in situ reflectances. Per site the number of matchups from M4RP is reported to give an insight of the amount of data provided and the relevance of the statistics.

Figure 3-31: Mean and standard deviation of differences between in situ and satellite fully-normalized water-leaving reflectances at 412 nm. M3RP IS and ISME: red and pink; M4RP IS and ISME: blue and cyan.

4th MERIS data reprocessing

Evolutions and Validation report

Ref.: MER4RP Validation Report

Version: 1.0

Date: 01/04/2019

Page: 82

Figure 3-32: Mean and standard deviation of differences between in situ and satellite fully-normalized water-leaving reflectances at 443 nm. M3RP IS and ISME: red and pink; M4RP IS and ISME: blue and cyan.
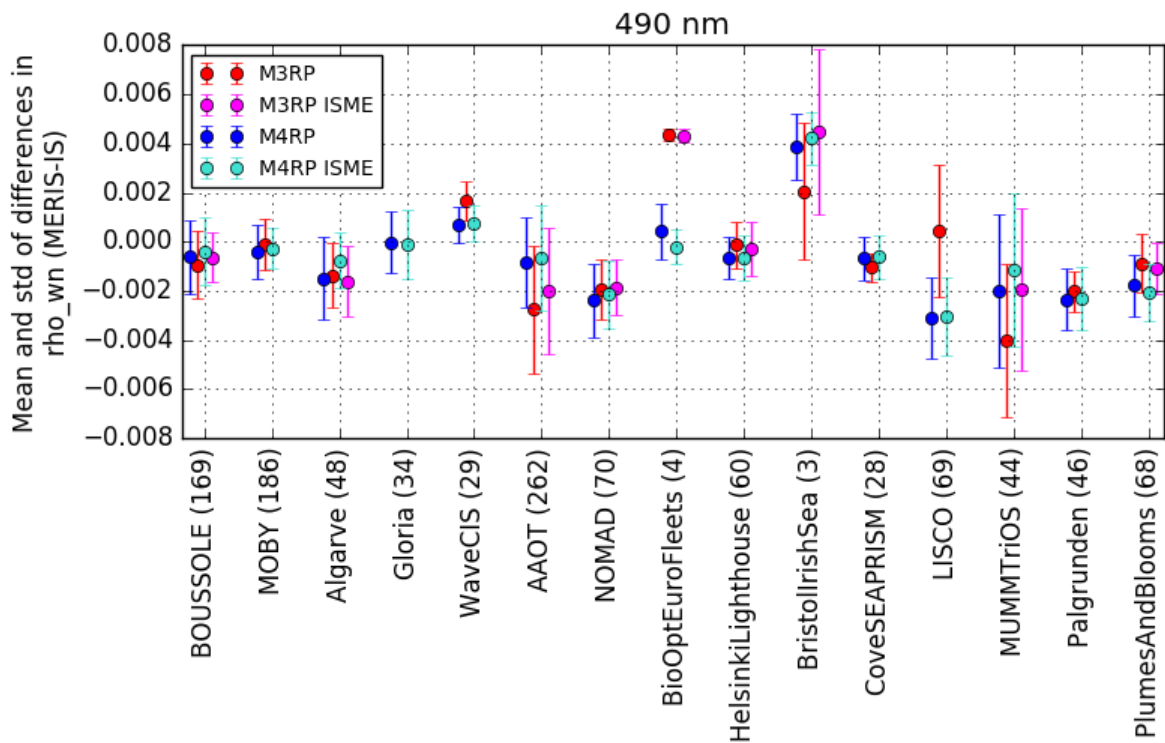
Figure 3-33: Mean and standard deviation of differences between in situ and satellite fully-normalized water-leaving reflectances at 490 nm. M3RP IS and ISME: red and pink; M4RP IS and ISME: blue and cyan.

4th MERIS data reprocessing

Evolutions and Validation report

Ref.: MER4RP Validation Report

Version: 1.0

Date: 01/04/2019

Page: 83
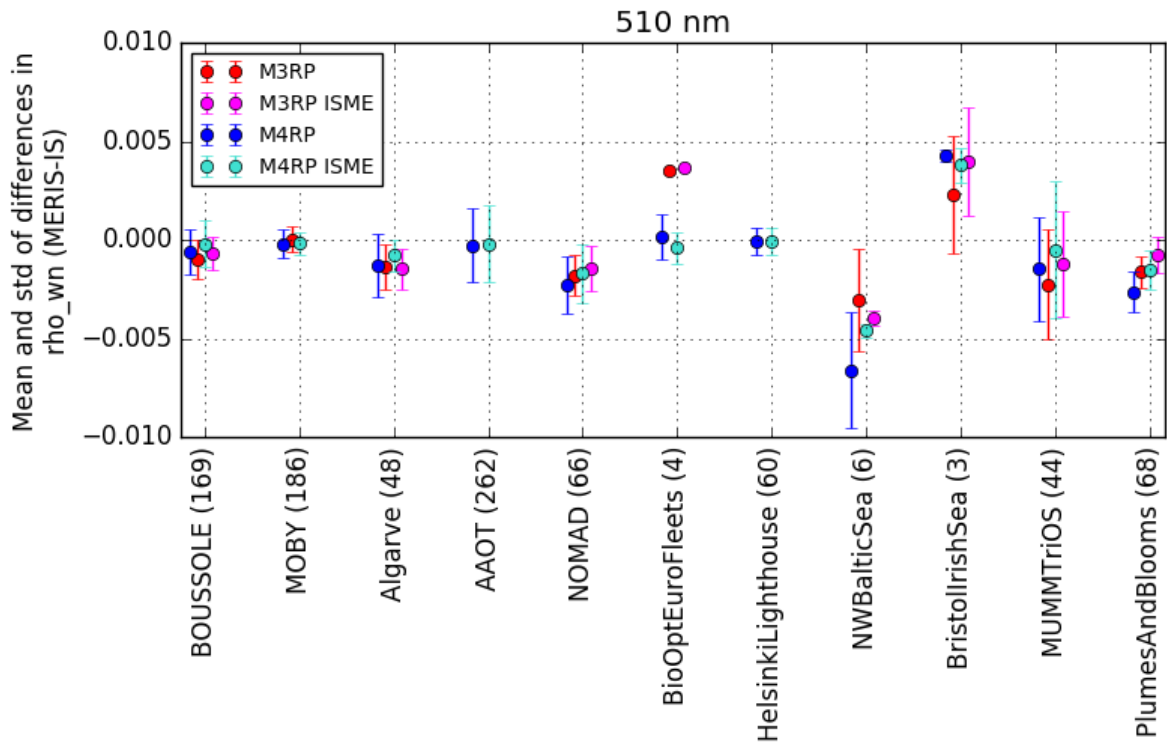
Figure 3-34: Mean and standard deviation of differences between in situ and satellite fully-normalized water-leaving reflectances at 510 nm. M3RP IS and ISME: red and pink; M4RP IS and ISME: blue and cyan.

Figure 3-35: Mean and standard deviation of differences between in situ and satellite fully-normalized water-leaving reflectances at 560 nm. M3RP IS and ISME: red and pink; M4RP IS and ISME: blue and cyan.

4th MERIS data reprocessing

Evolutions and Validation report

Ref.: MER4RP Validation Report

Version: 1.0

Date: 01/04/2019

Page: 84

Figure 3-36: Mean and standard deviation of differences between in situ and satellite fully-normalized water-leaving reflectances at 620 nm. M3RP IS and ISME: red and pink; M4RP IS and ISME: blue and cyan.

Figure 3-37: Mean and standard deviation of differences between in situ and satellite fully-normalized water-leaving reflectances at 665 nm. M3RP IS and ISME: red and pink; M4RP IS and ISME: blue and cyan.

4th MERIS data reprocessing

Evolutions and Validation report

Ref.: MER4RP Validation Report

Version: 1.0

Date: 01/04/2019

Page: 85

Figure 3-38: Mean and standard deviation of differences between in situ and satellite fully-normalized water-leaving reflectances at 681 nm. M3RP IS and ISME: red and pink; M4RP IS and ISME: blue and cyan.
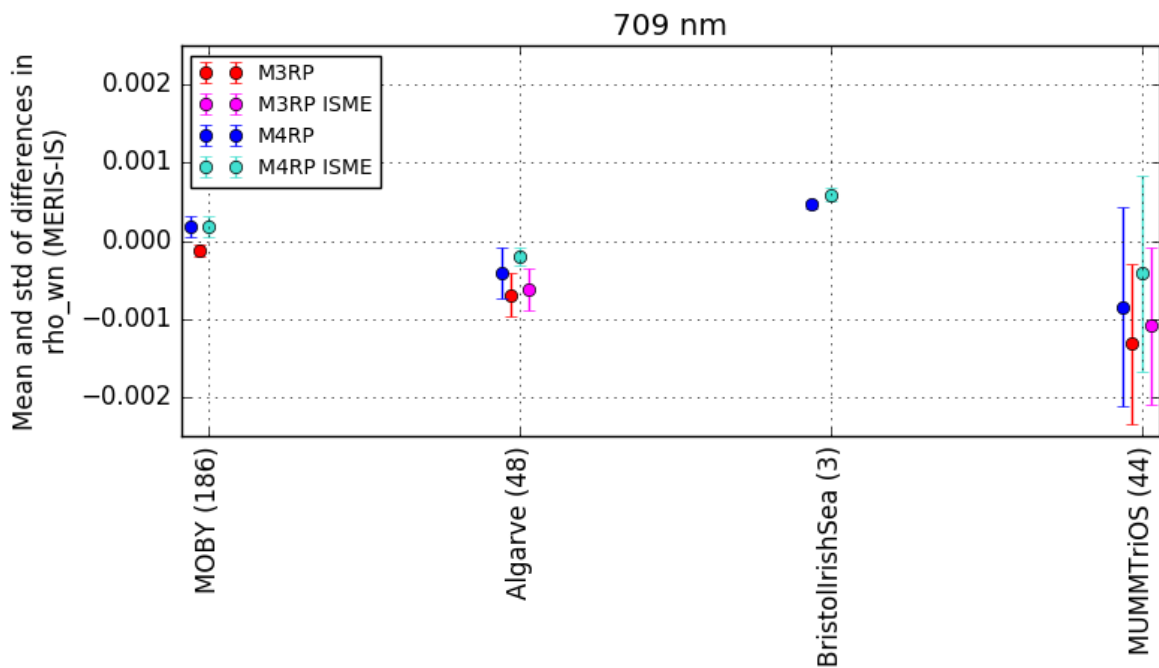
Figure 3-39: Mean and standard deviation of differences between in situ and satellite fully-normalized water-leaving reflectances at 709 nm. M3RP IS and ISME: red and pink; M4RP IS and ISME: blue and cyan.

4th MERIS data reprocessing

Evolutions and Validation report

Ref.:   MER4RP Validation Report

Version: 1.0

Date: 01/04/2019

Page: 86

Figure 3-40: Mean and standard deviation of differences between in situ and satellite fully-normalized water-leaving reflectances at 753 nm. M3RP IS and ISME: red and pink; M4RP IS and ISME: blue and cyan.

Figure 3-41: Mean and standard deviation of differences between in situ and satellite fully-normalized water-leaving reflectances at 778 nm. M3RP IS and ISME: red and pink; M4RP IS and ISME: blue and cyan.

4th MERIS data reprocessing

Evolutions and Validation report

Ref.: MER4RP Validation Report

Version: 1.0

Date: 01/04/2019

Page: 87

Figure 3-42: Mean and standard deviation of differences between in situ and satellite fully-normalized water-leaving reflectances at 865 nm. M3RP IS and ISME: red and pink; M4RP IS and ISME: blue and cyan.
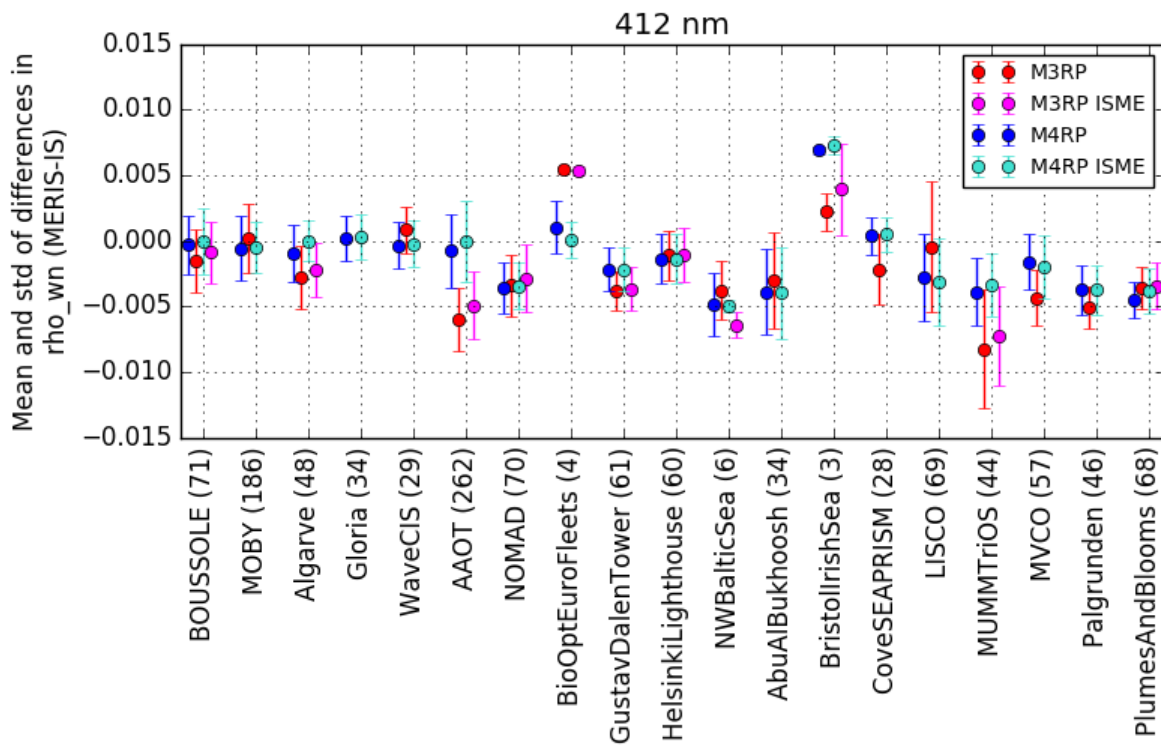

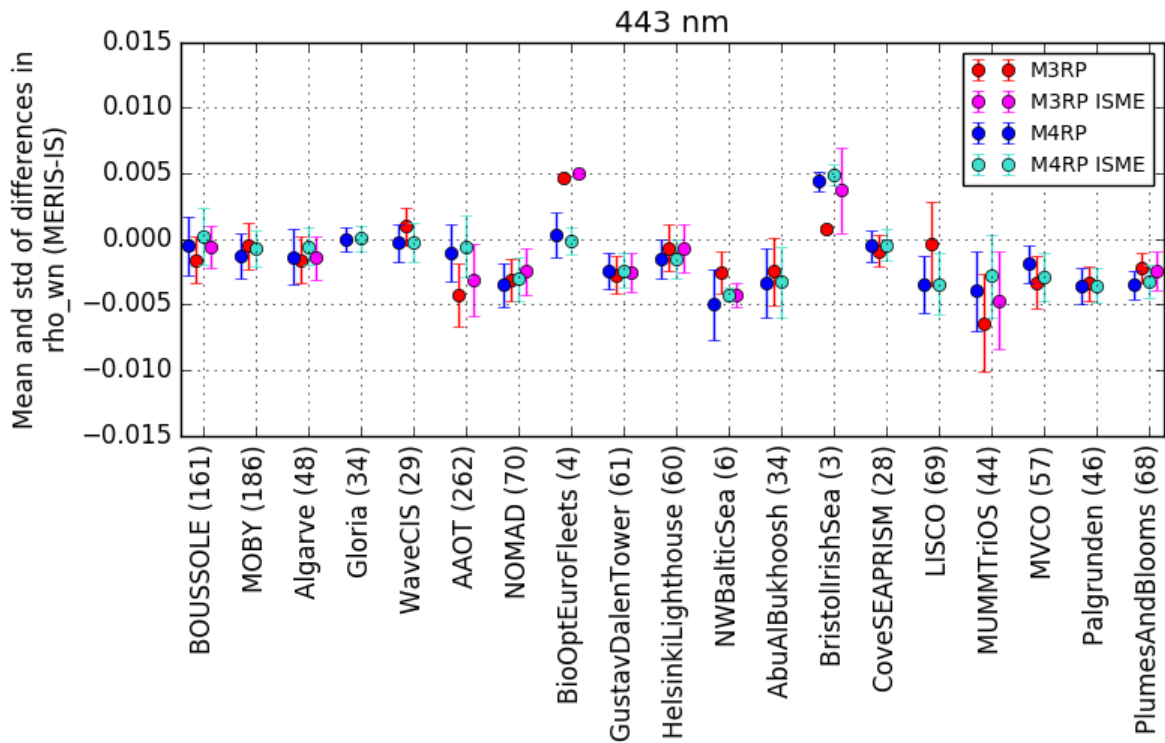*Figure 3-43: Mean and standard deviation of differences between in situ and satellite fully-normalized water-leaving reflectances at 885 nm. M3RP IS and ISME: red and pink; M4RP IS and ISME: blue and cyan.*

These results show that M4RP comparisons are slightly better than those of M3RP. Overall, "ISME" comparisons seem slightly better as well. Much improvement between M3RP and M4RP are shown at AAOT in the blue.

4th MERIS data reprocessing

Evolutions and Validation report

Ref.:   MER4RP Validation Report

Version: 1.0

Date: 01/04/2019

Page: 88

At most interesting sites these results can also be seen as a function of the wavelength in Figure 3-44.

The comparison at BOUSSOLE and MOBY reflects the choices and statistics used for vicarious calibration as only those two sites are chosen. M3RP used vicarious calibration using "IS" reflectances with more MOBY statistics while M4RP used vicarious calibration using "ISME" reflectances with equivalent MOBY and BOUSSOLE statistics. Therefore, validation on BOUSSOLE is best on M4RP "ISME" while it is best on MOBY on M3RP "IS".

Comparisons at AAOT and MUMMTriOS show better M4RP validation and indeed much improvement at AAOT.

Comparisons at NOMAD show better M3RP validation, differences are more chaotic at 560/620 nm as an effect of lower statistics at these two bands.

4th MERIS data reprocessing

Evolutions and Validation report

Ref.: MER4RP Validation Report

Version: 1.0

Date: 01/04/2019

Page: 89

MOBY, water case 1 REF

AAOT, water case 1/2 REF

4th MERIS data reprocessing

Evolutions and Validation report

Ref.:   MER4RP Validation Report

Version: 1.0

Date: 01/04/2019

Page: 90

NOMAD, water case 1/2 REF

4th MERIS data reprocessing

Evolutions and Validation report

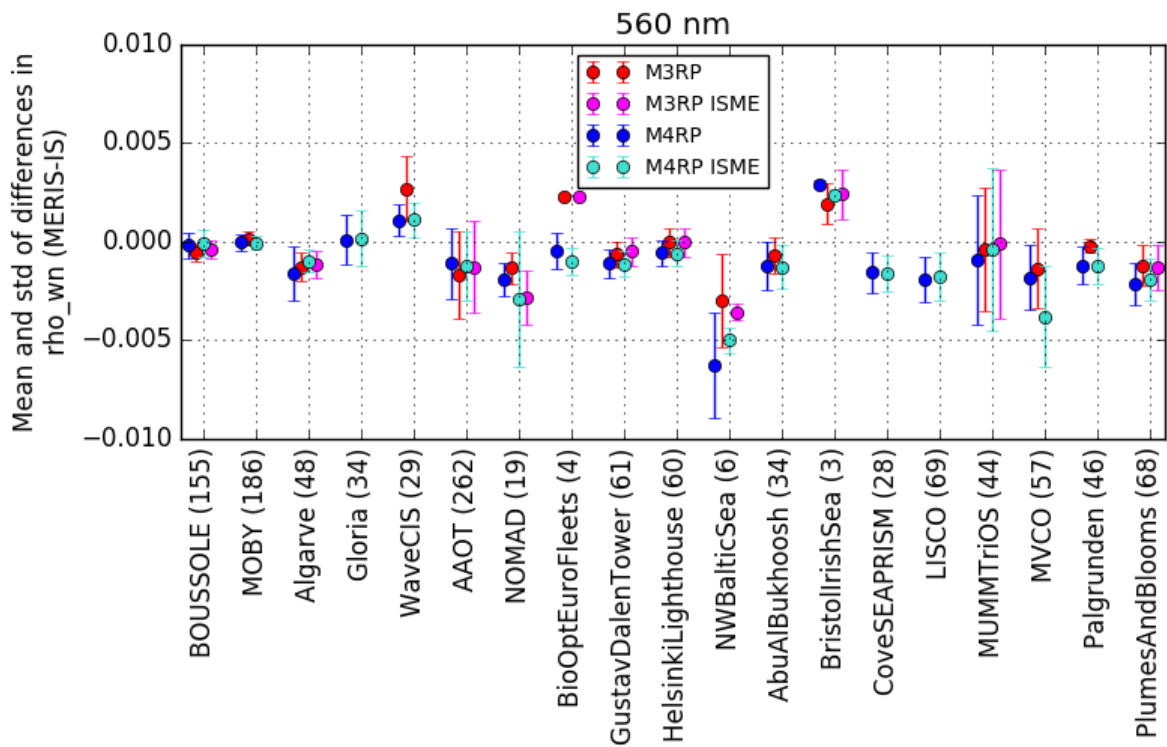Ref.: MER4RP Validation Report

Version: 1.0

Date: 01/04/2019

Page: 91

Figure 3-44: Mean and standard deviation of differences between in situ and satellite fully-normalized water-leaving reflectances as a function of the wavelength and at several sites (BOUSSOLE, MOBY, AAOT, NOMAD and MUMMTriOS). M3RP IS and ISME: red and pink; M4RP IS and ISME: blue and cyan.

Overall quality can be summarized by computing mean RPD (relative percent differences) and RMSE (root-mean-square errors) per site between 412 and 560 nm.

RPD results are displayed between Figure 3-45 and Figure 3-49. RMSE results are displayed between Figure 3-50 and Figure 3-54.

4th MERIS data reprocessing

Evolutions and Validation report

Ref.: MER4RP Validation Report

Version: 1.0

Date: 01/04/2019

Page: 92

Figure 3-45: RPD between in situ and satellite fully-normalized water-leaving reflectances at 412 nm. M3RP IS and ISME: red and pink; M4RP IS and ISME: blue and cyan.
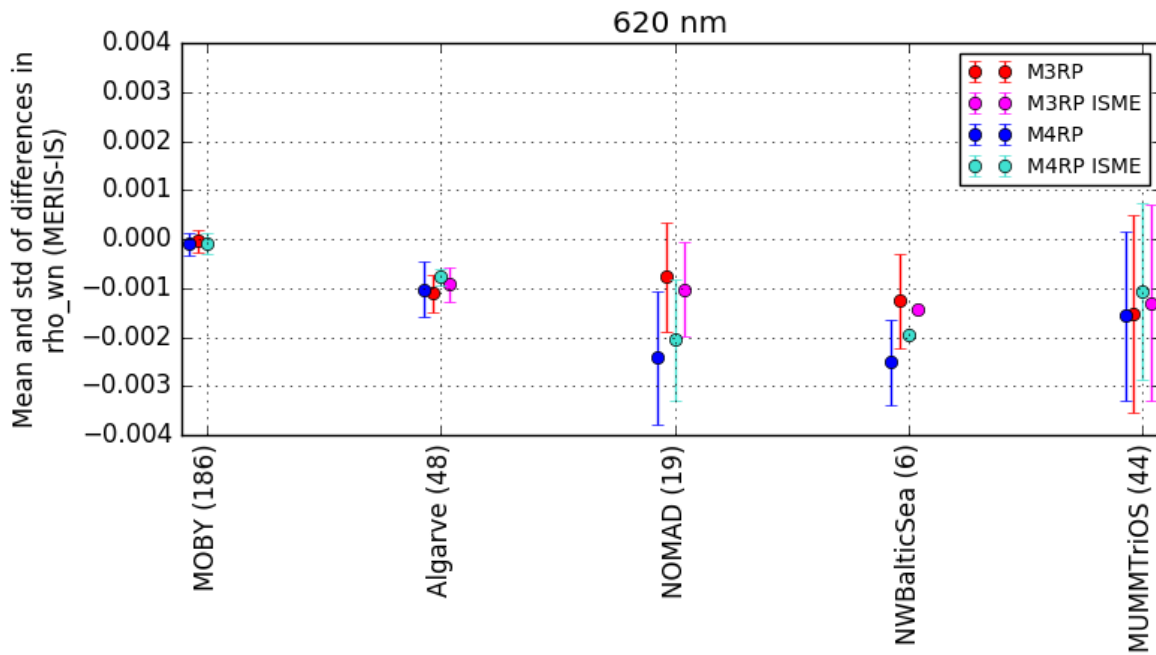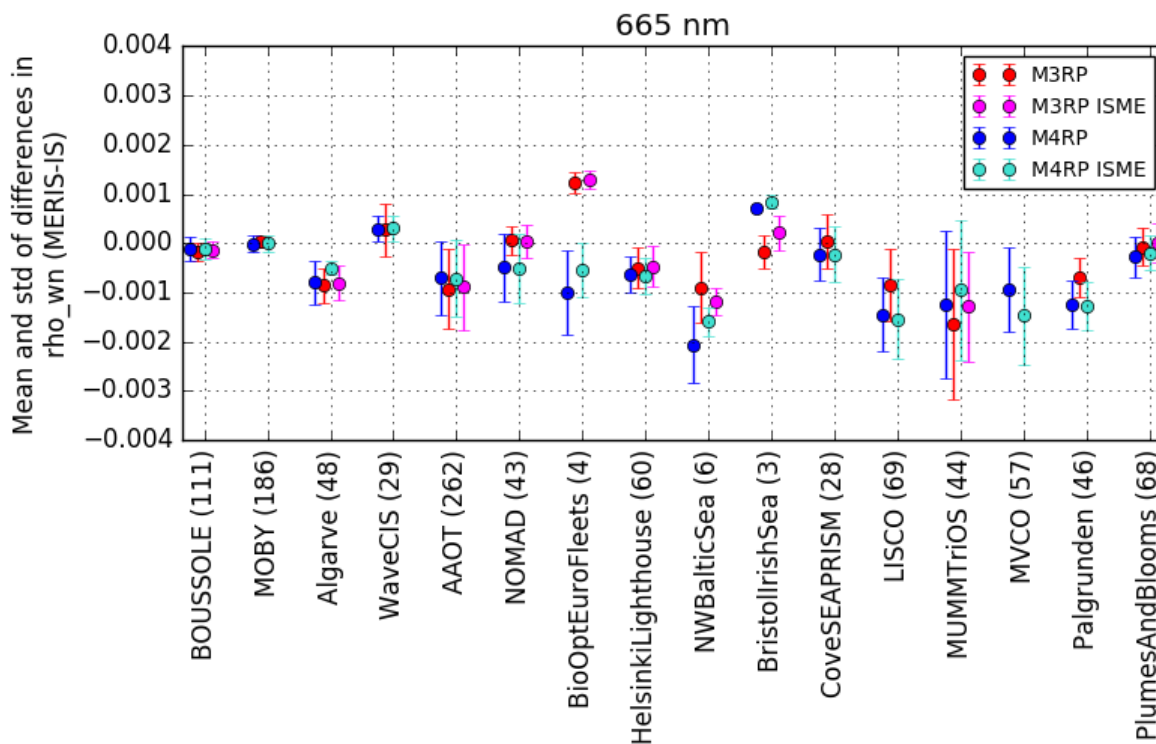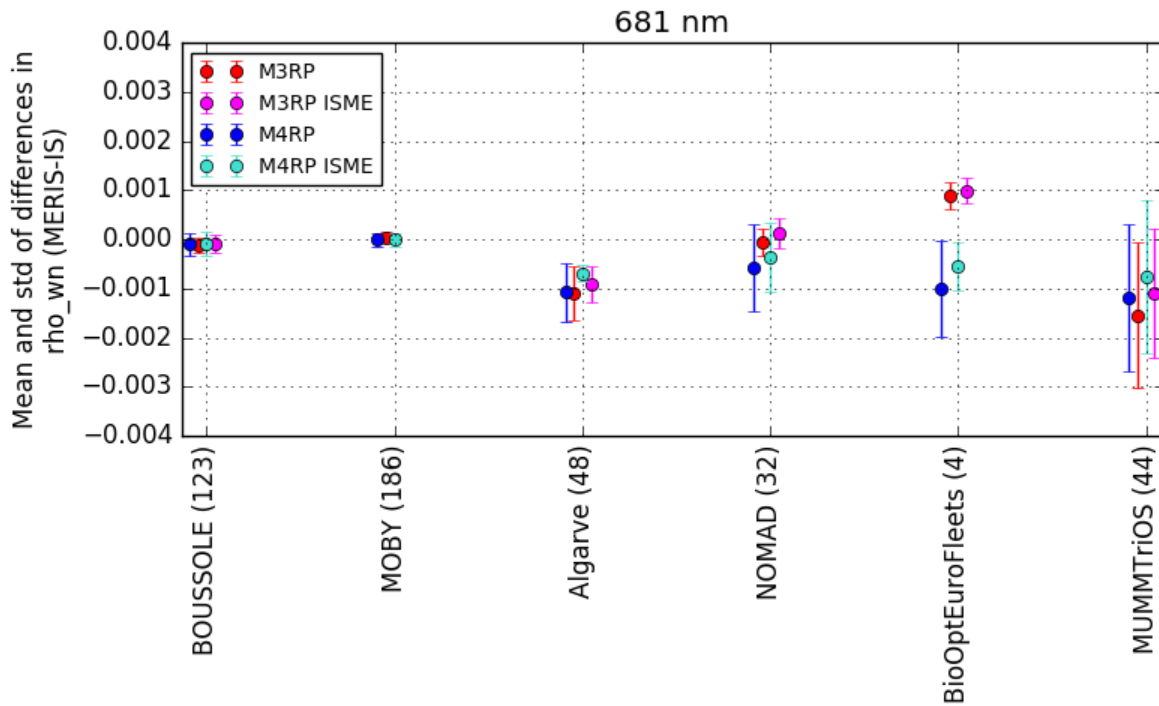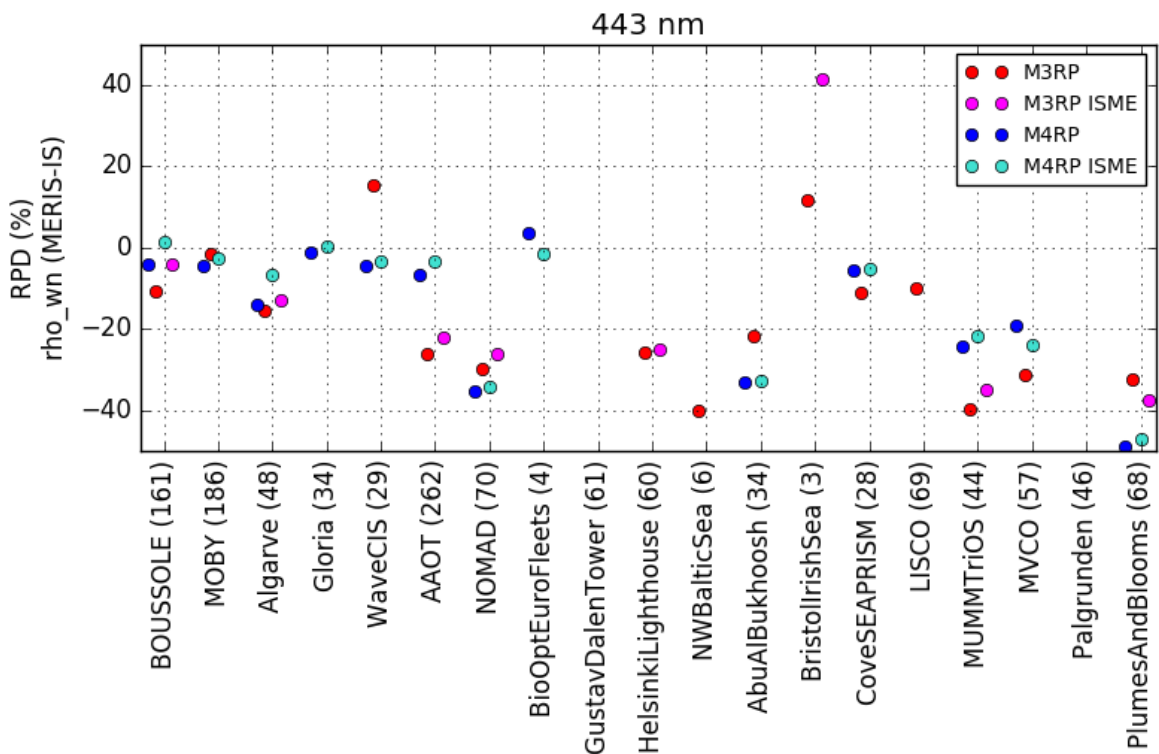

Figure 3-46: RPD between in situ and satellite fully-normalized water-leaving reflectances at 443 nm. M3RP IS and ISME: red and pink; M4RP IS and ISME: blue and cyan.

4th MERIS data reprocessing
Evolutions and Validation report

Ref.:   MER4RP Validation Report
Version: 1.0
Date: 01/04/2019
Page: 93
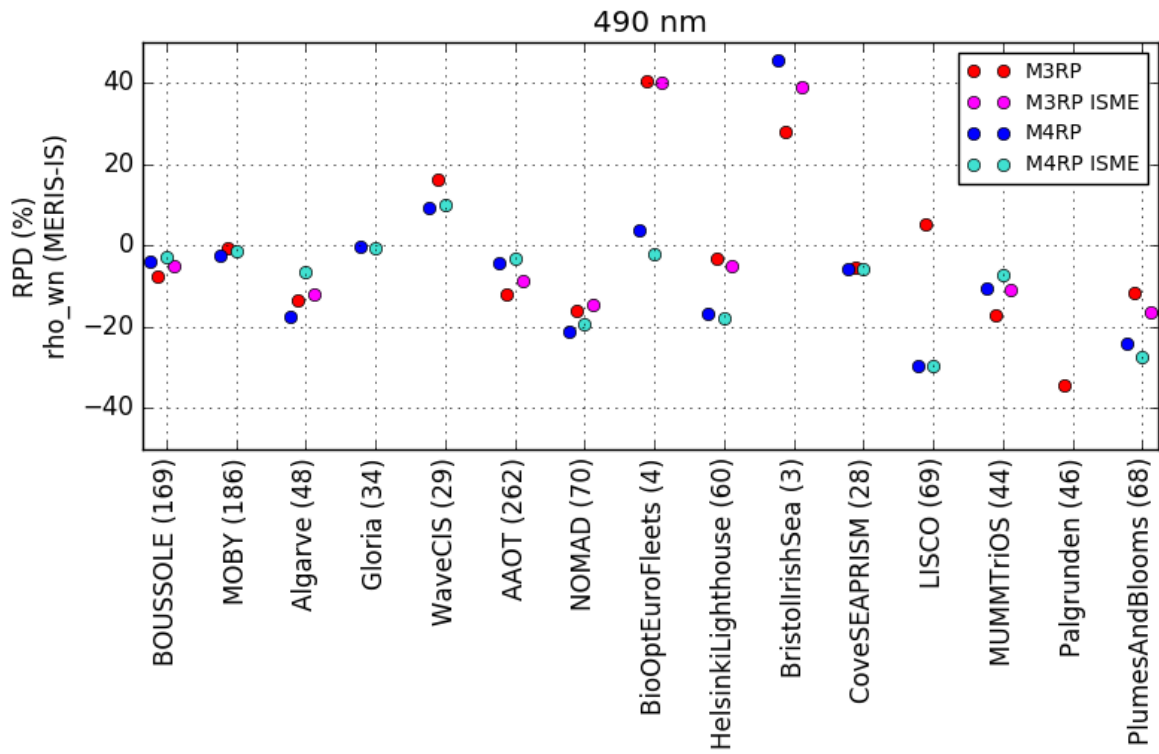
Figure 3-47: RPD between in situ and satellite fully-normalized water-leaving reflectances at 490 nm. M3RP IS and ISME: red and pink; M4RP IS and ISME: blue and cyan.
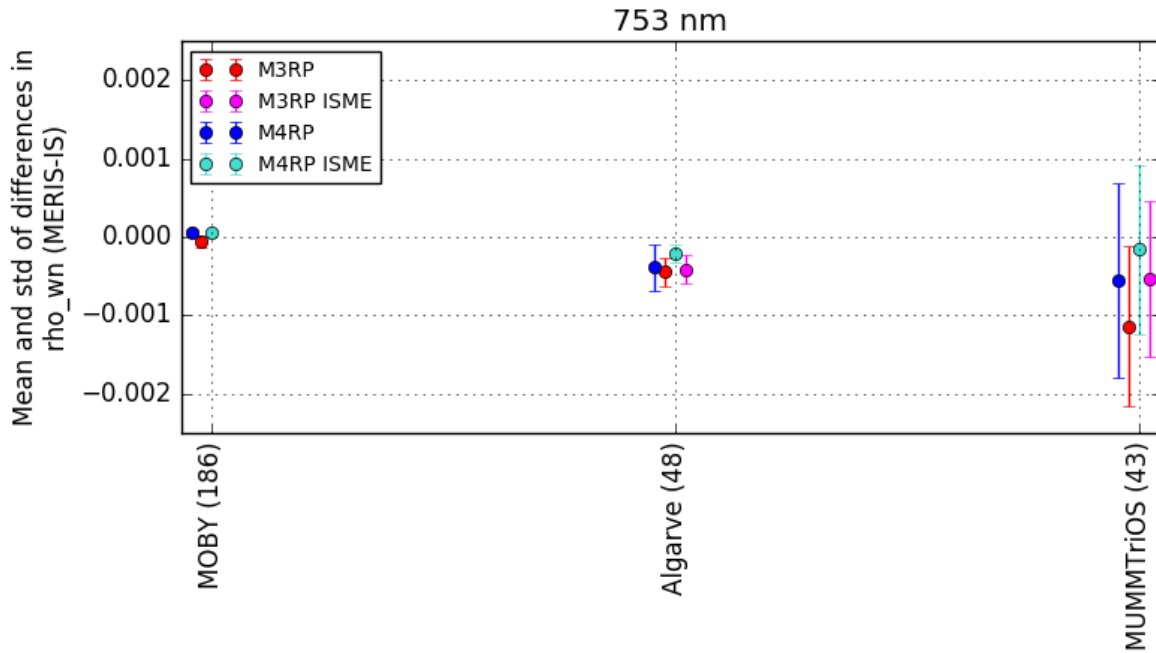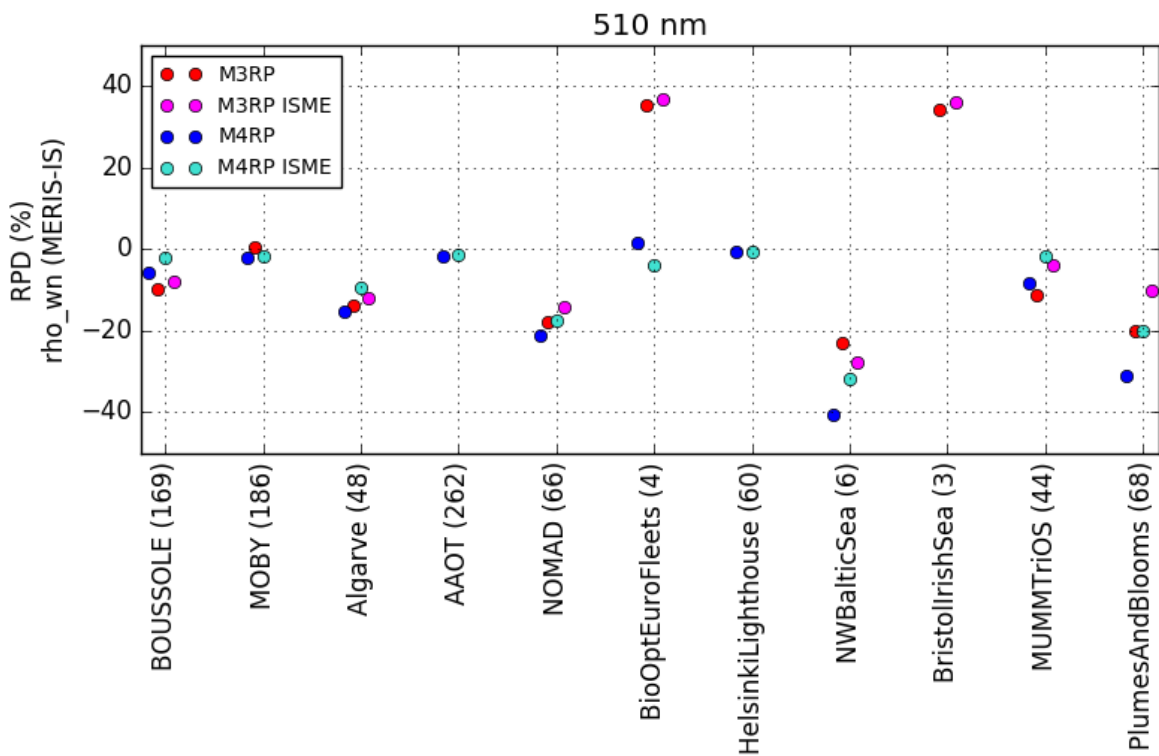

Figure 3-48: RPD between in situ and satellite fully-normalized water-leaving reflectances at 510 nm. M3RP IS and ISME: red and pink; M4RP IS and ISME: blue and cyan.

4th MERIS data reprocessing

Evolutions and Validation report

Ref.: MER4RP Validation Report

Version: 1.0

Date: 01/04/2019

Page: 94
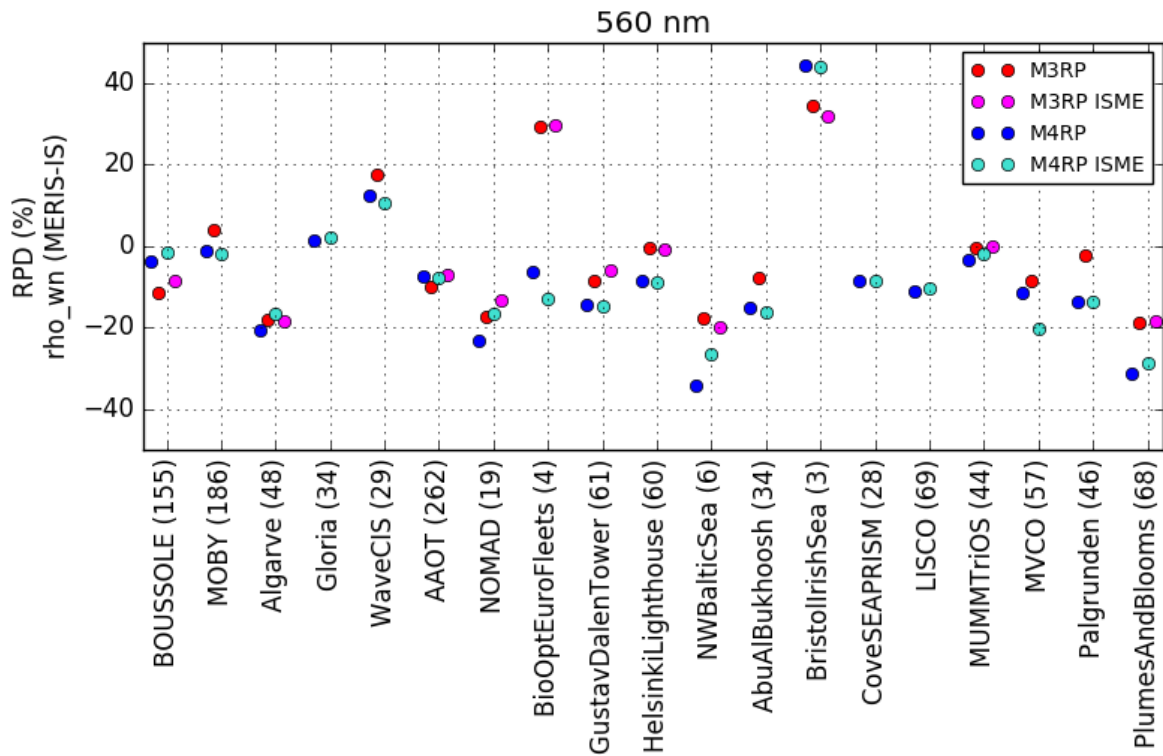
Figure 3-49: RPD between in situ and satellite fully-normalized water-leaving reflectances at 560 nm. M3RP IS and ISME: red and pink; M4RP IS and ISME: blue and cyan.
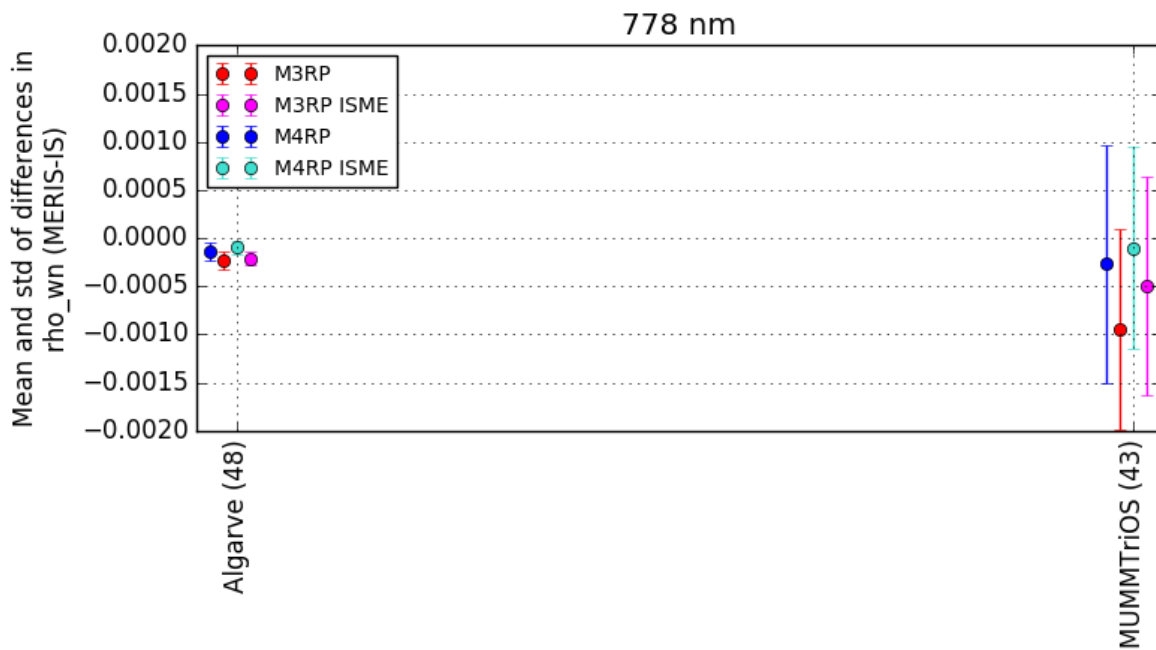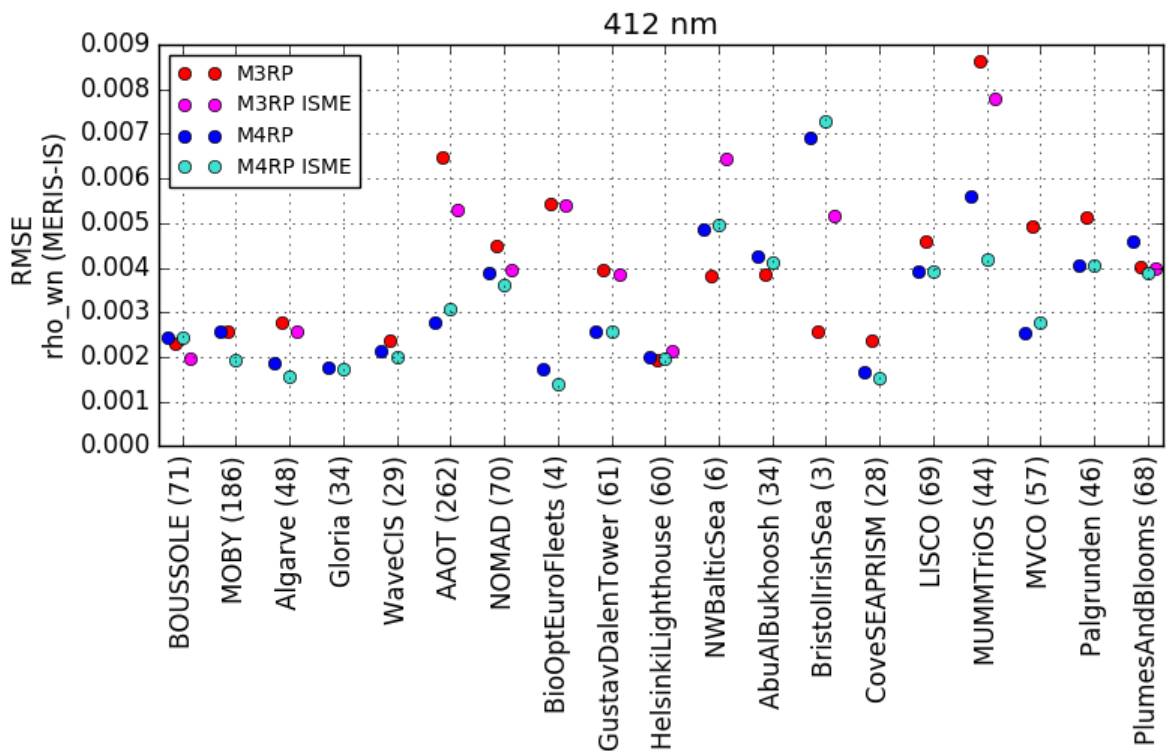

Figure 3-50: RMSE between in situ and satellite fully-normalized water-leaving reflectances at 412 nm. M3RP IS and ISME: red and pink; M4RP IS and ISME: blue and cyan.
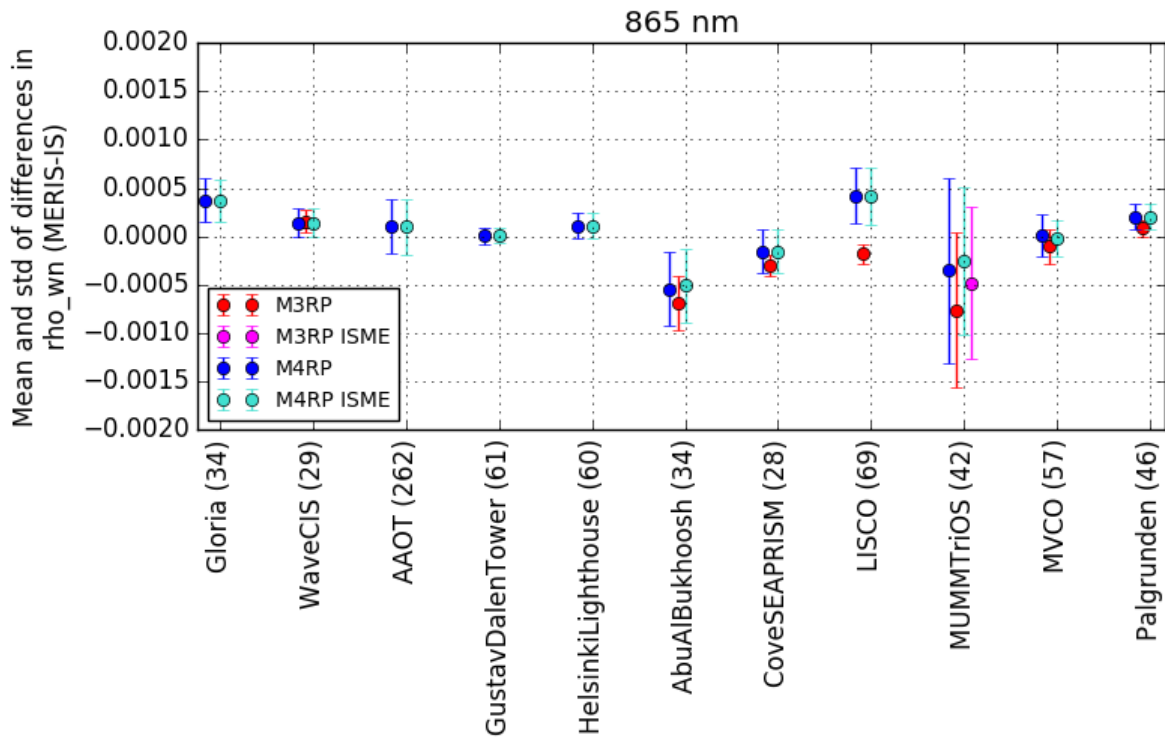
4th MERIS data reprocessing

Evolutions and Validation report

Ref.: MER4RP Validation Report

Version: 1.0

Date: 01/04/2019

Page: 95
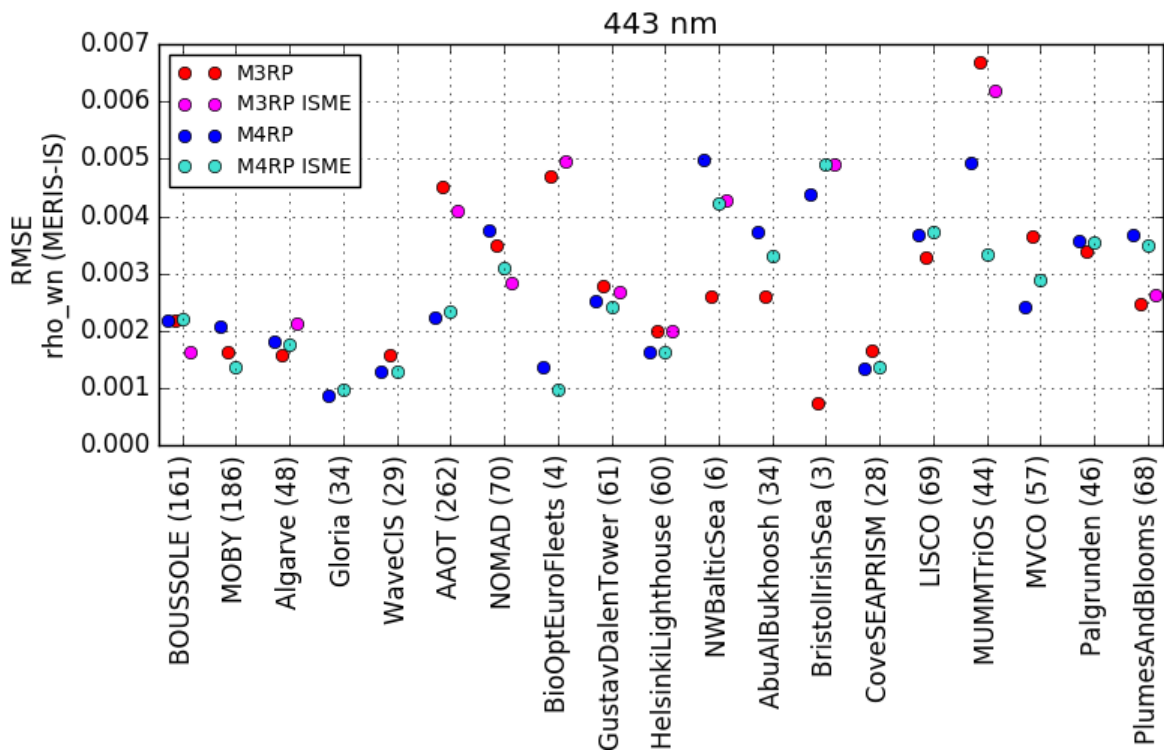
Figure 3-51: RMSE between in situ and satellite fully-normalized water-leaving reflectances at 443 nm. M3RP IS and ISME: red and pink; M4RP IS and ISME: blue and cyan.
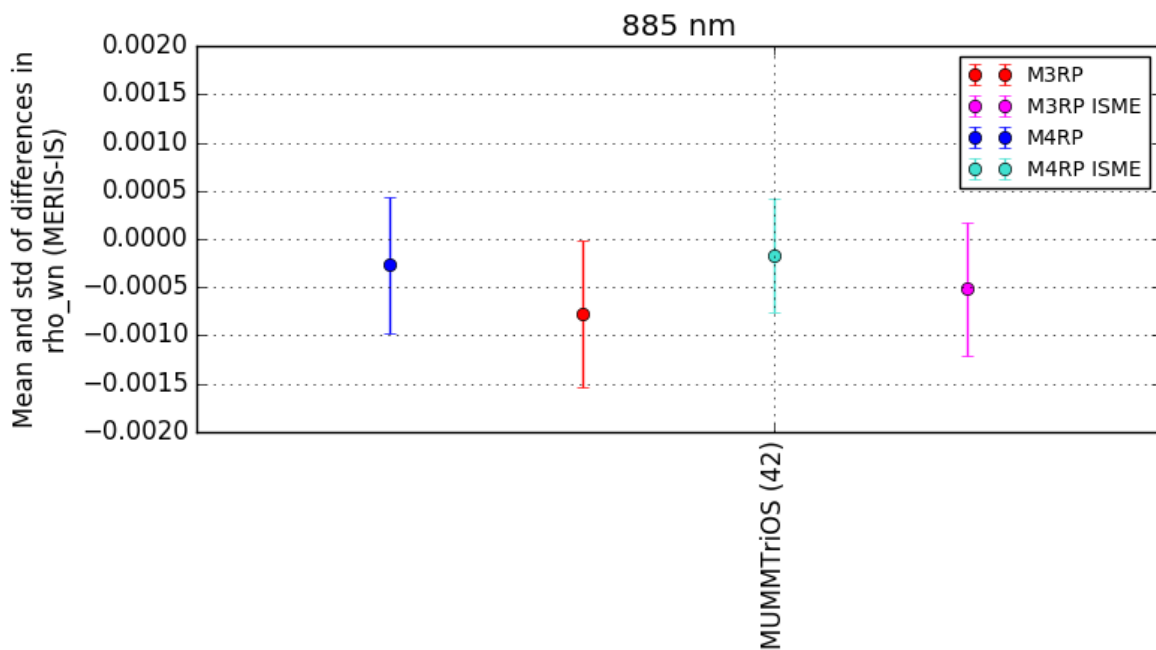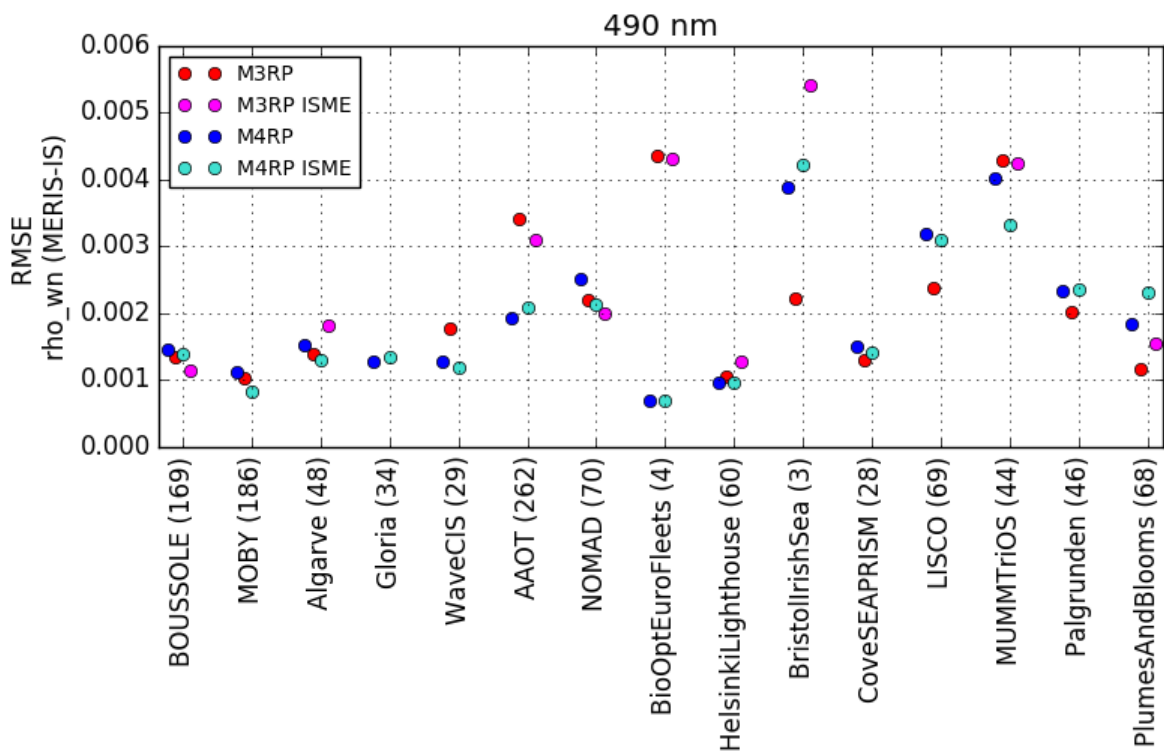

Figure 3-52: RMSE between in situ and satellite fully-normalized water-leaving reflectances at 490 nm. M3RP IS and ISME: red and pink; M4RP IS and ISME: blue and cyan.

4th MERIS data reprocessing
Evolutions and Validation report

Ref.:   MER4RP Validation Report
Version: 1.0
Date: 01/04/2019
Page: 96
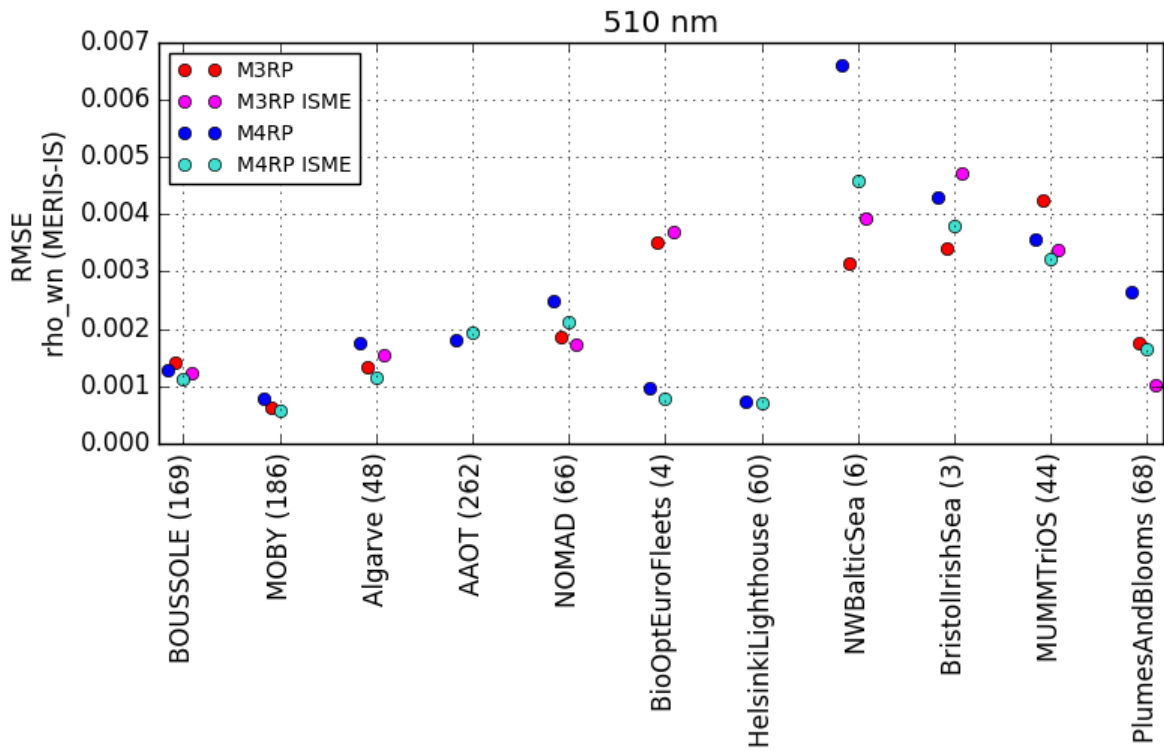
Figure 3-53: RMSE between in situ and satellite fully-normalized water-leaving reflectances at 510 nm. M3RP IS and ISME: red and pink; M4RP IS and ISME: blue and cyan.
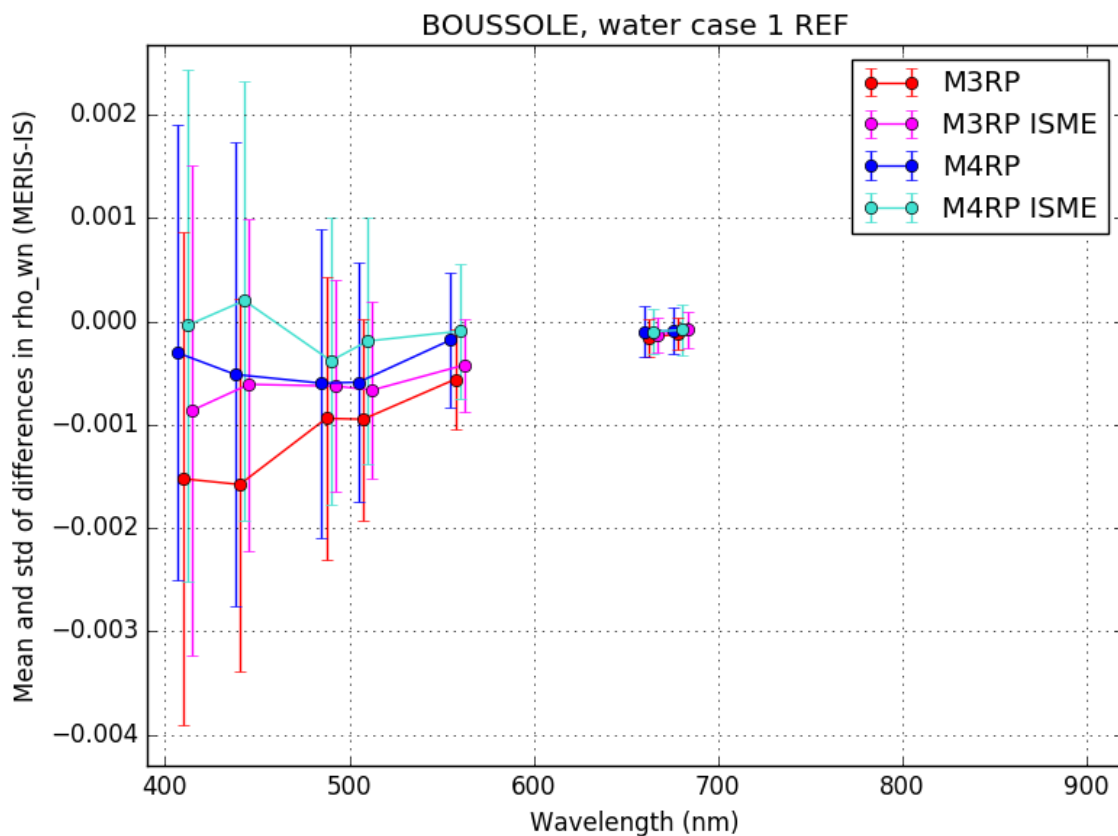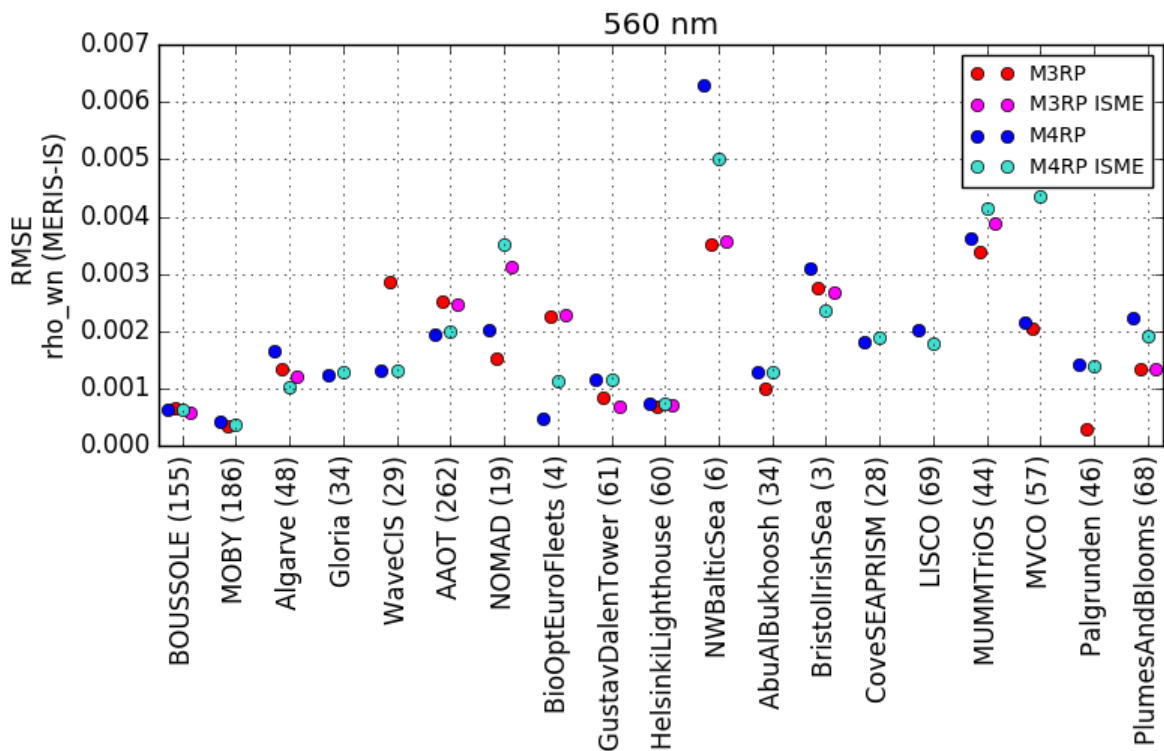

Figure 3-54: RMSE between in situ and satellite fully-normalized water-leaving reflectances at 560 nm. M3RP IS and ISME: red and pink; M4RP IS and ISME: blue and cyan.

4th MERIS data reprocessing
Evolutions and Validation report

Ref.: MER4RP Validation Report
Version: 1.0
Date: 01/04/2019
Page: 97

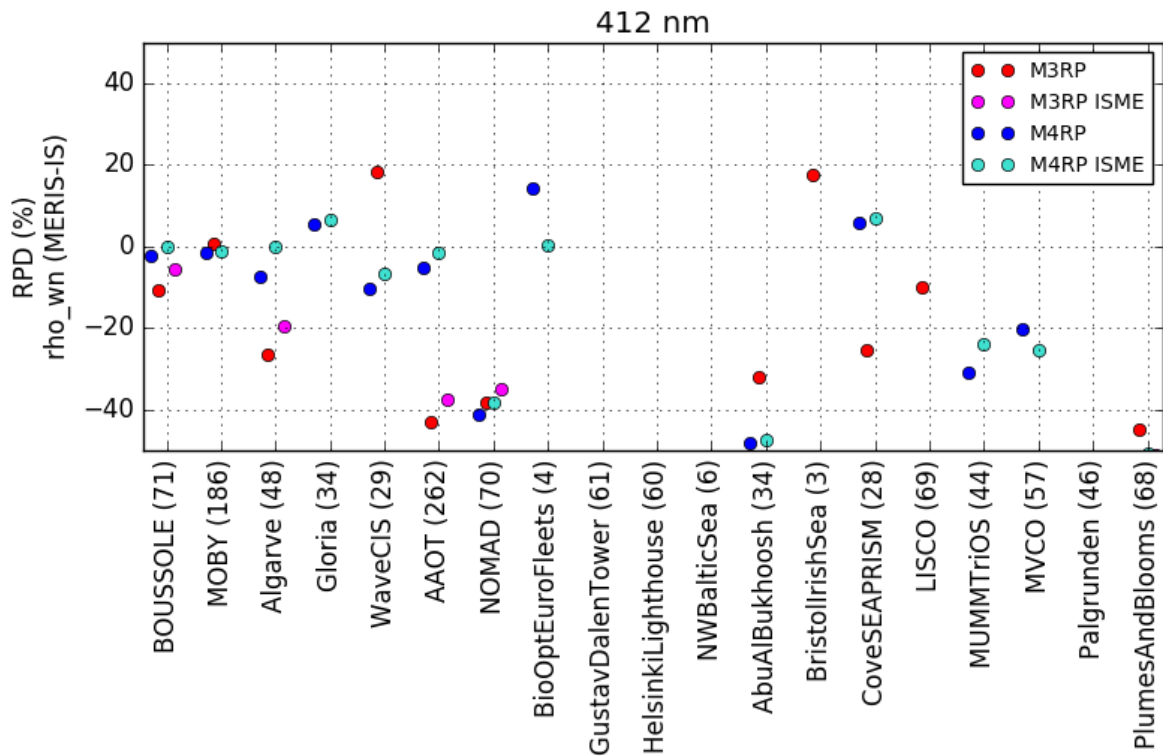Further grouping per category of sites allows to compare MER3RP and MER4RP on weighted-mean RPDs and weighted-mean RMSEs below (meaning that we weight according to the number of data points so as to consider a total statistic independent of the site).

MERIS 4RP are usually better (especially Case-1 and Case-1/2) or at least comparable with the results of MER3RP, almost achieving expectations of 0.002 RMSE in the blue or 5% RPD.

Table 3-3: MER3RP and MER4RP statistics comparison for Case-1 REF

Case-1 REF Band / Statistical parameter	RPD M3RP	RPD M4RP	RMSE M3RP	RMSE M4RP
412	-1.76	-1.71	0.00253	0.00252
443	-5.11	-4.40	0.00185	0.00212
490	-3.22	-2.98	0.00116	0.00129
510	-3.33	-3.65	0.00099	0.00104
560	-1.32	-2.30	0.00048	0.00053

Table 3-4: MER3RP and MER4RP statistics comparison for Case-1

Case-1 Band / Statistical parameter	RPD M3RP	RPD M4RP	RMSE M3RP	RMSE M4RP
412	-24.62	-2.18	0.00277	0.00196
443	-14.31	-5.30	0.00159	0.00138
490	-12.04	-1.11	0.00141	0.00141
510	-13.97	-5.69	0.00134	0.00083
560	-16.40	-3.93	0.00145	0.00140

Table 3-5: MER3RP and MER4RP statistics comparison for Case-1/2 REF

Case-1/2 REF Band / Statistical parameter	RPD M3RP	RPD M4RP	RMSE M3RP	RMSE M4RP
412	-41.37	-12.20	0.00583	0.00308
443	-27.63	-12.11	0.00416	0.00267
490	-13.61	-7.55	0.00302	0.00209
510	-17.89	-5.39	0.00185	0.00194
560	-12.77	-9.75	0.00221	0.00204

4th MERIS data reprocessing
Evolutions and Validation report

Ref.:   MER4RP Validation Report
Version: 1.0
Date: 01/04/2019
Page: 98

Table 3-6: MER3RP and MER4RP statistics comparison for Case-1/2

Case-1/2 Band / Statistical parameter	RPD M3RP	RPD M4RP	RMSE M3RP	RMSE M4RP
412	-117.58	-28.88	0.00351	0.00231
443	-49.00	-34.86	0.00266	0.00193
490	-13.97	0.57	0.00177	0.00087
510	-3.57	1.37	0.00327	0.00259
560	-4.60	-8.52	0.00145	0.00225

Table 3-7: MER3RP and MER4RP statistics comparison for Case-2

Case-2 Band / Statistical parameter	RPD M3RP	RPD M4RP	RMSE M3RP	RMSE M4RP
412	-75.99	-19.06	0.00526	0.00385
443	-31.28	-18.57	0.00402	0.00377
490	-6.54	-6.83	0.00420	0.00487
510	-7.96	-11.89	0.00565	0.00652
560	-5.73	-10.51	0.00558	0.00546

All these results provide consistency in the validation of the MER4RP for water-leaving reflectances, concluding that the quality is slightly enhanced compared to MER3RP.

Histograms are also obtained showing the agreement between MERIS and in situ normalized water-leaving reflectance with respect to the dynamics of water-leaving reflectance.
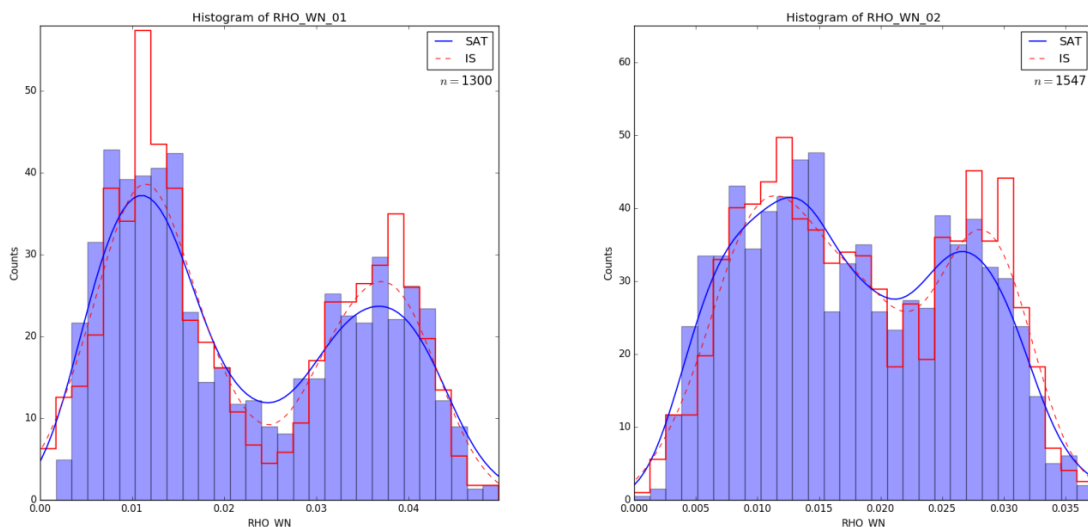
Figure 3-55: Histograms of 412 & 443 nm normalized water-leaving reflectance: MERIS (blue) and in situ (red)

4th MERIS data reprocessing

Evolutions and Validation report

Ref.:   MER4RP Validation Report

Version: 1.0

Date: 01/04/2019

Page: 99
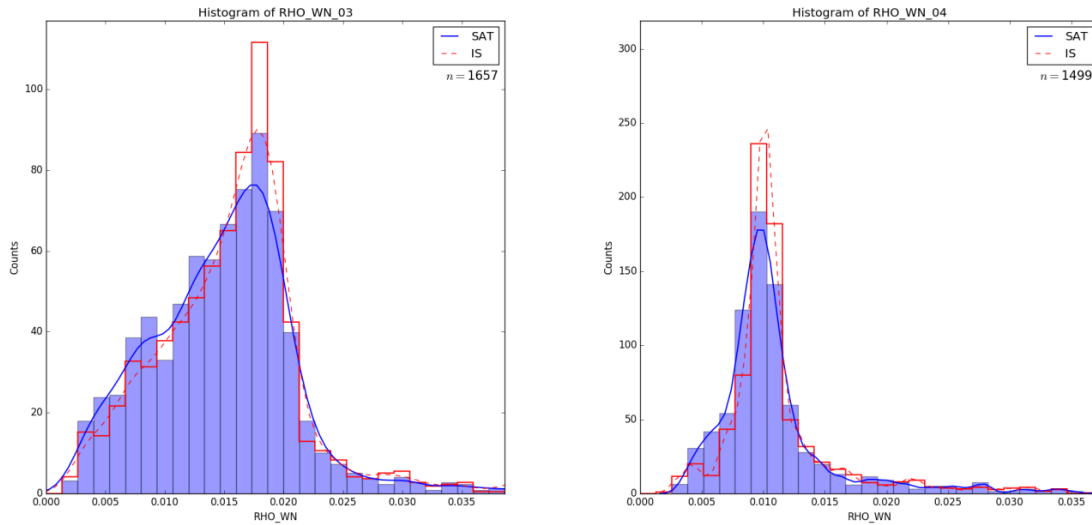
Figure 3-56: Histograms of 490 & 510 nm normalized water-leaving reflectance: MERIS (blue) and in situ (red)
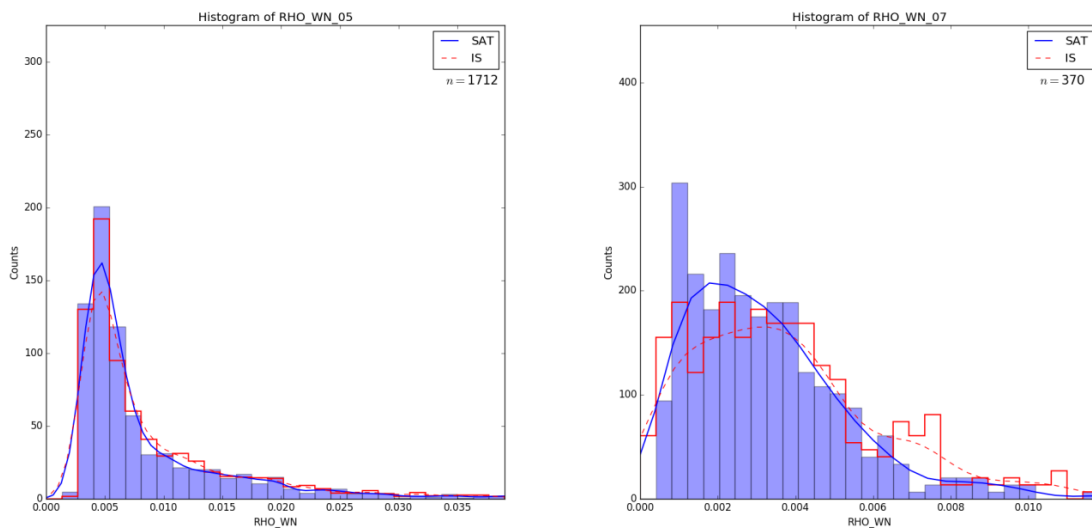
Figure 3-57: Histograms of 560 & 665 nm normalized water-leaving reflectance: MERIS (blue) and in situ (red)

3.3.1.2   *Comparisons of MER3RP and MER4RP L2 products*

Comparison over Black Sea

An intercomparison of the water reflectance from both MERIS 3RP and MERIS 4RP is carried out over the NW-Black Sea near Galata and Gloria stations (Figure 3-58) using the following products:

MER_RR__2PTACR20070512_081345_000001582058_00064_27172_0000.N1

ENV_ME_2_RRG____20070512T081345_20070512T081623_____0157_058_064_____ACR_R_NT____.SEN3

Both products show almost the same shape and behaviour, with maxima at 490 and 560 nm (chlorophyll contribution), and, then, a decrease and almost no signal in the IR range >750nm. We observe that MERIS 4RP products performs better in the short wavelength e.g. 412 nm, where one does not observe any more the negative reflectance as in the case of

4th MERIS data reprocessing
Evolutions and Validation report

Ref.: MER4RP Validation Report
Version: 1.0
Date: 01/04/2019
Page: 100

MERIS 3RP. In general, the results show higher water reflectance (5%-10%) in MERIS 4RP wrt MERIS 3RP (Figure 3-59 and Figure 3-60).
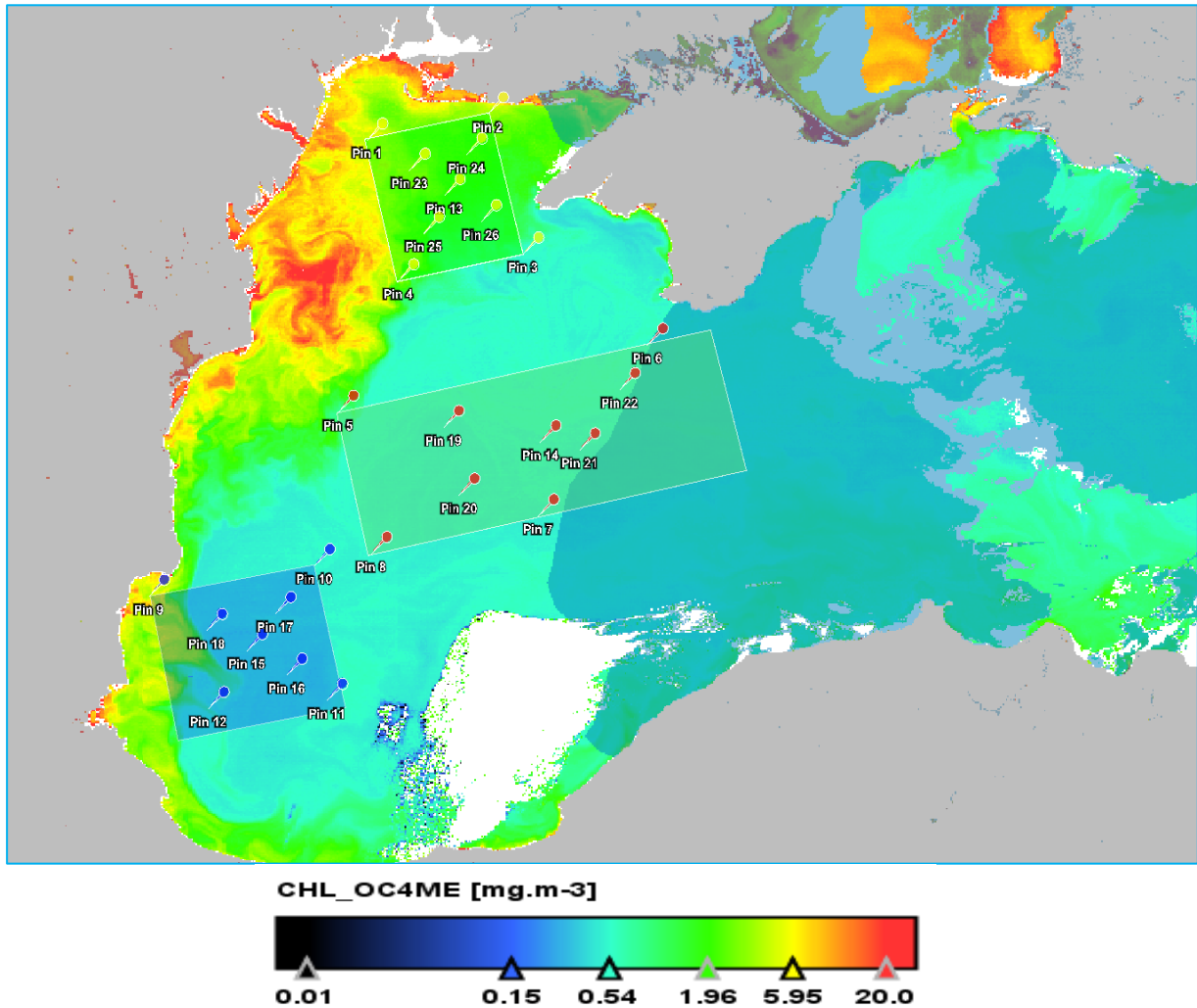
Figure 3-58: Chlorophyll-a (OC4ME) from MERIS-4RP of the Black sea showing the three ROIs (blue-pins) ROI-1, (red-pins) ROI-2 and (light-green-pins) ROI-3, as well the Pins location; The shaded area on the right part of the image indicates the Medium Glint Mask. MERIS acquisition is on 20070512.

4th MERIS data reprocessing
Evolutions and Validation report

Ref.: MER4RP Validation Report
Version: 1.0
Date: 01/04/2019
Page: 101
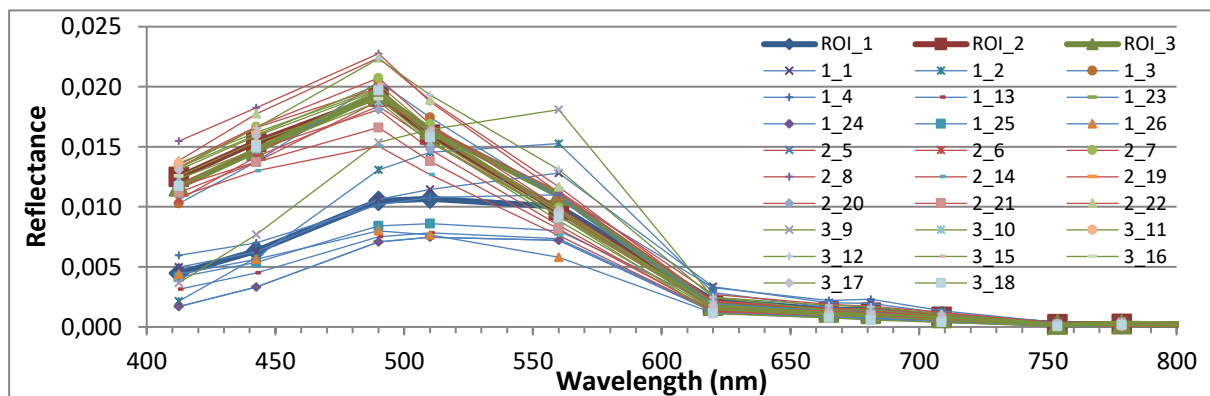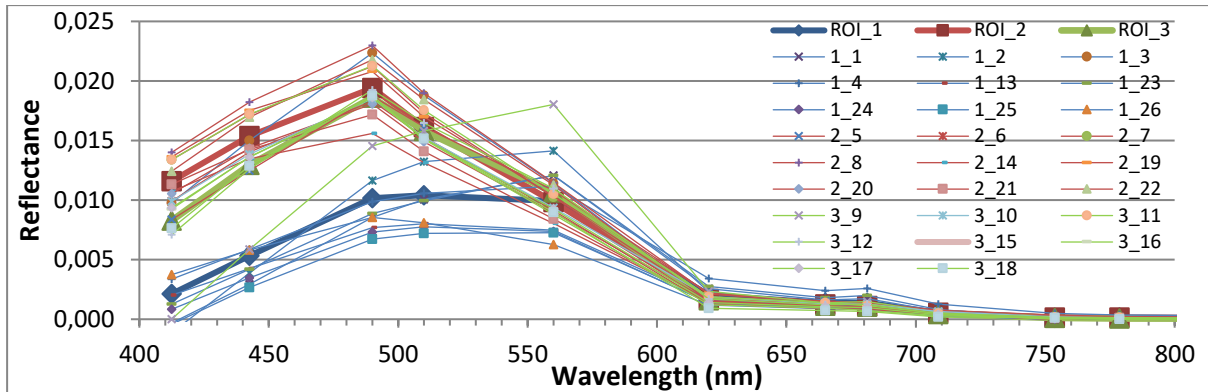
Figure 3-59: Spectral plots for each pin of (top) reflectance from MERIS 3RP and (bottom) M*_Rho_w from MERIS 4RP. Thick curves indicate the ROIs average over the valid pixels (see Figure 3-58).
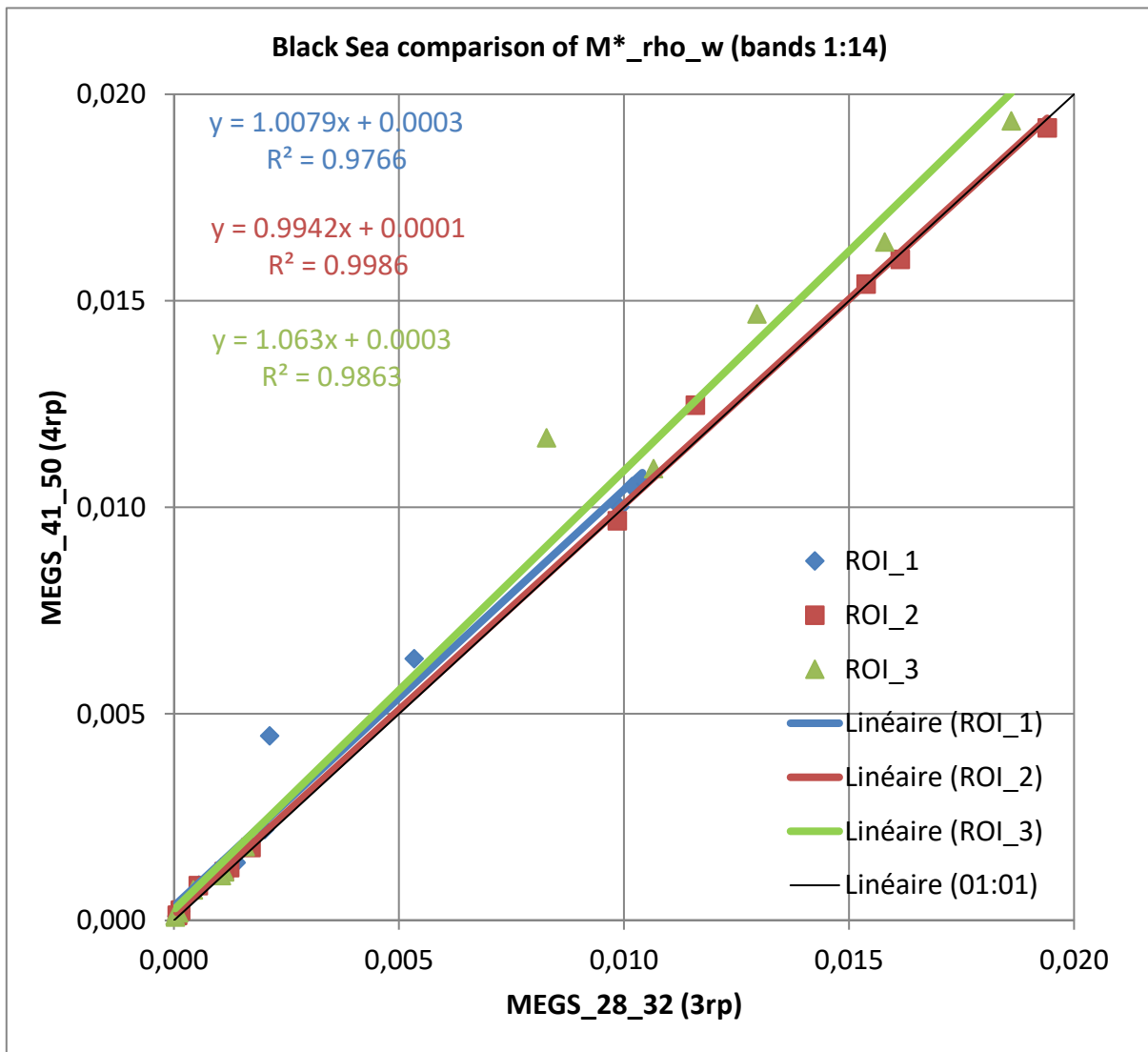
Figure 3-60: Scatterplot of Rho_w from MERIS 4P to water reflectance from MERIS 3RP from Black Sea averaged over the three ROIs (see Figure 3-58).

4th MERIS data reprocessing

Evolutions and Validation report

Ref.: MER4RP Validation Report

Version: 1.0

Date: 01/04/2019

Page: 102

Comparison over NW-European Seas

An intercomparison of the water reflectance from both MERIS 3RP and MERIS 4RP is carried out over the NW-European Seas near (Figure 3-61) using the following products:

MER_RR__2PTACR20080507_104518_000004482068_00223_32341_000.N1

ENV_ME_2_RRG____20080507T104518_20080507T105246_____0447_068_223_____ACR_R_NT____.SEN3

Both products show almost the same shape and behaviour for bands longer than 500 nm, but with clear higher reflectance values wrt to MERIS 3RP. Different behaviours could be observed in the blue-blue-green spectral range (412-490 nm) where MERIS 4RP shows higher reflectance for band 412 than for band 443, which is not the case for MERIS 3RP (Figure 3-62). In general, the results show systematically higher water reflectance (10%-20%) in MERIS 4RP wrt MERIS 3RP, particularly for ROI#4 (Figure 3-63).

CHL_OC4ME [mg.m-3]
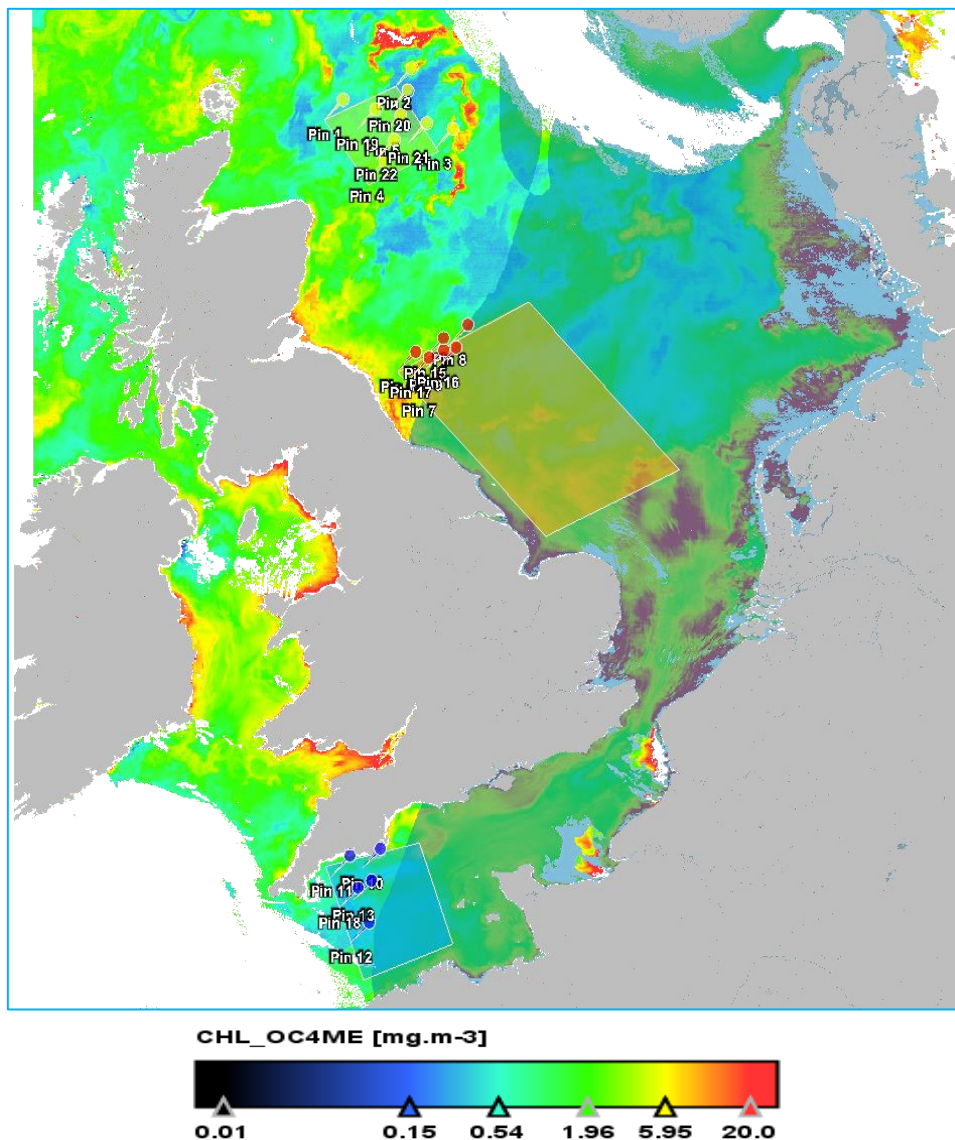
Figure 3-61: Chlorophyll-a (OC4ME) from MERIS-4RP of the NW-European Seas showing the three ROIs (blue-pins) ROI-1, (red-pins) ROI-2 and (light-green-pins) ROI-4, as well the Pins location; The shaded area on the right part of the image indicates the Medium Glint Mask. MERIS acquisition is on 20080507.

4th MERIS data reprocessing

Evolutions and Validation report

Ref.: MER4RP Validation Report

Version: 1.0

Date: 01/04/2019

Page: 103
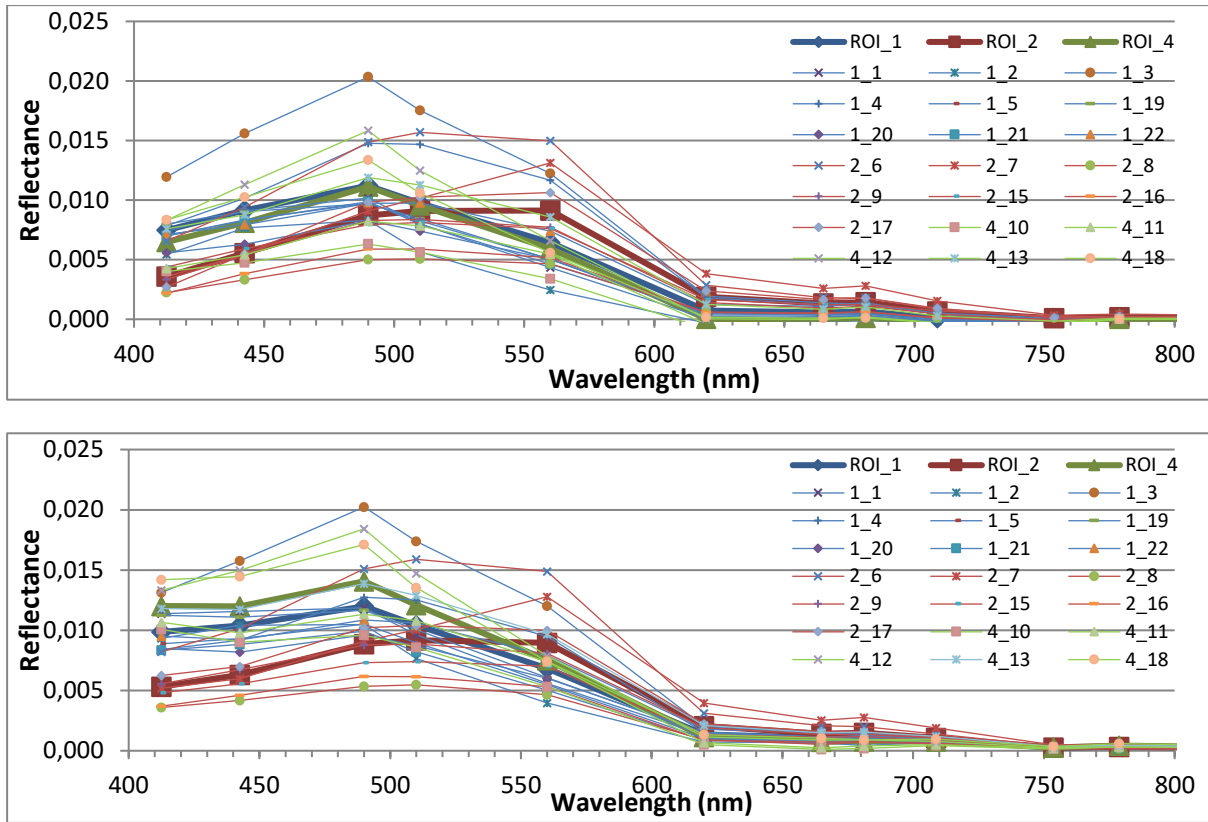
Figure 3-62: Spectral plots for each pin of (top) reflectance from MERIS 3RP and (bottom) M*_Rho_w from MERIS 4RP. Thick curves indicate the ROIs average over the valid pixels (see Figure 3-61).

4th MERIS data reprocessing
Evolutions and Validation report

Ref.:   MER4RP Validation Report
Version: 1.0
Date: 01/04/2019
Page: 104
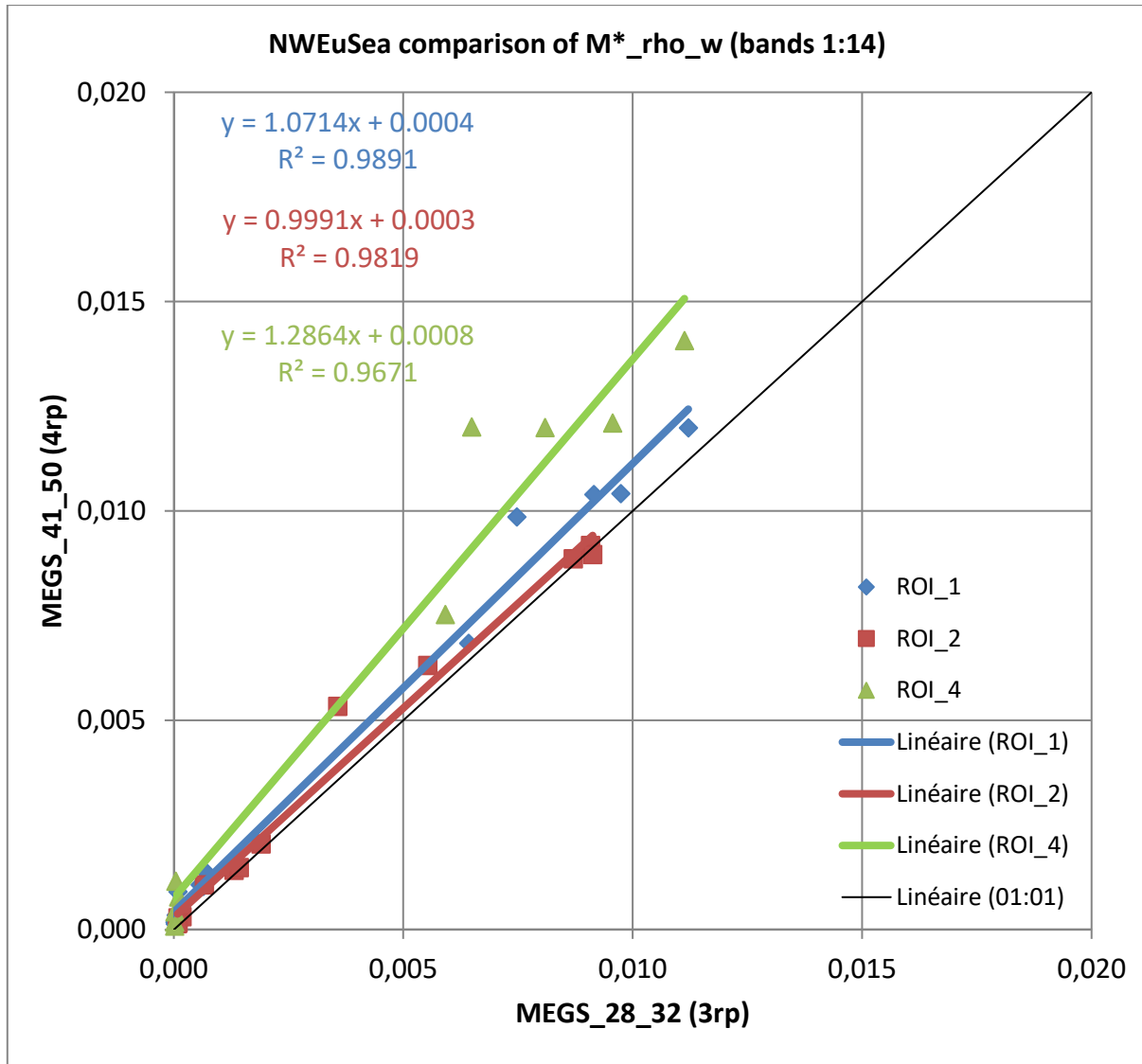
Figure 3-63: Scatterplot of M*_Rho_w from MERIS 4P to water reflectance from MERIS 3RP from NW-European Sea averaged over the three ROIs (see Figure 3-61).

Figure 3-64 displays scatterplot of the averaged water reflectance from both MERIS 4RP and MERIS 3RP over the different ROIs from both Black Sea and the NW-European Sea. Although MERIS 4RP shows systematically higher reflectance than MERIS 3RP, the NW-European seas exhibit stronger slope of about 10% than the Black Sea one, but lower correlation between both reprocessing datasets. This scatterplots per band from both Seas confirm the aforementioned results, where we observe the highest difference over M01 (412 nm) and M07 (665 nm) and longer wavelength (Figure 3-65).

4th MERIS data reprocessing

Evolutions and Validation report

Ref.: MER4RP Validation Report

Version: 1.0

Date: 01/04/2019

Page: 105
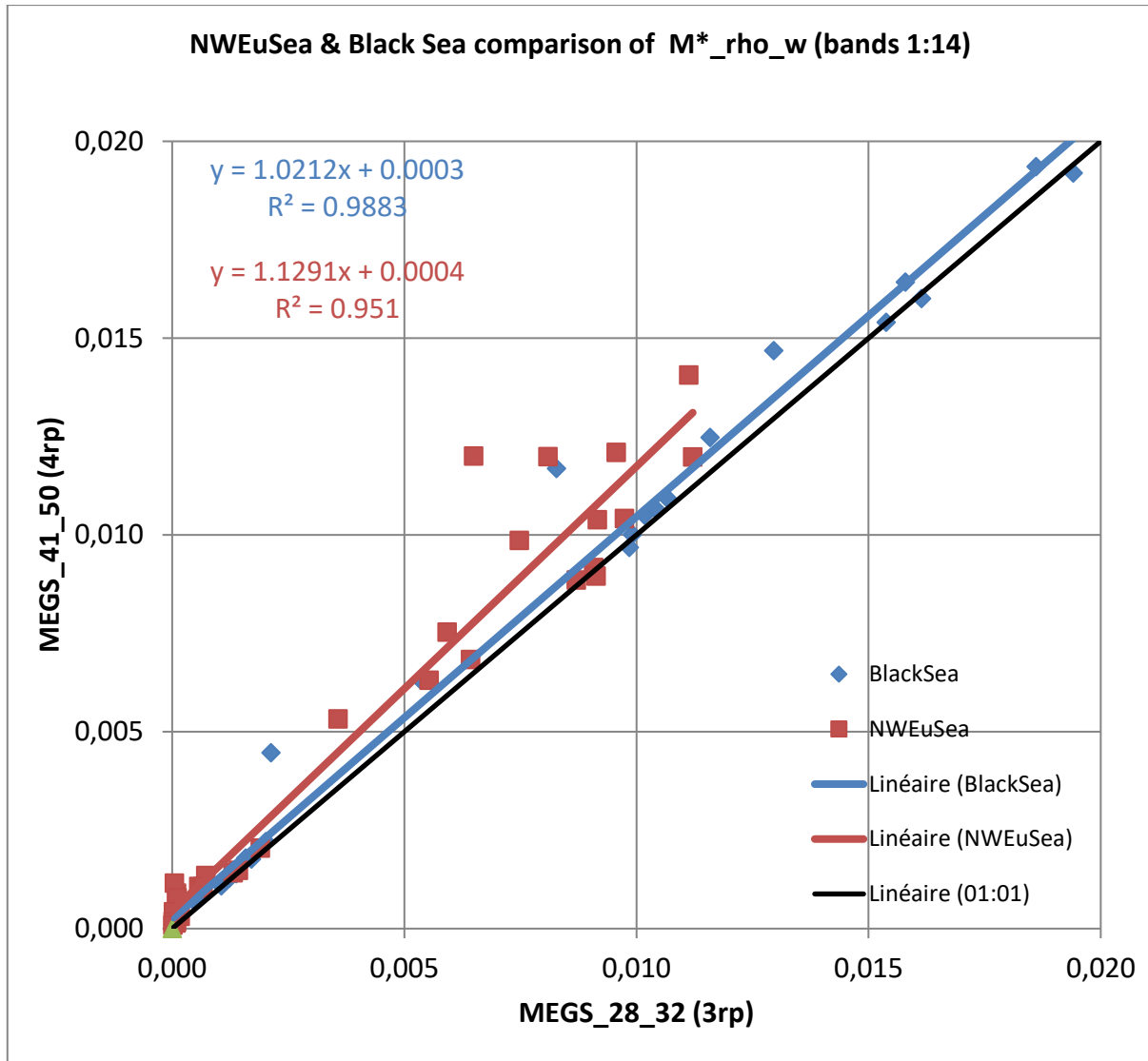
Figure 3-64: Scatterplot of Rho_w from MERIS 4P to water reflectance from MERIS 3RP from Black Sea and NW-European Sea averaged over the different ROIs (see Figure 3-58 and Figure 3-61).

4th MERIS data reprocessing

Evolutions and Validation report

Ref.: MER4RP Validation Report

Version: 1.0

Date: 01/04/2019

Page: 106

4th MERIS data reprocessing
Evolutions and Validation report

Ref.: MER4RP Validation Report
Version: 1.0
Date: 01/04/2019
Page: 107
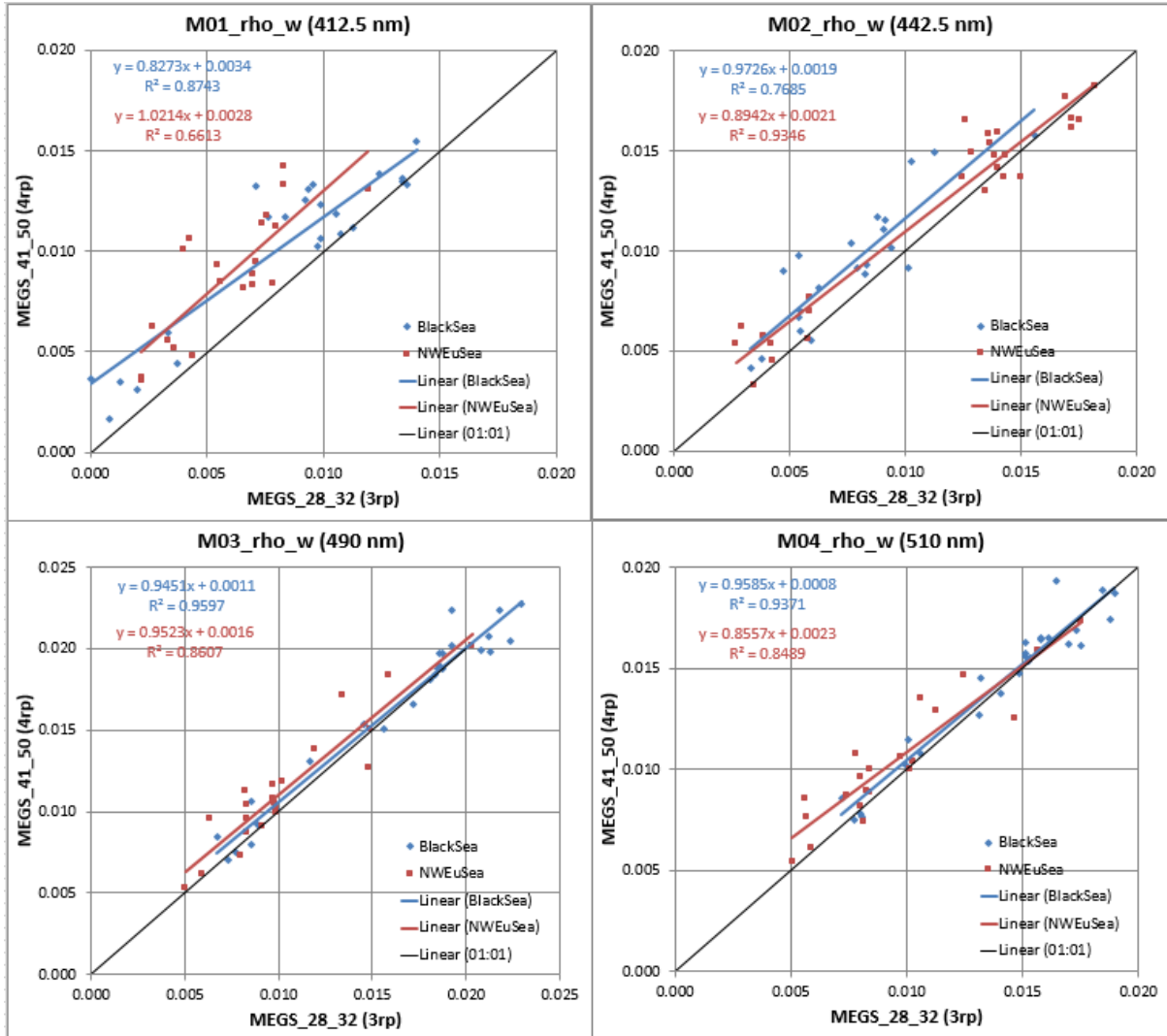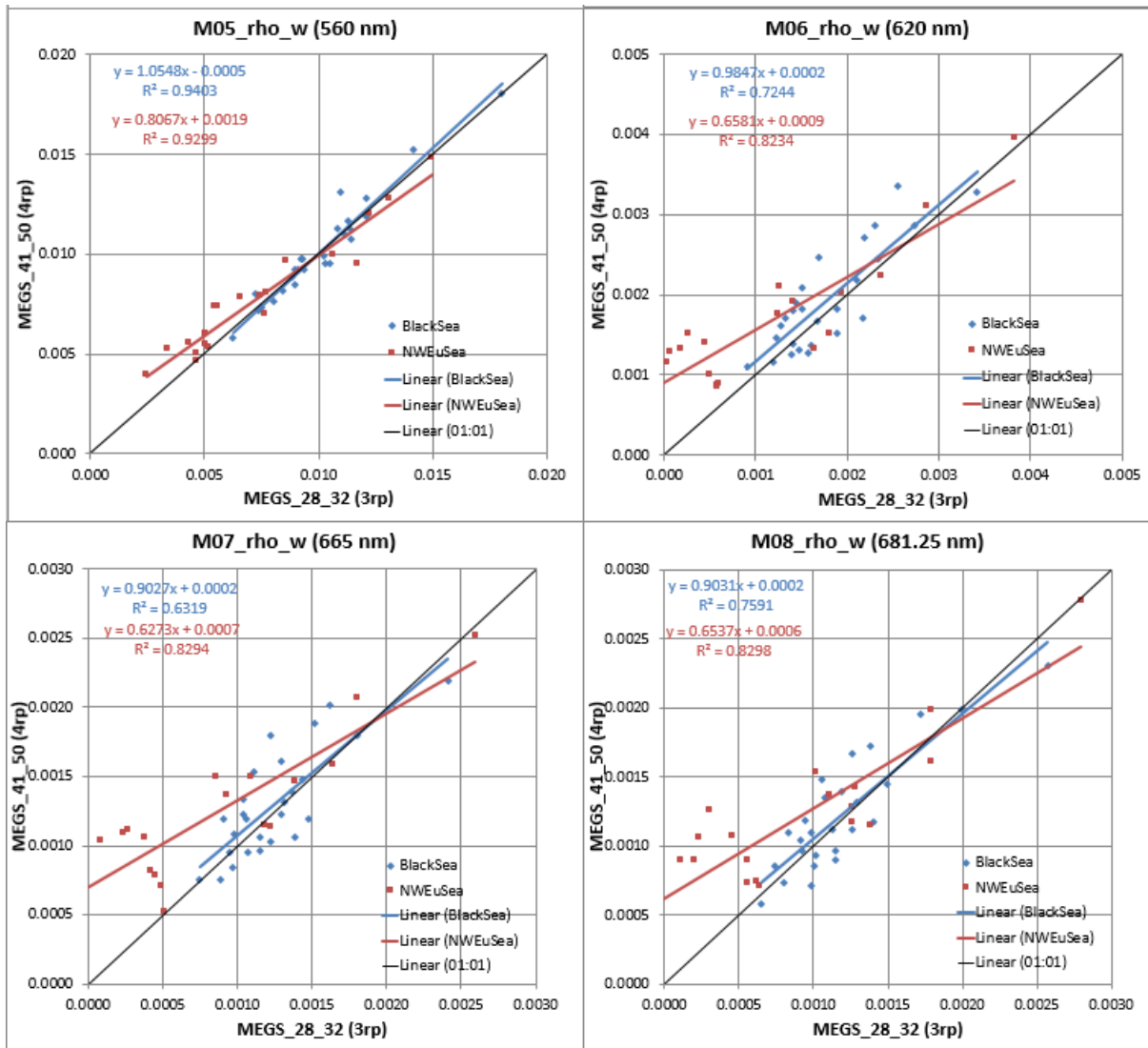
Figure 3-65: Scatterplot of M*_Rho_w from MERIS 4P to water reflectance from MERIS 3RP per band (top-bottom) M01-M08 from (blue) Black Sea and (red) NW-European Sea averaged over the different ROIs (see Figure 3-58 and Figure 3-61).

3.3.1.3   Validation based on L3 products intercomparison

The mer4val facility (http://mer4val.acri.fr/) provides Level 3 intercomparisons of the MER3RP and the MER4RP as well as MODIS and SeaWIFS (both, reprocessing version R2014.0) on a daily or monthly basis for the main L2 parameters.

Global maps of NRRS {412, 443, 490, 555, 670} nm can be compared between MERIS reprocessings and NASA sensors. Monthly means are displayed in Figure 3-66 to Figure 3-74 for Sept 2008. NRRS {510, 560, 620} nm can further be compared between M3RP and M4RP.

Overall geophysical consistency is checked at all bands. At 670 nm the water signal is very small and consequently more uncertainty, all sensors agree within an achievable precision.

4th MERIS data reprocessing

Evolutions and Validation report

Ref.: MER4RP Validation Report

Version: 1.0

Date: 01/04/2019

Page: 108
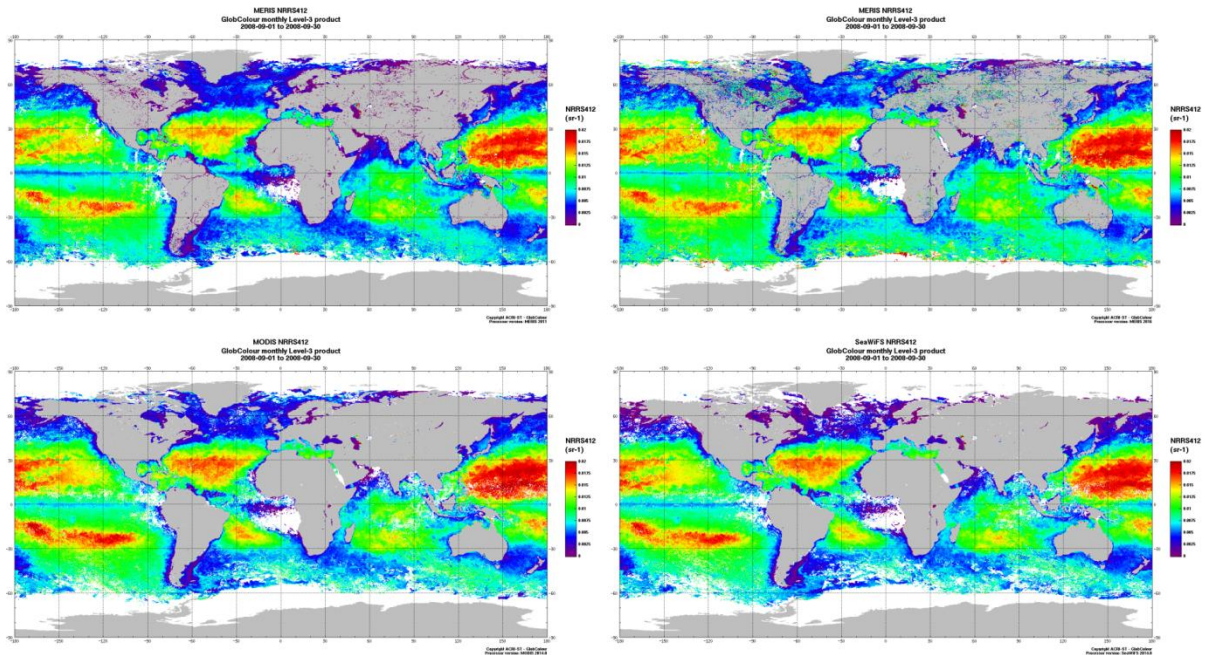
Figure 3-66: MER3RP (top left), MER4RP (top right), MODIS (bottom left), and SeaWIFS (bottom right) NRRS412 L3 map over Sept 2008.
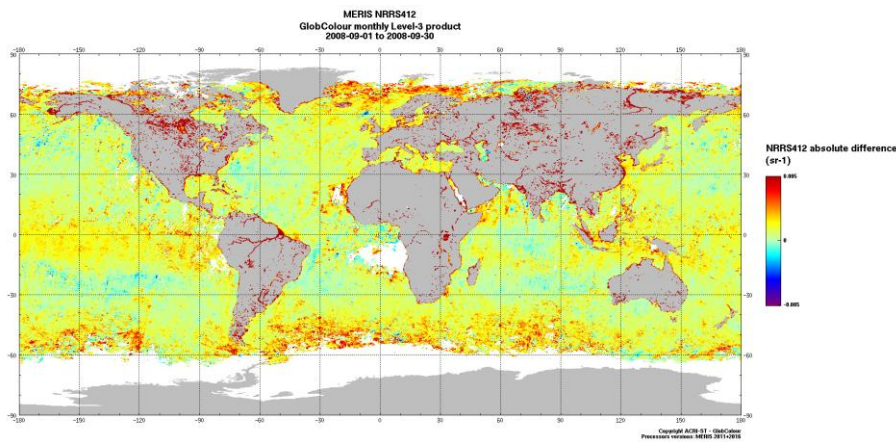
Figure 3-67: MER4RP - MER3RP absolute difference of NRRS412 L3 map over Sept 2008.

4th MERIS data reprocessing

Evolutions and Validation report

Ref.: MER4RP Validation Report

Version: 1.0

Date: 01/04/2019

Page: 109
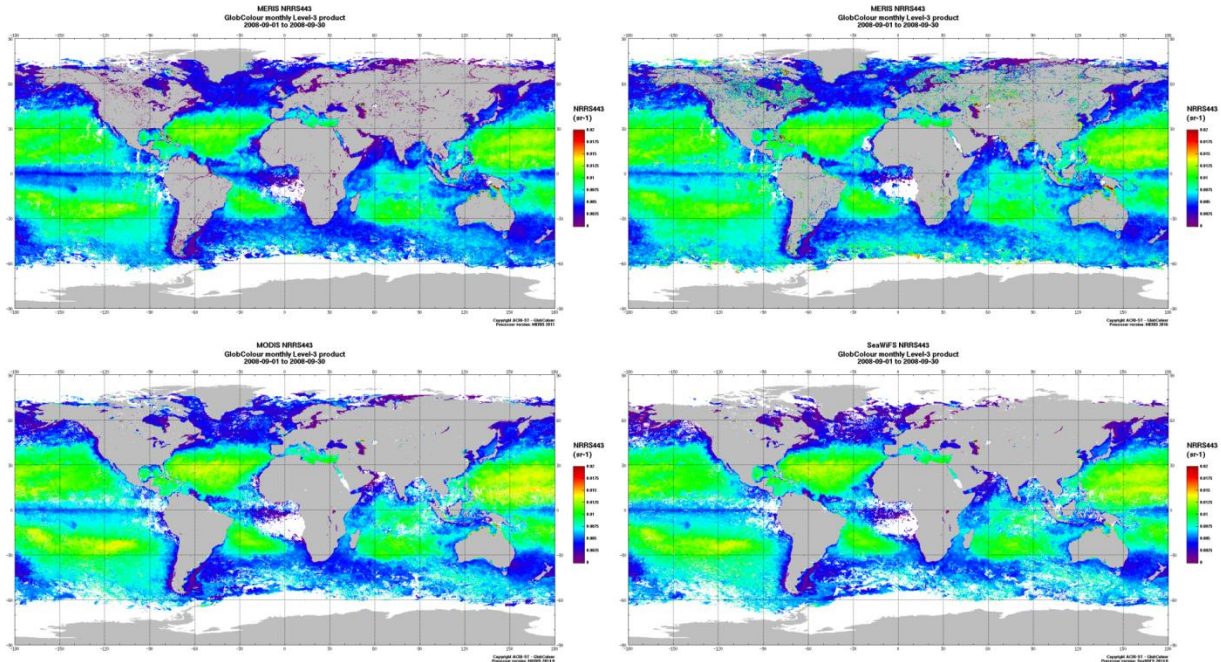
Figure 3-68: MER3RP (top left), MER4RP (top right), MODIS (bottom left), and SeaWIFS (bottom right) NRRS443 L3 map over Sept 2008.
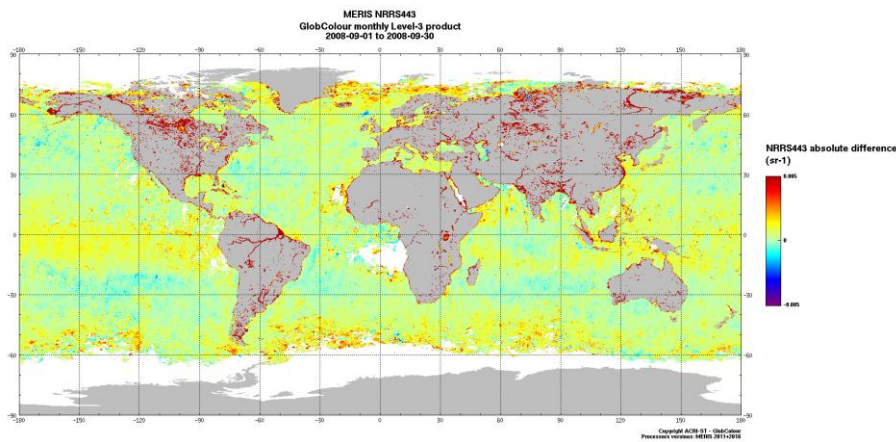
Figure 3-69: MER4RP - MER3RP absolute difference of NRRS443 L3 map over Sept 2008.

4th MERIS data reprocessing

Evolutions and Validation report

Ref.: MER4RP Validation Report

Version: 1.0

Date: 01/04/2019

Page: 110
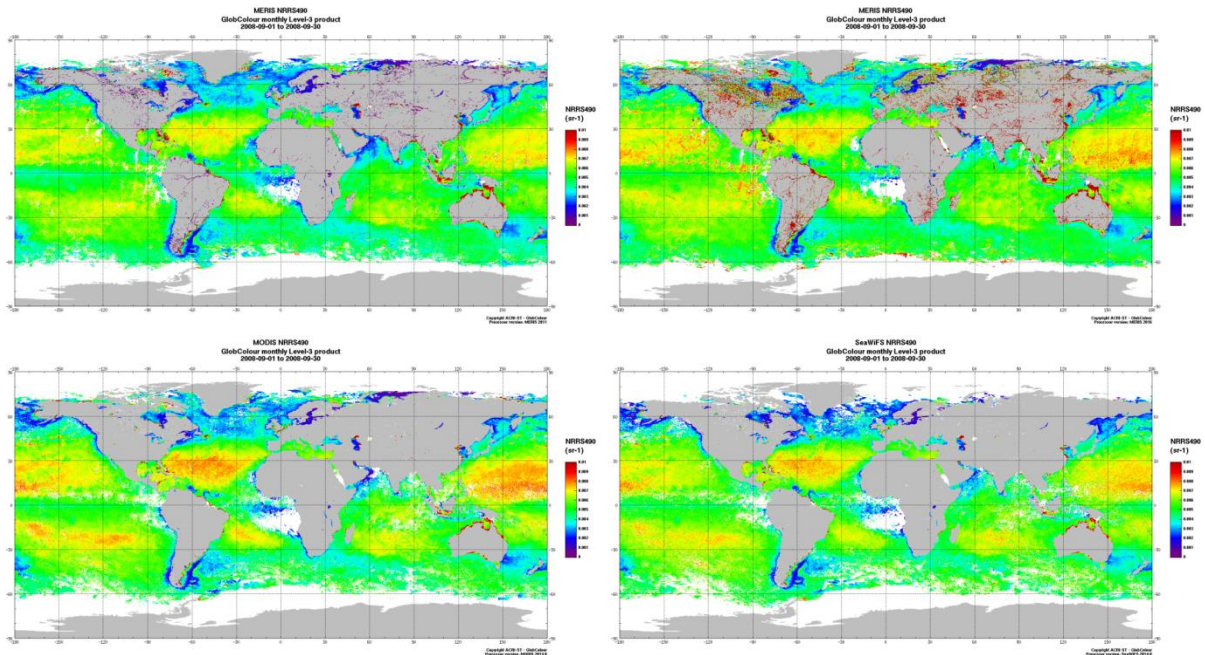
Figure 3-70: MER3RP (top left), MER4RP (top right), MODIS (bottom left), and SeaWIFS (bottom right) NRRS490 L3 map over Sept 2008.
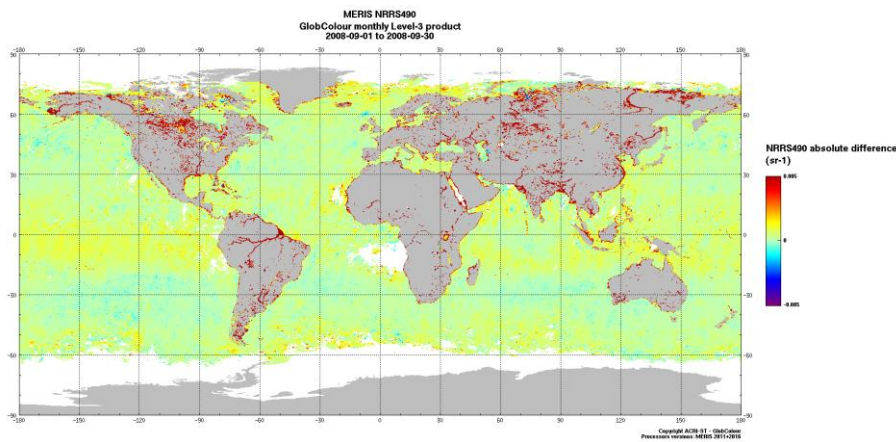
Figure 3-71: MER4RP - MER3RP absolute difference of NRRS490 L3 map over Sept 2008.

4th MERIS data reprocessing

Evolutions and Validation report

Ref.: MER4RP Validation Report
Version: 1.0
Date: 01/04/2019
Page: 111
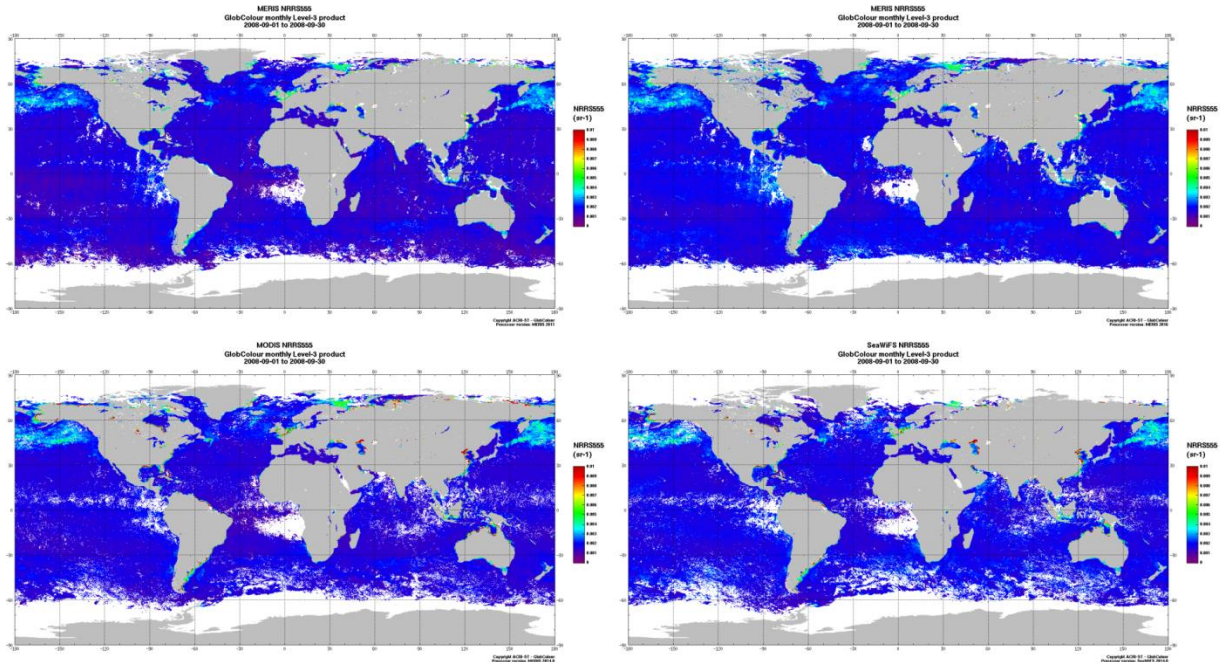
Figure 3-72: MER3RP (top left), MER4RP (top right), MODIS (bottom left), and SeaWIFS (bottom right) NRRS555 L3 map over Sept 2008.
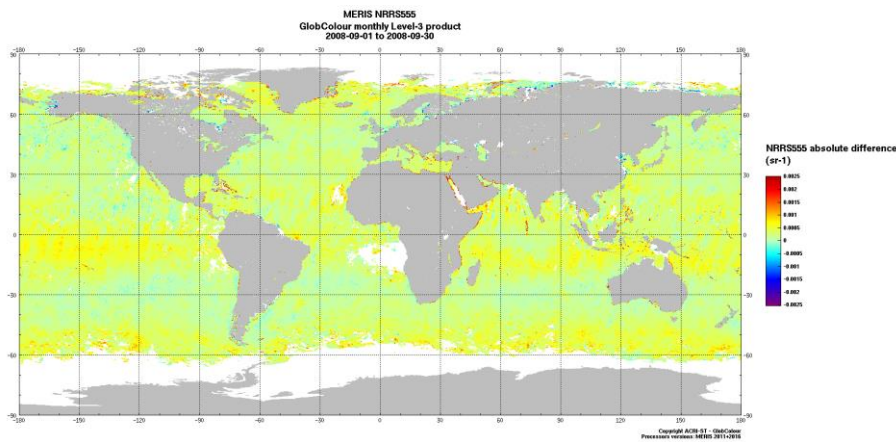
Figure 3-73: MER4RP - MER3RP absolute difference of NRRS555 L3 map over Sept 2008.

4th MERIS data reprocessing

Evolutions and Validation report

Ref.:   MER4RP Validation Report

Version: 1.0

Date: 01/04/2019

Page: 112

Figure 3-74: MER3RP (top left), MER4RP (top right), MODIS (bottom left), and SeaWIFS (bottom right) NRRS670 L3 map over Sept 2008.

Figure 3-75: MER4RP - MER3RP absolute difference of NRRS670 L3 map over Sept 2008.

Time series are also available showing comparisons of monthly means over three dedicated regions: South Indian Ocean (SIO), South Pacific Gyre (SPG), and North Sea. Examples are displayed in Figure 3-76.

4th MERIS data reprocessing

Evolutions and Validation report

Ref.:   MER4RP Validation Report

Version: 1.0

Date: 01/04/2019

Page: 113

Figure 3-76: Examples of NRRS time series from MER4VAL. Top: 443 nm on SPG, MER4RP vs MODIS. Bottom: 490 nm on SIO, MER4RP vs SeaWIFS.

For a more synthetic understanding NRRS monthly-means can be compared on the same sites as averages over the years covered jointly by all missions. Average monthly means are then computed from all available years, minimal and maximal years are displayed with dashed lines to see the natural variability. Results are displayed below in the following order: NRRS 412 to 670 each time by pair; North Sea on the top, SIO on the middle, and SPG on the right.

For North Sea the winter season (DJF) is less covered because of low solar zenith angle, consequences are low statistics and larger differences (all sensors disagree).

4th MERIS data reprocessing

Evolutions and Validation report

Ref.:   MER4RP Validation Report

Version: 1.0

Date: 01/04/2019

Page: 114

Overall, MER4RP performs equally compared to MER3RP in the comparisons with NASA sensors, NRRS being sometimes closer, sometimes farther. Between 412 and 490 nm MER4RP (or MER3RP) generally exhibit lower NRRS than NASA sensors, which is only false for MER4RP over North Sea.

Looking at the time-series over SPG and SIO, we see that the difference between MERIS4RP and SeaWiFS is roughy between 5E-4 and 1E-3 (depending on month), which is within the specification of the Antoine and Morel atmospheric correction.

Differences between MODIS and SeaWIFS can be on the same magnitude as differences with MERIS (3RP or 4RP).

At that point we must recall the differences in the calibration processes between NASA sensors and MERIS 3RP and 4RP:

NIR calibration:

- NASA: 865 fixed and 779 adjusted to have aerosol model forced at SPG

- MER3RP: 709 and 865 fixed, 779 adjusted to have log-log aerosol reflectance at SIO/SPG

- MERIS: BPAC adjusts NIR bands on a fitted aerosol model with weights per waveband inversely proportional to the signal, adjustment per pixel

VIS calibration:

- NASA: MOBY

- MER3RP: BOUSSOLE and MOBY combined but much more MOBY data

- MERIS: BOUSSOLE and MOBY combined, quite equivalent statistics, updated data

4th MERIS data reprocessing

Evolutions and Validation report

Ref.:   MER4RP Validation Report

Version: 1.0

Date: 01/04/2019

Page: 115
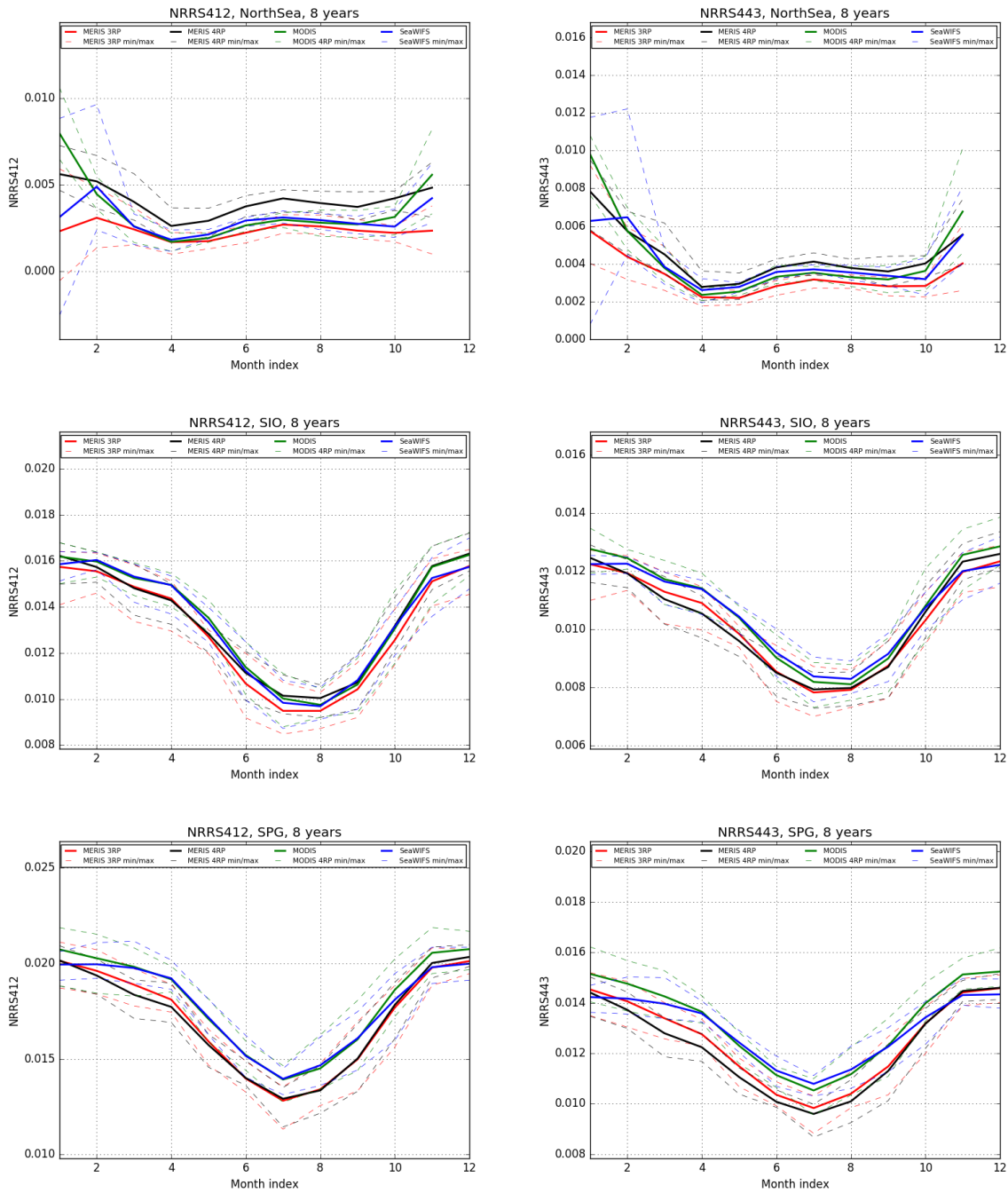
Figure 3-77: Monthly-mean comparisons of NRRS 412 (left) and 443 (right) between MER3RP (red), MER4RP (black), MODIS (green), and SeaWIFS (blue) on North Sea (top), SIO (middle) and SPG (right). Averages are over a period of eight years; minimal and maximal years are shown in dashed lines.

4th MERIS data reprocessing

Evolutions and Validation report

Ref.: MER4RP Validation Report

Version: 1.0

Date: 01/04/2019

Page: 116
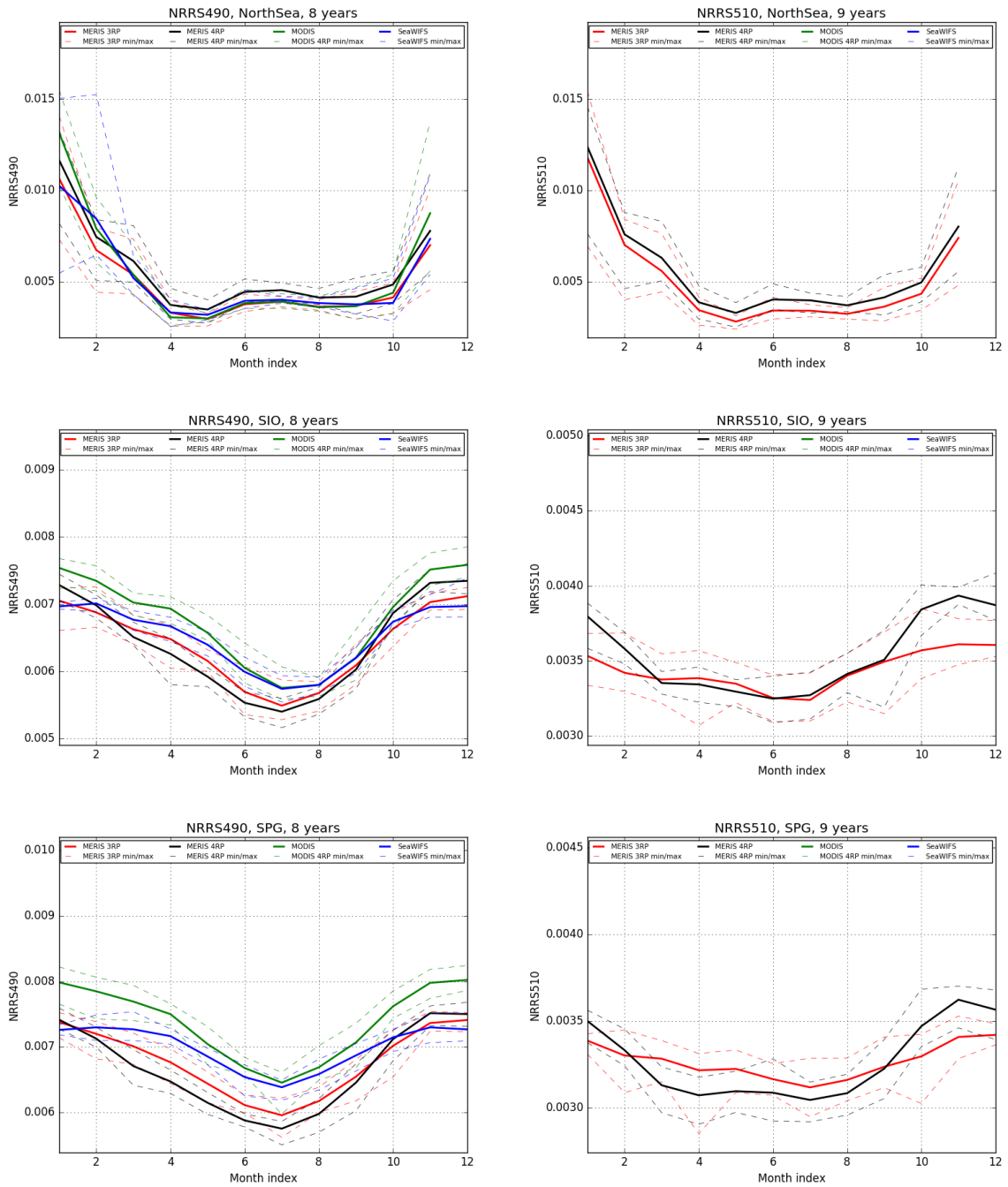
Figure 3-78: Monthly-mean comparisons of NRRS 490 (left) and 510 (right) between MER3RP (red), MER4RP (black), MODIS (green), and SeaWIFS (blue) on North Sea (top), SIO (middle) and SPG (right). Averages are over a period of eight years; minimal and maximal years are shown in dashed lines.

4th MERIS data reprocessing

Evolutions and Validation report

Ref.: MER4RP Validation Report

Version: 1.0

Date: 01/04/2019

Page: 117
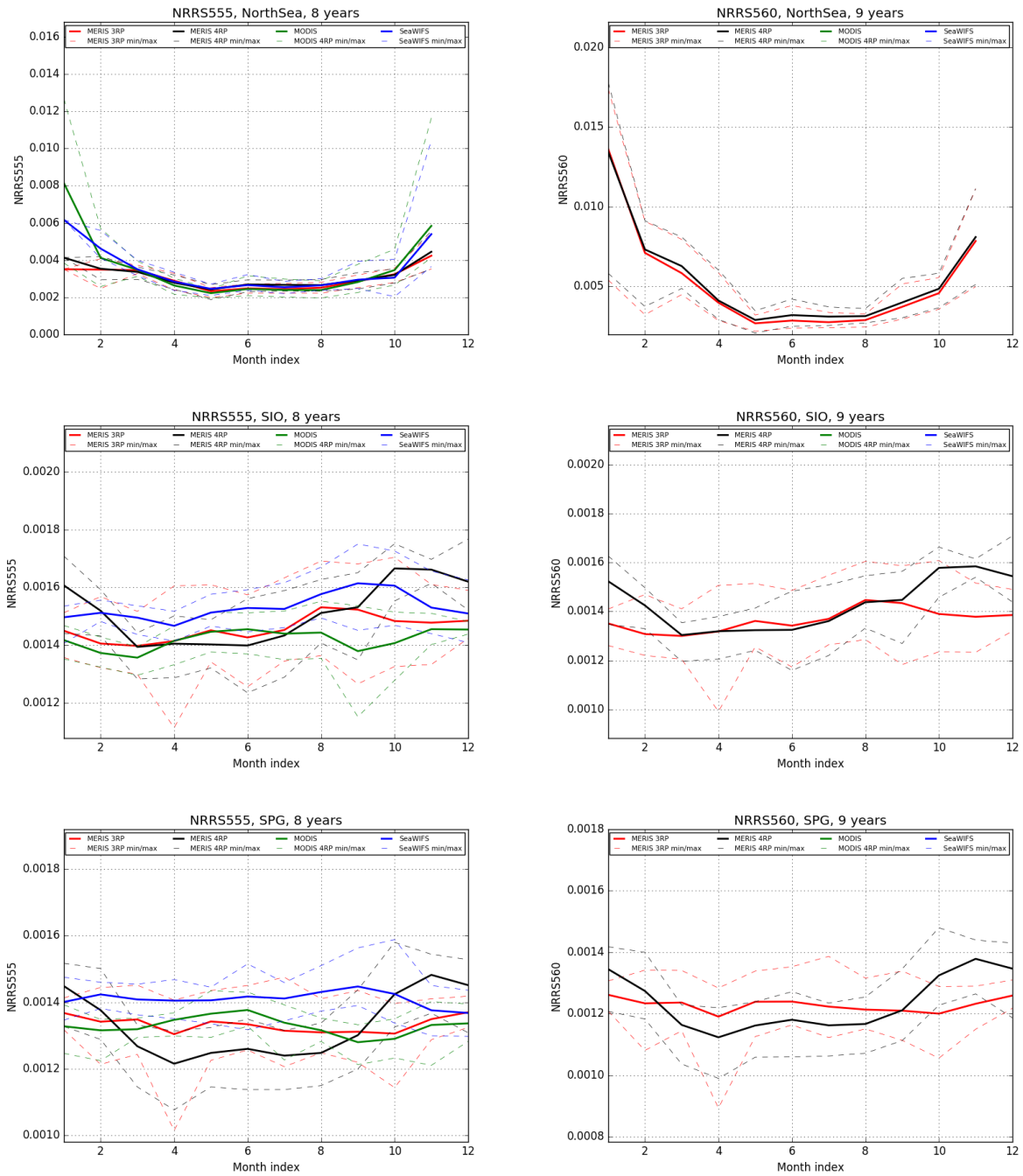
Figure 3-79: Monthly-mean comparisons of NRRS 555 (left) and 560 (right) between MER3RP (red), MER4RP (black), MODIS (green), and SeaWIFS (blue) on North Sea (top), SIO (middle) and SPG (right). Averages are over a period of eight years; minimal and maximal years are shown in dashed lines.

4th MERIS data reprocessing

Evolutions and Validation report

Ref.: MER4RP Validation Report

Version: 1.0

Date: 01/04/2019

Page: 118
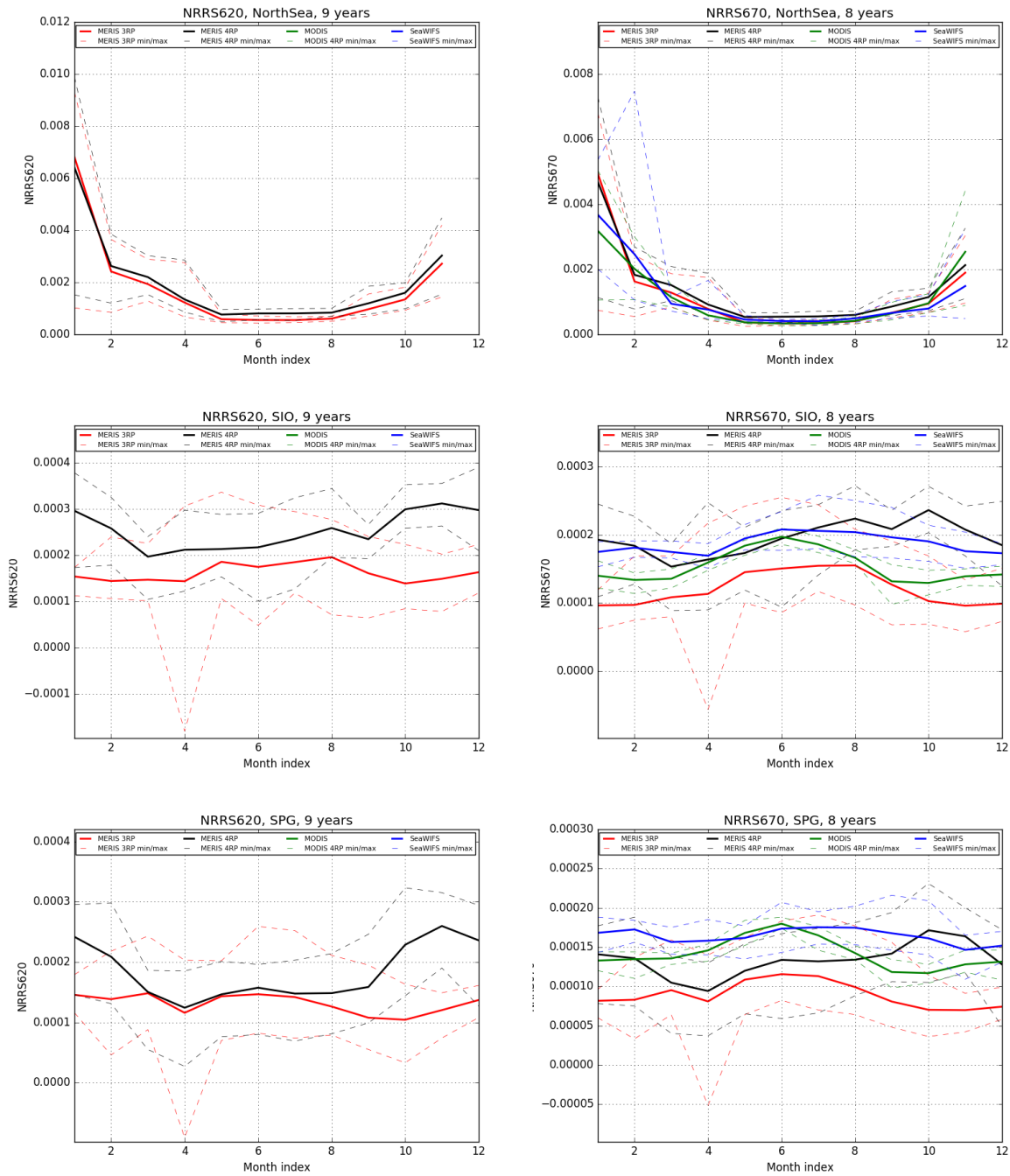
Figure 3-80: Monthly-mean comparisons of NRRS 620 (left) and 670 (right) between MER3RP (red), MER4RP (black), MODIS (green), and SeaWIFS (blue) on North Sea (top), SIO (middle) and SPG (right). Averages are over a period of eight years; minimal and maximal years are shown in dashed lines.

4th MERIS data reprocessing

Evolutions and Validation report

Ref.: MER4RP Validation Report

Version: 1.0

Date: 01/04/2019

Page: 119

3.3.2   Algal Pigment Concentration 1 (CHL_OC4ME)

Validation method

Comparisons with MER3RP, MODIS and SeaWIFS L3 monthly products and time series

Accuracy goal	MER3RP estimated quality	MER4RP estimated quality
Theoretical goal is to detect 10 classes of chlorophyll concentration with each of the 3 orders of magnitude between 0.03 and 30 mg/m3 decade, i.e. ~13%. Actual performance of OC4Me algorithm (ATBD 2.9, v4; 3 Jul 2011) is however to detect chlorophyll concentration within a factor of 0.5 to 2 (i.e. signed relative error between -50% and +100%).	▪ RPD (%) = - 12.0 ▪ RMSE = 0.278 ▪ MAD = 0.086	Comparable

Comparisons with MER3RP can be based on the monthly means maps as for the water-leaving reflectances. Example is given Figure 3-81 for March 2008, MER3RP OC4ME Chl, MER4RP OC4ME Chl, relative and absolute differences.

4th MERIS data reprocessing

Evolutions and Validation report

Ref.: MER4RP Validation Report

Version: 1.0

Date: 01/04/2019

Page: 120

MERIS CHL1 - OC4Me
GlobColour monthly Level-3 product
2008-03-01 to 2008-03-31

MERIS CHL1 - OC4Me
GlobColour monthly Level-3 product
2008-03-01 to 2008-03-31

4th MERIS data reprocessing

Evolutions and Validation report

Ref.: MER4RP Validation Report

Version: 1.0

Date: 01/04/2019

Page: 121

Figure 3-81: From top to bottom: MER3RP Chl, MER4RP Chl, relative and absolute differences L3 map, March 2008.

Relative differences can be very high due to the low values in oligotrophic regime. Strong differences are observed over coastal regions where notable changes have been made on the BPAC. Previous comparisons with reference measurements of AAOT provide more favourable nrrs values for MER4RP.

Validation of the OC4ME Chl algorithm can be made based on the mer4val time series, interestingly the SIO/SPG regions provide very oligotrophic regimes while the North Sea region provides high chl concentrations. Indeed, two observations can be made:

- in high Chl regimes the OC4ME algorithm performs very similarly to the NASA Chl (Figure 3-82);

- in low Chl regimes the OC4ME algorithm shows consistent bias with respect to the NASA Chl (Figure 3-83).

4th MERIS data reprocessing
Evolutions and Validation report

Ref.:   MER4RP Validation Report
Version: 1.0
Date: 01/04/2019
Page: 122
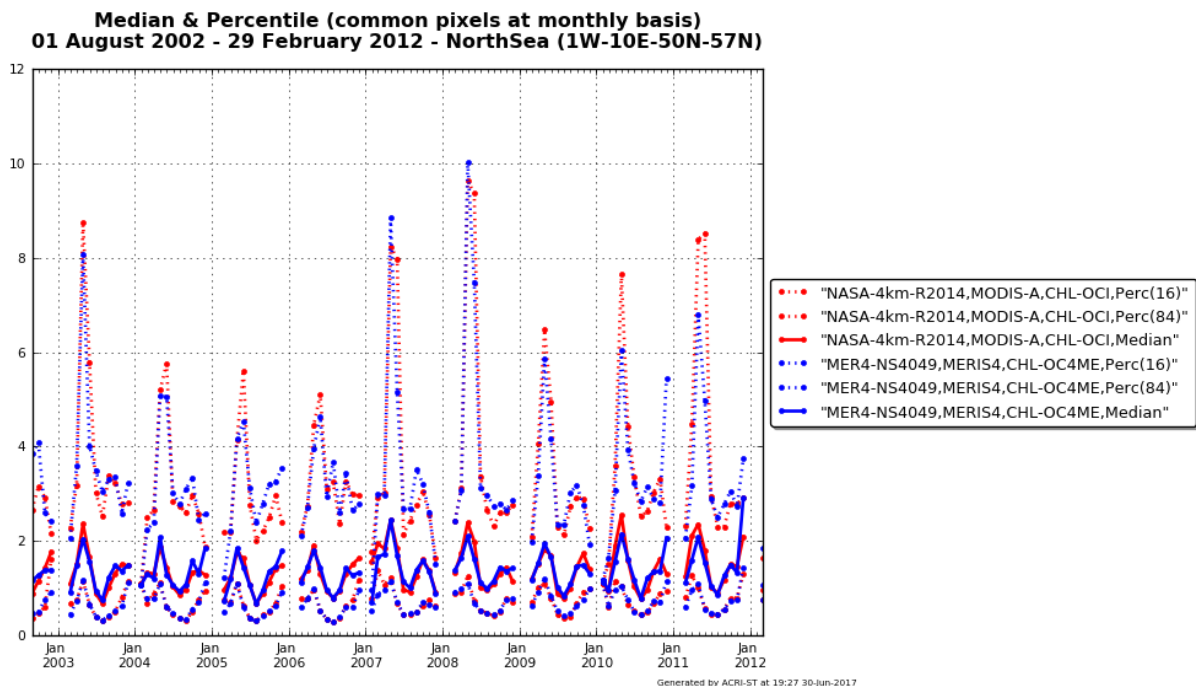
Figure 3-82: Time series of MER4RP CHL-OC4ME compared to MODIS CHL. North Sea region, high Chl concentrations
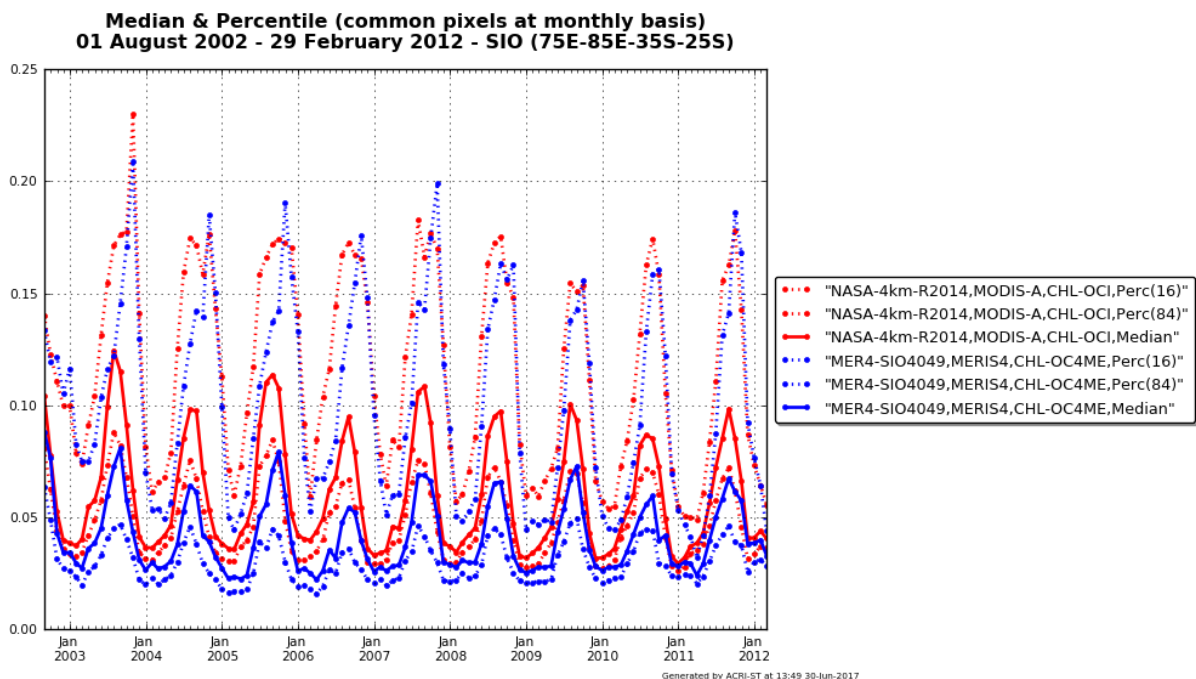
Figure 3-83: Time series of MER4RP CHL-OC4ME compared to MODIS CHL. SIO region, oligotrophic regime

The reason is not radiometric calibration; the reason is the OC4ME algorithm itself, which has been trained over very low Chl concentrations in oligotrophic regime. Indeed, using a common set of reflectances in oligotrophic regime, both OC4ME and NASA Color Index algorithms can be compared.

4th MERIS data reprocessing

Evolutions and Validation report

Ref.:   MER4RP Validation Report

Version: 1.0

Date: 01/04/2019

Page: 123

Results in Figure 3-84 and Figure 3-85 clearly show the resulting bias (lower values in OC4ME).
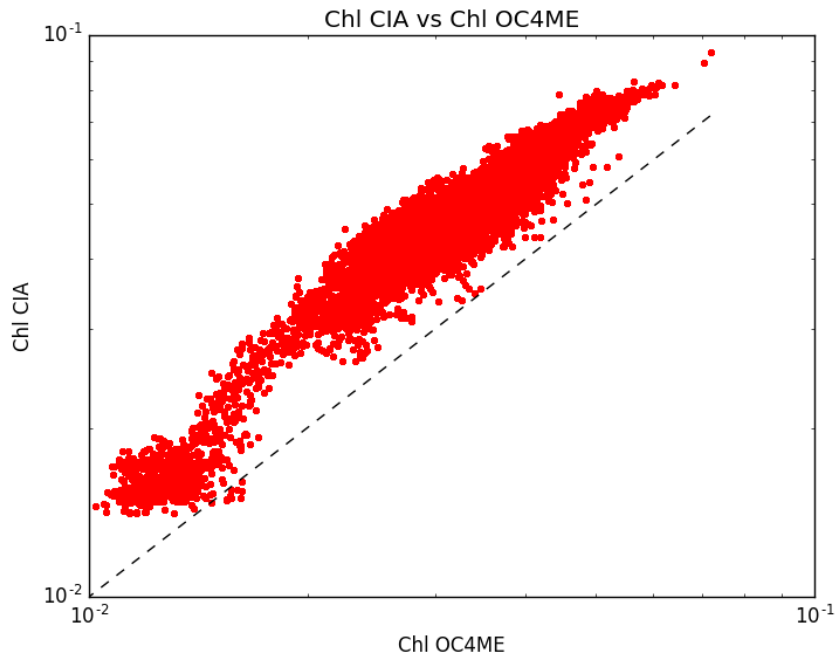
Figure 3-84: Comparisons of OC4ME and CI algorithms computed for a common set of reflectances in oligotrophic regime.
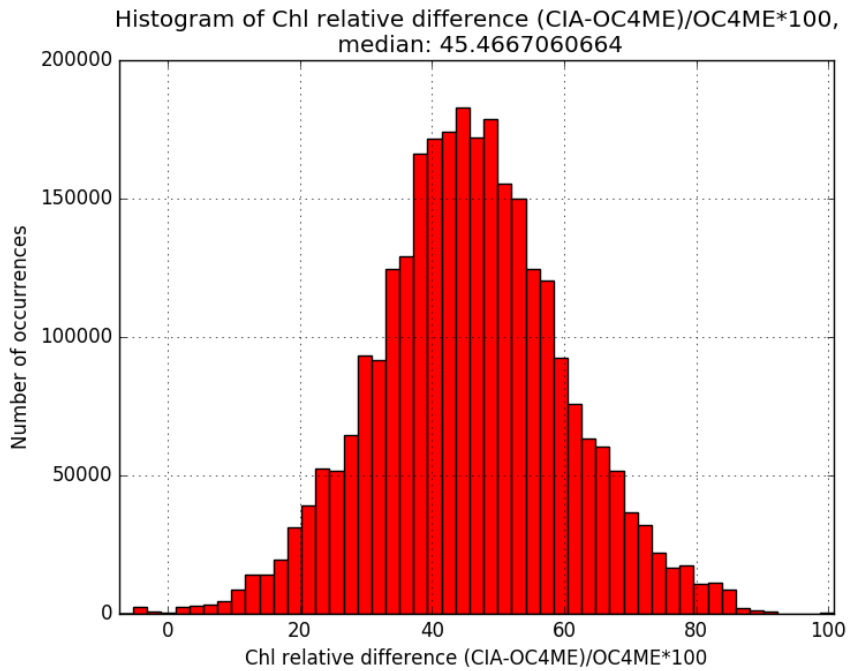
Figure 3-85: Comparisons of OC4ME and CI algorithms computed for a common set of reflectances in oligotrophic regime. Relative differences (CI-OC4ME)/OC4ME*100.

4th MERIS data reprocessing

Evolutions and Validation report

Ref.:   MER4RP Validation Report

Version: 1.0

Date: 01/04/2019

Page: 124

Validation over Black Sea and NW-European Seas

In order to assess the pigments behaviour in MERIS 4RP products, we compare them to that ones from MERIS 3RP products. As the data format changed following to SEN3-like format, the comparison was carried out on the Algal-1 (Algal-2) from MERIS 3RP to CHL_OC4Me (and CHL_NN) from to MERIS 4RP products respectively.

The following figures show the chlorophyll retrieved in case-1 waters from MERIS 3RP (Algal-1) and from MERIS 4RP (Chl-OC4Me) over the Black Sea. Both products display almost the same patterns with high chlorophyll values near the coast, which decrease toward the open ocean areas. MERIS 4RP product shows less invalid (no-data) pixels (e.g. NW-Black Sea area) than MERIS 3RP product, this decrease of pixels number could be attributed to the earned pixels with negative reflectance in MERIS 3RP. Another interesting feature could be observed on the Chl_OC4Me profile near the coast such as lower chlorophyll values and lower variability wrt that ones from the MERIS 3RP product. One can draw the same conclusion from the analysis over the NW-European Seas.

4th MERIS data reprocessing
Evolutions and Validation report

Ref.: MER4RP Validation Report
Version: 1.0
Date: 01/04/2019
Page: 125
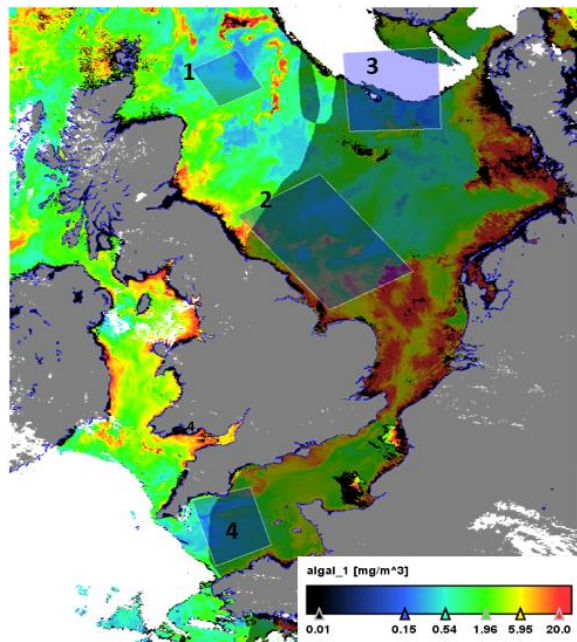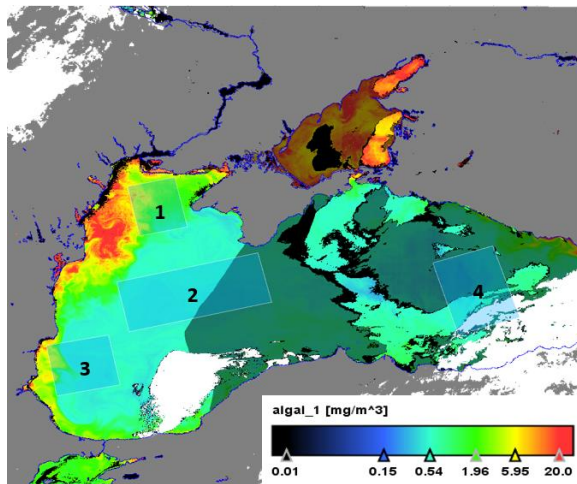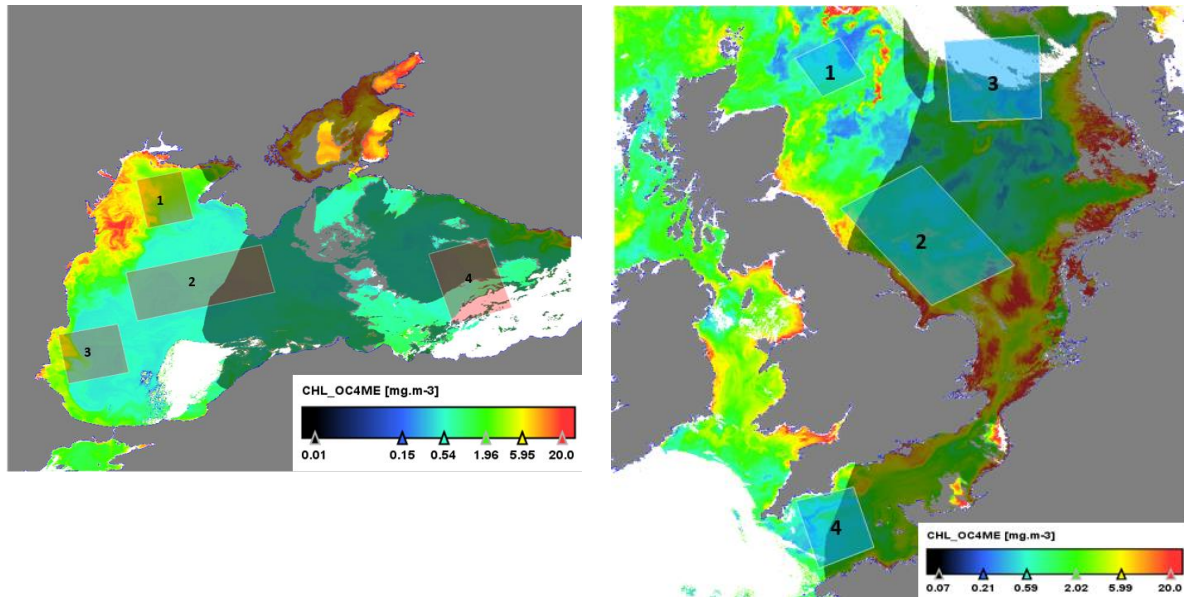
Figure 3-86: Black sea (left) and (right) NW-European Seas (upper row) Algal-1 from MER3RP and (lower row) Chl-OC4Me from MER4RP showing the ROIs locations. The shaded area on the right part of the image indicates the Medium Glint Mask. MERIS acquisitions are on 20070512 and 20080507 respectively.
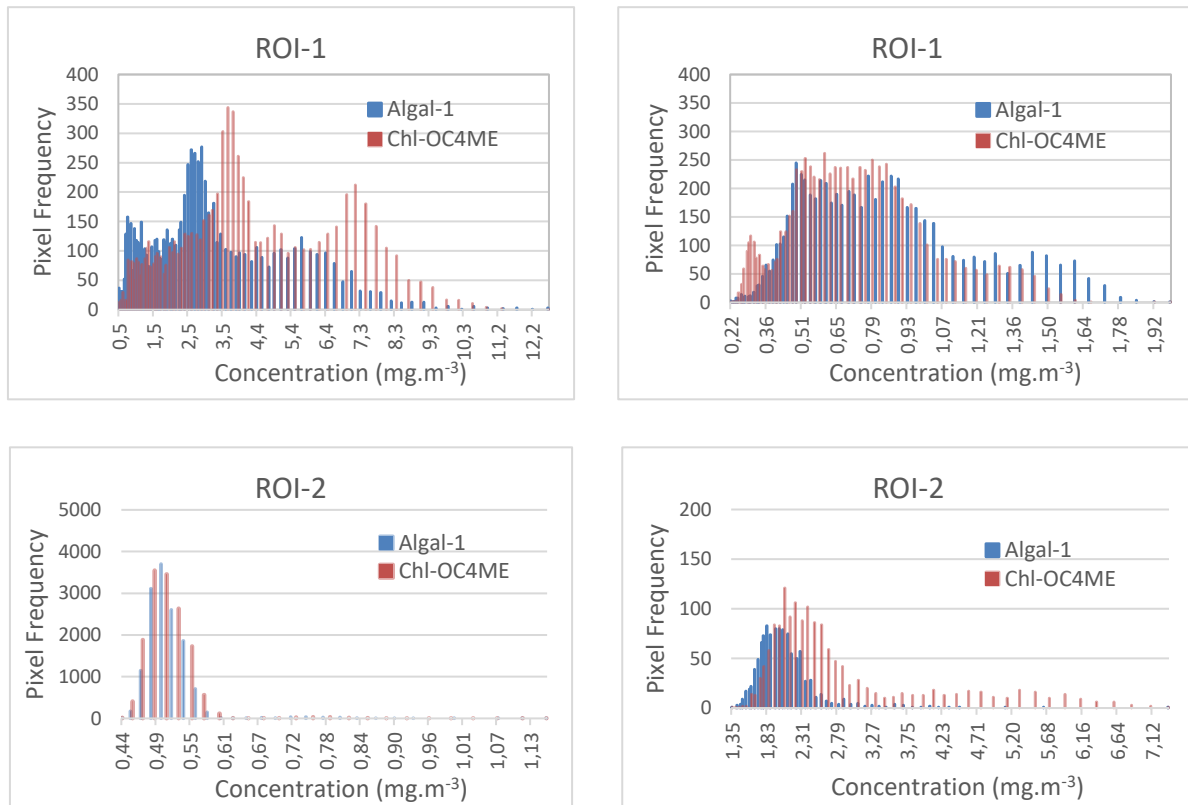
Figure 3-87: Histograms of Pigments (blue) algal-1 from MER3RP and (orange) Chl-OC4ME from MER4RP from different regions in (left) Black sea and (right) NW-European seas (see figure above).

4th MERIS data reprocessing

Evolutions and Validation report

Ref.: MER4RP Validation Report

Version: 1.0

Date: 01/04/2019

Page: 126

Table 3-8: Pigments (Algal-1, Algal-2, Chl-OC4Me and Chl-NN) from the MER3RP and MER4RP in mg/m³ over Black Sea and NW-European Seas for each pin shown in the above figure.

Area	ROI	Algal-1	N#	Chl-OC4Me	N#
Black Sea	ROI-1	2.876	7628	2.559	7639
	ROI-2	0.511	13678	0.505	14552
	ROI-3	0.983	10006	0.959	8624
	ROI-4	NA	NA	NA	NA
NW-European Seas	ROI-1	0.762	6317	0.705	7130
	ROI-2	2.550	1074	2.702	1490
	ROI-3	NA	NA	NA	NA
	ROI-4	0.660	1383	0.919	3279

3.3.3 Algal Pigment Concentration 2, output of the Case 2 algorithm (CHL_NN)

This product is not a standard product.

3.3.3.1 Introduction incl. alternative atmospheric correction

The algorithms to determine the three products *Algal Pigment Concentration 2 (CHL_NN)*, *Total Suspended Matter Concentration (TSM_NN)* and *CDM absorption coefficient (ADG_443_NN)* are connected to an alternative atmospheric correction procedure, which is used to derive water reflectance from top of atmosphere reflectances using also a neural network. This alternative AC procedure avoids the extrapolation of the path radiance reflectance from the NIR to the blue-green spectral range, which in some coastal waters with high concentration of light absorbing water constituents may lead to large errors and also negative water reflectances.

Input to this AC-NN is the TOA reflectances at 12 MERIS bands, which includes also the green and blue spectral bands. Training of this NN is based on simulated data, which are based on the same bio-optical model as used for deriving the water products.

For this reason we include here the validation also of the directional water reflectances, although they are not available as products but are used as input for the NN to determine the 5 water inherent optical properties (apig, ad, ag, bp, bw), from which the 3 concentrations products CHL_NN, TSM_NN, ADG443_NN are determined.

For the validation we have used the Helgoland transects, the MERMAID data base and the CEFAS data base.

The Helgoland transects are measurements from a ferry boat which connects the city of Cuxhaven at the mouth of the Elbe river (North Sea, German Bight) with the island of Helgoland. Along this transect measurements the reflectance of the water was measured

4th MERIS data reprocessing
Evolutions and Validation report

Ref.: MER4RP Validation Report
Version: 1.0
Date: 01/04/2019
Page: 127

continuously during the cruise with a TRIOS Ramses Spectrometer system from the bow of the ship, where the water is undisturbed during cruising. This system consists of 3 spectrometers, one is pointing to the water surface under a nadir angle of 45 degrees, the second one is pointing to the sky under the corresponding angle to determine the reflected sky light and the third spectrometer is used to measure the downwelling irradiance. Azimuth angle with respect to the sun was about 135 degrees. Water samples were taken during the cruise from the water surface and processed for phytoplankton pigments, suspended matter and the absorption by particulate matter and the filtered water.

The transects covers a large variety of water types including very turbid estuarine water with high detritus absorption coefficients as well as more clear blue-green water conditions with Secchi desk readings of > 6 meters. Since the water types have a patchy distribution and due to the strong tidal currents strict match-up conditions are rare, so that the relative distribution along the transect is a better criterium for the validation than a point-to-point comparison.
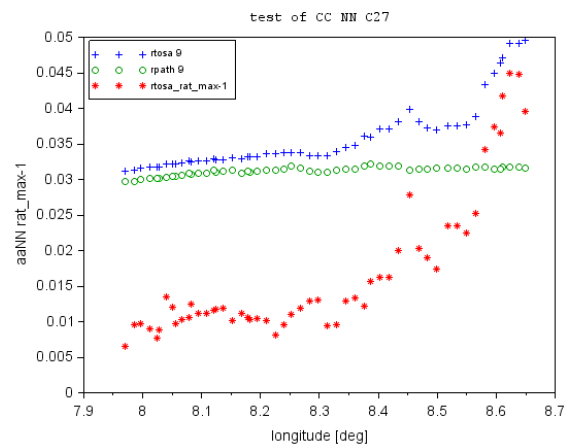
Figure 3-88: On the left location of the Helgoland transect. On the right transect with Rtosa and Rpath for band 9 (708 nm) and the maximum relative deviation from the autoassociative NN (red).

3.3.3.2 *Mermaid analysis of water leaving reflectances*

The comparison of rho_w_AAC (retrievals of the NN) with Rho_wn_IS (in situ) from different sites of MERMAID shows an acceptable agreement with respect to slope and bias (see from Figure 3-89 to Figure 3-92 showing different stations). The scatter of the data is larger than the desired 5% accuracy but with 16% on the log scale less than the results of the standard atmospheric correction procedure with 30%. Results which include data with high sun glint are within the same limits.

4th MERIS data reprocessing

Evolutions and Validation report

Ref.: MER4RP Validation Report

Version: 1.0

Date: 01/04/2019

Page: 128
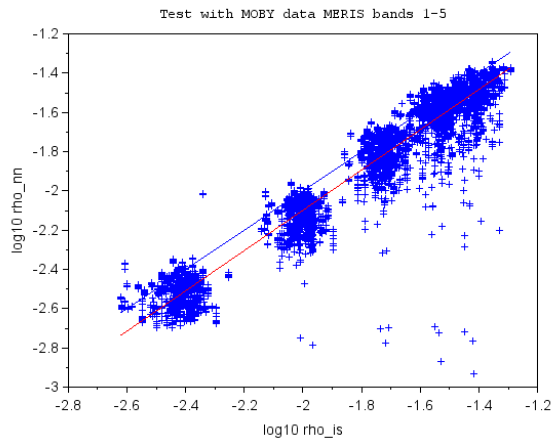
Slope (log10 scale) 1.02, bias -0.05, stdv 0.10
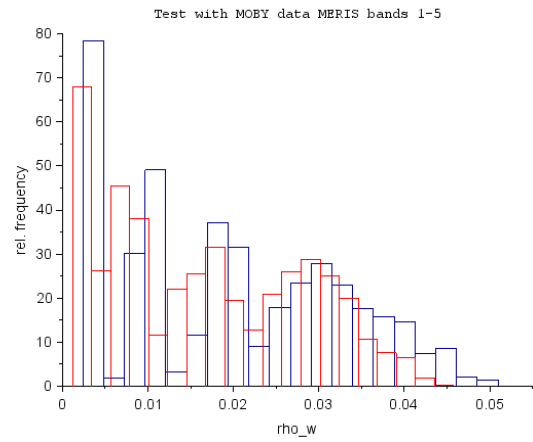
Blue: rho_wn_is, red: rho_w_nn

Figure 3-89: Water leaving reflectance at the MOBY station in Hawaii
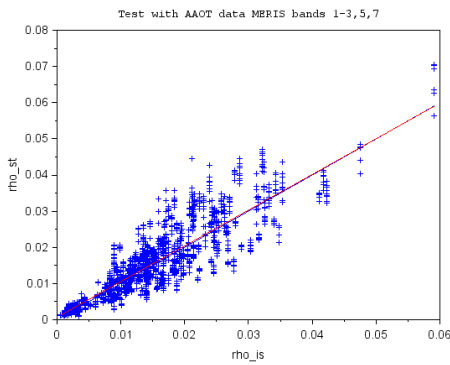
Slope: 0.99, bias:0.00066, stdv: 0.005n: 2298, flag: cloud, ice_haze, stdev of 9 pixels < 1.2 of toar band 5
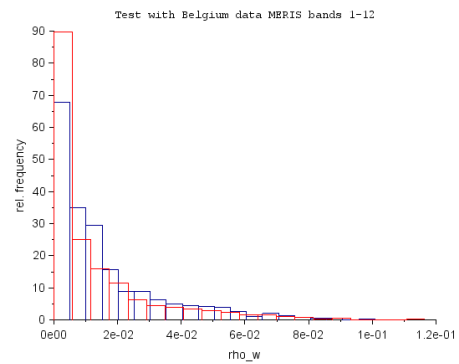
Relative frequency distribution of the water reflectances, blue: AAOT, red: MERIS NN data

Figure 3-90: Water leaving reflectance at the AAOT Venice Tower station in the Adriactic Sea
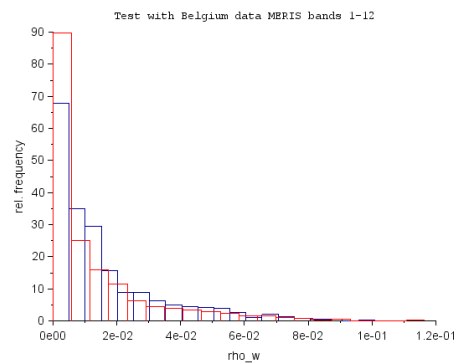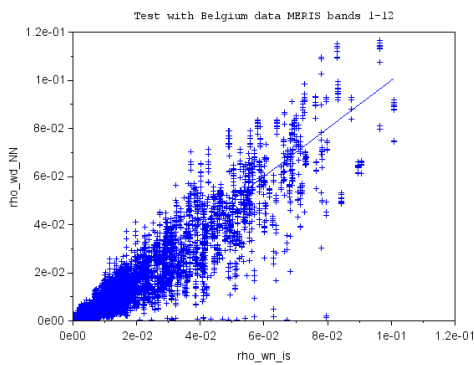
Figure 3-91: Comparison of water leaving reflectance with data of the Belgium coast (K. Ruddick), left on linear scale, right frequency distribution, blue in situ data, red MERIS data

4th MERIS data reprocessing

Evolutions and Validation report

Ref.: MER4RP Validation Report

Version: 1.0

Date: 01/04/2019

Page: 129
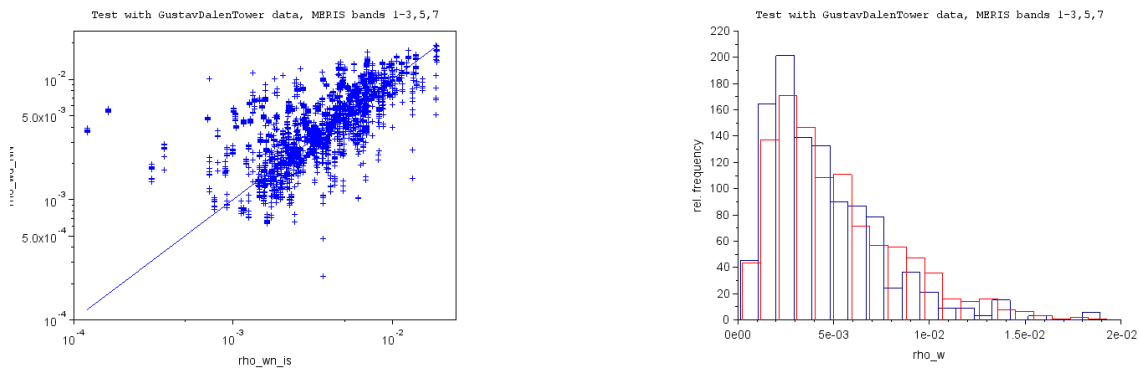
Figure 3-92: Comparison Comparison of water leaving reflectance with data of the Baltic Sea, Gustav Dalen Tower (G. Zibordi), left on log scale, right frequency distribution, blue in situ data, red MERIS data

Another way of comparison of in situ and satellite retrieval using the information of all data available for all stations is shown in Figure 3-93. The scatter plots show the results of the comparison by wavelength of all possible MERMAID stations. The number of points is higher than for the standard AC processor, because C2RCC NN does not generated negative spectra. Coefficients of determination range from 0.68 to 0.89, the bias from -9.8e-05 to 4.6e-04 and root mean square error form 1.1e-03 to 5.5e-03, with bigger uncertainties in the blue bands (rho_w_AAC). See Table 3-9 for comparison with the standard product (RHO_SURF) and the normalized versions of both, the standard (RHO_WN) and the NN (rho_wn_AAC) outputs. The C2RCC NN retrievals show a general underestimation of the reflectances, but with lower bias and RMSE than the standard procedure.

4th MERIS data reprocessing

Evolutions and Validation report

Ref.:   MER4RP Validation Report

Version: 1.0

Date: 01/04/2019

Page: 130
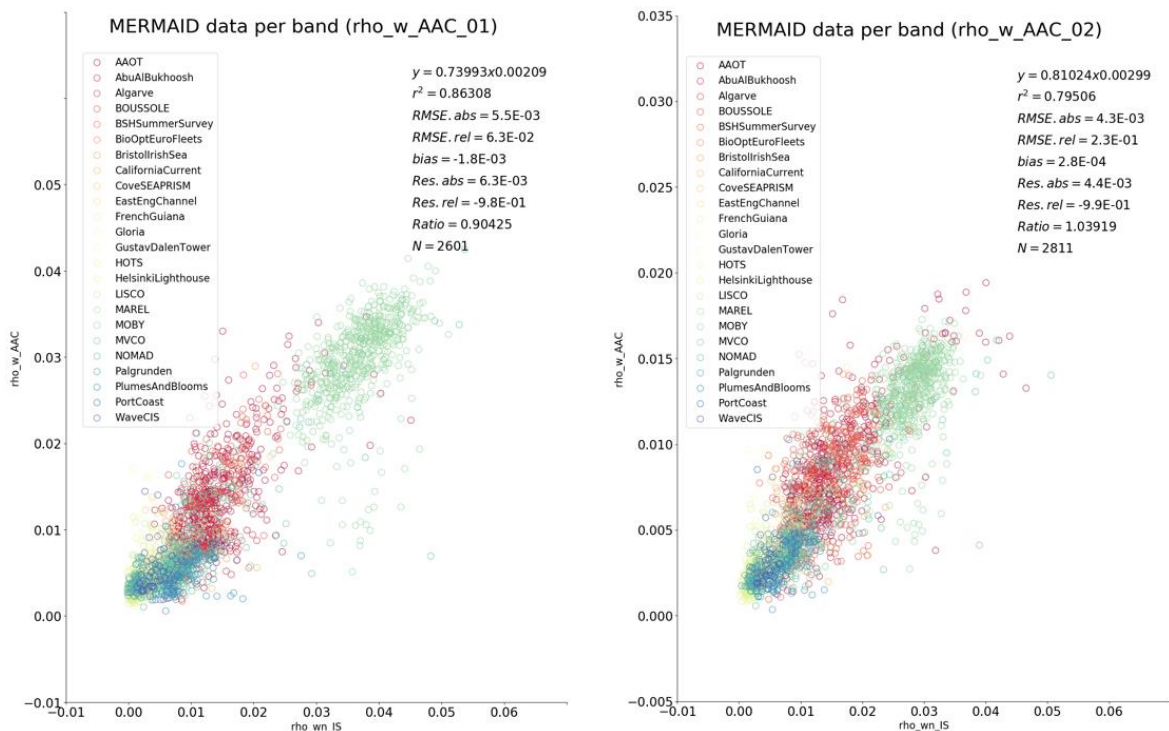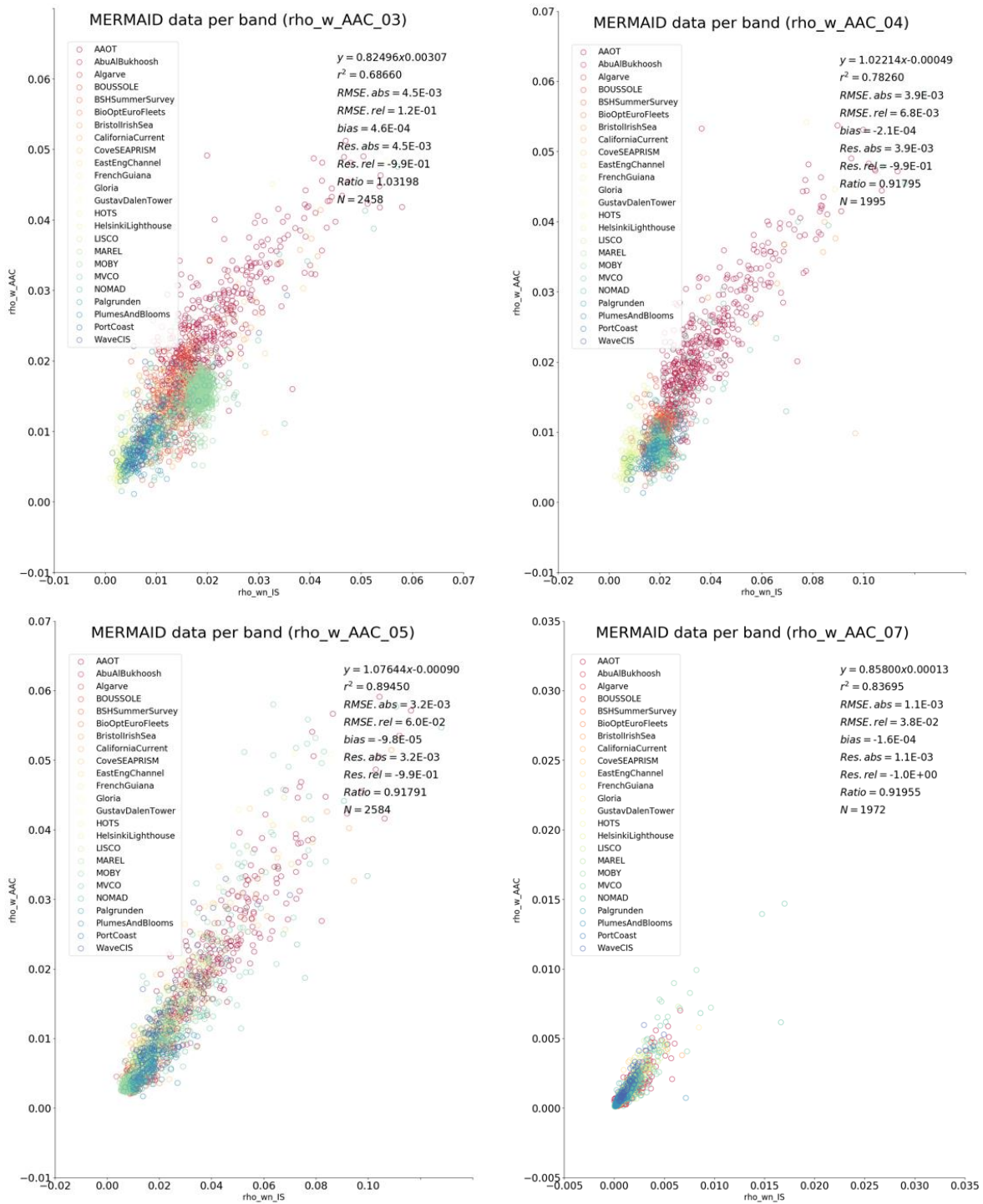
Figure 3-93: Scatter plots of Mermaid 4th reprocessing C2R NN water leaving reflectance vs. MERMAID in situ normalised water leaving reflectance (per wavelength)

4th MERIS data reprocessing
Evolutions and Validation report

Ref.: MER4RP Validation Report
Version: 1.0
Date: 01/04/2019
Page: 131

Table 3-9: Coefficient of determination and absolut root mean square error (RMSE abs) for Lw and Lwn of the MERIS 4th reprocessing standard product (RHO_SURF and RHO_WN) and the C2RNN AC (rho_w_AAC and rho_wn_AAC). In parentheses, the number of data points

R²/RMSE abs	Rho_w_AAC	Rho_wn_AAC	RHO_SURF	RHO_WN	Rho_w_AAC	Rho_wn_AAC	RHO_SURF	RHO_WN
412	0.86308 (2601)	0.86626 (2627)	0.87472 (1273)	0.88765 (1270)	5.5e-03	5.4e-03	4.7e-03	4.3e-03
443	0.79506 (2811)	0.80348 (2847)	0.8298 (1450)	0.84385 (1450)	4.3e-03	4.2e-03	3.8e-03	3.7e-03
490	0.6866 (2458)	0.70581 (2472)	0.83275 (1496)	0.84086 (1501)	4.5e-04	4.2e-03	3-5e-03	3.2e-03
510	0.7826 (1995)	0.78667 (2010)	0.83535 (1284)	0.83461 (1298)	3.9e-03	3.6e-03	3.7e-03	3.2e-03
560	0.8945 (2584)	0.89305 (2590)	0.87187 (1659)	0.86894 (1667)	3.2e-03	3.0e-03	4.0e-03	3.4e-03
665	0.83695 (1972)	0.83806 (1990)	0.54299 (535)	0.51359 (543)	1.5e-03	1.1e-03	3.4e-03	3.1e-03
865	0.00073 (1018)	-	0.00585 (336)	0.00585 (336)	1.5e-02	-	1.5e-03	1.5e-03

Since the underestimation of water leaving radiance is more visible in stations traditional considered Case 1 waters, a water type classification is applied to separate the data in clusters of Case 1 and several types of Case 2 following the approach developed by Lee et al., 2006. In the Lee paper four classes are grouped using the remote sensing reflectance as input: strict Case 1 (CS1), high CDOM vs. CHL content water (HCDOM), low CDOM vs. CHL content water (LCDOM), scattering waters (Bb). The classification was developed following Lee and Hu (2006), adapated as well for the Ocean Colour Climate Change Initiative (OC-CCI, PVSAR 2015). The classification is made on the in situ data spectrum, where some thresholds are applied with the purpose of separate Case 1 from other Case 2 waters. The Case 2 classification was later separated into three new classes, with focus on the CDOM to chlrophyll absorption ratio: high CDOM (HCDOM), low CDOM (LCDOM) and high backscattering (Bb).

Figure 3-94 shows three bands (443, 560 and 665 nm) for the scattering water type -Bb definition following the formulation above-. Histograms of the rho_w_IS (Mermaid) in situ vs. the rho_w_AAC retrieved by the NN accompanied the scatterplots. Many of the match-up points seem to be located in the AAOT, CoveSEAPRISM and LISCO stations. Histogram acompanyig the scatter plots show that for band 443 and 560 at least, the number of in situ data below 0.02 is higher than the EO data, but in general data are skewed to the left.

Table 3-10 summarizes the coefficient of determination in both cases for all bands and for the four water types. Coefficients of determination show better values in the blue bands for waters closer to Case 1 (CS1 and LCDOM) with decreasing values in the green and red parts of the spectrum. This behaviour seems to be the opposite for the HCDOM and Bb waters, at

4th MERIS data reprocessing

Evolutions and Validation report

Ref.:	MER4RP Validation Report
Version:	1.0
Date:	01/04/2019
Page:	132

least concerning the blue and green bands, with no so clear response in the red and NIR for the standard product, while the NN products give better coefficients for the red bands. The NIR results are very irregular and no conclusion can be extracted. RMSE are higher for the blue and green bands. Comparing with RHO-SURF, errors are slightly higher with the NN in the Case 1, Bb and LCDOM waters, but lower in the high CDOM content waters.

Histogram of rho_w_AAC_02

MERMAID data per band (rho_w_AAC_02)

$y = 0.74381x0.00430$
$r^2 = 0.63666$
$RMSE.abs = 4.7E\text{-}03$
$RMSE.rel = 1.7E\text{-}01$
$bias = 5.5E\text{-}04$
$Res.abs = 4.8E\text{-}03$
$Res.rel = -9.9E\text{-}01$
$Ratio = 1.05091$
$N = 729$

Histogram of rho_w_AAC_05

MERMAID data per band (rho_w_AAC_05)

$y = 1.00310x0.00082$
$r^2 = 0.83344$
$RMSE.abs = 4.7E\text{-}03$
$RMSE.rel = 4.5E\text{-}02$
$bias = 8.8E\text{-}04$
$Res.abs = 4.9E\text{-}03$
$Res.rel = -9.8E\text{-}01$
$Ratio = 1.02090$
$N = 589$

4th MERIS data reprocessing

Evolutions and Validation report

Ref.: MER4RP Validation Report

Version: 1.0

Date: 01/04/2019

Page: 133
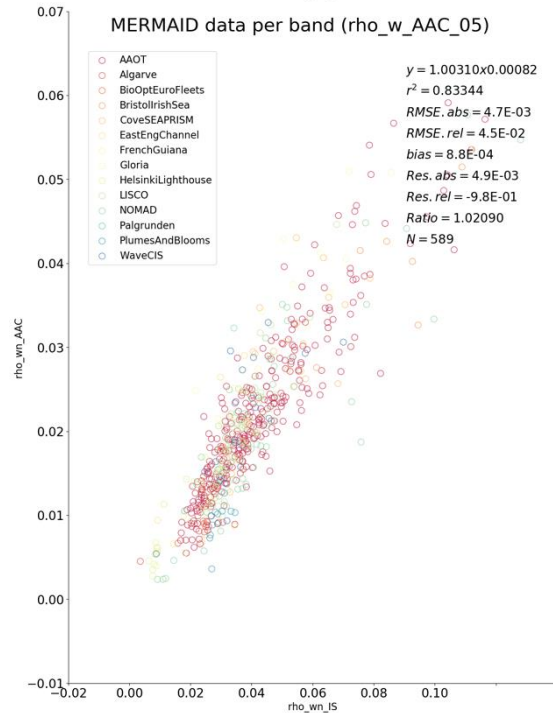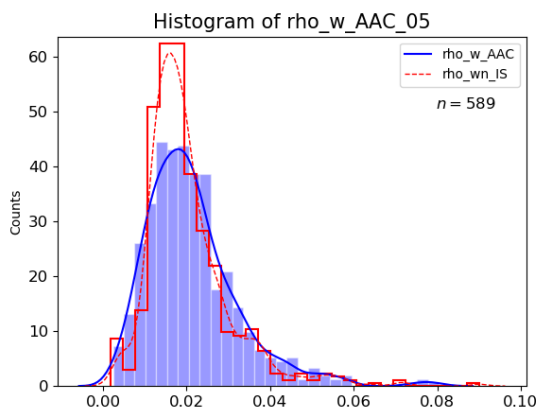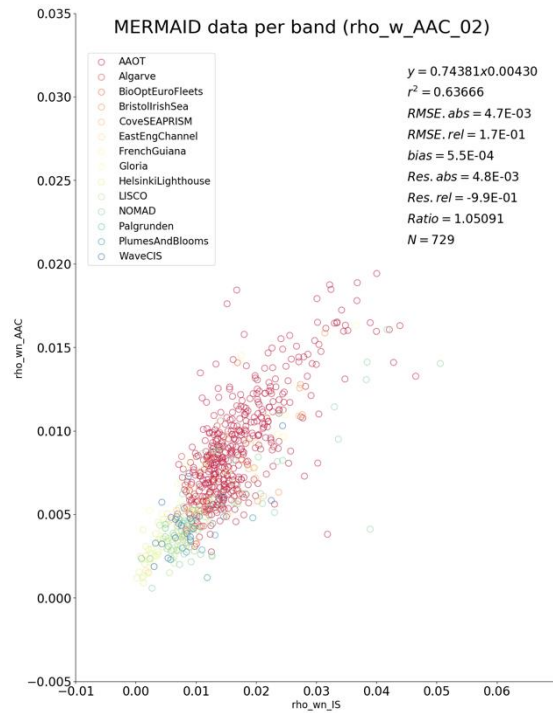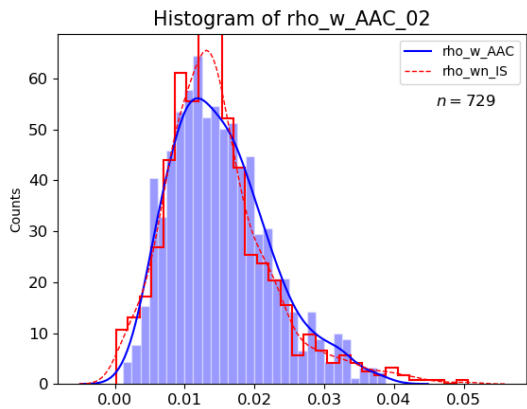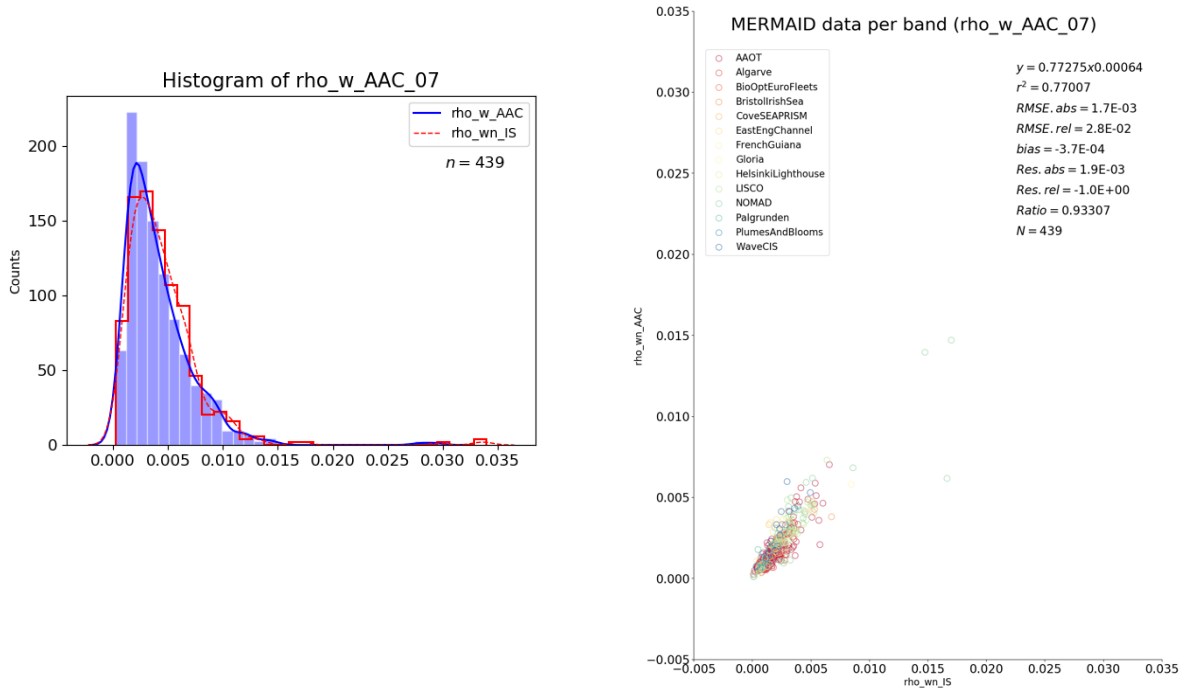
Figure 3-94: Scatter plots of Mermaid 4th reprocessing C2R NN water leaving reflectance vs. MERMAID in situ normalised water leaving reflectance (per wavelength) for the scattering water type defined by Lee et al. (2006)

*Table 3-10: Coefficient of determination (R²) and RMSE for Lw and Lwn of the MER4RP standard product (RHO_SURF) and the C2RNN AC (rho_w_AAC). In parentheses, the number of data points. *Negative reflectances have not been removed from the standard product*

R²	Rho_w_AAC	RHO_SURF*	Rho_w_AAC	RHO_SURF*	Rho_w_AAC	RHO_SURF*	Rho_w_AAC	RHO_SURF*
	CS1	CS1	Bb	Bb	LCDOM	LCDOM	HCDOM	HCDOM
412	0.849/7.5e-0.3 (871)	0.887/4.7e-03 (549)	0.556/4.8e-03 (711)	0.584/5.43-03 (434)	0.571/6.5e-03 (119)	0.877/3.5e-03 (50)	0.705/3.8e-03 (1062)	0.618/5.5e-03 (567)
443	0.8/4.4e-03 (866)	0.87/3.6e-03 (549)	0.636/4.7e-03 (729)	0.715/4.7e-03 (414)	0.489/4.4e-03 (117)	0.831/3.4e-03 (49)	0.749/4.2e-03 (1075)	0.745/4-6e-03 (523)
490	0.382/4.e-03 (882)	0.769/2.5e-03 (575)	0.739/5.3e-03 (721)	0.793/5.2e-03 (447)	0.272/4.e-03 (116)	0.774/2.e-03 (65)	0.829/4.6e-03 (1063)	0.841/4.6e-03 (596)
510	0.116/3.e-03 (858)	0.1559/1.9e-03 (567)	0.772/5.3e-03 (531)	0.768/6.5e-03 (329)	0.173/3.6e-03 (118)	0.195/2.4e-03 (66)	0.858/4.5e-03 (645)	0.825/5.7e-03 (397)
560	0.728/1.6e-03 (862)	0.651/1.4e-03 (553)	0.833/4.7e-03 (589)	0.769/6.9e-03 (389)	0.595/3.5e-03 (115)	0.555/2.3e-03 (64)	0.895/3.6e-03 (925)	0.833/5-6e-03 (574)
665	0.794/3.4e-04 (769)	0.742/7.4e-04 (128)	0.77/1.7e-03 (439)	0.451/5.e-03 (233)	0.345/1.5e-03 (98)	0.419/5.9e-04 (22)	0.798/1.4e-03 (689)	0.479/4.1e-03 (342)
865	0.306/2.8e-04 (46)	0.436/3.4e-04 (12)	0.0009/1.8e-02 (378)	0.002/1.6e-03 (158)	- -	- -	0.001/2.e-02 (591)	0.007/1.4e-03 (215)

4th MERIS data reprocessing
Evolutions and Validation report

Ref.: MER4RP Validation Report
Version: 1.0
Date: 01/04/2019
Page: 134
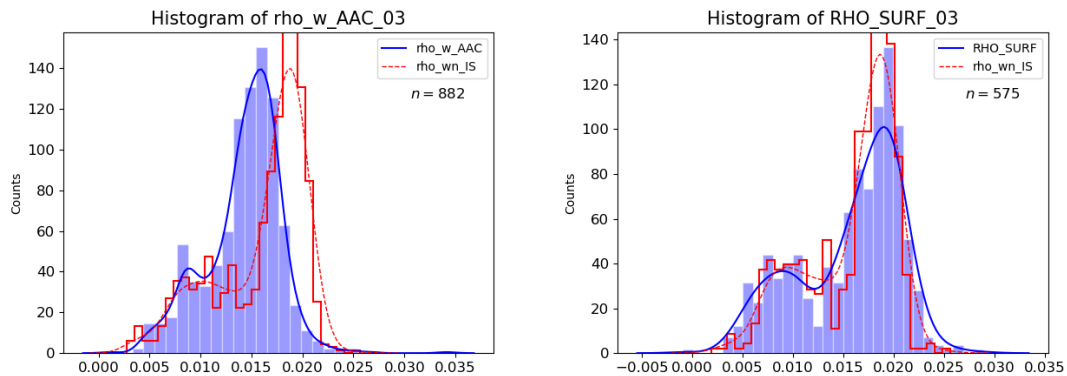
Figure 3-95: Histograms of the CS1 waters in the 490 nm band: on the left the rho_w_AAC and on the right the RHO_SURF reflectances

The histograms of the Figure 3-95 show the case of the match-ups for the stric Case 1 water. The number of points is again higher in the NN retrievals. What is interesting to see is how the peak of the histogram seems to be displaced to the left part (lower values) compare to the reflectances of the standard product.

3.3.3.3 Helgoland transects

As mentioned before, the Helgoland transect covers a large variety of water types including very turbid estuarine water with high detritus absorption coefficients as well as more clear blue-green water conditions with Secchi desk readings of > 6 meters. Eight days were selected for the comparison of the water leaving reflectance with in situ data (see Figure 3-96). For this first figure on the transects, the Lw NN is compared with in situ data for bands 443, 560 and 755 nm in all eight days. In the blue band (443 nm) and the NIR (755) is possible to observe certain underestimation of the NN retrievals when compare with the in situ for almost all days except in the 11 May 2006 and 12 June 2006. Correlations are better the farther we are from the coastal high turbid areas. This effect is visible in all transects for all wavelengths.

1.9.2005 Band 2, 443 nm   Band 5, 560 nm   Band 10, 755 nm

4th MERIS data reprocessing

Evolutions and Validation report

Ref.: MER4RP Validation Report

Version: 1.0

Date: 01/04/2019

Page: 135
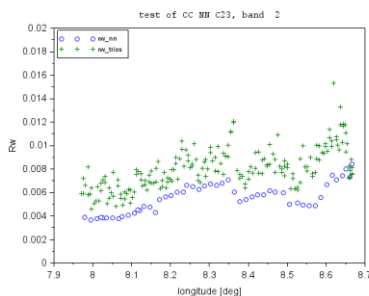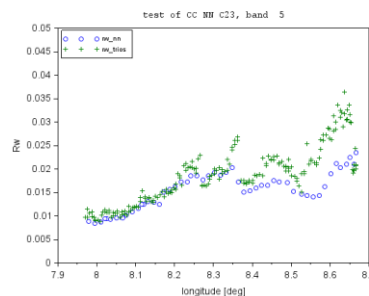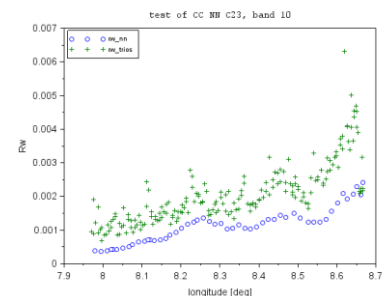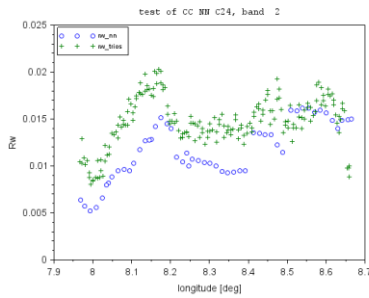
6.10.2005 Band 2, 443 nm
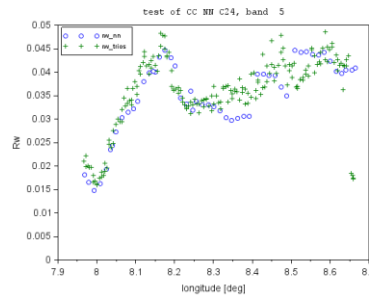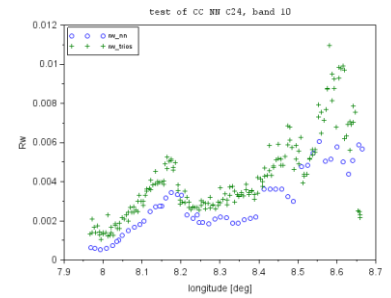
Band 5, 560 nm
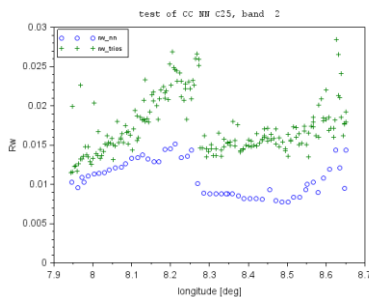
Band 10, 755 nm

13.10.2005 Band 2, 443 nm
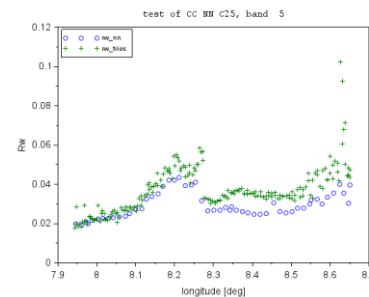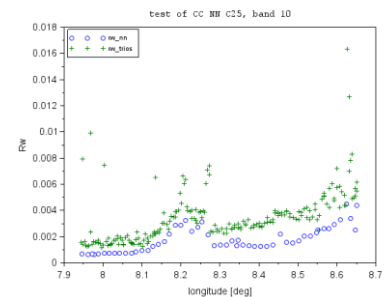
Band 5, 560 nm
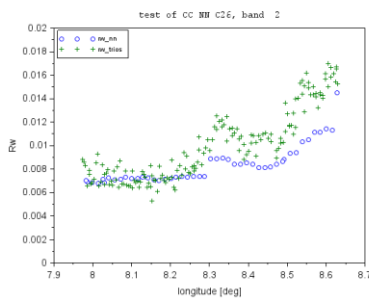
Band 10, 755 nm

8.5.2006 Band 2, 443 nm
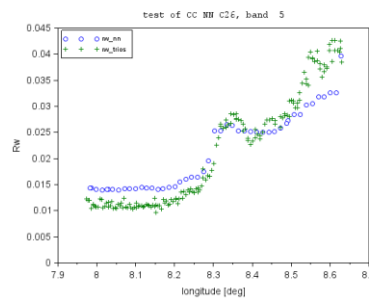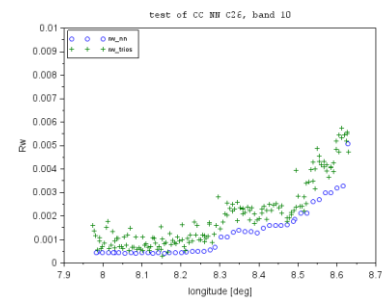
Band 5, 560 nm

Band 10, 755 nm

11.5.2006 Band 2, 443 nm

Band 5, 560 nm

Band 10, 755 nm

4th MERIS data reprocessing
Evolutions and Validation report

Ref.: MER4RP Validation Report
Version: 1.0
Date: 01/04/2019
Page: 136
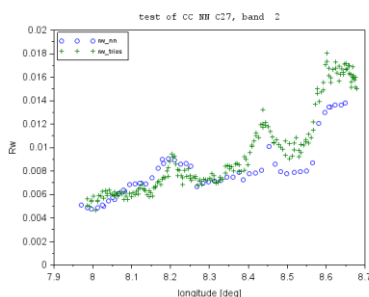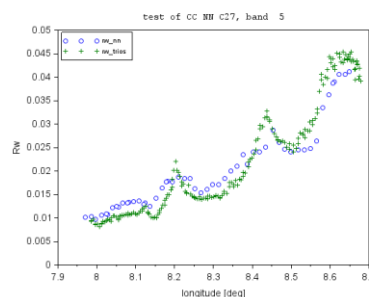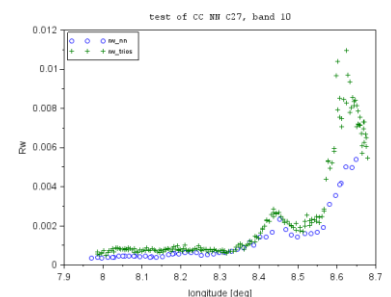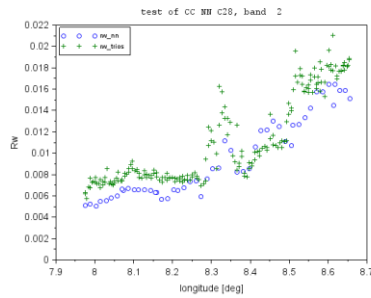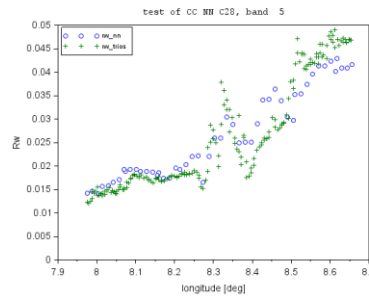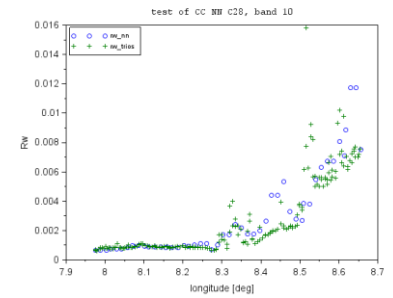
12.6.2006 Band 2, 443 nm   Band 5, 560 nm   Band 10, 755 nm
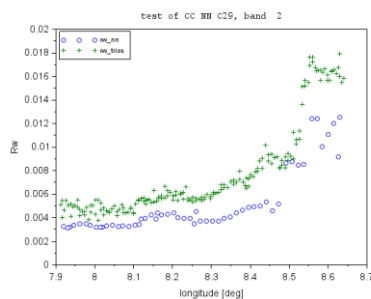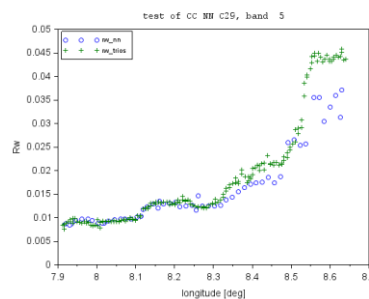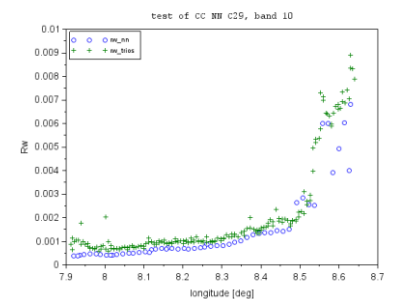
4.7.2006 Band 2, 443 nm   Band 5, 560 nm   Band 10, 755 nm
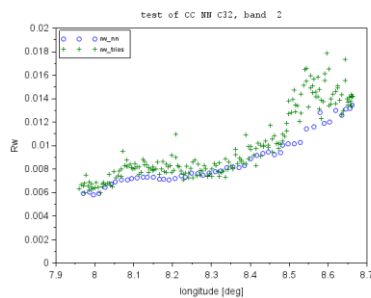
26.7.2006 Band 2, 443 nm   Band 5, 560 nm   Band 10, 755 nm
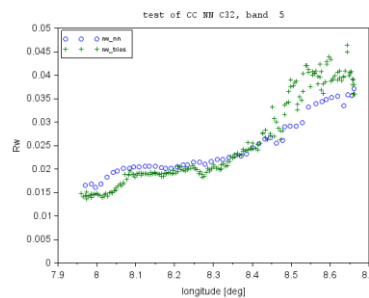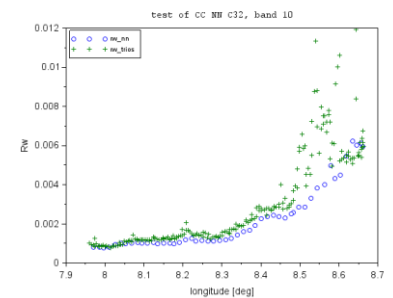
Figure 3-96: Lw NN is compared with in situ data for bands 443, 560 and 755 nm in eight different days following the Helgoland crusie transect

A comparison with the performance of the standard product is shown in Figure 3-97. Four examples with two different dates in different bands show a better performace of the NN retrievals approaching to the more complicated waters, with NN transects (blue and green lines for non-normalised and normalised data respectively) closer to the in situ data (black line) than the standard product (red line). In the second y-axis, a scale from 0 to 1 has been added to show the performance of the out_of_scope (OOS) and out_of_range (OOR) flags applied in the NN. For clarity, when the OOS flag is raised (AAC_OOS_true), a value of 0.6 is assigned. When the OOS is not raised (AAC_OOS_false), a value of 0.5 is assigned. When the OOR flag is raised (AAC_OOR_true), a value of 0.3 is assigned; and a value of 0.2 is assigned when the OOR flag is not raised (AAC_OOR_false). In the plots the labels AAC_OOR and AAC_OOS true or false help to understand them. The first day show an overtimation of the NN reflectances along the transects except for the pixels nearer to the coast. In the third plot

4th MERIS data reprocessing
Evolutions and Validation report

Ref.:   MER4RP Validation Report
Version: 1.0
Date: 01/04/2019
Page: 137

the disagreement is higher for the standard reflectances practically all the transects. Second and fourth plot look quite good, with bigger dispersion in pixels closer to the coast.
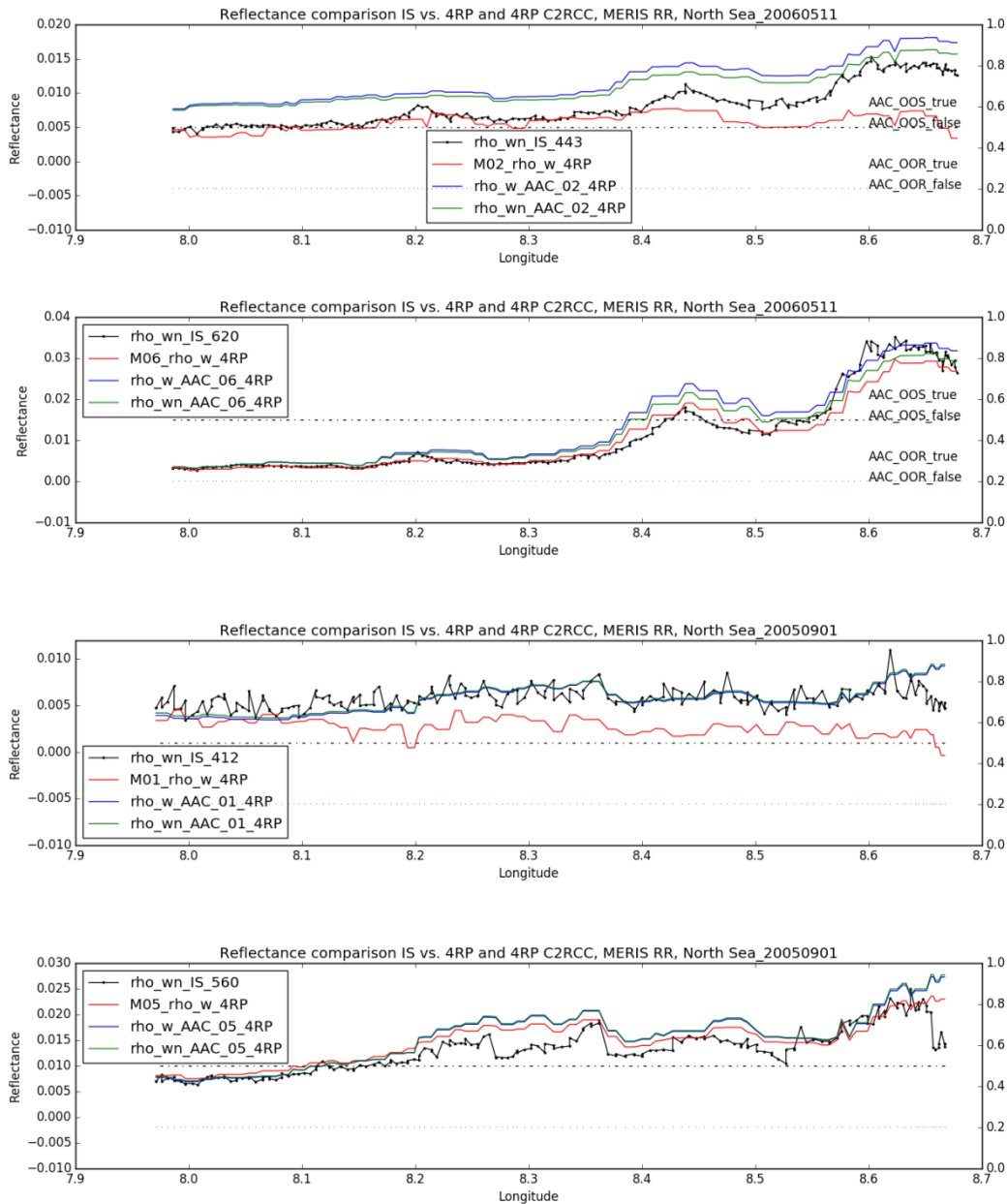
Figure 3-97: Comparison of in situ data on the Helgoland transects with the Lw NN retrievals and the standard product

3.3.3.4   *Algal Pigment Concentration 2 (CHL_NN)*

Mermaid

For the validation of the chlorophyll data two different MERMAID in situ data were used separately, which were measured using hplc (hplc_chla_total) with 514 samples (3x3 = 4626 pixels) and the fluorometric method (fluor_chla_is) with 239 samples (3x3 = 2637 MERIS

4th MERIS data reprocessing
Evolutions and Validation report

Ref.:   MER4RP Validation Report
Version: 1.0
Date: 01/04/2019
Page: 138

pixel). As already indicated in the NOMAD data set, the fluorometric data has a lower scatter. The output of the NN, i.e. apig, was converted into chlorophyll a concentration by <chl_conc> = 20 * apig^1.04.

The coefficients were derived from data of the North Sea by regression (Figure 3-99). As one can see in the following the coefficients, which were derived from regression with the MERMAID data set deviates from the coefficients, which were used up to now probably because they are more related to case 1 water.

The MERIS data were filtered using the following conditions: windm < 8 & cloud <1 &ice_haze < 1 & white_scatter < 1.
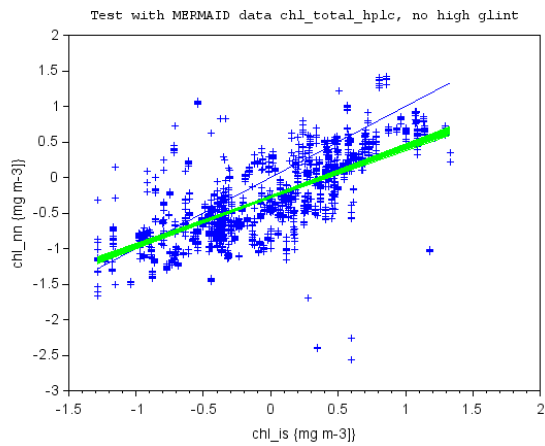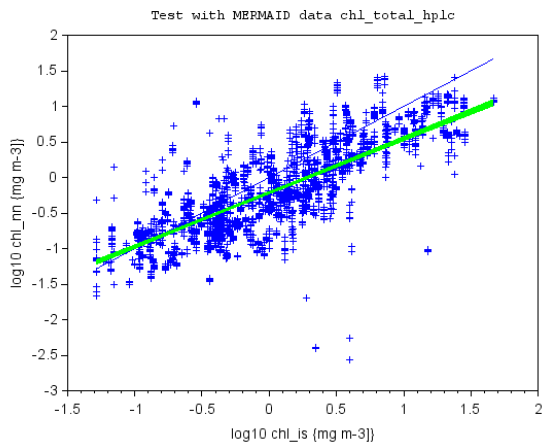
Test including high sun glint cases

mean slope of 100 random bootstrap samples: 0.7598

mean bias: -0.2123046

mean stedev: 0.38202

n= 4041 /9 = 449 in situ

Test for the cases without high sun glint

Mean slope of 100 random bootstrap samples: 0.6983953

mean bias: - 0.2708453

mean stdev: 0.3881643

n=2897 /9 = 321
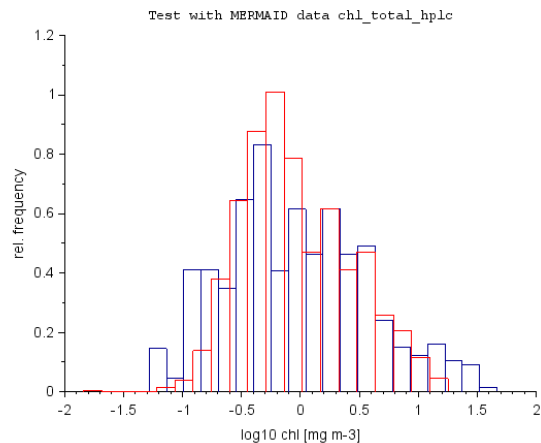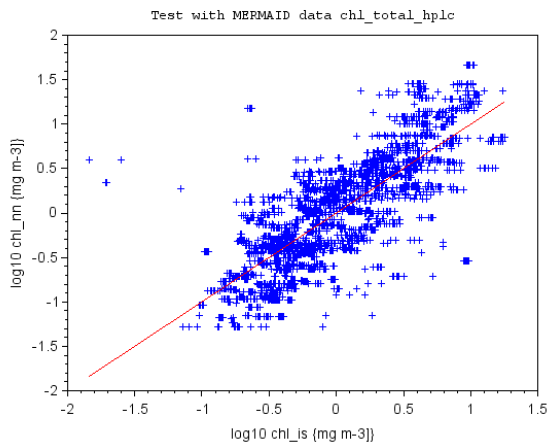
Conversion coefficients from this data set:

chl = 14.5 * apig_443 ^ 0.807

Frequency distribution after applying the optimum conversion coefficients

4th MERIS data reprocessing

Evolutions and Validation report

Ref.:   MER4RP Validation Report

Version: 1.0

Date: 01/04/2019

Page: 139

stdev of 0.388, = 38 % on the log scale

n= 4041 /9 = 449 in situ

Red: chl_nn, blue: hplc_chla_total
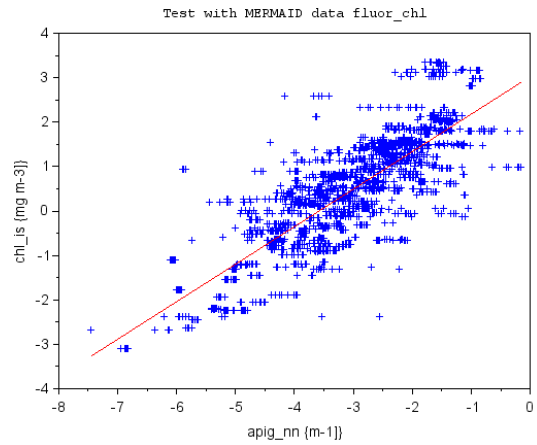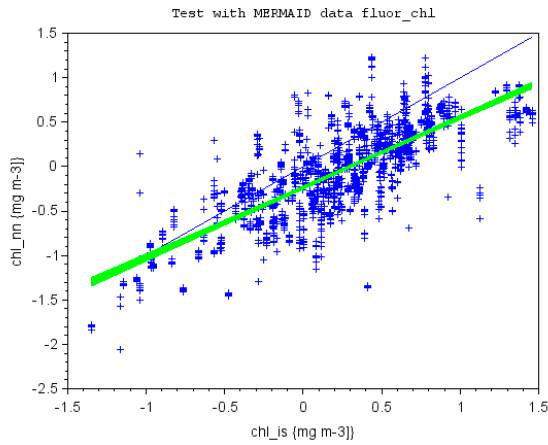
Mean slope: 0.786, mean bias: -0.233

mean stdev: 0.312, n= 2314   /9 = 257

New conversion factors:

Chl = 20.63 * apig^0.845

Figure 3-98: Test using the fluorometric chlorophyll data of MERMAID. Left the test, right the relationship between apig and the chlorophyll concentration for the determination of new
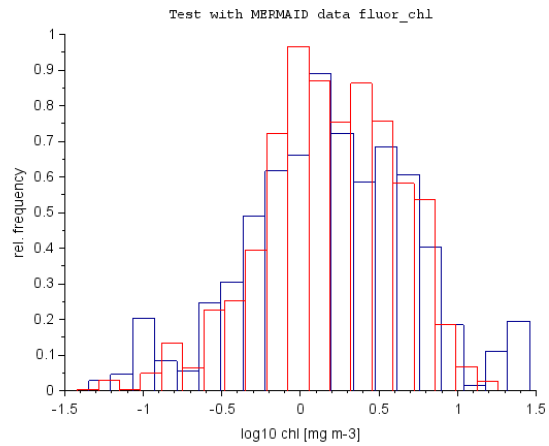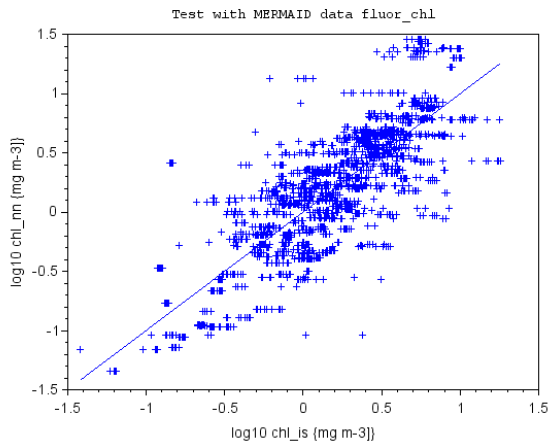
After applying the new conversion coefficients

Frequency distribution after applying the optimum conversion coefficients

Red: chl_nn, blue: fluor_chla_is

Figure 3-99: North Sea regressions using the hlpc and fluor matchups

4th MERIS data reprocessing

Evolutions and Validation report

Ref.: MER4RP Validation Report

Version: 1.0

Date: 01/04/2019

Page: 140
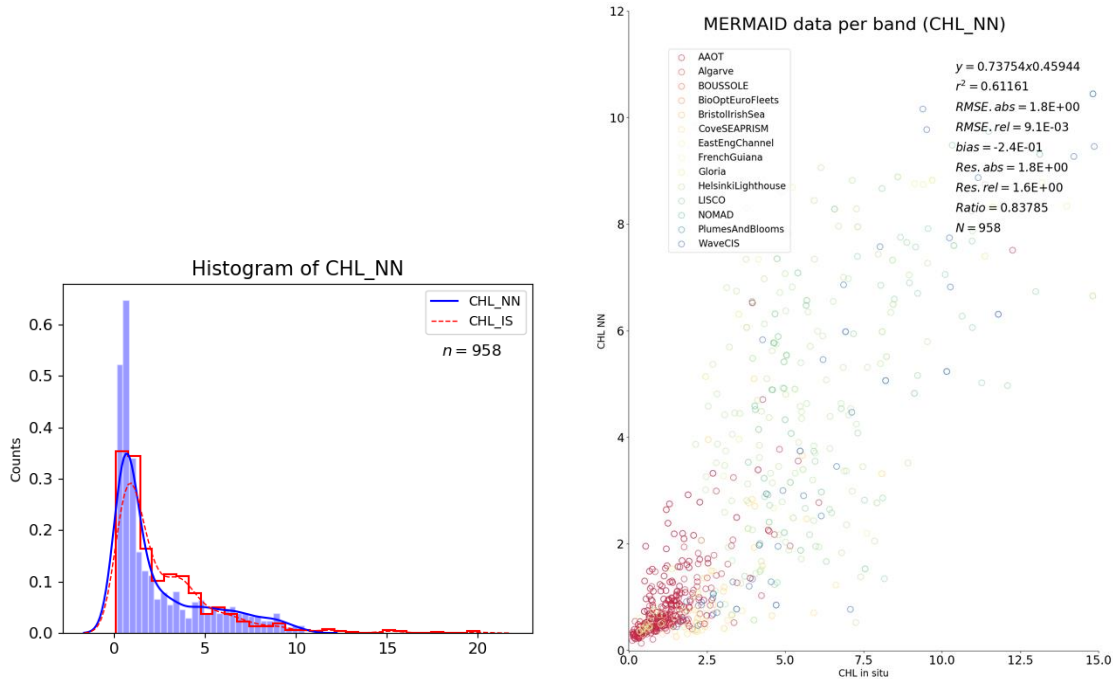
Figure 3-100: Scatter plot of the chlorophyll_a comparison: MERMAID in situ vs. C2R NN retrievals (top)and histogram of the in situ and satellite data (bottom)

Figure 3-100 shows the scatter plot and histogram of the total chlorophyll in situ contained in the Mermaid dataset (including 'FLUOR_chla_IS', 'AERONET_chla_IS', 'HPLC_chla_TOTAL_IS', 'FLUOR_chla_IS' 'chl_calc','SPECT_chla_IS') vs. the chlorphyll values derived from the NN. Total number of match-ups is 958. As can be seen in the histogram, satellite data shows one peak in lower chlorophyll vales (close to 0), while the in situ data has a broader distribution with two peaks. There are scarce CHL_NN values higher than 10 mg m^{-3}. The coefficient of determination is 0.61 with a bias of -0.24, with a slope of 0.73. The plot does not include the data flagged by'WP_PC_CHL_NN_FAIL', 'CC_CLOUD' and 'CC_CLOUD_AMBIGUOUS'.

The same exercise is done clustering the data per water types (Lee et al., 2006), as done with the reflectances in the previous section. In the following cases (Figure 3-101) there are four examples of the behavior of the regression CHL_NN vs. CHL_IS for high: a) high CDOM than CHL water types using the AERONET measurements (537); b) strict Case 1 against HLPC measurements (106); c) Case 2 scattering waters against AERONET (372); d) low CDOM than CHL content waters using HPLC measurements (55). These examples were chosen because the higher number of mtachups compared with the other in situ measurement types.

4th MERIS data reprocessing
Evolutions and Validation report

Ref.:   MER4RP Validation Report
Version: 1.0
Date: 01/04/2019
Page: 141

a) HCDOM AERONET_chla_IS vs. CHL_NN

MERMAID data per band (CHL_NN)

AAOT
CoveSEAPRISM
Gloria
HelsinkiLighthouse
LISCO
WaveCIS

$y = 0.74719x0.49361$
$r^2 = 0.57006$
$RMSE.abs = 1.8E+00$
$RMSE.rel = 2.0E-02$
$bias = -2.1E-01$
$Res.abs = 1.9E+00$
$Res.rel = 1.8E+00$
$Ratio = 0.85363$
$N = 537$
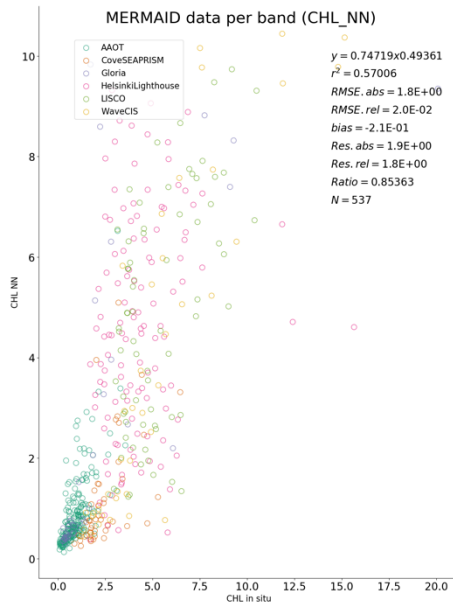
b) Case 1 HLPC_chla_TOTAL vs. CHL_NN

MERMAID data per band (CHL_NN)

Algarve
BOUSSOLE
EastEngChannel
NOMAD
PlumesAndBlooms

$y = 0.30686x-0.00038$
$r^2 = 0.89323$
$RMSE.abs = 1.8E+00$
$RMSE.rel = 5.7E-01$
$bias = -9.6E-01$
$Res.abs = 2.4E+00$
$Res.rel = 3.9E-01$
$Ratio = 0.33790$
$N = 106$
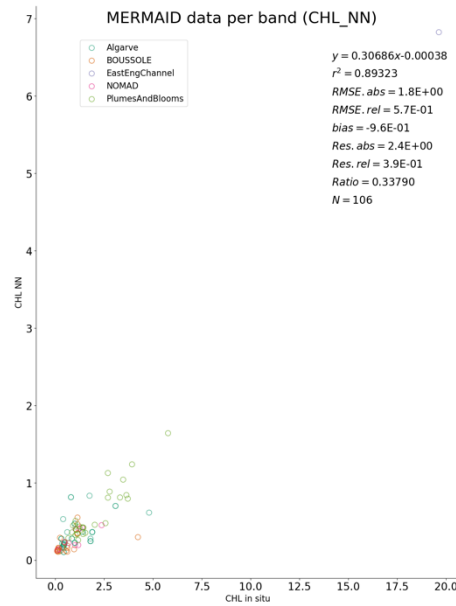
c) Case 2 AERONET_chla_IS vs. CHL_NN

MERMAID data per band (CHL_NN)

AAOT
CoveSEAPRISM
Gloria
HelsinkiLighthouse
LISCO
WaveCIS

$y = 0.72251x0.44026$
$r^2 = 0.64176$
$RMSE.abs = 1.7E+00$
$RMSE.rel = 2.3E-02$
$bias = -2.2E-01$
$Res.abs = 1.7E+00$
$Res.rel = 1.4E+00$
$Ratio = 0.83875$
$N = 372$
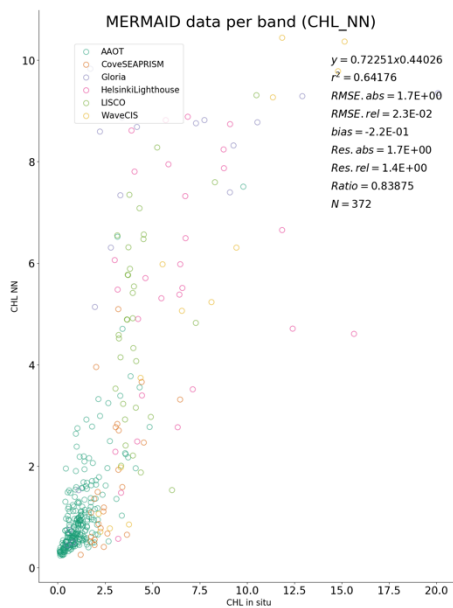
d) LCDOM HLPC_chla_TOTAL vs. CHL_NN

MERMAID data per band (CHL_NN)

Algarve
BOUSSOLE
NOMAD
PlumesAndBlooms

$y = 0.33315x0.59128$
$r^2 = 0.53830$
$RMSE.abs = 6.7E+00$
$RMSE.rel = 3.6E-01$
$bias = -3.5E+00$
$Res.abs = 9.0E+00$
$Res.rel = 5.1E+00$
$Ratio = 0.37265$
$N = 55$
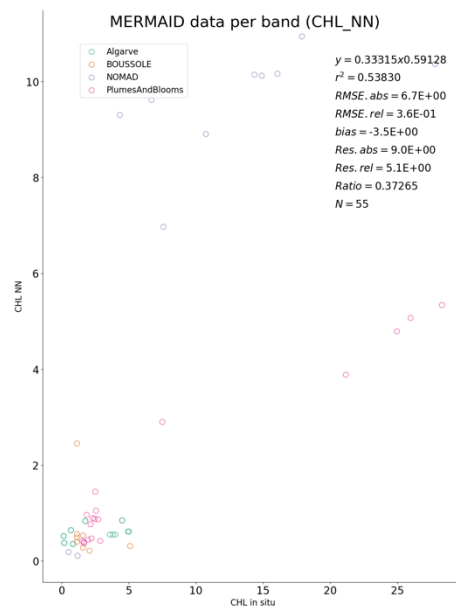
Figure 3-101: Scatter plot of CHL_NN vs. CHL_IS. Examples for fourdifferent water types and several types of in situ measurements

Coefficients of determination range from 0.57 in example a) with a RMSE of 1.8 mg m^{-3}; b) R^2 of 0.89 and again 1.8 mg m^{-3} of RMSE; c) R^2 of 0.64 and RMSE of 1.7 mg m^{-3}; and d) R^2 of 0.54 and RMSE of 6.7 mg m^{-3}.

As observed, most of the matchups for the MERMAID database are using the AERONET measurements (AAOT and LISCO). An important observation is that many of the points in AAOT seem to be classified as both HCDOM and Bb water types. This could be related to the

4th MERIS data reprocessing

Evolutions and Validation report

Ref.:   MER4RP Validation Report

Version: 1.0

Date: 01/04/2019

Page: 142

classification method that uses the in situ remote sensing reflectances with some thresholds, based exclusively in the NOMAD database.

Helgoland CHL

The retrieval of the CHL values is also tested using the data contained in the Helgoland transects dataset. Figure 3-102 shows the CHL values from MERIS (blue dots) compared with the in situ samples (red dots). The trend is similar in all eight transects, with in situ data showing higher uncertainties. It is assumed that in situ data have an uncertainty of a factor of 2.

4th MERIS data reprocessing

Evolutions and Validation report

Ref.: MER4RP Validation Report

Version: 1.0

Date: 01/04/2019

Page: 143
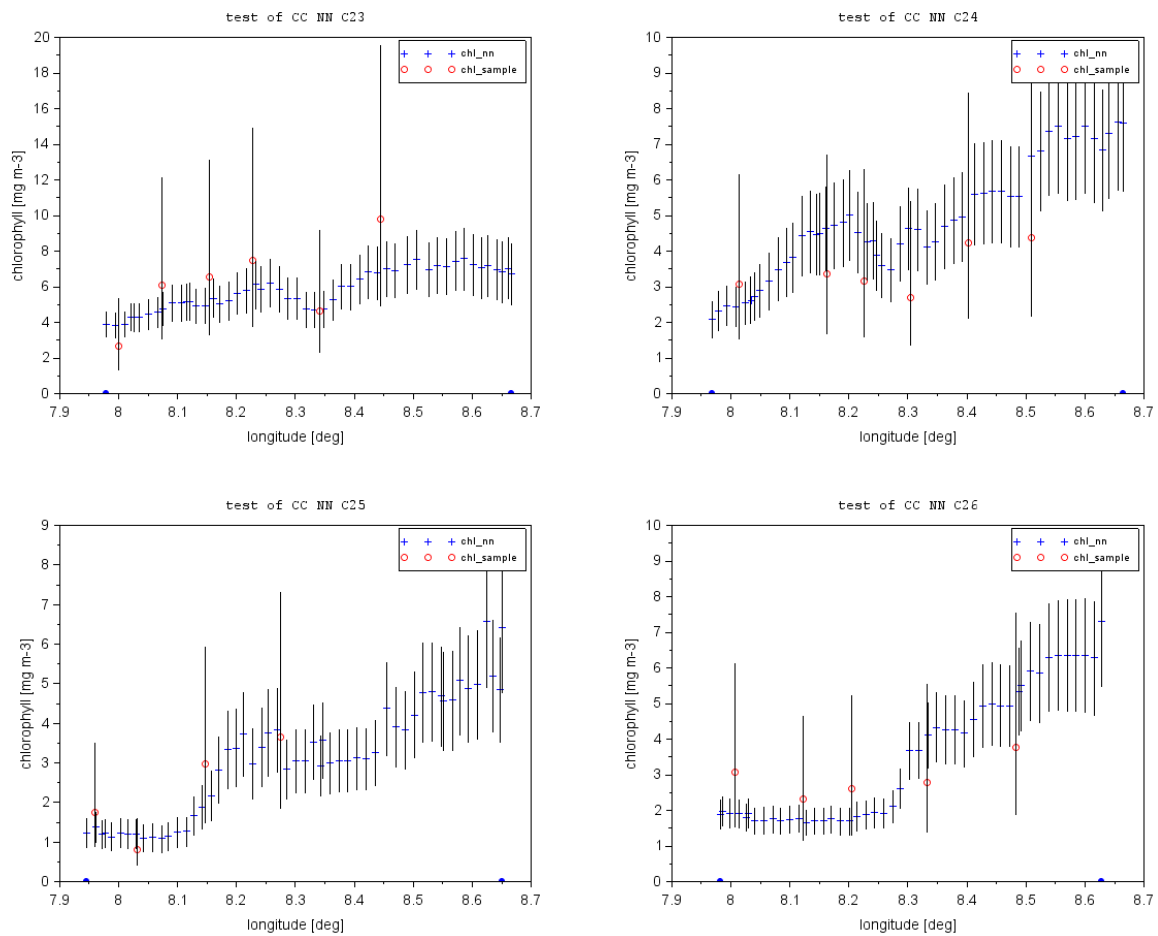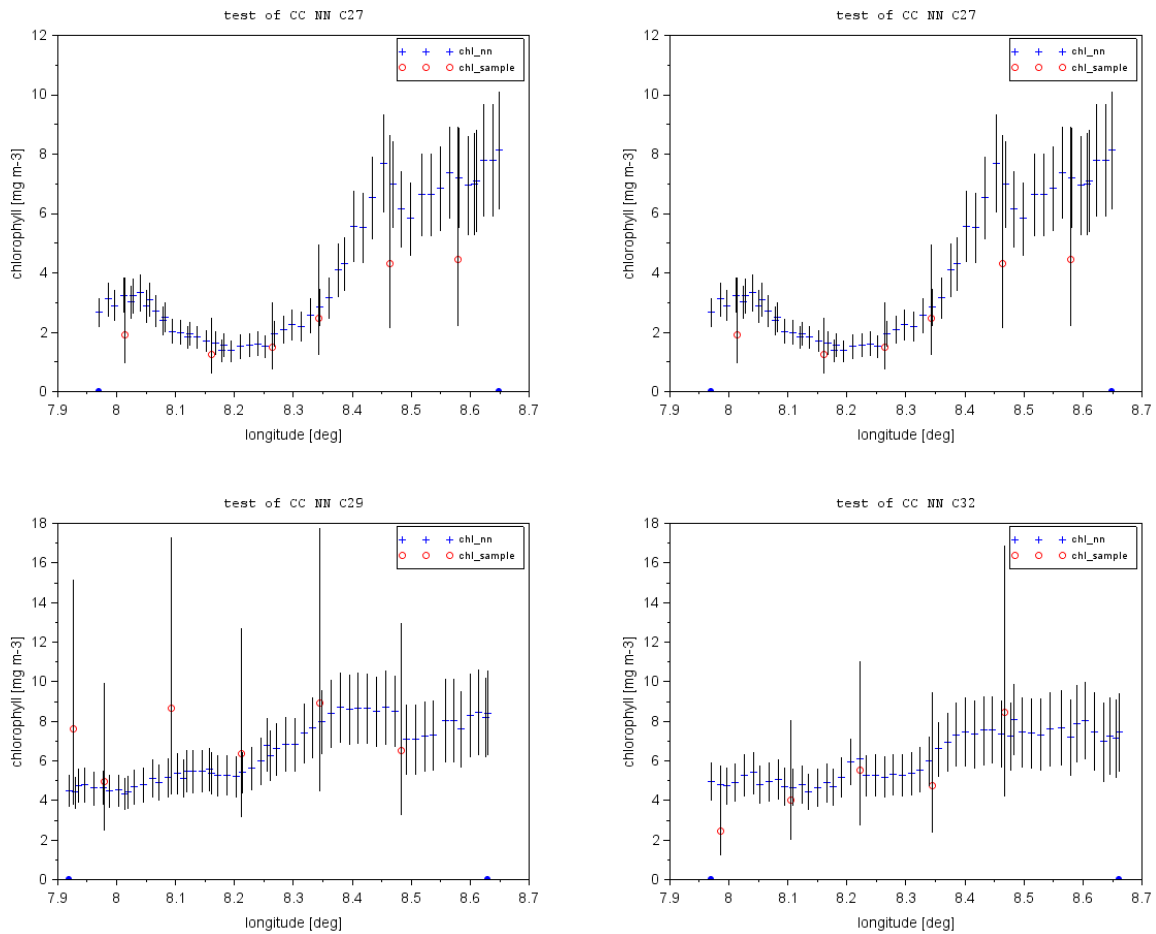
Figure 3-102: Chlorophyll concentration along the transect with the uncertainty range (vertical bars) and the chlorophyll concentration of the samples (red) with the factor 2 uncertainty range

3.3.4 Total Suspended Matter Concentration, output of the Case 2 algorithm (TSM_NN)

This product is not a standard product.

Helgoland transect

The transects of in situ measurements taken in the North Sea show the continuous increase of TSM concentrations from open water to the west coast of Germany. This trend is followed accurately by the TSM calculated with the C2RCC NN. We observe a slight overestimation in some of the transect when approaching the high TSM concentration areas near the coast.

4th MERIS data reprocessing

Evolutions and Validation report

Ref.: MER4RP Validation Report

Version: 1.0

Date: 01/04/2019

Page: 144

4th MERIS data reprocessing

Evolutions and Validation report

Ref.:   MER4RP Validation Report

Version: 1.0

Date: 01/04/2019

Page: 145
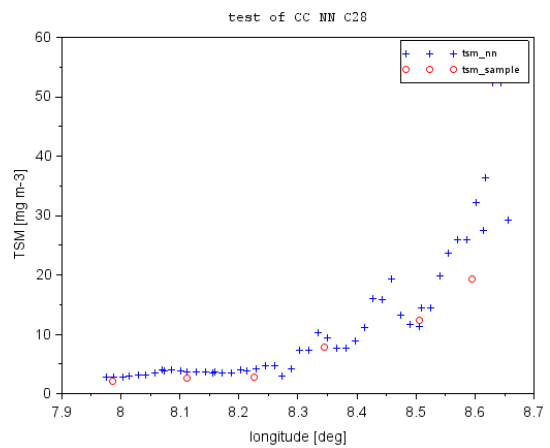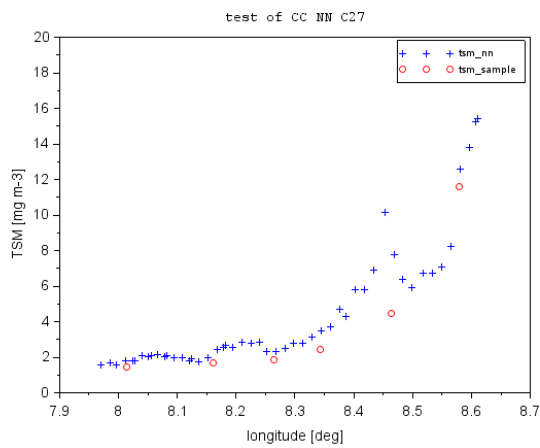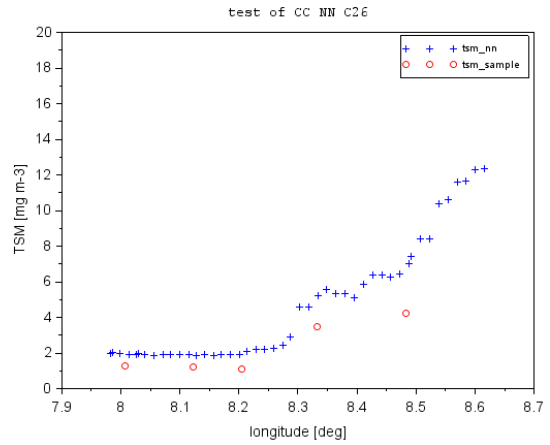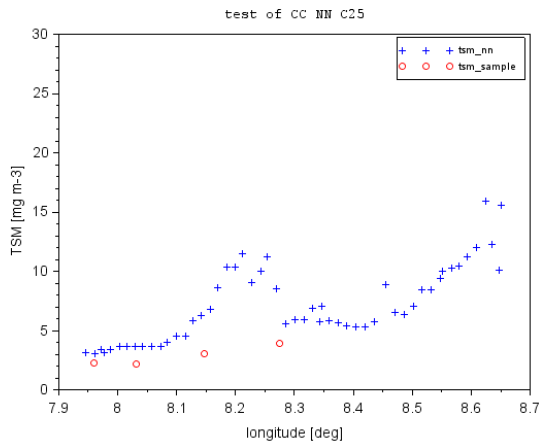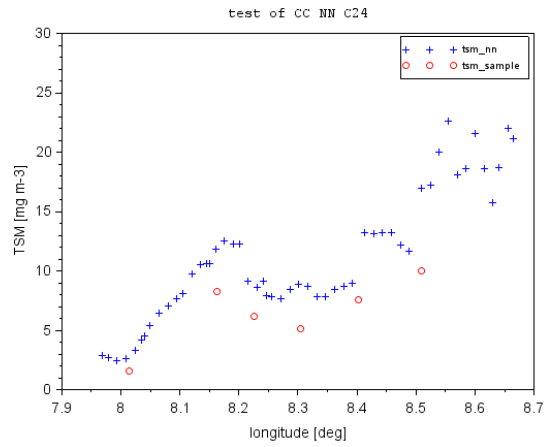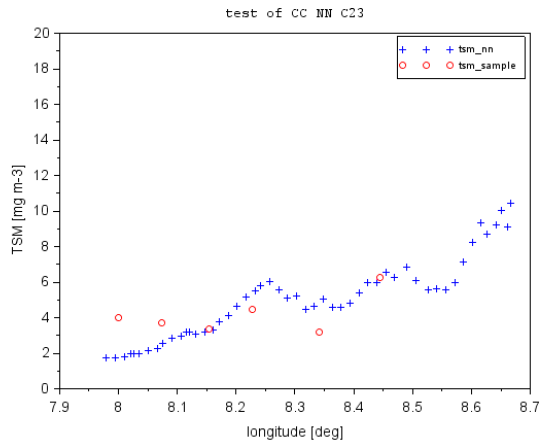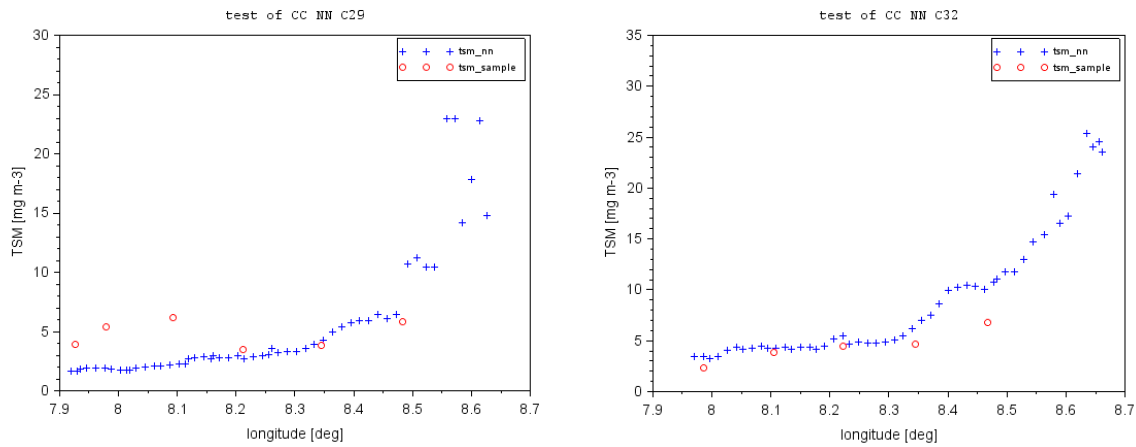
Figure 3-103: Comparison between water samples (red) and MERIS data (blue) for the total suspended matter dry weight (TSM) of all water constituents.

CEFAS

CEFAS is the Centre for Environment, Fisheries and Aquaculture Science (UK)[1] providing solution for the aquatic environment, biodiversity and food security. CEFAS provides a Defas Data Hub, an online portal for downloading datasets of water temperature, salinity, and sediment data across the UK continental self (in among other varaibles). CEFAS owns a system of SmartBuoys. Those are autonomous moored, automated and multiparameter recording platforms to collect marine environmental data. We used the data of four buoys: Dowsing, Liverpool, Warp and West Gabbard. Time series of CEFAS in situ data are available for the four stations matching most of the MERIS life span (2002-2012). Daily and weekly (not shown) values of turbidity are plot together with the TSM values extracted with the C2RCC NN (Figure 3-105).

In situ turbidity values and TSM EO data seem annual cycles very clear in all four stations, minimum values are shown in the central months of the year, while maximum values have a winter peak. This is especially visible in the Liverpool Bay area and West Gabbard. The Dowsing buoys collects data only from 2009, but in the few years shown, trends match quite well. In the Warp region the seasonal cycle is visible too, but data are more disperse. The Warp bouys is located closer to the Thymes river mouth, which could explain the irregularities in the trend.

---

[1] https://www.cefas.co.uk/about-us/

4th MERIS data reprocessing

Evolutions and Validation report

Ref.:   MER4RP Validation Report

Version: 1.0

Date: 01/04/2019

Page: 146
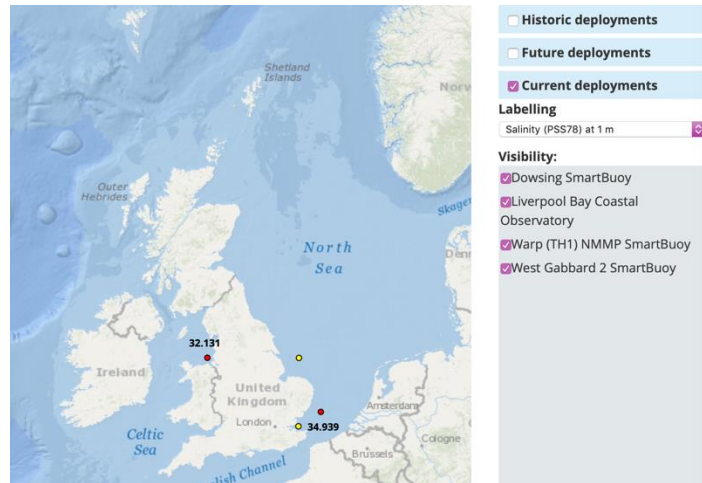
Figure 3-104: Location of the Cefas SmartBuoys system in the UK North Sea

4th MERIS data reprocessing

Evolutions and Validation report

Ref.: MER4RP Validation Report

Version: 1.0

Date: 01/04/2019

Page: 147
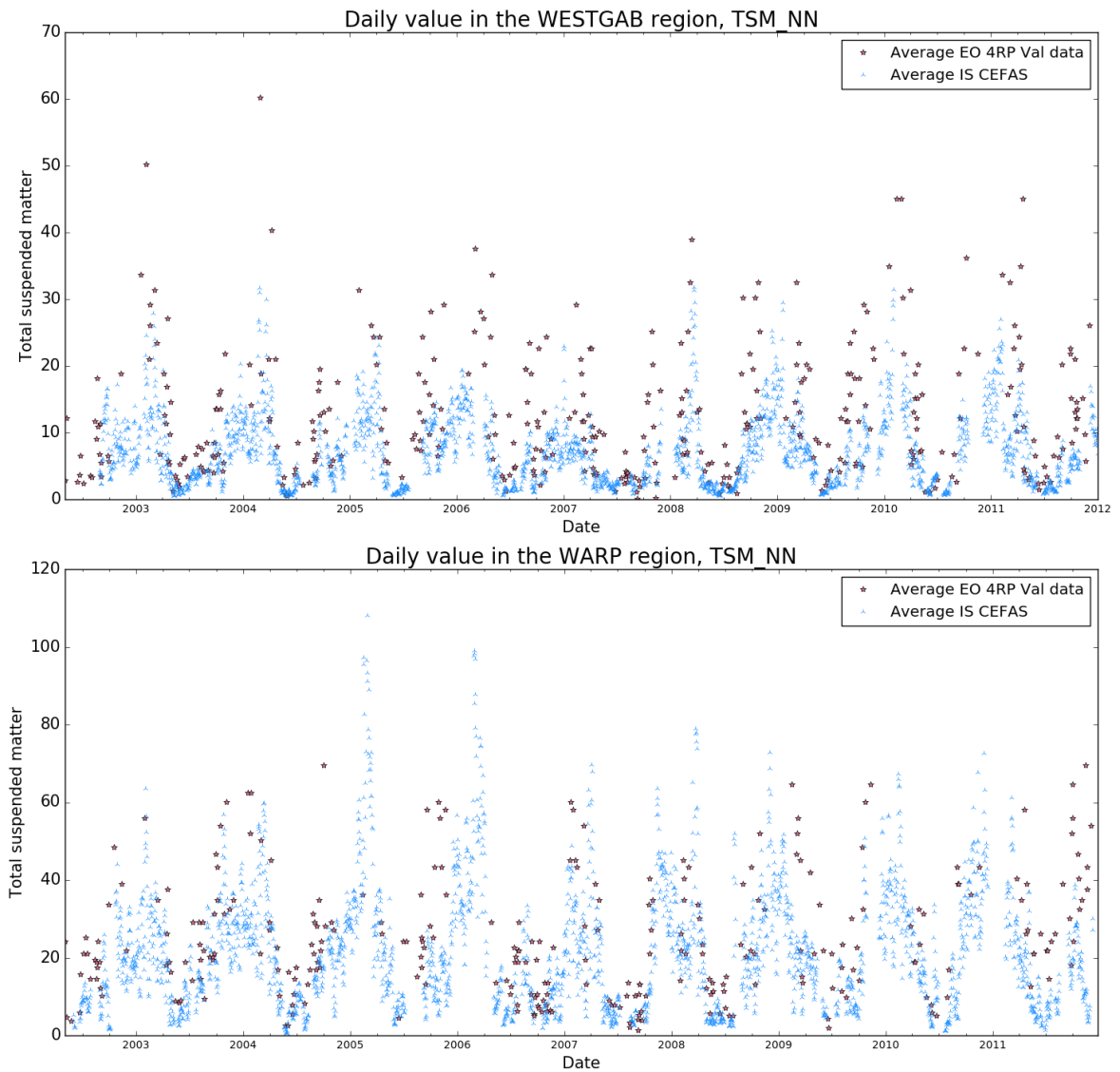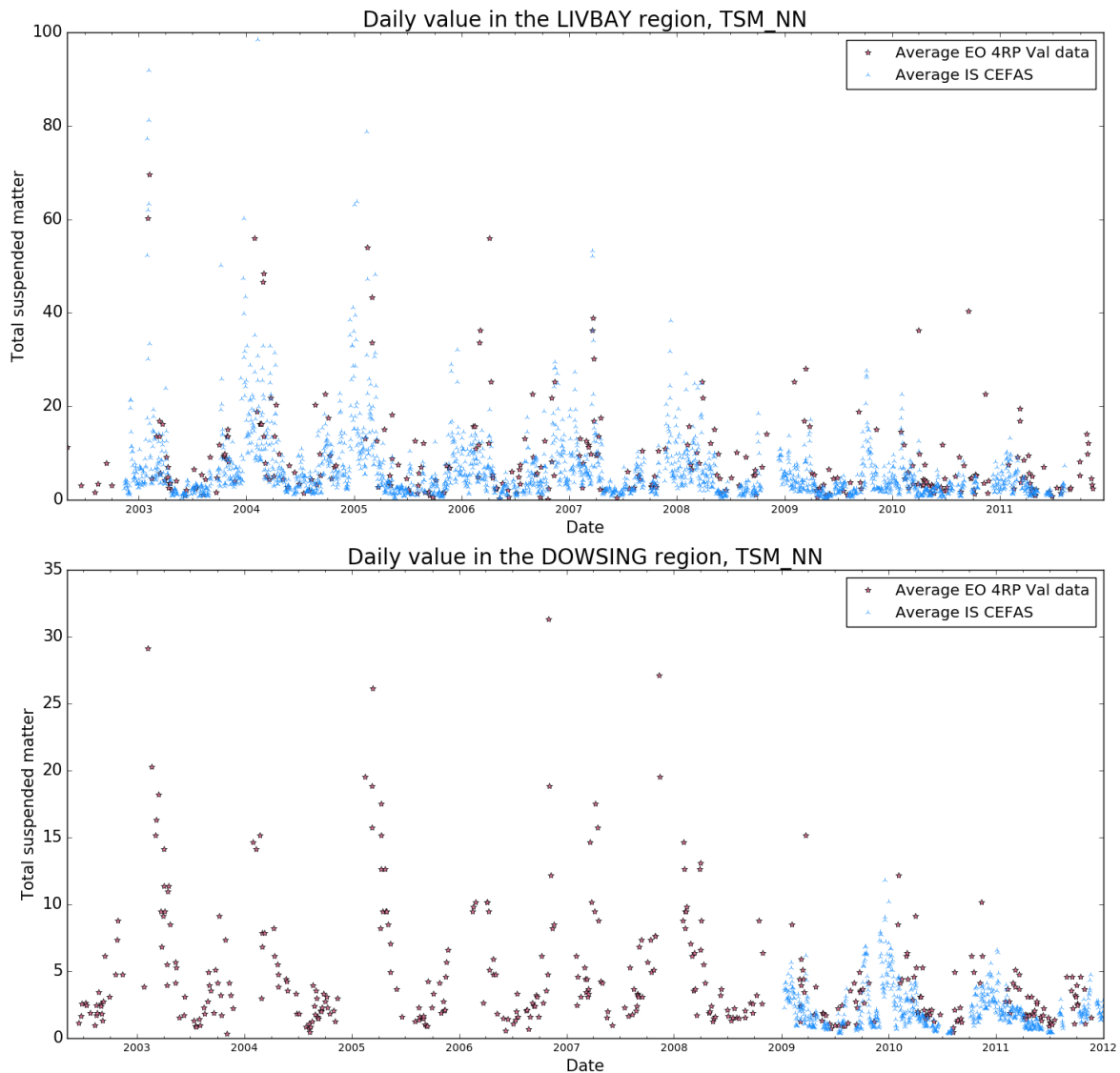
Figure 3-105: Time series (10 years) of the total suspended matter in situ vs. C2RNN TSM retrieval

3.3.5 CDM absorption coefficient, output of the Case 2 algorithm (ADG443_NN)

Helgoland transects

The transects of in situ measurements taken in the North Sea show the continuous increase of absorption coefficient from open water to the west coast of Germany. This trend is followed accurately by the absorption coefficient calculated with the C2RCC NN. In some of the transects, there is an overestimation of the NN product, but in most of them the values are very similar.

4th MERIS data reprocessing

Evolutions and Validation report

Ref.: MER4RP Validation Report

Version: 1.0

Date: 01/04/2019

Page: 148

4th MERIS data reprocessing

Evolutions and Validation report

Ref.:   MER4RP Validation Report

Version: 1.0

Date: 01/04/2019

Page: 149
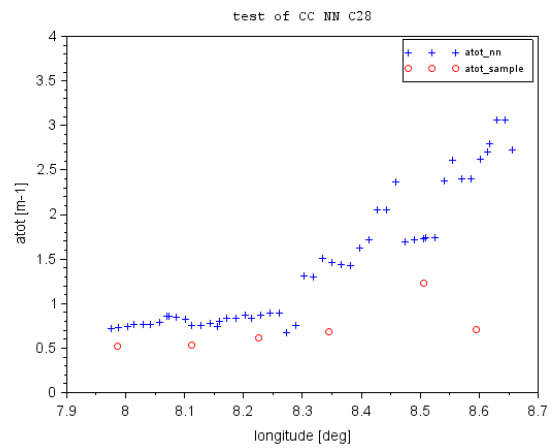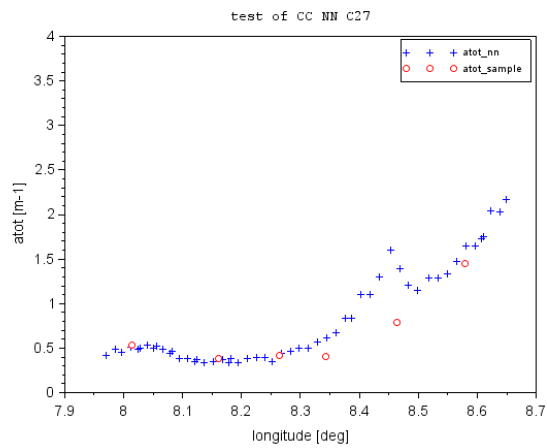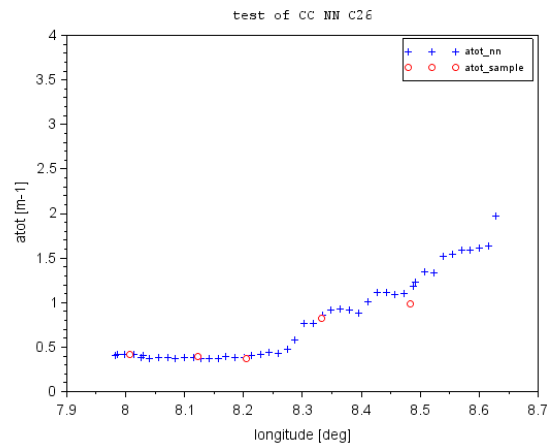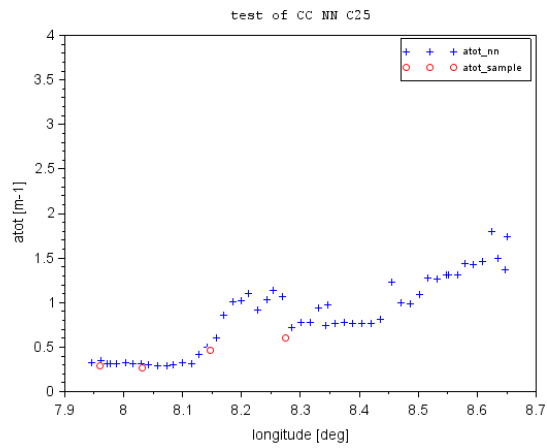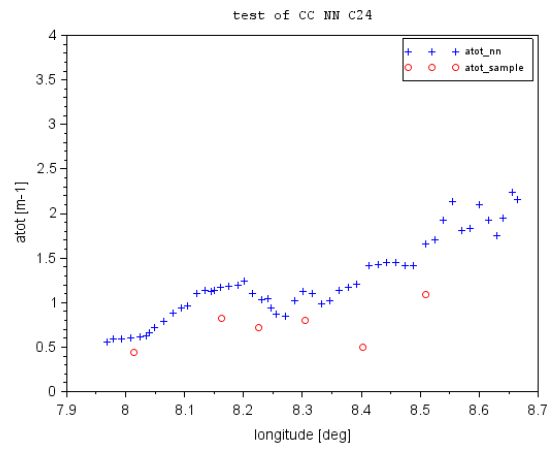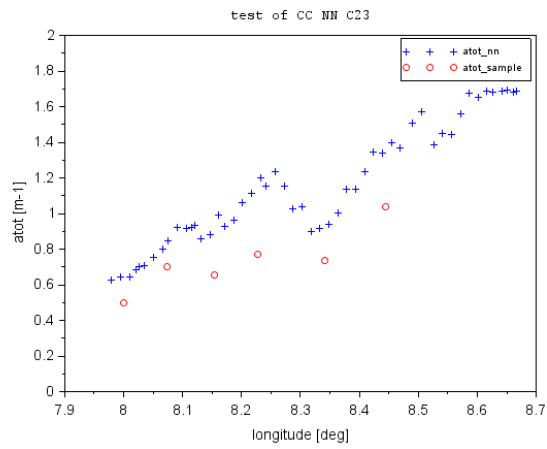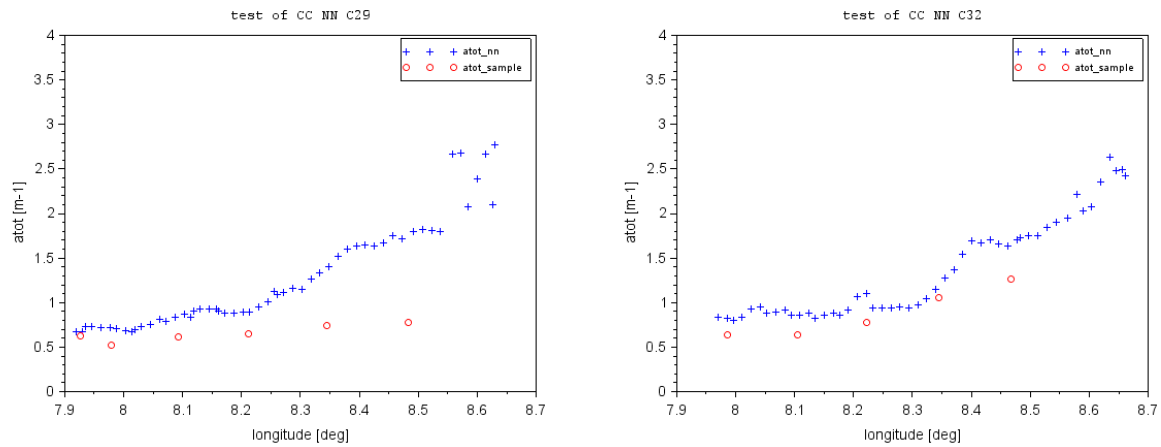
Figure 3-106: Comparison between water samples (red) and MERIS data (blue) for the absorption coefficient

3.3.6   Diffuse attenuation coefficient for downloading irradiance (KD490_M07)

Validation method

Match-up analysis with *in situ* radiometric profiles at BOUSSOLE.

Accuracy goal	MER3RP estimated quality	MER4RP estimated quality
Not availale	Not available	±15%

The diffuse attenation coefficient for downward plane irradiance at 490 nm product (KD490_M07) hase been introduced for the MER4RP and is derived with the Morel *et al*. (2007) algorithm (see S3-L2-SD-03-C10-LOV-ATBD).

The KD490_M07 has been validated against the *in situ* data collected at BOUSSOLE during monthly cruises for the whole MERIS mission with two radiometric profilers: a Satlantic SPMR (from 2001 to 2011) and a Biosperical C-OPS (starting from 2010).

Generally, three replicates of multispectral radiometric profiles of downward and upward irradiance (Ed and Eu) were collected at each station, along with Es, from which diffuse attenuation coefficients and reflectance spectra were derived (see Antoine *et al.* 2006).

The consistency of the two instruments was verified by performing consecutive deployments for ~1 year of monthly cruises. The mean unbiased percentage deviation of the reflectance was -1.40 % when the two instruments where deployed within 1h one from each other.

Quality control was performed through visual inspection of the reflectance spectra and compared to the Morel and Maritorena (2001) reflectance model constrained with *in situ* total Chlorophyll-a measured with HPLC method (Ras *et al*. 2008), suspect spectra were discarded. The *in situ*-MERIS matchups were extracted with ODESA over a 5x5 pixels grid centered on the sampling stations. The average of the valid pixels within the 5x5 grid and the available *in situ* replicates were considered for further analyses that resulted in 26 valid

4th MERIS data reprocessing

Evolutions and Validation report

Ref.: MER4RP Validation Report

Version: 1.0

Date: 01/04/2019

Page: 150

matchups (shown in Figure 3-107) with values ranging between 0.035 and 0.2 m^{-1} and a mean absolute percentage deviation of 13.5%.
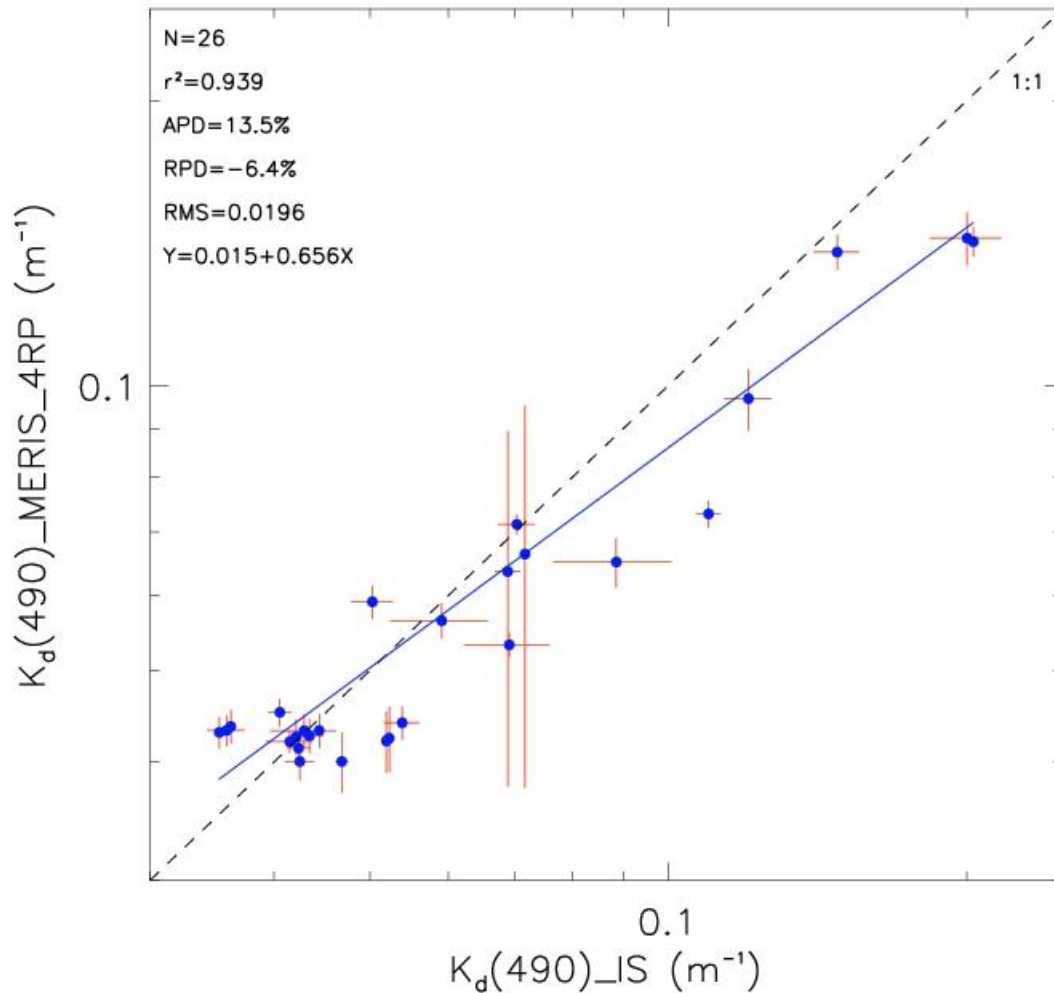
Figure 3-107: Kd(490) values derived from the MER4RP values and in situ measurements

3.3.7 Photosynthetically Available Radiation (PAR)

Validation method
PAR product validated in the frame of the MER2RP. Here, impact assessment of the MER4RP changes on the PAR products

Accuracy goal	MER3RP estimated quality	MER4RP estimated quality
The claimed accuracy for the PAR produt is +/- 3% according to the MERIS ATBD 2.18	+/- 3% (estimated from the MER2RP product validation)	+/- 3 % (estimated from the MER2RP product validation)

4th MERIS data reprocessing

Evolutions and Validation report

Ref.: MER4RP Validation Report

Version: 1.0

Date: 01/04/2019

Page: 151

No algorithm change has been performed for the PAR in the frame of the MER4RP (the PAR product remains in line with ATBD 2.18).

The PAR product from the MER2RP was verified and validated following Bouvet (2006). The accuracy of +/- 3% claimed in the MERIS ATBD 2.18 was confirmed. Since then there was no change in algorithm. The MER4RP PAR products can however differ significantly from the MER2RP and MER3RP PAR products due to changes in the products used as input to the PAR retrieval algorithm: the aerosol Angstrom exponent and optical thickness at 865 nm, the column water vapour and the total column ozone. Relative difference between PAR products from the MER4RP and MER3RP were found on few randomly selected scenes to be of the order of few percents but seem to locally reach up several tens of percents (see example in the next figure). No further validation of the MER4RP product was carried out. Such validation would be necessary to fully confirm for the MER4RP PAR data the ATBD claimed +/- 3% accuracy confirmed on the data from the MER2RP.

NB: the algorithm to derive the uncertainty associated to the PAR on a pixel basis is not defined. The 'PAR_err' is thus empty.
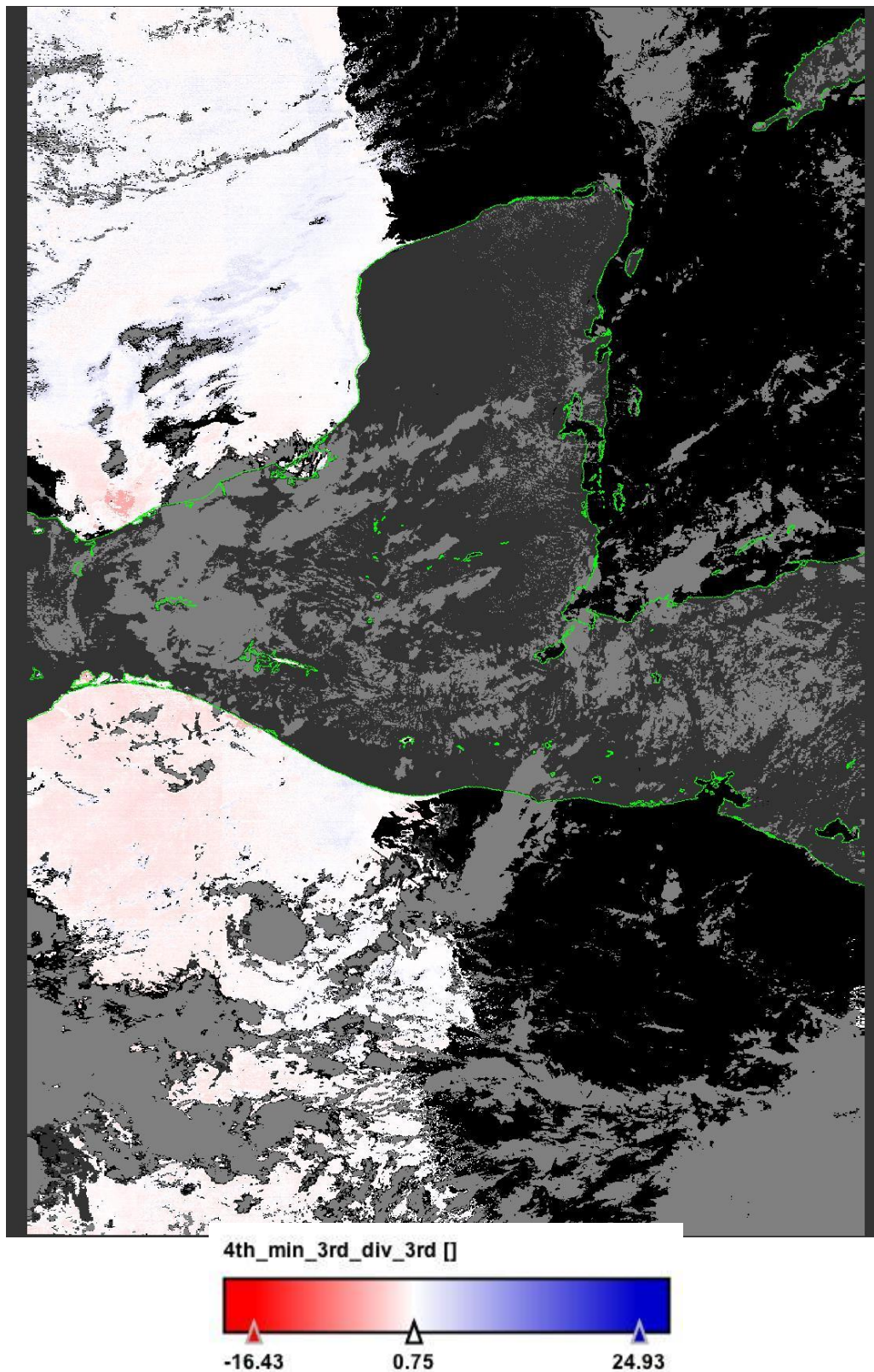
Figure 3-108: The relative difference in % between the PAR of the MER4RP and MER3RP: product ENV_ME_2_RRG____20080617T160908_20080617T161344_____0275_069_312_____ACR_R_ NT____.SEN3 and MER_RR__2PTACR20080617_160908_000002762069_00312_32931_0000.N1

4th MERIS data reprocessing
Evolutions and Validation report

Ref.: MER4RP Validation Report
Version: 1.0
Date: 01/04/2019
Page: 153

3.3.8 Aerosol Optical Thickness (AOT865) and Angstrom Coefficient at 865 nm (A865)

Validation method

T865 (aerosol optical thickness at 865 nm) and A865 (Angström exponent)

Comparisons with MER3RP, MODIS and SeaWiFS L3 monthly products

Comparisons with AERONET-OC aerosol optical thickness products

Accuracy goal	MER3RP estimated quality	MER4RP estimated quality
AOT865 15% accuracy or 0.02 for moderate values (~0.1-0.2), (ATBD 2.7 Iss 4.1 Feb 2000)	Retrieved for in situ values of AOT(870) < 0.03 ▪ RMSE = 0.08 ▪ MAD = 0.04	Retrieved for in situ values of AOT(870) < 0.03 ▪ RMSE = 0.038 ▪ MAD = -0.012
A865 Not specified in ATBD	Retrieved for in situ values of AOT(870)>0.03 ▪ RMSE = 0.66 ▪ MAD = 0.25	Retrieved for in situ values of AOT(870)>0.03 ▪ RMSE = 0.182 ▪ MAD = 0.084

Validation of the aerosol by-products is based on the mer4val facility: maps of T865 and A865 can be intercompared between MER3RP, MER4RP, MODIS, and SeaWIFS. These comparisons are intended to be qualitative as A865/T865 are atmospheric correction by-products, only indicative of the correct behaviour of the atmospheric correction.

The intercomparisons show that MER4RP T865 is closer to the ones of MODIS and SeaWIFS than MER3RP. A865 of MER4RP is closer to the one of SeaWIFS, MER3RP closer to MODIS.

Overall, A865/T865 have similar qualitative behaviour and quality for MER3RP than for MER4RP when compared to other sensors.

4th MERIS data reprocessing
Evolutions and Validation report

Ref.: MER4RP Validation Report
Version: 1.0
Date: 01/04/2019
Page: 154
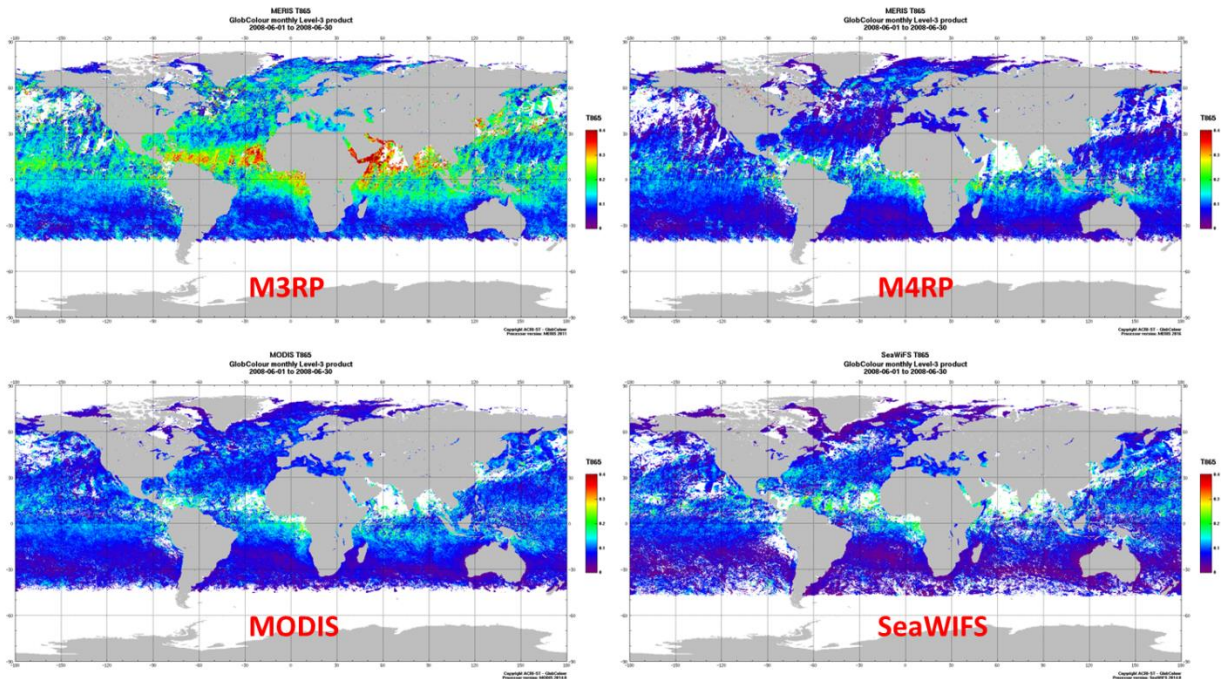
Figure 3-109: T865 monthly-means of Sept 2008. MER3RP, MER4RP, MODIS, and SeaWIFS.
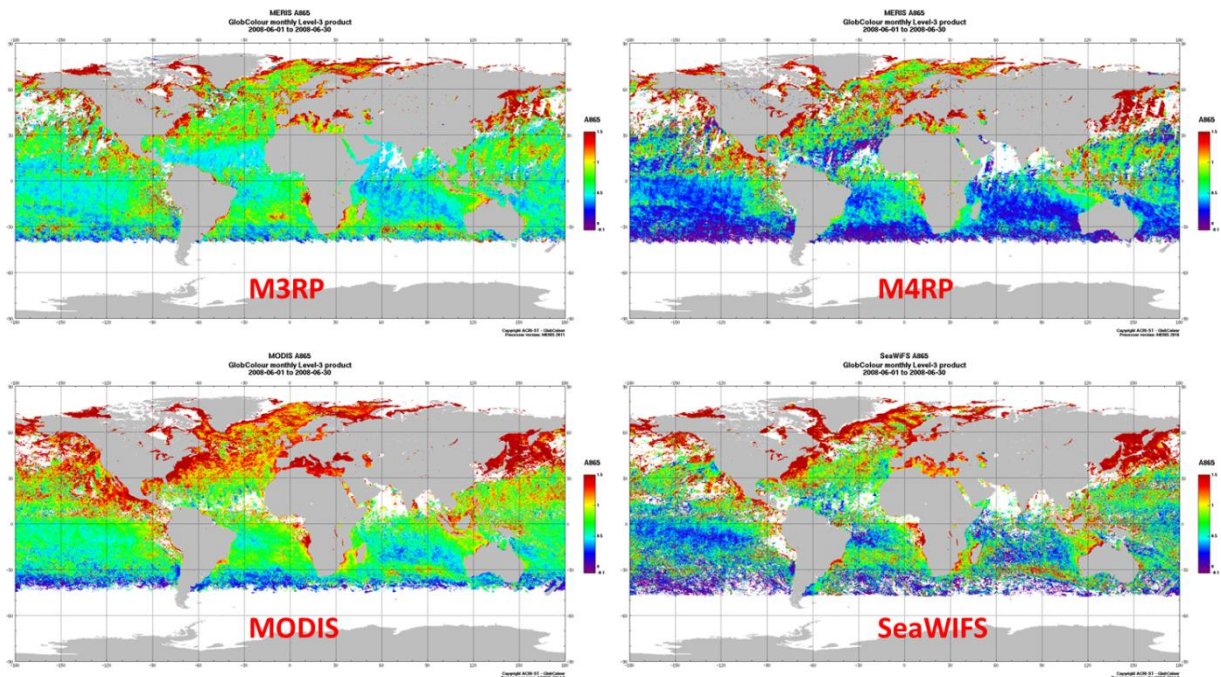
Figure 3-110: A865 monthly-means of Sept 2008. MER3RP, MER4RP, MODIS, and SeaWIFS.

Other means of comparisons are to compare with equipped in situ sites such as the AERONET-OC sites used in MERMAID. These sites include measurements of aerosol optical thickness at 870 nm and can directly be compared to the T865 product of MERIS. A bidimensional histogram of T865 vs in situ AOT is shown below which shows the relatively good values found from MERIS.

4th MERIS data reprocessing

Evolutions and Validation report

Ref.:   MER4RP Validation Report

Version: 1.0

Date: 01/04/2019

Page: 155

For retrieved AOTs < 0.03 we obtain RPD=0.233, MAD=-0.012, and RMSE=0.038.

For retrieved AOTs > 0.03 we obtain RPD=2.104, MAD=0.084, and RMSE=0.182.

These results are better than the ones obtained for MER3RP.
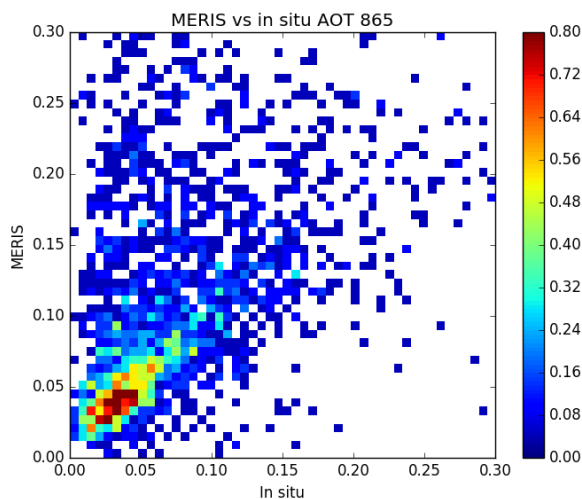
Figure 3-111: Bidimensional histogram of T865 (MERIS, y-axis) vs in situ AOT (x-axis) from AERONET-OC.

3.3.9   Focus on the Case2_S flag

The CASE2_S flag, which indicates high scattering, is raised when the TSM computed in the BPAC inversion is greater than a threshold. In the MER3RP, the threshold was set to 0.75 mg.l^{-1}. However, it should be noted that this flag reflects scattering in the NIR and as such does not strictly refer to the Case 1 / Case 2 distinction, since the flag can be raised by high levels of phytoplankton in mesotrophic waters. In the MER4RP, the new BPAC minimisation algorithm generally yields higher TSM, even over clear waters, and needs a revised threshold. Indeed, the particulate backscattering may compensate for any source of scattering not properly corrected, like white caps or Sun glint, which does not follow an atmospheric shape. An example is shown in Erreur ! Source du renvoi introuvable. over the South Pacific Gyre, where TSM can now reach values larger than 1.mg.l^{-1} over the glint (North-East region).

4th MERIS data reprocessing
Evolutions and Validation report

Ref.:   MER4RP Validation Report
Version: 1.0
Date: 01/04/2019
Page: 156
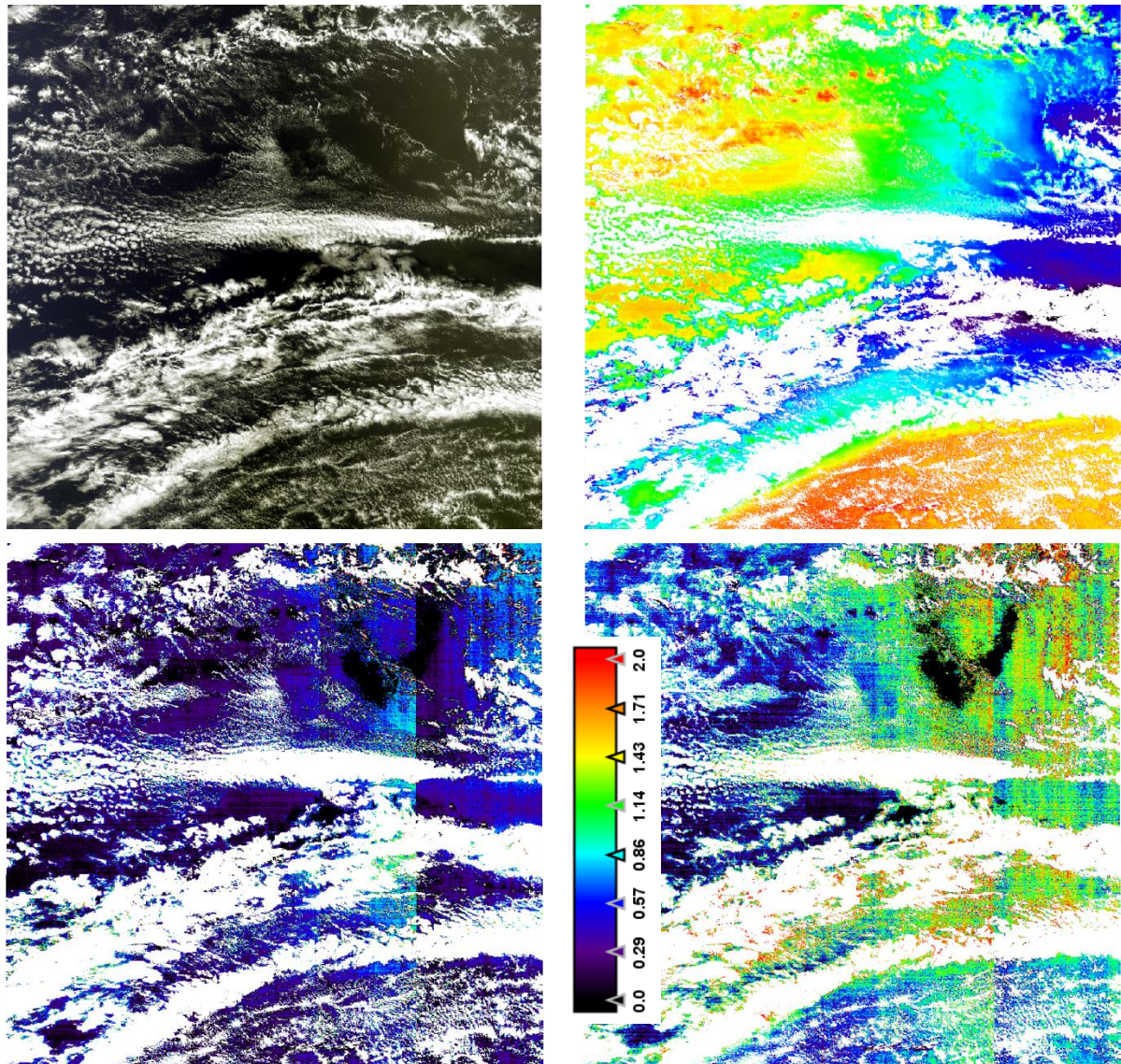
Figure 3-112: Example of BPAC inversion over the Shouth Pacific Gyre. Top left: RGB image of the Level-1 data. Top right: water vapour transmittance at 709 nm. Bottom: TSM retreived by MER3RP (left) and MER4RP (right) BPAC.

The water vapour transmittance is erroneously low over the glint, of easily 3%. Consequently, the signal entering the BPAC (corrected for gas, glint, and then for Rayleigh scattering) is erroneously too high at 709 nm. This affects the computed sediment backsctering, but not the aerosol content thanks to the residual of the optimisation.

An extended analysis over the MOBY and BOUSSOLE site is provided on Figure 3-113. Clearly, the previous threshold of 0.75 mg.l^{-1} is essentially reached when the pixels are impacted by HIGH GLINT, UNCORRECTED_GLINT (defined by HIGH_GLINT AND NOT MEDIUM_GLINT) and CLOUD_AMBIGUOUS (dotted line). These conditions are outside the domain of applicability of BPAC and should not artificially raise the CASE_2S flags. In the MER4RP, the threshold has thus been increased to 1.5 mg.l^{-1} (dashed line); furthermore the CASE_2S flag is never raised in case of CLOUD_AMBIGUOUS or UNCORRECTED_GLINT:

4th MERIS data reprocessing

Evolutions and Validation report

Ref.: MER4RP Validation Report

Version: 1.0

Date: 01/04/2019

Page: 157

CASE2_S = 1 if SPM > 1.5 AND NOT CLOUD_AMBIGUOUS AND NOT (HIGH_GLINT AND NOT MEDIUM_GLINT)
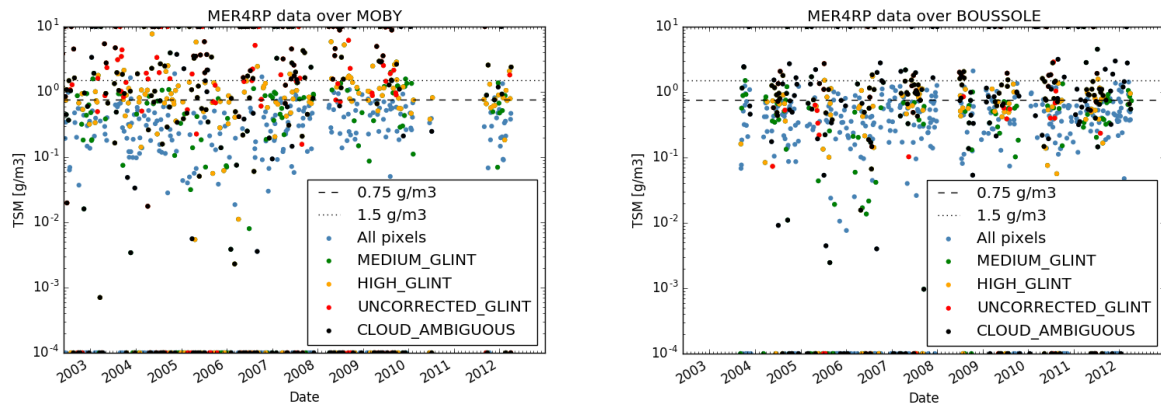
Figure 3-113: TSM computed by the MER4RP BPAC over the MOBY (left) and BOUSSOLE (right) sites. Colours depict the MER4RP flags (see legend).

4th MERIS data reprocessing
Evolutions and Validation report

Ref.: MER4RP Validation Report
Version: 1.0
Date: 01/04/2019
Page: 158

3.4 Land products

3.4.1 MERIS Global Vegetation Index / fAPAR (MGVI) and Rectified Channels

Validation method

The validation was mainly based on benchmark against third-party optical sensors products (mainly SeaWiFS and MODIS) using the same type of retrieval algorithm. In addition, several (but few) ground-based measurements, providing proxy of FAPAR, were used to assess the accuracy. More recently 3D-RT simulations of MERIS data help at inferring the performance of the retrieval algorithm over few virtual validation sites.

Accuracy goal	MER3RP estimated quality	MER4RP estimated quality
MGVI: The theoretical uncertainty of MGVI is set to -/+ 0.05 against FAPAR is estimated by a 1-D radiative transfer model. When comparing to interception ground-based estimates, the goal is -/+ 0.1 **Rectified Channels**: As these numbers are not 'measurable' parameters, the stability over long times is set to 5%.	**MGVI**: The estimated quality is -/+0.1 in average when comparing with ground-based estimates. However, this value depends on the radiative transfer regime over various land cover types. The algorithm is designed with the 'green leaf' concept and delivers instantaneous FAPAR values at time of overpass. **Rectified Channels:** Stability was assessed using daily anomalies from 2002-2009 and compass between 2 % in absolute value over a CEOS desert site.	**MGVI**: The root mean square deviation (RMSD) with third processing products is at about 1% with a bias of -0.006. Comparisons using two years of 3D-RT MERIS simulations over 9 virtual sites provide a mean RMSD of 0.16 with a mean bias and precision at ~-0.07 and 0.06, respectively. **Rectified Channels:** The root mean square deviations (RMSD) with third processing products are at about 0.4% and 2.7% with a bias of -0.006 in 681 nm and 865 nm bands, respectively (no bare soil in the 'validated' data).

3.4.2 MERIS Terrestrial Chlorophyll Index (MTCI)

Validation method

Intercomparisons of MER3RP and MER4RP FR scenes
Direct validation with in-situ canopy chlorophyll content data

Accuracy goal	MER3RP estimated quality	MER4RP estimated quality
	Good	Good, increased correlation with in-situ canopy chlorophyll content (r = 0.71 to 0.91)

3.4.2.1 *Intercomparison of 3RP and 4RP scenes*

Four full-resolution (FR) scenes produced using both the 3RP and 4RP processing baselines were examined for validation and verification of the MTCI in the 4RP. These scenes were acquired over France, Italy, Spain and the United Kingdom, covering both temperate and

4th MERIS data reprocessing

Evolutions and Validation report

Ref.: MER4RP Validation Report

Version: 1.0

Date: 01/04/2019

Page: 159

mediterranean biomes (Table 3-11). An intercomparison of the 3RP and 4RP products is provided.

Table 3-11: FR scenes examined for validation and verification of the MTCI in the 4RP

Location	3RP	4RP
France	MER_FRS_2PNACR20081223_101837_000002782075_00008_35633_0000.N1	ENV_ME_2_FRG____20081223T101837_20081223T102316_____0278_075_008_____ACR_R_NT_____.SEN3
Italy	MER_FRS_2PNACR20080626_093711_000002172069_00437_33056_0000.N1	ENV_ME_2_FRG____20080626T093711_20080626T094047_____0216_069_437_____ACR_R_NT_____.SEN3
Spain	MER_FRS_2PNACR20060722_103529_000001972049_00366_22965_0000.N1	ENV_ME_2_FRG____20060722T103529_20060722T103846_____0197_049_366_____ACR_R_NT_____.SEN3
United Kingdom	MER_FRS_2PNACR20060718_105659_000002202049_00309_22908_0000.N1	ENV_ME_2_FRG____20060718T105659_20060718T110039_____0219_049_309_____ACR_R_NT_____.SEN3

Between the 3RP and 4RP, MTCI values demonstrate highly consistent spatial patterns, with very few differences evident visually (Figure 3-114). The shape of the frequency distributions of MTCI values is similar in both the 3RP and 4RP, although differences in magnitude are observed in all the investigated scenes (Figure 3-115). This is the result of a greater number of valid pixels being present in the 4RP, presumably due to improvements in surface classification and cloud masking, in addition to the increased range limits. For example, 5,640,102 pixels are valid in the 4RP scene over the United Kingdom, as opposed to 5,435,284 in the 3RP scene. In absolute terms, the differences between MTCI values in the 3RP and 4RP are typically small (P_5 = -0.02, P_{95} = 0.05 to 0.12) (Table 3-12). Over all investigated scenes, differences are biased towards a slight increase in MTCI values, demonstrated by a positive mean difference of between 0.02 and 0.05. These differences demonstrate a spatial dependency, which appears to be related to slight changes in the calibration models of each MERIS camera in the 4RP (vertical stripes in Figure 99), in addition to the impact of smile correction (red areas in Figure 99). Thus, camera boundaries are clearly defined in difference images (Figure 3-116). Nevertheless, these changes are sufficiently small to include no evident cosmetic effects in the MTCI itself.

4th MERIS data reprocessing

Evolutions and Validation report

Ref.: MER4RP Validation Report

Version: 1.0

Date: 01/04/2019

Page: 160

Figure 3-114: MTCI in the 3RP (left) and 4RP (right) scenes covering France, Italy, Spain and the United Kingdom (top to bottom).

4th MERIS data reprocessing

Evolutions and Validation report

Ref.: MER4RP Validation Report

Version: 1.0

Date: 01/04/2019

Page: 161
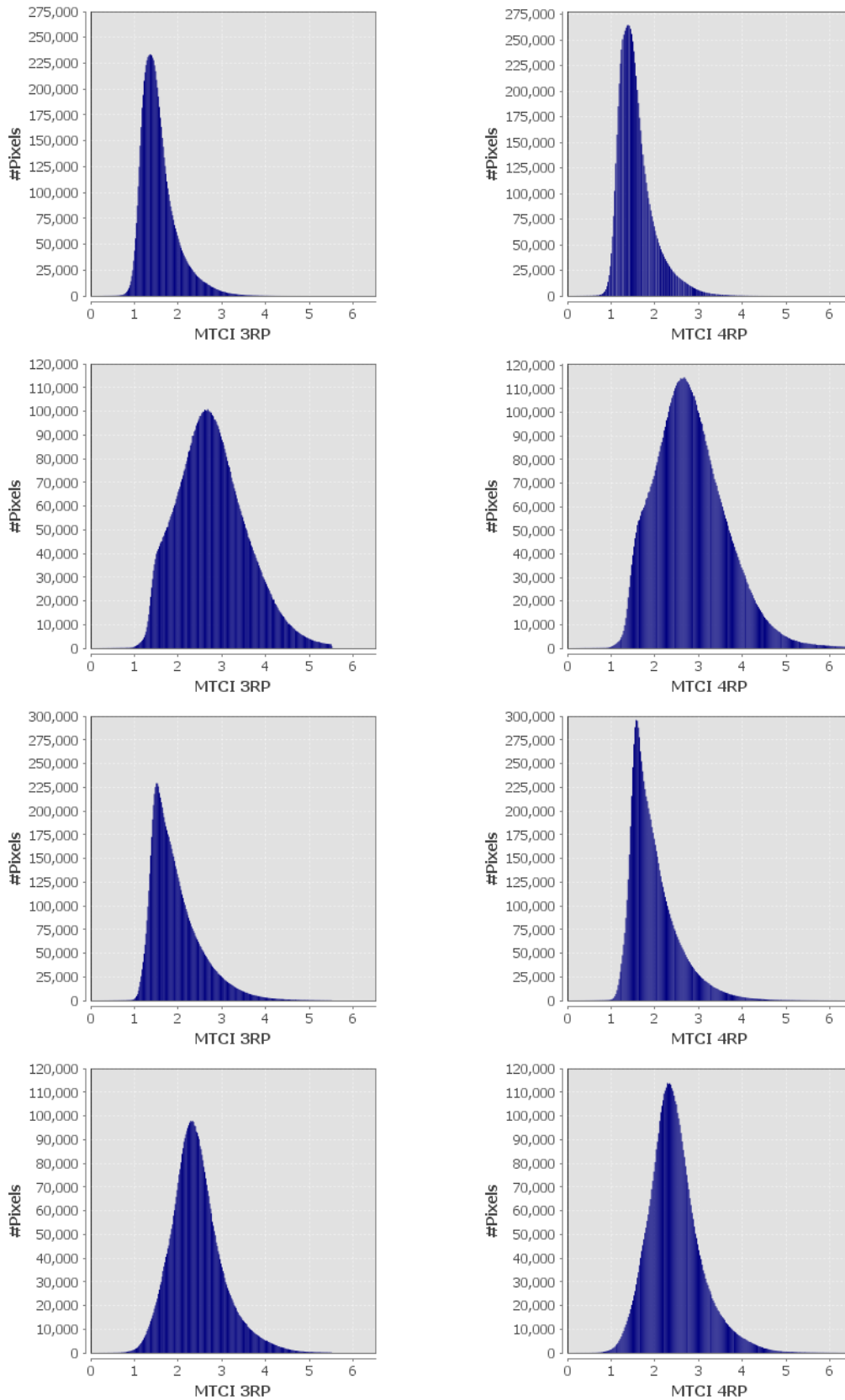
Figure 3-115: Frequency distribution of MTCI values for the 3RP (left) and 4RP (right) over the France, Italy, Spain and United Kingdom scenes (top to bottom).

4th MERIS data reprocessing

Evolutions and Validation report

Ref.: MER4RP Validation Report

Version: 1.0

Date: 01/04/2019

Page: 162

Table 3-12: Summary statistics relating to the absolute difference in MTCI values between the 3RP and 4RP for the France, Italy, Spain and United Kingdom scenes.

Statistic	Difference (4RP-3RP)			
	France	**Italy**	**Spain**	**UK**
Minimum	-0.32	-0.49	-0.45	-1.07
Maximum	0.68	0.43	0.79	0.94
Mean	0.02	0.02	0.04	0.02
Standard deviation	0.03	0.03	0.04	0.02
Coefficient of variation	1.61	1.25	0.95	0.95
Median	0.02	0.02	0.04	0.02
5th percentile	-0.02	-0.02	-0.01	-0.01
95th percentile	0.06	0.06	0.12	0.05
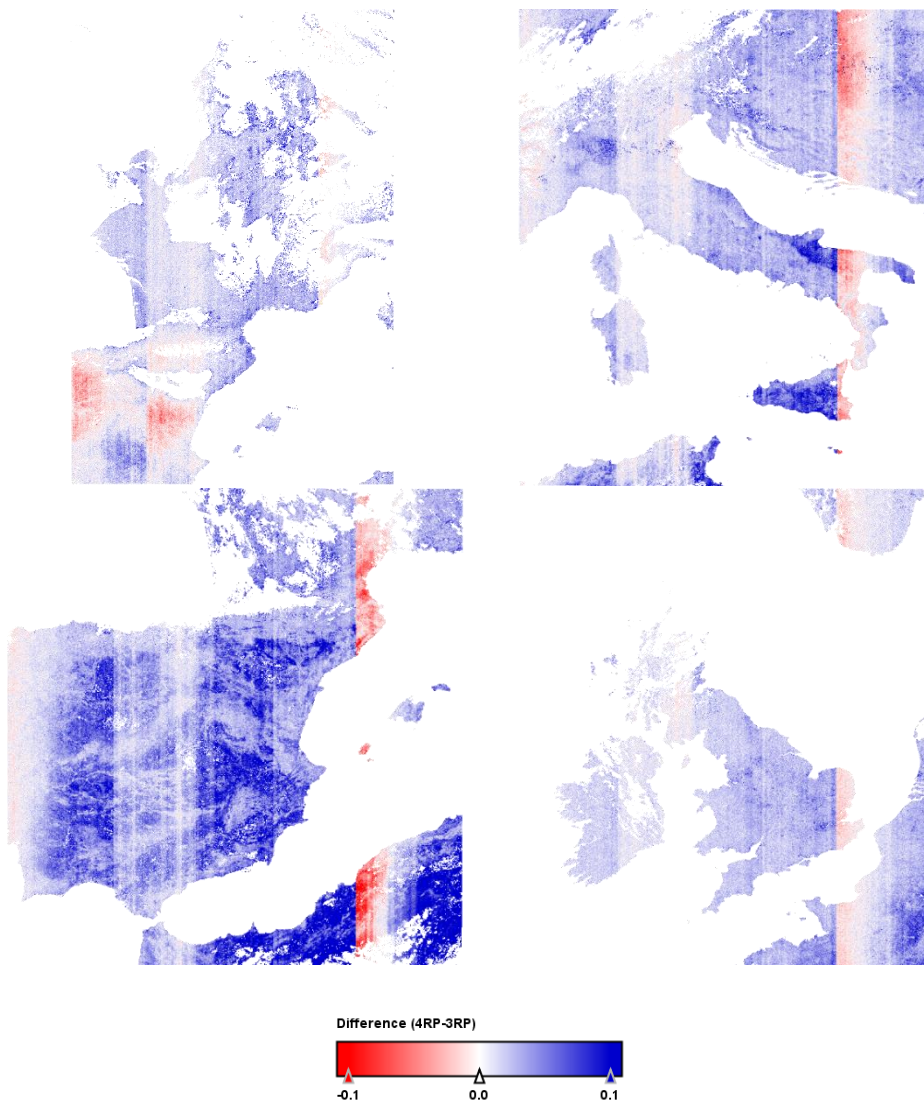
Figure 3-116: Difference in MTCI (4RP-3RP) for the France, Italy, Spain and United Kingdom scenes.

4th MERIS data reprocessing
Evolutions and Validation report

Ref.: MER4RP Validation Report
Version: 1.0
Date: 01/04/2019
Page: 163

3.4.2.2   Direct validation with in-situ canopy chlorophyll content data

In addition to the intercomparison exercise, in-situ canopy chlorophyll content (CCC) data collected in two previous campaigns were used to facilitate direct validation of the 3RP and 4RP products.

The first campaign took place in Southern England over an agricultural area between 11/07/2006 and 19/07/2006. The sampling strategy was based on 8 characterizing large, homoegenous fields, containing beans, linseed, wheat, grass, oats and maize. 3 to 5 elementary sampling units (ESUs) were established in each field, within which 25 measurements of leaf area index (LAI) and leaf chlorophyll concentration (LCC) were made (each an average of 4 to 8 replicates). LAI was estimated using the LI-COR LAI-2000, whilst LCC was estimated using a Konica Minolta SPAD-502 chlorophyll meter. Within each ESU, CCC was determined as the product of LAI and LCC. Further details of in-situ data collection are provided by Dash et al. (2010). For direct validation of the 3RP and 4RP products, MERIS data acquired on 18/07/2006 were investigated (Table 3-13). Additional georectification (i.e. beyond that provided in the product itself) was not undertaken, in constrast to Dash et al. (2010). Where a MERIS pixel was wholly composed of a single canopy type, the average CCC value of the ESUs contained within it was calculated.

Table 3-13: FR scenes examined for direct validation of the MTCI in the 4RP

Location	3RP	4RP
United Kingdom	MER_FRS_2PPBCM20060718_105924_000000422049_00309_22908_0002.N1	ENV_ME_2_FRG____20060718T105905_20060718T111150_____0765_049_309_____ACR_R_NT____.SEN3
Italy	MER_FRS_2PPDSI20090817_092720_000005092081_00394_39025_0665.N1	ENV_ME_2_FRG____20090817T092720_20090817T093802_____0642_081_394_____ACR_R_NT____.SEN3

The second campaign took place in Southern Italy over an irrigated agricultural area between 23/08/2009 and 25/08/2009. 36 ESUs of 20 m x 20 m were established over the site, which is mainly comprised of forage crops (alfalfa, maize), fruit trees (plum, apricot, kiwi, peach) and vegetables (aubergine, pepper, artichoke). As in the first campaign, LAI and LCC were derived using the LAI-2000 and SPAD-502. Within each ESU, 18 LAI and 30 LCC measurements were made. Further details of in-situ data collection and provided by Vuolo et al. (2012). To upscale in-situ data, a high spatial resolution CCC reference map was produced from RapidEye data acquired on 17/08/2009, by look-up table (LUT) inversion of the coupled Leaf Optical Properties Spectra (PROSPECT) and Scattering by Arbitrarily Inclined Leaves (SAIL) radiative transfer models (RTMs). Further details on RTM parameterization are described by Vuolo et al. (2010). This reference map was then validated using the in-situ data (r = 0.87, RMSE = 0.39 g m^{-2}). For direct validation of the 3RP and 4RP products, both MERIS data and the high spatial resolution CCC reference map were reprojected to the same coordinate system and aggregated to a common spatial resolution of 1 km. Only 1 km cells in with vegetation cover of > 80% were considered, following Vuolo et al. (2012). The investigated MERIS data were acquired on 17/08/2009 (Table 3-13).

4th MERIS data reprocessing

Evolutions and Validation report

Ref.: MER4RP Validation Report

Version: 1.0

Date: 01/04/2019

Page: 164

Agreement between the MTCI and in-situ CCC was assessed in terms of the Pearson product moment correlation coefficient. In the case of both campaigns, the 4RP products demonstrate an increased correlation when compared to the corresponding 3RP products (Figure 3-117 and Figure 3-118).
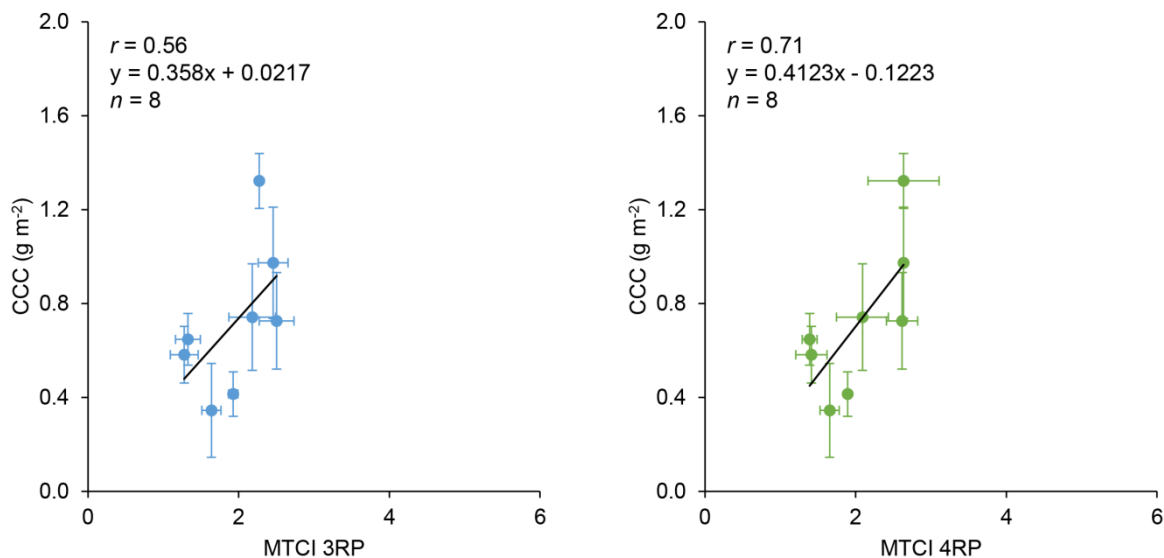
Figure 3-117: Comparison between CCC and the MTCI for the 3RP (left) and 4RP (right) in the case of the first campaign in Southern England.
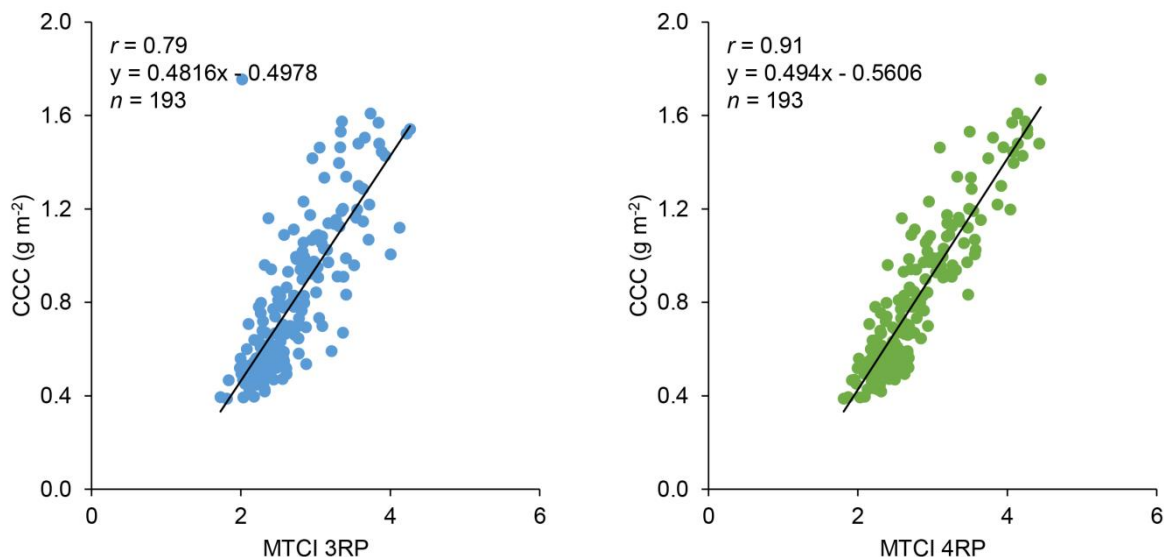
Figure 3-118: Comparison between CCC and the MTCI for the 3RP (left) and 4RP (right) in the case of the second campaign in Southern Italy.

4th MERIS data reprocessing

Evolutions and Validation report

Ref.: MER4RP Validation Report

Version: 1.0

Date: 01/04/2019

Page: 165

3.4.3 Aerosol Optical Thickness at 442 nm (T442) and Angstrom Coefficient (A442)

Validation method

Validation against AERONET matchups. Extractions of 11RRx1RR pixels boxes around AERONET sites representative of various aerosols models and surfaces (*AltaFloresta, Banizoumbou, Beijing, Dakar, Evora, GSFC, Ispra, Hamburg, Kanpur, Lille, TableMountain*). AERONET data were averaged in ±0.5 hour intervals centred on MERIS overpass time. The `CLOUD` mask was extended using the morphological operator `dilate` with a width of 10 pixels. Moreover, matchups whose standard deviation of AOT exceeded 0.1 were discarded from the regression analysis This conservative approach is chosen to avoid cloud contamination that was the main issue with the MER3RP product. However, these filtering criteria could bias MERIS AOT toward lower values.

No filtering based on the quality index `Q` has been applied.

| **Accuracy goal** | **MER3RP / MER4RP estimated quality** |

Standard published accuracy of aerosol products over land (i.e. MODIS):

AOT(443, 550)=0.05+0.15 AOT[1]

(2004-2010) MODIS coll. 5: N=5448, r^2=0.871, rmse=0.137, gfrac=0.62 (*Bréon et al. 2011*)

gfrac is the fraction of matchups satisfying [1]

AOT at 442 nm (see Figures below)

Site		T_442 MER3RP	T_442 MER4RP	T_ALPHA_442 MER4RP
Alta Floresta	N	127	**259**	236
	r^2	0.73	**0.79**	0.77
	RMSE	0.44	0.21	**0.18**
	Gfrac	0.24	0.59	**0.67**
Banizoumbou	N	0	2	2
	r^2		-	-
	RMSE		-	-
	Gfrac		-	-
Beijing	N	216	**374**	233
	r^2	**0.50**	0.43	0.33
	RMSE	0.49	**0.34**	0.38
	Gfrac	**0.29**	0.26	0.15
Dakar	N	0	**100**	86
	r^2		0.25	**0.31**
	RMSE		0.30	**0.29**
	Gfrac		0.16	**0.21**
Evora	N	**335**	288	259
	r^2	**0.60**	0.33	0.51
	RMSE	0.11	**0.10**	0.12
	Gfrac	0.33	**0.78**	0.30
GSFC	N	384	**518**	259
	r^2	0.63	**0.81**	0.51
	RMSE	0.19	**0.11**	0.12
	Gfrac	0.30	**0.61**	0.30
Ispra	N	169	**224**	91
	r^2	0.69	0.69	**0.71**
	RMSE	0.17	**0.15**	0.19
	Gfrac	**0.54**	0.44	0.33
Hamburg	N	**113**	90	68
	r^2	0.75	**0.75**	0.74
	RMSE	0.11	**0.09**	0.10
	Gfrac	0.63	**0.63**	0.54

4th MERIS data reprocessing

Evolutions and Validation report

Ref.: MER4RP Validation Report

Version: 1.0

Date: 01/04/2019

Page: 166

Kanpur	N	**503**	451	167
	r^2	**0.72**	0.47	0.29
	RMSE	0.34	**0.33**	0.36
	Gfrac	0.21	**0.31**	0.31
Lille	N	**127**	108	81
	r^2	0.63	**0.68**	0.56
	RMSE	0.12	**0.08**	0.11
	Gfrac	0.57	**0.75**	0.56
Table Mountain		6	**6**	6
	r^2	-	-	-
	RMSE	0.27	**0.10**	0.12
	Gfrac	0.00	**0.50**	0.50

Statistics of the matchup's regressions. Best indicators are in bold.

The quality of the regressions has slightly increased between MER3RP and MER4RP. The differences between sites are important. The main improvements of MER4RP are a better cloud screening and a better LARS BRDF. Benefits of the introduction of a new aerosol Angström exponent climatology are not demonstrated. T_ALPHA_442 is almost always systematically worse than T_442. The discrepancies between MER4RP and AERONET are the largest for large absorbing aerosols loading (desert dust/ biomass burning/ urban pollution). The absence of absorption in the aerosols models used for retrieval may explain partly those discrepancies.

Angström coefficient

Though a slight increase in performance between 3RP and 4RP, the Angström exponent over land is still not validated and poorly correlated to AERONET.

4th MERIS data reprocessing
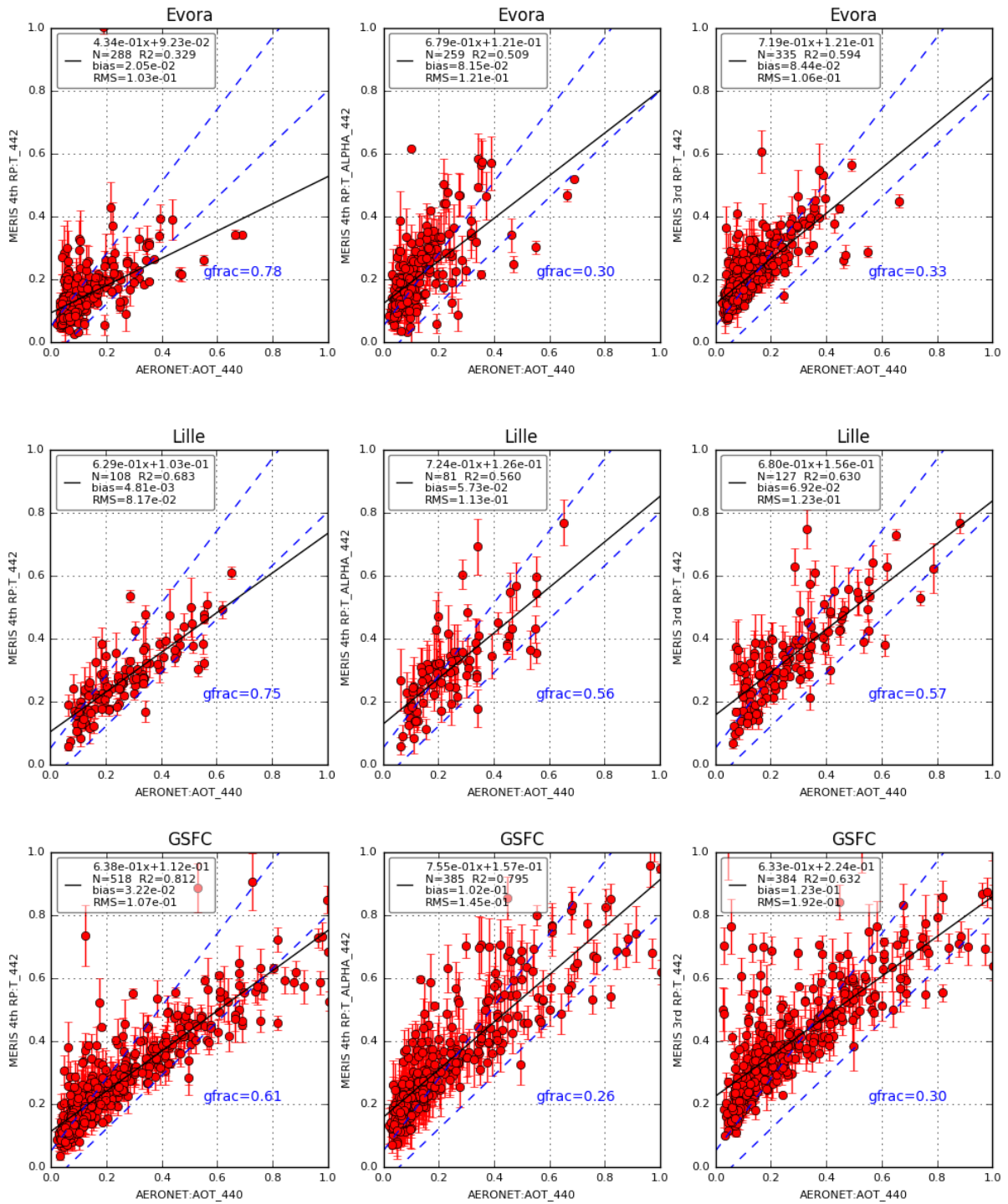
Evolutions and Validation report

Ref.:   MER4RP Validation Report
Version: 1.0
Date: 01/04/2019
Page: 167

4th MERIS data reprocessing

Evolutions and Validation report

Ref.: MER4RP Validation Report

Version: 1.0

Date: 01/04/2019

Page: 168

4th MERIS data reprocessing

Evolutions and Validation report

Ref.: MER4RP Validation Report

Version: 1.0

Date: 01/04/2019

Page: 169

4th MERIS data reprocessing

Evolutions and Validation report

Ref.: MER4RP Validation Report

Version: 1.0

Date: 01/04/2019

Page: 170
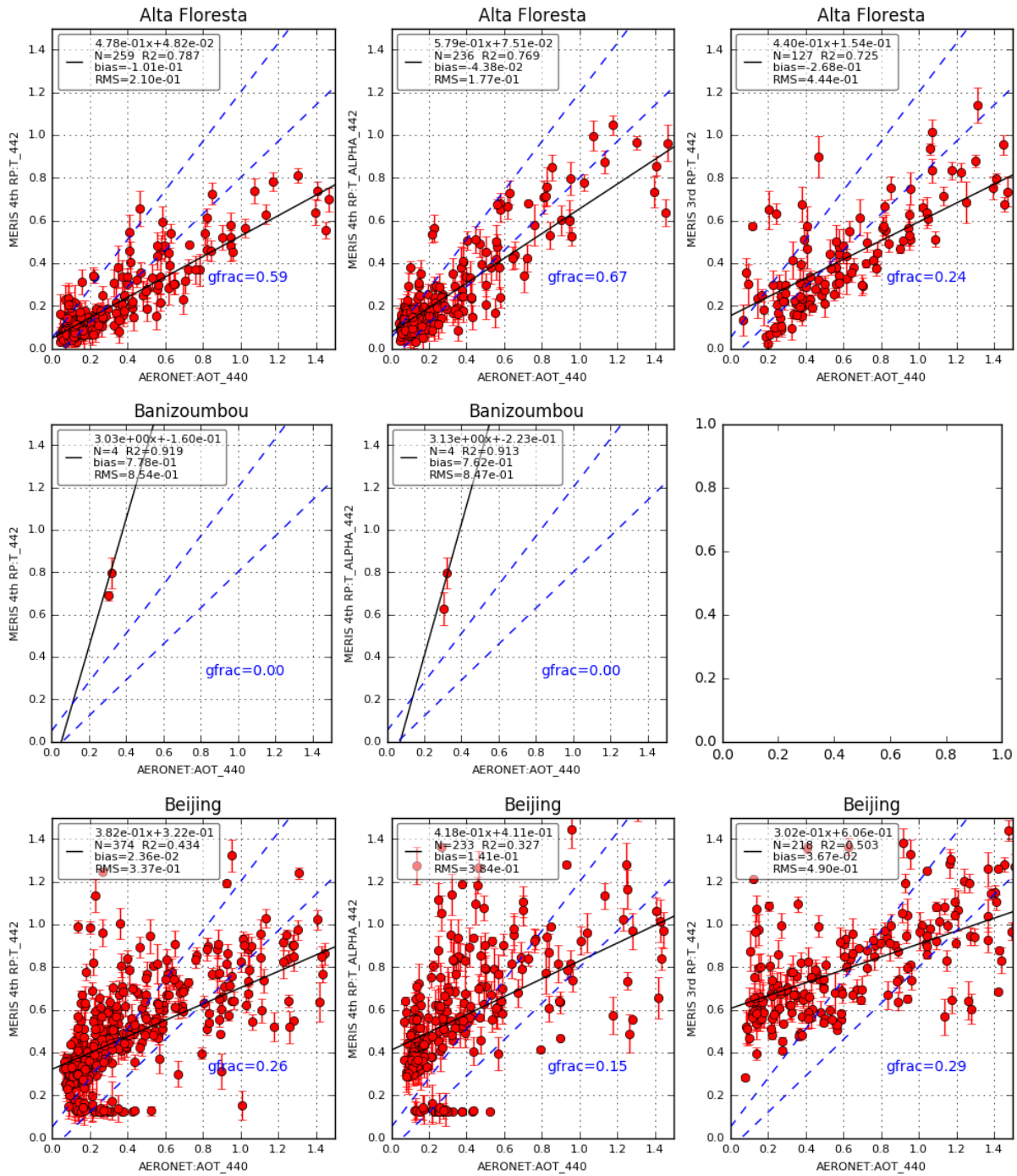
4th MERIS data reprocessing
Evolutions and Validation report
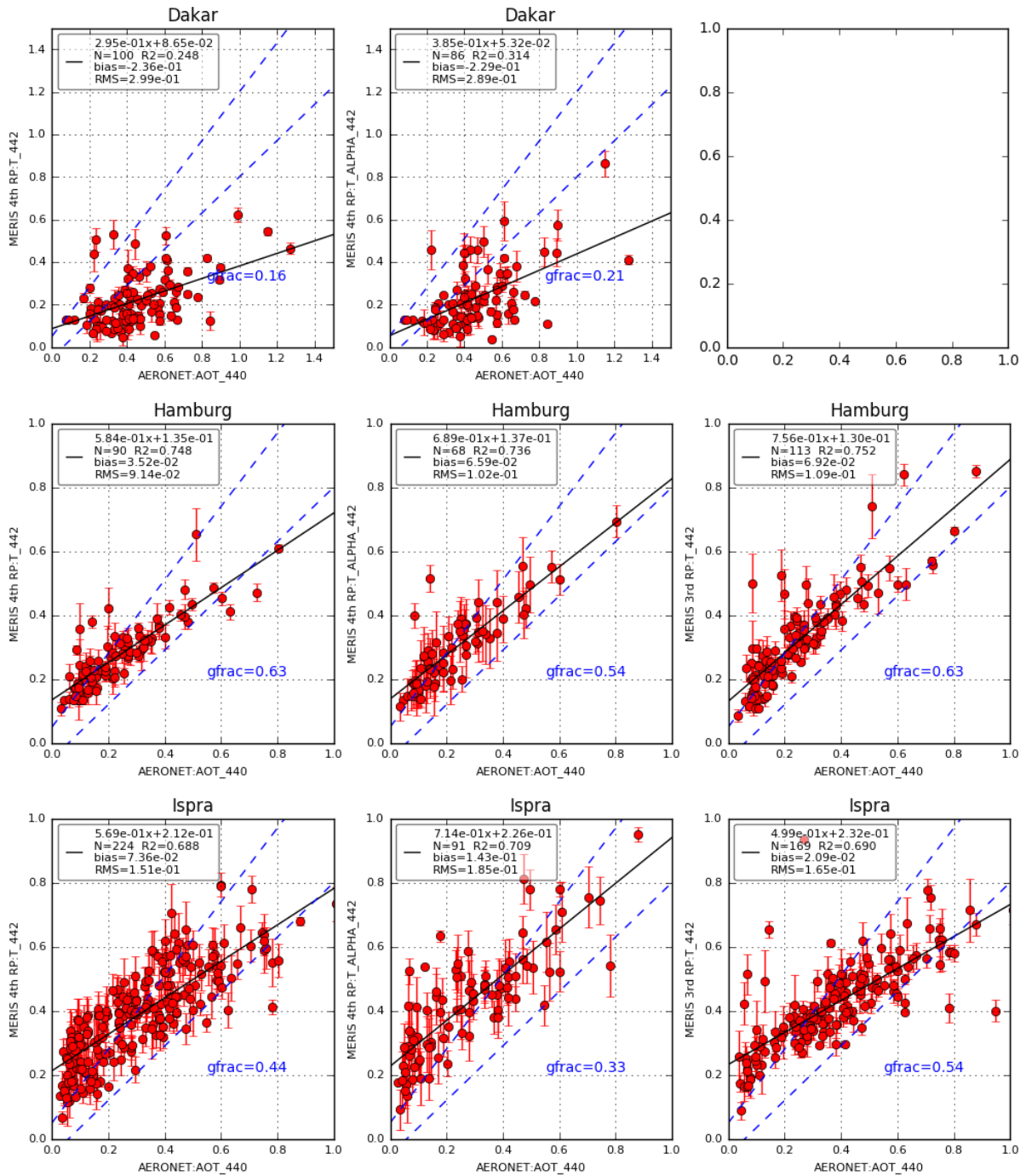
Ref.: MER4RP Validation Report
Version: 1.0
Date: 01/04/2019
Page: 171
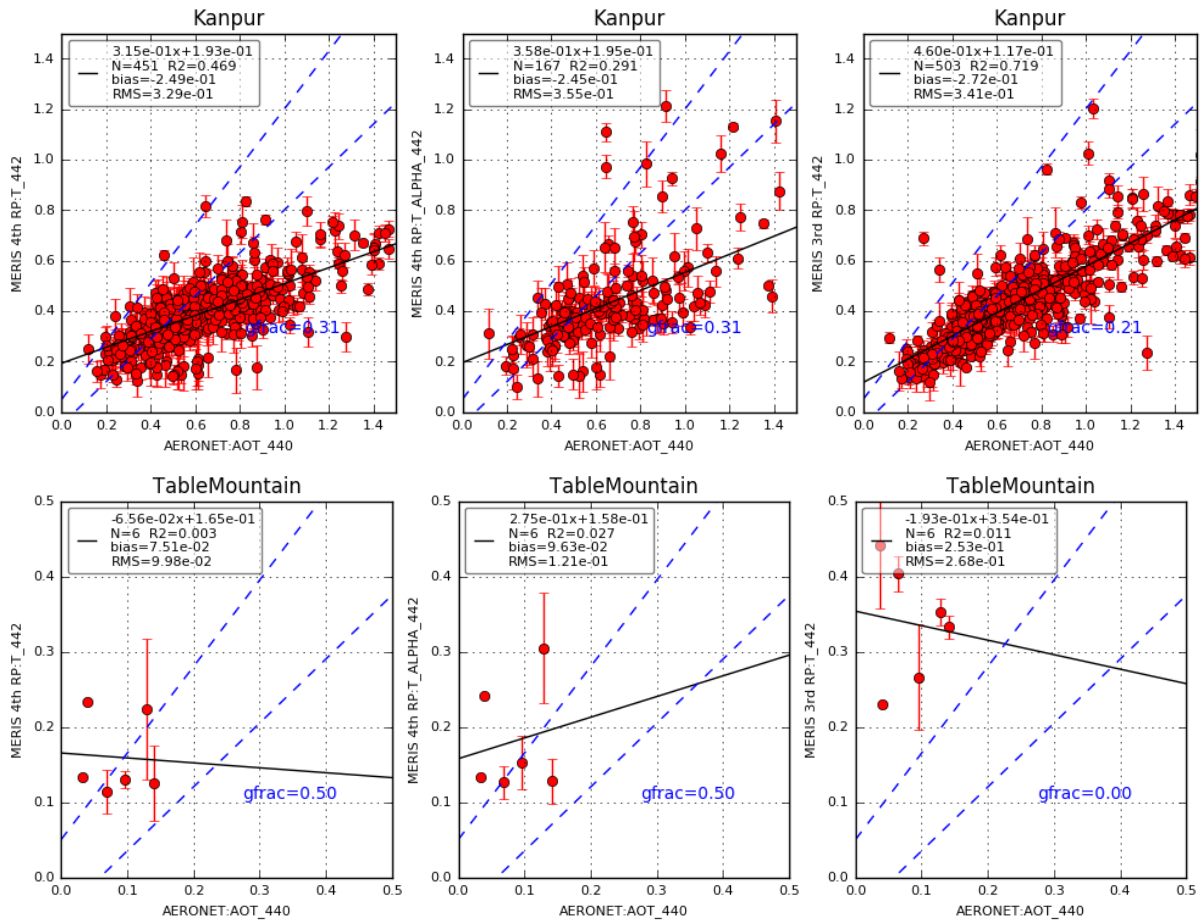
4 Acknowledgement to *in situ* data contributors

A large part of the MER4RP over the ocean has been possible thanks to the *in situ* measurements, which constitute essential independent reference data to calibrate and validate the algorithms.

The MERIS Quality Working Group is much grateful to all the scientists and associated laboratories who share their datasets within **MERMAID**, the validation facility used to extract MERIS matchups.

The **MERMAID** website http://hermes.acri.fr/mermaid contains details about the datasets, contact emails and a measurements protocols document for all available datasets (*MERIS Optical Measurement Protocols - Part A: In situ water reflectance measurements*). MERMAID validation facility is maintained by ACRI-ST, ARGANS and ESA.

In particular, the MERIS Quality Working Group thanks the following Principle Investigators and mission responsibles who currently contribute to the MERIS validation:

- **Giuseppe Zibordi** (Joint Research Center, Italy) for providing data at four AERONET- OC sites: the Acqua Alta Oceanographic Tower, Abu Al Bukhoosh, Gustav Dalen Tower and Helsinki Lighthouse.
  - G. Zibordi, B. Holben, I. Slutsker, D. Giles, D. D'Alimonte, F. Mélin, J.-F. Berthon, D. Vandemark, H. Feng, G. Schuster, B. Fabbri, S. Kaitala, J. Seppälä. AERONET-OC: a network for the validation of Ocean Color primary radiometric products. *Journal of Atmospheric and Oceanic Technology*, 26, 1634-1651, 2009.
  - G. Zibordi, J.-F. Berthon, F. Mélin, D. D'Alimonte and S. Kaitala. Validation of satellite ocean color primary products at optically complex coastal sites: northern Adriatic Sea, northern Baltic Proper and Gulf of Finland. *Remote Sensing of Environment*, 113, 2574-2591, 2009.

- **David Antoine** (Laboratoire d'Océanographie de Villefranche, France) for the BOUSSOLE dataset, used in particular for the vicarious adjustment.
  - Antoine, D. M. Chami, H. Claustre, F. D'Ortenzio, A. Morel, G. Bécu, B. Gentili, F. Louis, J. Ras, E. Roussier, A.J. Scott, D. Tailliez, S. B. Hooker, P. Guevel, J.-F. Desté, C. Dempsey and D. Adams. 2006, BOUSSOLE: a joint CNRS-INSU, ESA, CNES and NASA Ocean Color Calibration And Validation Activity. NASA Technical memorandum N° 2006 – 214147.
  - Antoine, D., P. Guevel, J.-F. Desté, G. Bécu, F. Louis, A. J. Scott and P. Bardey, 2008, The «BOUSSOLE» buoy: A new transparent-to-swell taut mooring dedicated to marine optics: design, tests and performance at sea, *Journal of Atmospheric and Oceanic Technology*, 25, 968-989.

- **David McKee** (University of Strathclyde, UK) for the Bristol Channel and Irish Sea datasets.

- **Kenneth Voss** (NOAA) for the MOBY dataset used for the vicarious adjustment.

4th MERIS data reprocessing
Evolutions and Validation report

Ref.: MER4RP Validation Report
Version: 1.0
Date: 01/04/2019
Page: 172

- Clark, D. K., Yarborough, M. A., Feinholz, M. E., Flora, S., Broenkow, W., Kim, Y. S., Johnson, B. C., Brown, S. W., Yuen, M. & Mueller, J. L. (2003).MOBY, A Radiometric Buoy for Performance Monitoring and Vicarious Calibration of Satellite Ocean Colour Sensors: Measurements and Data Analysis Protocols. In Ocean Optics Protocols for Satellite Ocean Colour Sensor Validation, NASA Technical Memo. 2003-211621/Rev4, Vol VI, 3-34 (Eds J. L. Muller, G. Fargion and C. McClain). Greenbelt, MD.: NASA/GSFC.

- **Kevin Ruddick** (MUMM, Belgium) for the MUMMTriOS dataset.

  - Ruddick, K. G., V. De Cauwer, Y. Park and G. Moore (2006). Seaborne measurements of near infrared water-leaving reflectance - the similarity spectrum for turbid waters. Limnology and Oceanography 51(2): 1167-1179.

- **Hui Feng** (University of New Hampshire, US) and **Heidi Sosik** (Woods Hole Oceanographic Institution) for the AERONET-OC MVCO dataset.

  - G. Zibordi, B. Holben, I. Slutsker, D. Giles, D. D'Alimonte, F. Mélin, J.-F. Berthon, D. Vandemark, H. Feng, G. Schuster, B. Fabbri, S. Kaitala, J. Seppälä. AERONET-OC: a network for the validation of Ocean Color primary radiometric products. *Journal of Atmospheric and Oceanic Technology*, 26, 1634-1651, 2009.

- **Jeremy Werdell** (NASA), **Ajit Subramaniam** (University of Maryland, US), **Dariusz Stramski** (University of California, US), **Greg Mitchell** (University of California, US), **William Balch** (Bigelow Laboratory for Ocean Sciences, US), **Frank Muller-Karger** (University South Florida, US), **Ken Carder** (Professor Emeritus University South Florida, US), **Norman Nelson** (University of California, US), **Rick Stumpf** (NOAA, US), **William Balch** (Bigelow Laboratory for Ocean Sciences) and **Stan Hooker** (NASA) for the NOMAD dataset.

  - Werdell, P.J. and S.W. Bailey, 2005: An improved bio-optical dataset for ocean color algorithm development and satellite data product validation. *Remote Sensing of Environment*, 98(1), 122-140.

- **David Siegel** (University of California, US) for the Plumes and Blooms dataset.

- **Bill Gibson** (Coastal Studies Institut, LSU) and **Alan Weidemann** (Naval Research Laboratory, NRLSSC) for the AERONET-OC WaveCIS dataset.

- **Greg Shuster** (NASA GSFC) and **Brent Holben** (NASA GSFC) for the AERONET-OC CoveSEAPRISM dataset.

  - G. Zibordi, B. Holben, I. Slutsker, D. Giles, D. D'Alimonte, F. Mélin, J.-F. Berthon, D. Vandemark, H. Feng, G. Schuster, B. Fabbri, S. Kaitala, J. Seppälä. AERONET-OC: a network for the validation of Ocean Color primary radiometric products. *Journal of Atmospheric and Oceanic Technology*, 26, 1634-1651, 2009.

- **Vanda Brotas** (Universidade de Lisboa) for the Portcoast dataset.

- **Vittorio Brando** (CSIRO, Australia) for the AERONET-OC LJCO dataset.

- **Suzanne Kratzer** (University of Stockholm, Sweden) for the North-Western Baltic Sea and AERONET-OC Palgrunden dataset.

4th MERIS data reprocessing

Evolutions and Validation report

Ref.: MER4RP Validation Report

Version: 1.0

Date: 01/04/2019

Page: 173

Kratzer, S., Brockmann, C. & Moore, G. F. (2008). Using MERIS full resolution data (300 m spatial resolution) to monitor coastal waters– a case study from Himmerfjärden, a fjord-like bay in the north-western Baltic Sea. Remote Sensing of the Environment 112(5): 2284-2300.

4th MERIS data reprocessing
Evolutions and Validation report

Ref.: MER4RP Validation Report
Version: 1.0
Date: 01/04/2019
Page: 174

5 References

▪ Ahmad, Z., B.A. Franz, C.R. McClain, E.J. Kwiatkowska, J. Werdell, E.P. Shettle, and B.N. Holben, 2010. "New aerosol models for the retrieval of aerosol optical thickness and normalized water-leaving radiances from the SeaWiFS and MODIS sensors over coastal regions and open oceans", *Applied Optics*, 49 (29): 5545–5560.

▪ Antoine, D., and A. Morel, 1999. "A multiple scattering algorithm for atmospheric correction of remotely sensed ocean color (MERIS instrument): Principle and implementation for atmospheres carrying various aerosols including absorbing ones", International Journal of Remote Sensing, 20: 1875–1916.

▪ Antoine D., Chami M., Claustre H., D'Ortenzio F., Morel A., Bécu G., Gentili B., Louis F., Ras J., Roussier E., Scott AJ., Tailliez D., Hooker SB., Guevel P., Desté J-F., Dempsey C., Adams D. (2006) BOUSSOLE: a joint CNRS-INSU, ESA, CNES and NASA Ocean Color Calibration And Validation Activity. NASA Technical memorandum N° 2006–214147, NASA/GSFC, Greenbelt, MD, 61 pp.

▪ Bodhaine, B.A., N.B. Wood, E.G. Dutton, and J.R. Slusser, 1999. "On Rayleigh optical depth calculations", *Journal of Atmospheric and Oceanic Technology*, 16: 1854-1861.

▪ Bogumil, K., J. Orphal, T. Homann, S. Voigt, P. Spietz, O.C. Fleischmann, A. Vogel, M. Hartmann, H. Bovensmann, J. Frerick, and J.P. Burrows, 2003. "Measurements of molecular absorption spectra with the SCIAMACHY pre-flight model: Instrument characterization and reference data for atmospheric remote sensing in the 230-2380 nm region", *Journal of Photochemistry and Photobiology A: Chemistry*, 157: 167–184.

▪ Bouvet M., 2006, MERIS Photosynthetically Available Radiation: a product quality assessment, Proceedings of the Second Working Meeting on MERIS and AATSR Calibration and Geophysical Validation (MAVT-2006), 20-24 March 2006, ESRIN, Frascati, Italy (ESA SP-615, July 2006) - http://envisat.esa.int/workshops/mavt_2006/papers/56_bouve.pdf

▪ Bouvet, M., 2017. "Comparison of ozone absorption cross section", *ESA Technical Note for the MERIS 4th Reprocessing*, ESA/ESTEC, Noordwijk, The Netherlands: 27p.

▪ Brockmann, Kirches, Militzer, Stelzer: "SENTINEL 3 – LAND-WATER MASK" Technical Note, v1.2 dated on 14.08.2015.

▪ Bréon, F.-M., A. Vermeulen, J. Descloitres, 2011. "An evaluation of satellite aerosol products against sunphotometer measurements", Remote Sensing of Environment, 115 (12): 3102–3111; doi: 10.1016/j.rse.2011.06.017.

▪ Chehade, W, V. Gorshelev, A. Serdyuchenko, J.-P. Burrows, and M. Weber, 2013. "Revised temperature-dependent ozone absorption cross-section spectra (Bogumil et al.) measured with the SCIAMACHY satellite spectrometer", *Atmospheric Measurement Techniques*, 6: 3055–3065.

▪ Fanton d'Andon, O. and Mangin, A. and Lavender, S. and Antoine, D. and Maritorena, S. and Morel, A. and Barrot, G. et al. 2009. "GlobColour - the European Service for Ocean Colour", in Proceedings of the 2009 IEEE International Geoscience & Remote Sensing Symposium, Jul 12-17 2009, Cape Town South Africa: IEEE Geoscience and Remote Sensing Society.

4th MERIS data reprocessing

Evolutions and Validation report

Ref.: MER4RP Validation Report

Version: 1.0

Date: 01/04/2019

Page: 175

- Francois-Marie Bréon, Anne Vermeulen, Jacques Descloitres, An evaluation of satellite aerosol products against sunphotometer measurements, Remote Sensing of Environment, Volume 115, Issue 12, 2011, Pages 3102-3111, ISSN 0034-4257, https://doi.org/10.1016/j.rse.2011.06.017.

- Gordon and Wang, 1999. "Retrieval of water-leaving radiance and aerosol optical thickness over the oceans with SeaWiFS: a preliminary algorithm", *Applied Optics*, 33 (3): 443–452; doi: 10.1364/AO.33.000 443.

- Hansen, J.E., and L. Travis, 1974. "Light scattering in planetary atmospheres", Space Science Reviews, 16: 527-610.

- Hsu, N. C., M.-J. Jeong, C. Bettenhausen, A. M. Sayer, R. Hansell, C. S. Seftor, J. Huang, and S.-C. Tsay (2013), Enhanced Deep Blue aerosol retrieval algorithm: The second generation, *J. Geophys. Res. Atmos.*, **118**, 9296–9315, doi:10.1002/jgrd.50712

- Morel, André & Maritorena, Stéphane. (2001). Bio-optical properties of oceanic waters: A reappraisal. Journal of Geophysical Research. 106. 7163-7180. 10.1029/2000JC000319.

- Morel, A., Huot, Y., Gentili, B., Werdell, P.J., Hooker, S.B. and B.A. Franz (2007). Examining the consistency of products derived from various ocean color sensors in open ocean (Case 1) waters in the perspective of a multi‐sensor approach. Remote Sensing of Environment, 111, 69‐88.

- Moulin, C., H.R. Gordon, V.F. Banzon, and R.H. Evans, 2001. "Assessment of Saharan dust absorption in the visible from SeaWiFS imagery", *Journal of Geophysical Research*, 106: 18239-18249.

- Nunes, L., and F. Zagolski, 2008. "MERISAT porting in linux – MERISAT detail design of optimization & complementary recipes for LUTs generation", GMV-Skysoft/PARBLEU Report (D-06), MERISAT-SKS-SDD-006-1A, GMV/Skysoft, Lisbon, Portugal: 158p.

- Neiva, P., and F. Zagolski, 2011. "MERISAT porting in linux; Phase-II – MERISAT software requirements specification for the third LUTs generation", GMV-Skysoft/PARBLEU Report (D-02), MERISAT-SKS-REQ-SRS-1B, GMV/Skysoft, Lisbon, Portugal: 37p.

- Ras, J., Claustre, H., and Uitz, J.: Spatial variability of phytoplankton pigment distributions in the Subtropical South Pacific Ocean: comparison between in situ and predicted data, Biogeosciences, 5, 353-369, https://doi.org/10.5194/bg-5-353-2008, 2008.

- Santer, R., V. Carrère, P. Dubuisson, and J.C. Roger, 1999. "Atmospheric corrections over land for MERIS", International Journal of Remote Sensing, 20 (9): 1819–1840.

- Santer, R., and F. Zagolski, 2010. "The blue aerosols over ocean", PARBLEU/ADRINORD Report on the 'Inherent Optical Properties of the Aerosols over Ocean': 20p.

- Sayer, A. M., N. C. Hsu, C. Bettenhausen, and M.-J. Jeong (2013), Validation and uncertainty estimates for MODIS Collection 6 "Deep Blue" aerosol data, *J. Geophys. Res. Atmos.*, **118**, 7864–7872, doi:10.1002/jgrd.50600

- Shettle, E.P., and R.W. Fenn, 1979. "Models for the aerosols of the lower atmosphere and the effects of humidity variations on their optical properties", *Air Force Geophysical Laboratory, Technical Report AFGL-TR-79-0214*, Hanscom Air Force Base (Mass.).

	Ref.: MER4RP Validation Report
4th MERIS data reprocessing	Version: 1.0
Evolutions and Validation report	Date: 01/04/2019
	Page: 176

- Vermote, E., C.O. Justice and F.-M. Bréon, (2009), Towards a Generalized Approach for Correction of the BRDF Effect in MODIS Directional Reflectances, *IEEE Transactions on Geoscience and Remote Sensing*, Vol 47, No 3, pp-898-908

End Of Document